THE DYNAMIC PSEUDO-JAHN-TELLER PROBLEM IN CUBIC SYMMETRY

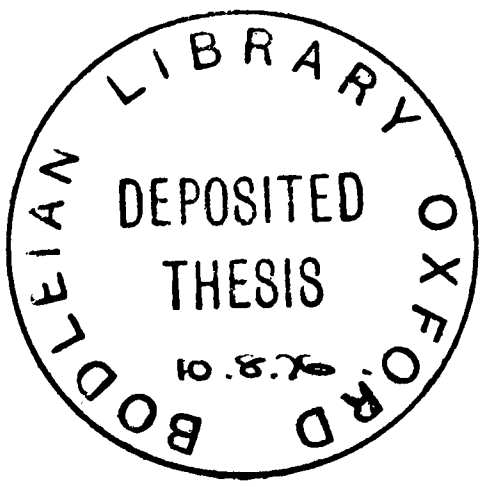
AND A

VIBRONIC MODEL FOR THE RELAXED EXCITED STATE OF THE F CENTRE

IN SOME ALKALI HALIDES

Hans Ulrich Grevsmühl

The Queen's College



Thesis submitted for the degree of Doctor of Philosophy

in the University of Oxford

Department of Theoretical Physics

April 1976

ABSTRACT

The results of recent experiments on Stark effects in F-band luminescence of various alkali halides have suggested a model for the relaxed excited state of the F centre in which non-degenerate 2s and 2p electronic states interact in cubic symmetry via a triply degenerate odd-parity (T_{1u})vibrational mode. A general exact solution of this vibronic problem has been given by Ham (1973a).

We extend the work by a numerical investigation of this ideal pseudo-Jahn-Teller problem. Vibronic energy levels and wave functions, emission spectra at various temperatures, absorption lines and spectra at T=0, and reduction factors are calculated for various values of the vibronic coupling strength and of the electronic 2s-2p spacing. The results are compared with explicit expressions of the weak and strong coupling limit. In addition, the absorption line shape is calculated in semi-classical approximation.

The relaxed excited state of the F centre is investigated within this model by a perturbation analysis for the case of weak electron-phonon coupling. The resulting predictions are compared with available data on radiative lifetimes, Stark effects, magnetic circular polarization, and stress-induced polarization of F-band luminescence. It is shown that a consistent quantitative interpretation of most of these data is possible on this basis if the 2s electronic state lies below the 2p state in the relaxed cubic configuration.

To my wife Jacqueline

ACKNOWLEDGEMENTS

I would like to thank Professor Sir R. Peierls for accepting me in his department, for his interest in the completion of this work and for his efforts in raising additional grants.

I would also like to thank Dr. M.C.M. O'Brien for accepting the supervision of this thesis and for many helpful discussions, as well as making available to me some of her unpublished work and that of Dr. R. Englman.

I am particularly grateful to Dr. F.S. Ham for giving me the opportunity to work for a while in collaboration with him on an exciting topic of the time, for his continuous encouragement and stimulating influence throughout this work.

I am indebted to The Queen's College, Oxford, for its support and for awarding me one of their Florey European Studentships which enabled me to persue this research. In particular, I wish to thank Dr. J. Moffatt for his personal interest in my welfare.

My sincere thanks go to my parents and parents-in-law for their loving assistance and support in turbulent times.

Finally, I am grateful to Mrs. E. Browne for the speedy and accurate typing of this thesis.

CONTENTS

		Page
§ 1	Introduction	1
PART I:	FUNDAMENTAL THEORY	5
§ 2	The Quasi-Molecular Model	5
§ 3	The Jahn-Teller Theorem	11
§ 4	Static and Dynamic Jahn-Teller Effect	15
§ 5	Linear Vibronic Interactions	19
§ 6	Ideal $(s + p) \otimes T_{1u}$ System	25
	(a) Model Hamiltonian	25
	(b) The Static Problem	27
§ 7	The Dynamic $(s + p) \otimes T_{1u}$ Problem	31
	(a) Exact Solution	31
	(b) The Strong-Coupling Limit	35
PART II:	FURTHER INVESTIGATIONS OF THE IDEAL $(s + p) \otimes T_{1u}$ SYSTEM	39
§ 8	Group Theoretical Considerations	39
§ 9	Matrix Elements of the Pseudo-Jahn-Teller Interaction	45
	(a) Introduction of Irreducible Tensors	45
	(b) Reduced Matrix Elements	48
	(c) Matrix Elements of H_{PJT}	56
§ 10	Numerical Diagonalization of the Energy Matrix	59
§ 11	Energy Levels and Vibronic Wave Functions	63
	(a) Weak Coupling - Perturbation Approach	63
	(b) The Strong-Coupling Limit	67
	(c) Computational Results	68
	(i) Low-Lying Energy Levels	68
	(ii) Electronic Admixtures in the Vibronic States	71
	(iii) High-Lying Energy Levels - Type A, B, and C States	72
§ 12	Optical Emission and Absorption	80
	(a) General Expressions	80
	(b) Weak-Coupling - Perturbation Approach	82

		Page
§ 13	Numerical Calculation of the Emission Spectrum	85
	(a) At Zero Temperature	85
	(b) At Higher Temperatures	90
§ 14	Numerical Calculation of the Absorption Spectrum at Zero Temperature	94
	(a) Absorption Lines	94
	(b) Absorption Spectra	98
§ 15	Emission and Absorption Lines in the Strong Coupling Limit	102
§ 16	Absorption Line Shape in Semi-Classical Approximation	106
§ 17	Reduction Factors	112
§ 18	Summary and Discussion	119
PART III:	VIBRONIC MODEL FOR THE RELAXED EXCITED STATE OF THE F CENTRE	127
§ 19	Experimental Evidence and Theoretical Background	127
§ 20	Weak Coupling Limit - Perturbation Treatment	137
	(a) Low-Energy Vibronic States with no External Perturbation	137
	(b) Stark Effects in Emission	141
	(c) Stress-Induced Polarization of Emission	144
	(d) Magnetic Circular Polarization of Emission	147
§ 21	Comparison with Experiment	151
§ 22	Discussion	160
§ 23	Final Comments	166

References

Graph Index

Appendix: Jahn-Teller Systems in WKB Approximation

§ 1 Introduction

The F centre in alkali halides, an electron trapped at a negative-ion vacancy, has been the object of many experimental and theoretical studies and most of its important features are by now well established. For a thorough review on the subject we refer to Fowler (1968) and Markham (1966).

It is known that optical absorption occurs from a 1s-like (A_{1g}) ground state of a 2p-like (T_{1u}) excited state where Stark-effect experiments (Chiarotti et al. 1966, 1969) appear to indicate that a 2s-like state lies above the 2p-like state. After the optical absorption takes place, the surrounding ions relax to a new equilibrium configuration appropriate to the excited state and the potential which characterise the F-electron changes. Consequently, the energies and wave functions of the electronic states of the excited F centre differ from those for the ground-state lattice configuration. Until recently, much less has been known about the character of these so-called relaxed excited states (abbr. as RES).

Whereas the earlier view (Fowler 1968) has been that absorption and luminescence in the F band involved only diffuse hydrogenic 2p excited states, recent theoretical studies have suggested that the 2s electronic state may be degenerate with, or lie slightly below, the 2p states after lattice relaxation (Fowler et al. 1967, Wood et al. 1969). These states should be coupled by odd-parity (T_{1u}) vibrational modes, and the resulting vibronic levels of the coupled electron-lattice system will then be mixtures of the 2s and 2p electronic states.

This view is supported by a number of recent experiments on luminescence in the F band of various alkali halides, particularly Stark-effect studies by Kühnert (1967), Bogan and Fitchen (1970), Stiles et al. (1970), Ohkura et al. (1974). These experiments have been interpreted on the basis of a semiclassical approximate theory developed by Bogan and Fitchen (1970) which assumes that in the cubic configuration the 2s electronic state is slightly lower in energy than the 2p state and that these states are strongly mixed by a fluctuating electric field due to longitudinal-optical phonons.

Ham (1972b, 1973a) has given an exact solution of the vibronic problem which incorporates the principle features indicated by the recent work, namely, nondegenerate 2s and 2p electronic states interacting in cubic symmetry via triply degenerate odd-parity (T_{1u}) vibrational mode. Using this ideal (s+p) ⊠ T_{1u} system, a so-called pseudo-Jahn-Teller (abbreviated as PJT) system, as a model for the RES of the F centre, he has been able to show that the coupling to the T_{1u}-modes is actually rather weak for at least some of the alkali halides, contrary to the previous assumption.

This thesis consists of three parts. Part I deals with the fundamental background and basic theory of the (s+p) ⊠ T_{1u} system. After setting up the vibronic model for the RES of the F centre in § 2 and 5, we outline in § 6 and 7 the static and dynamic solution of this PJT system, as given by Ham. This problem would not in a strict sense be said to involve a Jahn-Teller (abbreviated as JT) effect, since the coupling due to the vibrational modes here is between nondegenerate electronic states and the Jahn-Teller theorem (Jahn and

Teller 1937) is therefore not applicable. Nevertheless, as the physics of the two situations is essentially the same, we present in § 3 and 4 some of the fundamental theory of the JT effect. For good surveys on this subject to refer to Ham (1972a), Englman (1972a) and Sturge (1967).

In part II the ideal (s+p) ⊠ T_{1u} system is investigated numerically by employing the full rotational symmetry of the model Hamiltonian. After some introductory group theoretical considerations (§ 8), matrix elements of the PJT interaction are calculated by making use of the irreducible tensor method (§ 9). The resulting eigenvalue problem is solved by numerical diagonalization (§ 10). Energy levels and wave functions (§ 11), emission (§ 13) and adsorption spectra (§ 14) and reduction factors (§ 17) are computed for representative values of the electronic 2s-2p-spacing and of the coupling strength. In order to compare the properties with the results of weak and strong coupling simple perturbation treatment in full rotational symmetry (§ 11) and Ham's orthogonal transformation (§ 7, 11) are used, respectively (§ 12, 15). In addition the absorption line shape is calculated in semi-classical approximation (§ 16). In § 18 we summarize and discuss our numerical results with reference to other JT and PJT systems. Emphasis is laid on the optical resonance effect in absorption which is thought to be a direct consequence of the dynamic PJT effect. Reference is also made to O'Brien's WKB approximation for the higher energy eigenstates (see Appendix).

Finally, in part III our vibronic model for the RES of the F centre is compared with the experimental data and a

perturbation analysis for the weak-coupling limit is presented (§ 19 to 21). In § 22 our results are discussed in detail and possible improvements of our model by including further vibrational modes are indicated (§ 23).

We note that, although connected of course, parts II and III are treated on the whole as separate entities, reflecting a purely theoretical interest in this PJT system on the one hand and an application to a physical system on the other. The weak-coupling analysis in part III is the result of a joint investigation by Ham and the author (1973b) which was carried out after the general solution (Ham 1973a) presented in part I had been established.

PART I : Fundamental Theory

§2 The Quasi-Molecular Model

Most theoretical studies of the RES of the F centre have been made along two lines. On the one hand we have the polaron coupling theory where the problem of conduction electrons and their interaction with the lattice has been carried over to the impurity problem (bound polaron problem). The question of adiabatic, or strong, coupling versus weak or intermediate coupling has been studied in great detail, and various theories for different coupling regions have been developed (Fowler 1968). In particular, this approach has been formulated for the nearly degenerate states of a bound lattice polaron and applied to the RES of the F centre (Wang et al 1973). Alternatively, one can set up vibronic models by taking into account the coupling between the electronic states of the F electron and the various vibrational modes of the lattice (Ham 1972b, 1973a, Iida et al. 1972, Kayanuma and Toyozawa 1974). In our thesis we shall exclusively take this approach which, as we shall see, will lead us to the Jahn-Teller and pseudo-Jahn-Teller problem.

Both types of studies are concerned with the serious problem of separating the motion of the electron from that of the lattice. In general, it is very difficult to find the stationary states of a system which consists of several coupled particles. Often, however, like with the F centre (in absorption), we can divide the system into a "fast" part (the electron) and a "slow" part (the ions) because of the large differences in the masses wheras the forces acting on the electron and ions are of comparable order of magnitude. As long as the electronic energy levels of the system (or at least those which are coupled by changes in the vibrational coordinates $\underset{\sim}{Q}$ of the lattice) are widely separated in energy compared to the phonon energies, we can treat

the two parts separately and the Born-Oppenheimer approximation (1927) is appropriate. The vibronic eigenfunctions of the coupled system then take the form (Born and Huang 1954).

$$\Xi_n(\underset{\sim}{q}, \underset{\sim}{Q}) = \psi_n(\underset{\sim}{q}, \underset{\sim}{Q})\, \chi_{nm}(\underset{\sim}{Q}) \tag{2.1}$$

Here $\underset{\sim}{q}$ denotes the electronic coordinates, while $\underset{\sim}{Q}$ represents symbolically all the vibrational coordinates of the lattice. The electronic wave function is normalized under integration over $\underset{\sim}{q}$ alone and depends parametrically on $\underset{\sim}{Q}$, satisfying the Schrödinger equation

$$H_e(\underset{\sim}{Q})\psi_n(\underset{\sim}{q}, \underset{\sim}{Q}) = E_n^{(e)}(\underset{\sim}{Q})\,\psi_n(\underset{\sim}{q}, \underset{\sim}{Q}) \tag{2.2}$$

with the electronic Hamiltonian

$$H_e(\underset{\sim}{Q}) = \underset{\sim}{p}^2/2m_e + V(\underset{\sim}{q}, \underset{\sim}{Q}) \tag{2.3}$$

Here we assume that there is only one "active" electron, as for the F centre. In the case of two or more electrons expression (2.3) has to be modified by including further terms for the kinetic energies.

$V(\underset{\sim}{q},\underset{\sim}{Q})$ is the total potential energy as a function $\underset{\sim}{q}$ and $\underset{\sim}{Q}$ (we neglect spin-orbit interaction and external fields). The vibrational wave function depends on the quantum number m and parametrically on n but not on $\underset{\sim}{q}$, and is a solution of the vibrational equation

$$\left(U^{(e)}(\underset{\sim}{Q}) + \sum_v P_v^2/2M_v\right)\chi(\underset{\sim}{Q}) = E^{(L)}\chi(\underset{\sim}{Q}) \tag{2.4}$$

where P_v is the momentum conjugate to Q_v and M_v is the associated ionic mass. $E^{(L)}$ is the vibronic energy eigenvalue. $U^{(e)}(\underset{\sim}{Q})$ is given by

$$U^{(e)}(\underset{\sim}{Q}) = E^{(e)}(\underset{\sim}{Q}) + \int \psi^*(\underset{\sim}{q}, \underset{\sim}{Q}) \sum_v \left(P_v^2/2M_v\right)\psi(\underset{\sim}{q}, \underset{\sim}{Q})\, dq \tag{2.5}$$

Physically this means that the electrons move in a potential well determined by the actual positions of the neighbouring ions, i.e. the instantaneous vibrations of the lattice, whereas the equilibrium positions and vibrational states of the nuclei are determined by the average positions of the electrons and so depend

only upon the electronic state.

When the electronic energy levels are either degenerate or nearly degenerate, i.e. when their separation in energy is small compared to $\hbar\omega$ of the lattice phonons, the Born-Oppenheimer approximation is in general no longer valid, and the system may exhibit a Jahn-Teller or pseudo-Jahn-Teller effect. However, the vibronic eigenfunctions of the system may now be taken as linear combinations of a number of Born-Oppenheimer products where in this case the vibrational functions satisfy a number of coupled differential equations in place of (2.4).

Before pursuing this matter further, we shall briefly outline the logic of the so-called "quasi-molecular" model. The total instantaneous potential seen by an electron in some nuclear framework (molecular or crystalline) can be divided into two parts: the static part $V_o\ (\underset{\sim}{q}, \underset{\sim}{Q}_o)$ in which the mean nuclear positions $\underset{\sim}{Q}_o$ are contained parametrically, and the dynamic part $V\ (\underset{\sim}{q},\underset{\sim}{Q})$ which depends on the displacements $\underset{\sim}{Q}$ of the nuclei from their mean positions. We assume that $V\ (\underset{\sim}{q},\underset{\sim}{Q})$ can be expanded in powers of $Q_{i\alpha}$ where i labels the nuclei and α their cartesian directions of displacement. However the $Q_{i\alpha}$ do not transform in a simple manner under the operations of the symmetry group of the system, and it is more convenient to introduce normal coordinates Q_K (see comments below) which do transform according to the irreducible representations (abbreviated as I.R.) of the group involved. We then find

$$V(\underset{\sim}{q}, \underset{\sim}{Q}) = V_o(\underset{\sim}{q}) + \sum_K \left(\frac{\partial V}{\partial Q_K}\right)_{Q_K=0} \cdot Q_K + \frac{1}{2}\sum_{K,L}\left(\frac{\partial^2 V}{\partial Q_K\, \partial Q_L}\right)_{Q_K, Q_L = 0} Q_K\, Q_L + \cdots \quad (2.6)$$

where the coefficients $\partial V/\partial Q_K$, $\partial^2 V/\partial Q_K\, \partial Q_L$, ... depend on q only. Since V is invariant, $\partial V/\partial Q_K$ transforms in the same way as Q_K.

In the following we shall assume that only the motions of the

defect and its immediate neighbours contribute appreciably to $V(\underset{\sim}{q},\underset{\sim}{Q})$. As regards to the F centre we shall particularly be interested in the octahedral XY_6 complex.

To classify the possible modes of vibration of this complex, we label the vertices from 1 to 6 as shown in Fig.1 and mount a cartesian coordinate frame to measure the displacements $Q_{i\alpha}$, denoted now as x_i,y_i,z_i, of the centre of mass of each atom Y. In order to find out how the 18 possible displacements (x_i,y_i,z_i) transform under the operations of O_h, we have to seek the I.R.'s of O_h for which certain linear combinations of the displacements serve as bases. For this procedure we refer to the textbooks by Tinkham (1964), Heine (1964) and Wilson et al (1955). The final result is expressed as the symbolic sum

$$\Gamma_w = A_{1g} + E_g + T_{1g} + 2T_{1u} + T_{2g} + T_{2u} \qquad (2.7)$$

With this expression we are now able to construct the normal coordinates, i.e. the linear combinations of the displacements (x_i,y_i,z_i) that form bases for the I.R.'s occurring on the right-hand side of (2.7). We find that the bases for T_{1g} correspond to pure rotations of the octahedral complex and are therefore not of physical interest. All the other normal coordinates Q_κ are listed in Table 1. In columns a and b we use the notations of Van Vleck (1939) and of Heine (1964), respectively. In odd parity modes we hold the central point X, rather than the centre of mass, fixed. Some of the nuclear motions associated with those Q_κ which are important for the JT effect are illustrated in Fig.2. The totally symmetric coordinate Q_1 is called the "Breathing" mode A_{1g} and does not reduce the original symmetry. Q_3 represents tetragonal (even parity) distortion of the octahedron, lowering the symmetry from O_h to D_{4h}. Similarly, the combination

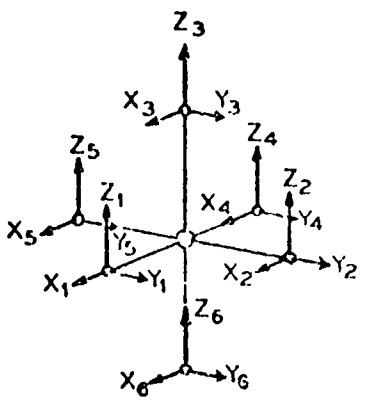


FIG. 1

THE OCTAHEDRAL xy_6 COMPLEX

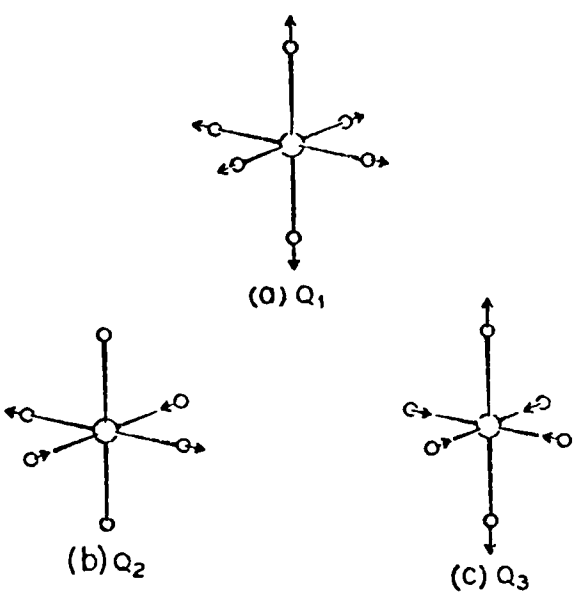


FIG. 2

SYMMETRY COORDINATES FOR THE xy_6 COMPLEX

a	*b*	*c*
Q_1	A $_{1g}$	$(x_1 - x_4 + y_2 - y_5 + z_3 - z_6)/6^{1/2}$
Q_2	E $_g(v)$	$(x_1 - x_4 - y_2 + y_5)/2$
Q_3	E $_g(u)$	$(2z_3 - 2z_6 - x_1 + x_4 - y_2 + y_5)/2(3)^{1/2}$
Q_4	T $_{2g}(\xi)$	$(z_2 - z_5 + y_3 - y_6)/2$
Q_5	T $_{2g}(\eta)$	$(x_3 - x_6 + z_1 - z_4)/2$
Q_6	T $_{2g}(\zeta)$	$(y_1 - y_4 + x_2 - x_5)/2$
Q_7	T $_{1u}{}^a(x)$	$(x_2 + x_3 + x_5 + x_6)/2$
Q_8	T $_{1u}{}^a(y)$	$(y_1 + y_3 + y_4 + y_6)/2$
Q_9	T $_{1u}{}^a(z)$	$(z_1 + z_2 + z_4 + z_5)/2$
Q_{10}	T $_{1u}{}^b(x)$	$(x_1 + x_4)/2^{1/2}$
Q_{11}	T $_{1u}{}^b(y)$	$(y_2 + y_5)/2^{1/2}$
Q_{12}	T $_{1u}{}^b(z)$	$(z_3 + z_6)/2^{1/2}$
Q_{13}	T $_{2u}(\xi)$	$(x_2 + x_5 - x_3 - x_6)/2$
Q_{14}	T $_{2u}(\eta)$	$(y_3 + y_6 - y_1 - y_4)/2$
Q_{15}	T $_{2u}(\zeta)$	$(z_1 + z_4 - z_2 - z_5)/2$

TABLE 1

SYMMETRY COORDINATES AND VIBRATIONAL MODES FOR THE XY_6 COMPLEX

$(Q_4 + Q_5 + Q_6)$ or $(Q_7 + Q_8 + Q_9)$ represent trigonal distortion lowering the symmetry to D_{3d}.

In a real crystal, the Q_κ are not normal coordinates, since the potential energy of the lattice is not diagonal in Q_κ. However, since (2.6) is still valid, we can employ the "quasi-molecular" approximation in which the Q_κ are treated approximately as normal coordinates and all interactions are limited to the nearest neighbours of the point defect, i.e. to the first "shell" of this "cluster" model. In this context the Q_κ are referred to a collective or symmetry coordinates (Sturge 1967). In any particular case, Table 1 can easily be extended to further shells if these turn out to be important (Jahn and Teller 1937 Table 1). The Q_κ belonging to a particular I.R. Γ_γ represent therefore in some average sense the various lattice coordinates which belong to Γ_γ and are often referred to as "interaction modes" (Toyozawa and Inone 1966). A justification and limitation of the cluster model has recently been given by O'Brien(1972a).

In the following we shall employ the quasi-molecular model for the F centre in which the central electron and its nearest neighbour ions form a XY_6 complex. The nuclear Hamiltonian can now be written in the harmonic approximation as

$$H_L = \frac{1}{2} \sum_\kappa \left(P_\kappa^2 / \mu_\kappa + \mu_\kappa \omega_\kappa^2 Q_\kappa^2 \right) \tag{2.8}$$

where P_κ is the momentum operator conjugate to Q_κ of Table 1, μ_κ is the effective mass, and ω_κ is the frequency of the κth normal mode.

The Hamiltonian of the F centre electron may be rewritten as

$$H_e(\underset{\sim}{Q}) = H_{eo} + \sum_\kappa \left(\frac{\partial V}{\partial Q_\kappa} \right)_{Q_\kappa = 0} Q_\kappa + \frac{1}{2} \sum_{\kappa, L} \left(\frac{\partial^2 V}{\partial Q_\kappa \partial Q_L} \right)_{Q_\kappa, Q_L = 0} Q_\kappa Q_L + \cdots \tag{2.9}$$

where the spin-orbit coupling is again neglected, and where

$$H_{eo} = \underset{\sim}{p}^2 / 2m_e + V_o(\underset{\sim}{q}) \tag{2.10}$$

is the electronic Hamiltonian for a given symmetric configuration, i.e. with the lattice fixed at $\underset{\sim}{Q} = 0$, the equilibrium position of the lattice ions when the F centre is in its orbital ground state.

The F centre has cubic octahedral symmetry, and so does $H_{eo}(\underset{\sim}{q})$. The orbital wave functions comprising a multiplet will then have the same symmetry as the set of basis functions of one of the I.R. Γ_α of O_h. The singlet ground and excited states transform according to A_{1g} like $x^2 + y^2 + z^2$. The orbital triplet excited states transform according to T_{1u} like (x, y, z). Our attention will be restricted to these three states only, i.e. we shall neglect all higher lying states.

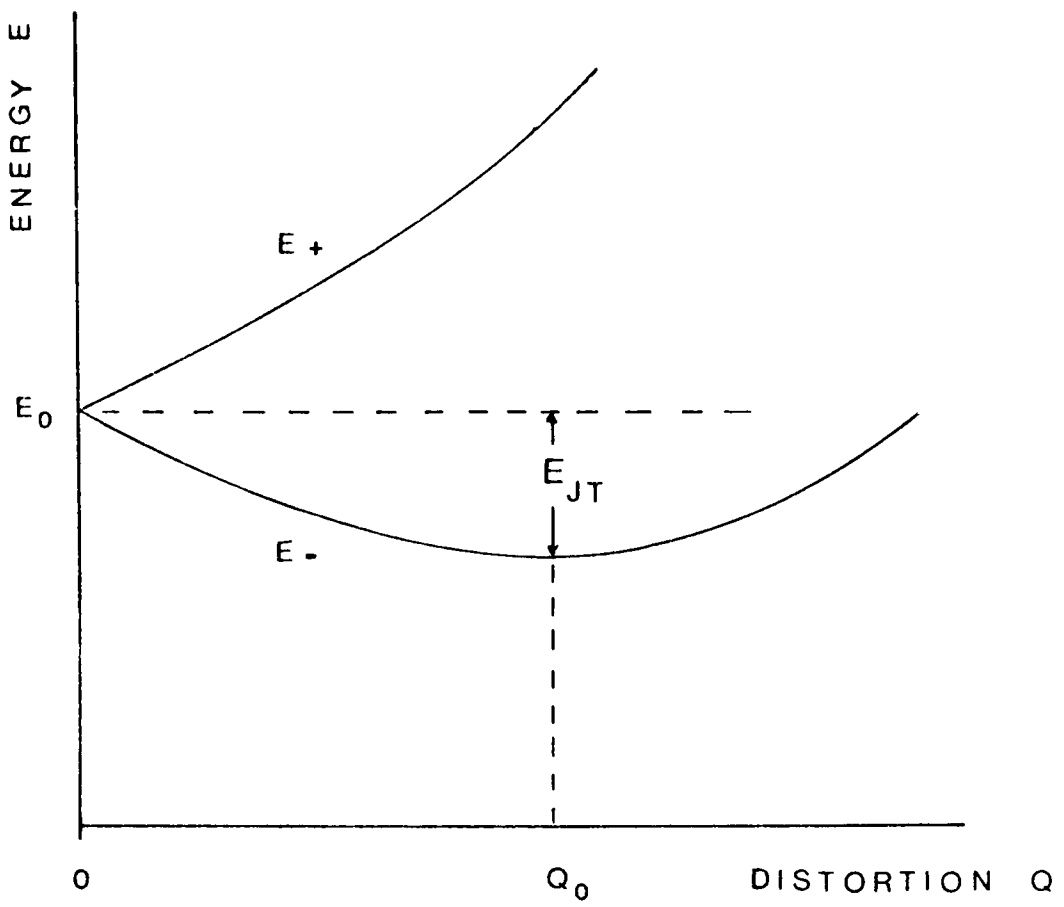
§3 The Jahn-Teller Theorem

The fundamental theorem of the JT effect (Jahn and Teller 1936, 1937) reads: If a molecule or crystalline defect has orbital electronic degeneracy when the nuclei are in a symmetrical configuration, then the molecule or defect is unstable with respect to at least one asymmetric displacement of the nuclei which lifts the degeneracy. The only exception to the rule is the linear molecule (Ham 1972a).

The instability arises because a linear splitting of a degenerate electronic level necessarily leads to a state with lower energy than that of the unsplit level, the centre of gravity of the level being unshifted to first order. Ultimately the distortion is limited to a finite value by the quasi-elastic forces (i.e. the $V(\underset{\sim}{q},\underset{\sim}{Q})$ of (2.6)) that resist it. Since the elastic energy associated with the distortion is proportional to Q_K^2 (the symmetrical configuration denoted by $Q_K^2 = 0$ is assumed to be a configuration of stable equilibrium apart from the coupling to the degenerate electronic state), the system can lower its energy by distorting to finite Q_K, to the so-called "JT distortion". The symmetrical configuration is therefore unstable with respect to this distortion. Thus, a new position of equilibrium is reached in which the local symmetry is lower than the point symmetry of the crystal. In general, this new symmetry will be low enough to remove all orbital electronic degeneracy. Now a distortion that removes electronic degeneracy must itself be degenerate, so there will be more than one position of equilibrium with equal energy. This means that the original purely electronic degeneracy is replaced by a "vibronic" one (Sturge 1967).

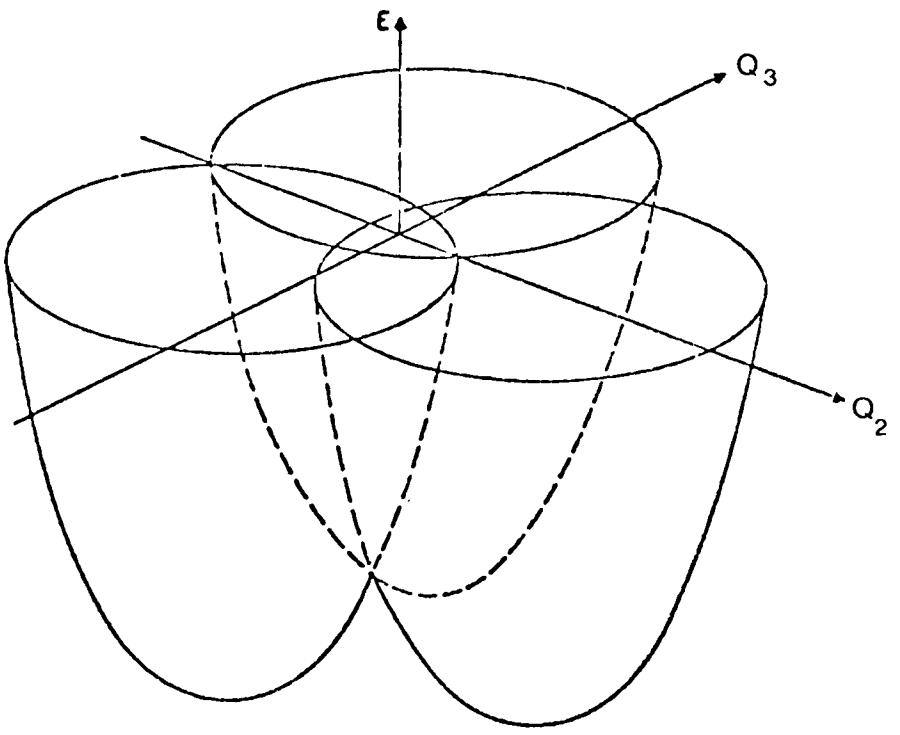
Fig. 3 shows the energy splitting of a doubly degenerate

FIG. 3



JAHN–TELLER INSTABILITY OF A DOUBLY DEGENERATE ELECTRONIC STATE

FIG. 4



ENERGY SURFACES FOR T ⊗ E

electronic state under a distortion that lifts the degeneracy in first order, showing the JT instability of the symmetrical configuration. The two split electronic states are the two eigenstates of (2.2) that become degenerate at Q = 0, and their E_+ (Q) and E_- (Q) are the associated eigenvalues.

Originally, Jahn and Teller (1937) proved their theorem with the help of perturbation theory and from an exhaustive examination of the properties of the point symmetry group in each possible case. Alternatively, one may use the Hellman-Feynman theorem which rest on the assumption that it is possible to write down the total potential energy of a system of electrons and nuclei as an explicit function of the coordinates, $V(\underset{\sim}{q}, \underset{\sim}{Q})$, and that the first derivative with respect to each of the nuclear coordinates exists (Sturge 1967).

Using this latter approach we can write the electronic energy eigenvalues of the system in analogy to (2.6) and (2.9) as

$$E^{(e)}_{n\alpha i}(Q) = E^{(e)}_{0,n\alpha i} + \sum_K \left(\frac{\partial E^{(e)}_{n\alpha i}}{\partial Q_K}\right)_{Q_k=0} Q_K + \cdots \qquad (3.1)$$

where the subscripts n,α, i denote the principal quantum number, I.R. label, and component label of the electronic states, respectively. K ≡(pγj) stands for a similar collection of vibrational quantum numbers.

In elementary vibration theory the vanishing of the linear term in (3.1) is taken as a condition for the establishment of an equilibrium configuration Q_o. However, as Jahn and Teller could show, this equilibrium configuration does usually not exist if $\psi_{n\alpha i}$ is orbitally degenerate. Since the normal coordinates Q_K of the nuclei are regarded as parameters in the electronic eigenvalue equation (2.2), we can apply the Hellman-Feynman theorem

$$\left(\frac{\partial E^{(e)}_{n\alpha i}}{\partial Q_\kappa}\right)_{Q_\kappa = 0 \text{ for all } \kappa} = \left\langle \psi_{n\alpha i} \middle| \frac{\partial H_e}{\partial Q_\kappa} \middle| \psi_{n\alpha i} \right\rangle \qquad (3.2)$$

where H_e is the electronic Hamiltonian and $\psi_{n\alpha i}$ is its exact and normalised eigenfunction.

If the matrix element in (3.2) is non-vanishing for a certain nuclear configuration, the configuration is unstable and will sponteneously distort until $(\partial E^{(e)}_{n\alpha i}/\partial Q_\kappa)_o$ is zero. The JT theorem states that if there is an orbitally degenerate electronic state when $Q_\kappa = 0$, the matrix element in (3.2) exists for some Q_κ, $\kappa \neq 1$, i.e. for some nontotally symmetric coordinate. For the fully symmetric coordinate Q_1, this matrix element is zero.

We prove this statement by group theory. $\psi_{n\alpha i}$ transforms according to some component of the I.R. Γ_α. $Q_{p\gamma j}$ transforms according to Γ_γ, and so does $(\partial/\partial Q_{p\gamma j})$ in order for $(\partial/\partial Q_{p\gamma j})\, Q_{p\gamma j}$ to be a scalar, transforming as Γ_1 (we assume the I.R.'s to be real). If the matrix element (3.2) is not to vanish identically, $\Gamma_\alpha x \Gamma_\gamma x \Gamma_\alpha$ must contain Γ_1, i.e. Γ_γ must be contained in the symmetric product $[\Gamma_\alpha{}^2]$ (Heine 1964).

If Γ_α is nondegenerate, $[\Gamma_\alpha{}^2] = \Gamma_1$. The spontaneous distortion which occurs now is totally symmetric and does not lower the symmetry of the system. In equilibrium, therefore $Q_\kappa = 0$ unless $\Gamma_\gamma = \Gamma_1$. The system readjusts until (3.2) is "accidentally zero" in a group-theoretical sense.

If Γ_α is degenerate, there will be one or more non-symmetric I.R. contained in $[\Gamma_\alpha{}^2]$. If the complex has a normal coordinate Q_κ transforming as one of these I.R.'s there is no reason from symmetry why (3.2) should be zero. In general, equilibrium is reached only through lowering of the symmetry, i.e. at some finite value of Q_κ.

An important consequence of the requirement that $[\Gamma_\alpha{}^2]$ contains Γ_γ is that in a centrosymmetric system Γ_γ must be of even parity. This often reduces the number of Q_κ with which we have to deal. In §5 we shall see that in the case of the F centre (O_h symmetry) the triply degenerate p (T_{1u}) electronic state can only be split by the vibrational E_g and T_{2g} modes, the so-called "Jahn-Teller modes".

The above form of the JT theorem applies only to an electronic system having orbital degeneracy. As Jahn (1938) has shown, the same theorem applies in principle to spin degeneracy as well, with the further exception that simple Kramers degeneracy cannot be lifted by any distortion. However, the direct coupling between the spin levels and lattice distortion is sufficiently weak so that in practice JT effects are not significant when spin degeneracy alone is present.

The JT theorem is an existence theorem concerning the availability in each case of at least one mode of distortion that can in principle cause a linear splitting. However, it says nothing about the magnitude of the coupling coefficient appropriate in any case, and of course it is the size of this coefficient that determines whether in a given situation we see a static JT effect, a dynamic effect, or no significant effect at all (Ham 1972a). In the following paragraph we shall probe further into this problem.

§4 The Static and Dynamic Jahn-Teller Effect

We consider now the eigenvalues $E^{(e)}(\underset{\sim}{Q})$ of the electronic Hamiltonian (2.3) where the ionic kinetic energy has been completely omitted. These energy surfaces $E^{(e)}(\underset{\sim}{Q})$ corresond to a completely static treatment of the lattice where the dependence of the various lattice coordinates $\underset{\sim}{Q}$ is taken only parametrically. As we have seen above, when there is a JT effect the surfaces intersect with a finite slope in the symmetrical configuration $\underset{\sim}{Q} = 0$, which is therefore unstable. There are a number of absolute minima lying at finite $\underset{\sim}{Q}$ which thus correspond to the configurations of stable equilibrium. In these stable distorted configurations the lowest electronic state has no remaining orbital degeneracy, for by the JT theorem a further distortion could otherwise lead to a still lower value of $E^{(e)}(\underset{\sim}{Q})$. The energy difference E_{JT}, or E_{PJT} in the case of the pseudo-Jahn-Teller effect, by which $E^{(e)}(Q)$ at these absolute minima, including the elastic energy, lies below the energy $E_o^{(e)}$ of the symmetrical configuration is thus the energy of stablization of the distorted configuration, the so-called "Jahn-Teller energy" (or PJT energy) (see Fig.3).

In §5 we shall see that the E_g and T_{2g} lattice modes in O_h symmetry give rise to JT instabilities by coupling to the 2p (T_{1u}) electronic states, whereas the T_{1u} mode forms a PJT problem by interacting with 2s (A_{1g}) and 2p (T_{1u}) electronic states. For the static treatment of these systems we refer to Van Vleck (1939), Moffitt and Thorson (1957), Öpik and Pryce (1957), Liehr (1963). The PJT problem will be discussed in detail in §6.

Fig.4 shows the energy surfaces for the $T \otimes E$ case, i.e. for the vibronic problem of an orbital triplet electronic state with JT

coupling only with a pair of E vibrational modes, Q_2 and Q_3. One can show that since the vibronic interaction Hamiltonian is diagonal in the space of the electronic basis states $|x\rangle, |y\rangle, |z\rangle$, no mixing of the electronic states can occur for any Q_2, Q_3, and we talk of a "trivial JT case". The resulting energy surfaces are thus three disjoint paraboloids corresponding to the electronic basis $|x\rangle, |y\rangle, |z\rangle$.

In the case of $T \otimes T_2$, i.e. the orbital triplet electronic states interact only with a T_2 lattice mode, the JT interaction Hamiltonian cannot be diagonalized simultaneously with the nuclear kinetic and potential energy, and we now have a "non-trivial JT case". The energy surfaces are now not easily visualized, but various cross sections have been illsutrated by Liehr (1963). The stable configurations are few in number and represent distortions of trigonal symmetry.

We now take account of the kinetic energy of the lattice ions. Unless the linear vibronic interaction Hamiltonian is diagonal within the space of the (degenerate) electronic basis states, this interaction causes the nuclear motion to mix electronic states, and the Born-Oppenheimer approximation is invalid. We therefore seek to solve directly the vibronic Schrödinger equation

$$H(\underset{\sim}{P}, \underset{\sim}{Q})\Psi(\underset{\sim}{q}, \underset{\sim}{Q}) = E\,\Psi(\underset{\sim}{q}, \underset{\sim}{Q}) \tag{4.1}$$

where the full vibronic Hamiltonian (without the spin-orbit term and external fields) is given by

$$H(\underset{\sim}{P}, \underset{\sim}{Q}) = \sum_{\nu} \frac{P_\nu}{2M_\nu} + \frac{\underset{\sim}{p}^2}{2m_e} + V(\underset{\sim}{q}, \underset{\sim}{Q}) \tag{4.2}$$

It is very important that the vibronic Hamiltonian in (4.1) has the full symmetry of the symmetrical configuration of the

complex or of the lattice site at which the JT ion is situated, since the total potential energy $V(\underset{\sim}{q},\underset{\sim}{Q})$ has this symmetry under simultaneous transformation of the electronic coordinates $\underset{\sim}{q}$ and the displacements $\underset{\sim}{Q}$ of the nuclei. Consequently, the vibronic eigenstates of (4.1) may be classified according to the point symmetry group of the symmetrical configuration, and states have the degeneracy of the I.R.'s of this group. We see, therefore, that the JT coupling does not lift the degeneracies of the vibronic states which belong as partners to the same I.R. of the group of the original symmetrical configuration. Whereas the degeneracy of the electronic states which satisfy (2.2) is split for a fixed $\underset{\sim}{Q}$ different from that of the symmetrical configuration, there is no such splitting of the vibronic eigenstates of the coupled system. Even for the static JT effect the degeneracy is preserved, since the several energetically equivalent distorted configurations and the associated electronic states represent vibronic states which belong as partners to one (or sometimes more) I.R. of the original symmetry group (Ham 1972a).

For weak or intermediate coupling, the minima of the adiabatic potentials are separated by not very high barriers (their magnitudes are in the order of the energy of vibration), and the system can go over from one potential minimum to another by thermal activation over the barriers, or even at zero temperature by quantum-mechanical tunnelling. This is because the wave functions describing the system as localized in one or another valley are not orthogonal and are therefore not true eigenfunctions. The system will oscillate between its stable configurations, and the original point symmetry is maintained in the average.

For very strong coupling (also often referred to as static JT effect) we still have vibrational ionic motion within the well in $E^{(e)}(\underset{\sim}{Q})$ corresponding to the distorted configuration, so that there may still be significant dynamic corrections, even from zero-point ionic motion in the ground state. In this situation the Born-Oppenheimer approximation may be applicable in describing the low-energy states in each well. For a discussion of the dynamic JT effect of various systems we refer to Ham (1972a) and Englman (1972a).

§5 Linear Vibronic Interactions

The electronic state of the F centre will be coupled by vibronic interactions, spin-orbit coupling and external fields. For the further treatment it is therefore useful to consider all the possible matrix elements with the s(A_{1g}) electronic ground and excited states and the p (T_{1u}) electronic excited states. In calculating these matrix elements we use the irreducible tensor method. This has been extensively developed for systems with Hamiltonians having full spherical symmetry (e.g. free atoms) (Fano et al 1959 , Wigner 1959) but also applied to lower symmetry characteristic of the internal modes of motion of molecules and of the states of ions in solids (Griffith 1962).

The generalized Wigner-Eckart Theorem is given by Griffith (1962, eqn. (2.15))

$$\langle a\alpha \mid g^b_\beta \mid c\gamma \rangle = \langle a \| g^b \| c \rangle \cdot V\begin{pmatrix} a & c & b \\ \alpha & \gamma & \beta \end{pmatrix} \qquad (5.1)$$

where $|a\alpha\rangle$ and $|c\gamma\rangle$ are basis functions of the I.R.'s Γ_a and Γ_c, respectively, and the set of operators g^b_β span Γ_b.

The intrinsic, or scalar, part $\langle a||g^b||c\rangle$ is the so-called reduced matrix element and is not determined by group-theoretical considerations, whereas the V coupling coefficients depend on symmetry, i.e. upon which particular components have been selected. The V coefficients for the octahedral group are tabulated in Griffith (1962), Appendix C.

By definition $\langle a||g^b||c\rangle = 0$ (5.2a)

Whenever $\delta(a, b, c) = 0.$ (5.2b)

For $a \neq c$, $\delta(a, b, c) = 1$ only if A_1 (or A_{1g}) is contained in the triple direct product a x b x c, or c in a x b, or a in b x c, or b in a x c; $\delta(a, b, c) = 0$ otherwise.

Thus, in the case of the F centre (O_h symmetry) we find for the direct product

$$A_{1g} \times T_{1u} = T_{1u} \tag{5.3}$$

thus only operator transforming according to T_{1u} can have non-vanishing matrix elements between the electronic s- and p-states. These will be vibrations of symmetry T_{1u} as well as the electric dipole operator.

Eqn. (5.1) gives

$$\langle A_{1g}\, \iota \,|\, g_\beta^{T_{1u}} | T_{1u}\, \gamma \rangle = \langle A_{1g} \| g^{T_{1u}} \| T_{1u} \rangle \cdot \frac{\delta_{\beta\gamma}}{\sqrt{3}} \tag{5.4}$$

where $$\langle A_{1g} \| g^{T_{1u}} \| T_{1u} \rangle = \langle T_{1u} \| g^{T_{1u}} \| A_{1g} \rangle$$

if all the basis functions and operators involved are real.

For a = c, the direct product of a with itself may be split up into two parts - the symmetrized and the antisymmetrized squares $\left[a^2\right]$ and $\{a^2\}$, and so can the matrix elements. In order for the symmetric part of $\langle a\alpha | g_\beta^b | a\alpha' \rangle$ to be non-zero, the symmetric product $\left[\Gamma_a{}^2\right]$ must contain Γ_b. Similarly, for the antisymmetric part to be non-zero, $\{\Gamma_a{}^2\}$ must contain Γ_b.

For the F centre we find,

$$\left[T_{1u}{}^2\right] = A_{1g} + E_g + T_{2g} \tag{5.5a}$$

$$\left\{T_{1u}{}^2\right\} = T_{1g} \tag{5.5b}$$

In the electron-lattice interaction, the coefficients $(\partial V/\partial Q_\kappa)$ represent the change in potential energy of the F-centre electron as a result of a lattice distortion. Since $(\partial V/\partial Q_\kappa)$ is real and Hermitian, its matrix elements are symmetric, and according to (5.5a) the only non-zero matrix elements of the electron-lattice interaction will be for vibrations of symmetry A_{1g}, E_g and T_{2g}.

Similarly, we find that the applied stress interaction with the F-centre electron should have non-zero matrix elements

for applied stress of symmetry A_{1g}, E_g and T_{2g}.

The orbital part of the spin-orbit interaction is an imaginary Hermitian operator of symmetry T_{1g}, and its antisymmetric matrix elements will therefore be non-zero according to (5.5b). Similarly, we expect ℓ_z to have some non-zero matrix elements.

The corresponding symmetric matrix elements are obtained with the help of (5.1),

$$\langle T_{1u}\alpha \mid g_\iota^{A_{1g}} \mid T_{1u}\gamma\rangle = \langle T_{1u} \| g^{A_{1g}} \| T_{1u}\rangle \frac{\delta_{\alpha\gamma}}{\sqrt{3}} \tag{5.6}$$

$$\begin{aligned}\langle T_{1u}x \mid g_\theta^{E_g} \mid T_{1u}x\rangle &= \langle T_{1u}y \mid g_\theta^{E_g} \mid T_{1u}y\rangle = \\ &= -2\langle T_{1u}z \mid g_\theta^{E_g} \mid T_{1u}z\rangle = -\sqrt{3}\langle T_{1u}x \mid g_\epsilon^{E_g} \mid T_{1u}x\rangle = \\ &= \sqrt{3}\langle T_{1u}y \mid g_\epsilon^{E_g} \mid T_{1u}y\rangle = \langle T_{1u} \| g^{E_g} \| T_{1u}\rangle \cdot \frac{1}{2\cdot\sqrt{3}}\end{aligned} \tag{5.7}$$

$$\langle T_{1u}\alpha \mid g_\beta^{T_{2g}} \mid T_{1u}\gamma\rangle = -\langle T_{1u} \| g^{T_{2g}} \| T_{1u}\rangle \cdot \frac{|\varepsilon_{\alpha\beta\gamma}|}{\sqrt{6}} \tag{5.8}$$

where $\varepsilon_{\alpha\beta\gamma}$ is the so-called alternating tensor which is defined to be zero if any two of $\alpha,\beta,$or γ equal, to be (+1) if $\alpha\beta\gamma$ is an even permutation of xyz and (-1) if it is an odd permutation. Thus $|\varepsilon_{\alpha\beta\gamma}| = 1$ for any permutation.

Similarly, we find for the antisymmetric matrix element,

$$\langle T_{1u}\alpha \mid g_\beta^{T_{1u}} \mid T_{1u}\gamma\rangle = \langle T_{1u} \| g^{T_{1g}} \| T_{1u}\rangle \cdot \frac{\varepsilon_{\alpha\beta\gamma}}{\sqrt{6}} \tag{5.9}$$

For the electronic s-(A_{1g}) states one obtains,

$$A_{1g} \times A_{1g} = \left[A_{1g}^2\right] = A_{1g} \tag{5.10}$$

No antisymmetric product exists so that only vibrations and strains of symmetry A_{1g} can interact with the electronic ground and s-like excited state.

We are now in the position to write down the linear electron-lattice interaction for the F centre which arises from the coupling to the lattice modes A_{1g}, E_g, T_{2g}, T_{1u}. As can be seen from Table 1,

the F electron is coupled to two types of T_{1u} lattice modes. However, the T_{1u} mode of the (Q_7, Q_8, Q_9) coordinates represents a pure translation of the F centre environment, and we shall neglect in the following the coupling to this mode as the influence of the T_{1u} mode associated with (Q_{10}, Q_{11}, Q_{12}) is expected to dominate. This enables us to treat the T_{1u} vibrations in a similar way as the even parity vibrational modes.

We suppose that the electronic eigenfunctions of §2 for the F centre are the solutions of the static problem. Assuming that the excited levels are well separated from the ground state, we may use first-order perturbation theory for the vibronic coupling. With the general results given above, we find the matrix elements of the linear vibronic interaction Hamiltonians acting within the excited electronic p (T_{1u}) states given by $|x\rangle$, $|y\rangle$, $|z\rangle$. Going over to Hamilton operator equivalents we end up with

$$H_{int,1} = H_{eL}(A_{1g}) + H_{JT}(E_g) + H_{JT}(T_{2g}) \qquad (5.11)$$
$$= \sum_{\Gamma_\gamma = A_{1g}, E_g, T_{2g}} L(\Gamma_\gamma) \cdot \sum_{i} \sum_{\alpha,\beta = x,y,z} Q_i^{\Gamma_\gamma} \cdot V \begin{pmatrix} T_{1u} & T_{1u} & \Gamma_\gamma \\ \alpha & \beta & i \end{pmatrix} |\alpha\rangle\langle\beta|$$

where $L(\Gamma_\gamma)$ is a measure of the strength of the electron-lattice coupling and is given by the reduced matrix element

$$L(\Gamma_\gamma) = \langle T_{1u} \| \partial H_e / \partial Q^{\Gamma_\gamma} \| T_{1u} \rangle \qquad (5.12)$$

and $Q_i^{\Gamma\gamma} \equiv Q_K$ of Table 1.

Similarly, we obtain within the excited electronic p (T_{1u}) and 2s (A_{1g}) states (we neglect the coupling to the electronic ground state!),

$$H_{int,2} = H_{pJT}(T_{1u}) \qquad (5.13)$$
$$= L(T_{1u}) \cdot \sum_{\alpha,\beta = x,y,z} Q_\beta^{T_{1u}} \cdot V \begin{pmatrix} A_{1g} & T_{1u} & T_{1u} \\ i & \alpha & \beta \end{pmatrix} \cdot \{ |s\rangle\langle\alpha| + |\alpha\rangle\langle s| \}$$

where $$L(T_{1u}) = \langle A_{1g} \| \frac{\partial H_e}{\partial Q^{T_{1u}}} \| T_{1u} \rangle \qquad (5.14)$$

and $Q_x^{T_{1u}} \equiv Q_{10}$, $Q_y^{T_{1u}} \equiv Q_{11}$, $Q_z^{T_{1u}} \equiv Q_{12}$ of Table 1.

The total linear vibronic interaction Hamiltonian is then given by the sum of the fully symmetric electron-lattice interaction term $H_{eL}(A_{1g})$, the two Jahn-Teller terms $H_{JT}(E_g)$ and $H_{JT}(T_{2g})$, and the pseudo-JT term $H_{pJT}(T_{1u})$.

$$H_{eL}(A_{1g}) = \frac{L(A_{1g})}{\sqrt{3}} Q_1 \cdot \{ |x\rangle\langle x| + |y\rangle\langle y| + |z\rangle\langle z| \} \qquad (5.15)$$

$$H_{JT}(E_g) = \frac{L(E_g)}{2\sqrt{3}} \cdot \{ (Q_2 - \sqrt{3} Q_3) \cdot |x\rangle\langle x| + (Q_2 + \sqrt{3} Q_3) \cdot |y\rangle\langle y| - 2 Q_2 |z\rangle\langle z| \} \qquad (5.16)$$

$$H_{JT}(T_{2g}) = - \frac{L(T_{2g})}{\sqrt{6}} \cdot \{ Q_4 (|y\rangle\langle z| + |z\rangle\langle y|) + Q_5 (|x\rangle\langle z| + |z\rangle\langle x|) + Q_6 (|x\rangle\langle y| + |y\rangle\langle x|) \} \qquad (5.17)$$

$$H_{pJT}(T_{1u}) = \frac{L(T_{1u})}{\sqrt{3}} \cdot \{ Q_{10} \cdot (|s\rangle\langle x| + |x\rangle\langle s|) + Q_{11} \cdot (|s\rangle\langle y| + |y\rangle\langle s|) + Q_{12} \cdot (|s\rangle\langle z| + |z\rangle\langle s|) \} \qquad (5.18)$$

We note, if $\Gamma_\gamma = A_{1g}$, then

$$V \begin{pmatrix} T_{1u} & T_{1u} & A_{1g} \\ \alpha & \beta & i \end{pmatrix} = \frac{\delta_{\alpha\beta}}{\sqrt{3}} \qquad (5.19)$$

so there is an overall shift but no splitting. If $\Gamma_\gamma \neq A_{1g}$, then we find with Griffith (1962, equ. 2.21),

$$\sum_\alpha V \begin{pmatrix} T_{1u} & T_{1u} & \Gamma_\gamma \\ \alpha & \alpha & i \end{pmatrix} = 0 \qquad (5.20)$$

for the JT interaction the centroid of T_{1u} is therefore not shifted to first order in Q_K. From this follows that at least one of the eigenvalues, resulting from the vibronic interaction and the static Hamiltonian, decreases initially linearly, with

increasing Q_κ (see §3 Jahn-Teller theorem).

We have assumed that there is no coupling between the electronic s-states and the A_{1g}-lattice modes. In particular, when the F electron is in its ground state 1s, the equilibrium position of the lattice ions is by definition $Q_\kappa = 0$ for all κ. In order that the linear vibronic interaction H_{int} does not change this equilibrium position, we require that

$$\langle 1s \left| \frac{\partial H_e}{\partial Q_\kappa} \right| 1s \rangle = 0 \qquad (5.21)$$

even for vibrations of symmetry A_{1g}. As the A_{1g} modes affect only a shift of the levels, it is sensible to assume a similar condition for the 2s state.

§6 Ideal $(s + p) \otimes T_{1u}$ System

(a) Model Hamiltonian

A system having a symmetrical configuration of the nuclear framework and involving electronic states which may be non-degenerate but which are not sufficiently separated in energy compared to $\hbar\omega$ of the lattice phonons for the Born-Oppenheimer approximation to be accurate can exhibit a PJT effect (Ham 1972a). From the general consideration that the properties of a physical system cannot change discontinuously when a parameter specifying the system varies continuously, we must expect, as Öpik and Pryce (1957) have noted, a similar physics to the JT effect to arise in systems with nearly degenerate electronic states.

In our further treatment we shall mainly be interested in treating the vibronic coupling to the T_{1u} mode, and for this it is of advantage to express the model Hamiltonian in a more convenient form. The electronic 2s (A_{1g}) and 2p (T_{1u}) states interact in cubic symmetry (point group O_h) via a triply degenerate T_{1u} vibrational mode Q_x, Q_y, Q_z. The vibrational Hamiltonian may thus be written as

$$H_L = \frac{1}{2\mu} \left\{ P^2 + (\mu\omega)^2 Q^2 \right\} \tag{6.1}$$

where $P^2 = \sum_{i=x,y,z} P_i^2$, $Q^2 = \sum_{i=x,y,z} Q^2$.

In the configuration of cubic symmetry ($Q_x = Q_y = Q_z = 0$) the excited electronic singlet state $|2s\rangle$ is taken to have an energy E_{sp} relative to the excited triplet state $|x\rangle, |y\rangle, |z\rangle$. The purely electronic part of the model Hamiltonian is therefore taken to be

$$H_e = \frac{1}{2} E_{sp} \cdot \rho_0 \tag{6.2}$$

where ρ_o denotes the Hermitean electronic operator

$$\rho_0 = |2s\rangle\langle 2s| - \sum_{i=x,y,z} |i\rangle\langle i| \tag{6.3}$$

Denoting $G = L\,(T_{1u})/\sqrt{3}$ and $Q_x = Q_{10}$, $Q_y = Q_{11}$, $Q_z = Q_{12}$ in the PJT interaction above we find

$$H_{PJT}(T_{1u}) = G \sum_{i=x,y,z} Q_i \rho_i \tag{6.4}$$

with the Hermitean electronic operators

$$\rho_i = |i\rangle\langle 2s| + |2s\rangle\langle i| \qquad (i = x,y,z) \tag{6.5}$$

The model Hamiltonian is given by

$$H = H_L + H_e + H_{PJT} \tag{6.6}$$

Following Messiah (1969, p.433) we introduce the dimensionless Hermitean operators q_i, p_i which are related to Q_i, P_i by

$$Q_i = \sqrt{\frac{\hbar}{\mu\omega}}\, q_i \quad , \quad P_i = \sqrt{\mu\hbar\omega}\, p_i \quad (i = x,y,z) \tag{6.7}$$

where $p_j = -i\frac{\partial}{\partial q_j}$ and $[p_k, q_j] = i\,\delta_{kj}$ (Note, do not confuse q_i, p_i with the electronic coordinates $\underset{\sim}{q}$, $\underset{\sim}{p}$, of §2).

Furthermore, we define the dimensionless quantities,

$$\varkappa = \frac{G}{\hbar\omega}\sqrt{\frac{\hbar}{2\mu\omega}} \tag{6.8}$$

$$\delta = \frac{E_{sp}}{2\hbar\omega} \tag{6.9}$$

$$\varepsilon = \frac{E}{\hbar\omega} \quad , \quad h = \frac{H}{\hbar\omega} \tag{6.10}$$

The model Hamiltonian then reads

$$h = h_L + h_e + h_{PJT} \tag{6.11}$$

where

$$h_L = \tfrac{1}{2}\cdot(p^2 + q^2) \tag{6.12}$$

$$h_e = \delta\cdot\rho_0 \tag{6.13}$$

$$h_{PJT} = \sqrt{2}\,\varkappa \cdot \sum_{i=x,y,z} q_i \rho_i \tag{6.14}$$

where $p^2 = \sum_{i=x,y,z} p_i^2$, $q^2 = \sum_{i=x,y,z} q_i^2$. One can show that the model Hamiltonian is invariant under a continuous group of simultaneous rotations of the electronic and vibrational coordinates. As a result of this, the static problem of the next section exhibits spherical symmetry. Ham has used these symmetry properties to

derive exact expressions for the vibronic eigenstates (§7).

(b) The Static Problem

As for the static JT effect we omit the vibrational kinetic energy terms in our model Hamiltonian h. Then the linear combinations of the electronic states $|x\rangle, |y\rangle, |z\rangle, |2s\rangle$ that diagonalize h for any choice of q_x, q_y, q_z are found by solving the secular equation.

Two of the states are linear combinations of 2s and 2p and have the energies

$$\varepsilon_{1/2} = \frac{q^2}{2} \pm \sqrt{\delta^2 + 2\varkappa^2 q^2} \qquad (6.15)$$

Note that $\varepsilon_{1/2}$ do not depend on the sign of δ. The two states which involve the 2p states alone correspond to the double root of the secular equation

$$\varepsilon_{3/4} = \frac{q^2}{2} - \delta \qquad (6.16)$$

These solutions are independent of $\varkappa$.

The adiabatic energy surfaces have spherical symmetry in q-space and are given for representative cases in Fig.5. The configuration of minimum energy is obtained by finding the stationary points of ε_2. The minimum occurs at $q = q_0$ given by

$$q_0^2 = 2\varepsilon_G \left\{ 1 - \left(\frac{\delta}{2\varepsilon_G}\right)^2 \right\} \qquad (6.17)$$

provided the coupling is sufficiently strong so that

$$2\varepsilon_G > |\delta| \qquad (6.18)$$

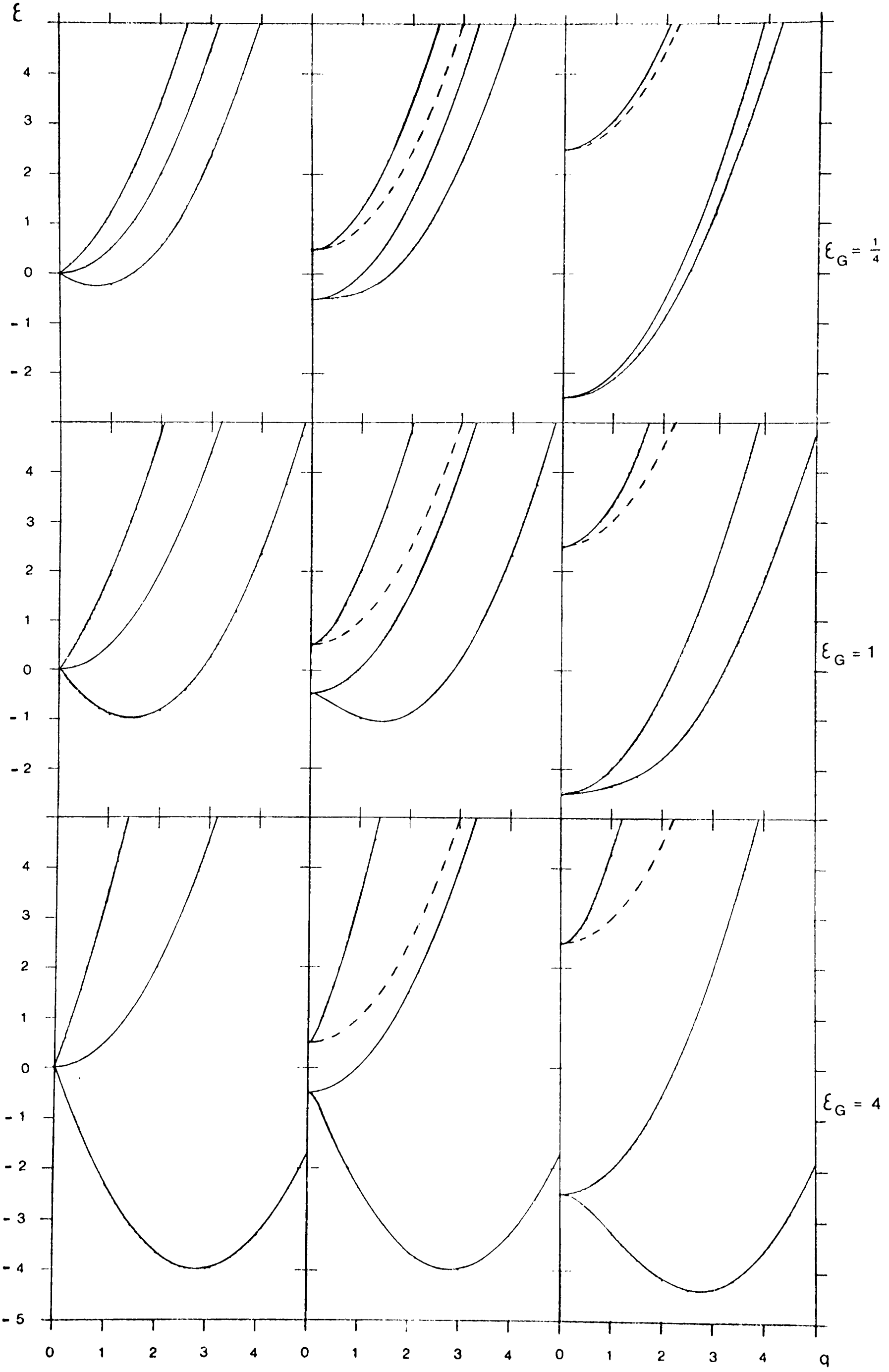
where the stablization energy $\varepsilon_G \equiv E_G/\hbar\omega$ for this PJT system is defined by

$$\varepsilon_G = \varkappa^2 \qquad (6.19)$$

The energy at the minimum is

$$\varepsilon_2^{min}(q=q_0) = -\varepsilon_G \left\{ 1 + \left(\frac{\delta}{2\varepsilon_G}\right)^2 \right\} \qquad (6.20a)$$

FIG. 5 ADIABATIC ENERGY SURFACES for $(s + p) \otimes T_{1u}$



The values of the other energy surfaces for $q = q_o$ are

$$\varepsilon_1(q = q_o) = \varepsilon_G \left\{ 3 \pm \left(\frac{\delta}{2\varepsilon_G}\right)^2 \right\} \qquad (6.20b)$$

$$\varepsilon_{3/4}(q = q_o) = \varepsilon_G \left\{ 1 - \left(\frac{\delta}{2\varepsilon_G}\right)^2 \right\} - \delta \qquad (6.20c)$$

For weaker coupling, i.e. when we have

$$2\varepsilon_G \leq |\delta| \qquad (6.21)$$

The minimum occurs in $q = 0$ and is given by

$$\varepsilon_2^{min}(q = 0) = -|\delta| \qquad (6.22)$$

No well develops in this case and the cubic configuration remains stable. Furthermore, we note

$$\left.\frac{\partial \varepsilon_i}{\partial q}\right|_{q=0} = 0 \qquad (i = 1,2,3,4) \qquad (6.23)$$

If the 2s and 2p states are accidentally degenerate, i.e. $\delta = 0$, the occurring instability involves a linear splitting of the electronic degeneracy exactly as in the JT effect, and we find

$$\left.\frac{\partial \varepsilon_i}{\partial q}\right|_{q=0} = (-1)^{i+1} \qquad (i = 1,2) \qquad (6.24a)$$

$$\left.\frac{\partial \varepsilon_j}{\partial q}\right|_{q=0} = 0 \qquad (j = 3,4) \qquad (6.24b)$$

The energy surfaces $\varepsilon_{1/2}$ in q-space have now a similar form as the 'mexican hat' in Q_2, Q_3 space of the E-E JT system (Englman 1972 p.23). Because of the linear splitting of the energy surfaces near $q = 0$ we find that a well develops now even for weak coupling; its depth is given by

$$\varepsilon_2^{min}(q = q_o) = -\varepsilon_G \qquad (6.25)$$

with

$$q_o = \sqrt{2\varepsilon_G} \qquad (6.26)$$

In the limit of strong coupling (§7b) the adiabatic energy surfacesfor $\delta \neq 0$ go over into the ones for $\delta = 0$. For $\delta = 0$ this limit is reached for smaller values of ε_G than for $\delta \neq 0$.

In this case the only necessary condition for strong coupling is $\varepsilon_G >> 1$ whereas in the case of $\delta \neq 0$ we find $\varepsilon_G >> 1$ and $2\varepsilon_G >> |\delta|$. Fig.5 shows the energy surfaces for the $(s + p) \otimes T_{1u}$ system. The 3 columns belong to $\delta = 0, \pm \frac{1}{2}, \pm \frac{5}{2}$, and the 3 rows to $\varepsilon_G = \frac{1}{4}$, 1, 4, respectively. Whereas the lowest and upper energy surfaces are independent of the sign of δ, the doubly degenerate middle ones are not. The dashed lines indicate the middle energy surfaces for $\delta < 0$.

Öpik and Pryce (1957) considered the more general static problem of s and p states, including linear JT coupling of the p states to E_g and T_{2g} modes. The stationary points that occur have cubic, tetragonal, trigonal, or rhombic symmetry. Ham (1973a) could show that the configurations of minimum energy are those given in Table 2 for the various regions defined by the relative strengths of the coupling with different modes. In particular, the rhombic stationary points are never minima. There are two types of minima having tetragonal or trigonal symmetry. In one of these the electronic state in the minimum configuration is pure p; we have $Q_x = Q_y = Q_z = 0$, and the minimum results from the JT coupling of the p states to the E_g or T_{2g} modes alone and does not involve the s state in any way. In the other type of minimum (which we call the s-p mixed type in Table 2), the electronic state is a mixture of s and p, and there is a non-zero distortion <u>both</u> in the space of the T_{1u} coordinates and in that of the Q's of <u>either</u> E_g <u>or</u> T_{2g}. In this latter case, energetically equivalent minima occur at points related by inversion symmetry in T_{1u} Q-space, thus doubling the number of minima compared to what is found for the case of pure JT coupling alone.

TABLE 2

Configuration of minimum energy for simultaneous coupling of nondegenerate s and p electronic states to modes of symmetry E_g, T_{2g} and T_{1u}. The range of the coupling energies E_G, $(E_{JT})_E$ and $(E_{JT})_T$, over which the indicated configuration is the minimum, is given below [a]. Also given are the minimum energy [b], the number of energetically equivalent minima, and the irreducible representations of O_h spanned by the distorted states.

(taken from Ham (1973 a))

Configuration:	Cubic s state, $r=0$	$(E_{JT})_E > (E_{JT})_T$ Tetragonal Jahn-Teller type	Tetragonal s-p mixed type
$E_{sp}<0$ $(E_{JT})_E < \lvert E_{sp}\rvert$	$E_G < \frac{1}{4}\lvert E_{sp}\rvert$		$E_G > \frac{1}{4}\lvert E_{sp}\rvert$
$E_{sp}<0$ $(E_{JT})_E > \lvert E_{sp}\rvert$		$E_G < \frac{1}{2}(E_{JT})_E - \frac{1}{4}\lvert E_{sp}\rvert$	$E_G > \frac{1}{2}(E_{JT})_E - \frac{1}{4}\lvert E_{sp}\rvert$
$E_{sp}>0$		$E_G < \frac{1}{2}(E_{JT})_E + \frac{1}{4}E_{sp}$	$E_G > \frac{1}{2}(E_{JT})_E + \frac{1}{4}E_{sp}$
Energy [b]	$E = E_{sp}$	$E = -(E_{JT})_E$	$E = -\left(\frac{(4E_G - E_{sp})^2 + 4(E_{JT})_E^2 - E_{sp}}{4[4E_G - (E_{JT})_E]}\right)$
No. of equivalent minima	1	3	6
Irreducible reps. spanned (O_h)	A_{1g}	T_{1u}	$A_{1g} + E_g + T_{1u}$

Configuration:	Cubic s state, $r=0$	$(E_{JT})_T > (E_{JT})_E$ Trigonal Jahn-Teller type	Trigonal s-p mixed type
$E_{sp}<0$ $(E_{JT})_T < \lvert E_{sp}\rvert$	$E_G < \frac{1}{4}\lvert E_{sp}\rvert$		$E_G > \frac{1}{4}\lvert E_{sp}\rvert$
$E_{sp}<0$ $(E_{JT})_T > \lvert E_{sp}\rvert$		$E_G < \frac{1}{2}(E_{JT})_T - \frac{1}{4}\lvert E_{sp}\rvert$	$E_G > \frac{1}{2}(E_{JT})_T - \frac{1}{4}\lvert E_{sp}\rvert$
$E_{sp}>0$		$E_G < \frac{1}{2}(E_{JT})_T + \frac{1}{4}E_{sp}$	$E_G > \frac{1}{2}(E_{JT})_T + \frac{1}{4}E_{sp}$
Energy [b]	$E = E_{sp}$	$E = -(E_{JT})_T$	$E = -\left(\frac{(4E_G - E_{sp})^2 + 4(E_{JT})_T^2 - E_{sp}}{4[4E_G - (E_{JT})_T]}\right)$
No. of equivalent minima	1	4	8
Irreducible reps. spanned (O_h)	A_{1g}	$A_{2u} + T_{1u}$	$A_{1g} + A_{2u} + T_{1u} + T_{2g}$

[a] E_{sp} is the energy of the s electronic state relative to that of the p state in the cubic configuration. The PJT energy E_G and the JT energies $(E_{JT})_E$ and $(E_{JT})_T$ are defined in the text.

[b] In this table the energy of the minimum is given relative to the zero of energy taken to coincide with the energy of the electronic p state in the cubic configuration.

The JT energies in Table 2 are related to the coupling coefficients, effective masses, and frequencies of the modes as follows (see §5)

$$\left(E_{JT}\right)_E = \frac{L^2(E_g)}{6\mu_E \omega_E^2} \quad , \quad \left(E_{JT}\right)_T = \frac{L^2(T_{2g})}{9\mu_T \omega_T^2} \tag{6.27}$$

Including the JT coupling to the E_g and T_{2g} modes has the important effect of destryoing the spherical symmetry found above, except in the exceptional case in which $(E_{JT})_E = (E_{JT})_T$.

§7 The Dynamic $(s + p) \otimes T_{1u}$ Problem

(a) Exact Solution

In the following we outline Ham's general solution of the dynamic $(s + p) \otimes T_{1u}$ problem (Ham 1973a). This solution is based on the full rotational symmetry of the model Hamiltonian (6.11), which is invariant under a continuous group of simultaneous rotations of the electronic and vibrational coordinates.

From the experience with ideal JT systems (see §4) we know that exact solutions can usually only be obtained when the electronic operators (or their matrices) of the vibronic interaction term commute as the total Hamiltonian may then be brought to diagonal form by means of a unitary transformation. In the case of non-commuting electronic operators, however, such a transformation is not possible (Messiah 1969 p.287) and, in general, exact eigenstates cannot be obtained. Occasionally, as done by Moffitt and Thorson (1957), it is possible to carry out a second-order perturbation treatment in which the system can have spherical symmetry "accidentally" and to express the second-order energy matrix by operators which - together with the unperturbed Hamiltonian- form a set of commuting observables. It is therefore very remarkable that an extended treatment along the same lines could provide exact solutions for the T_{1u} - PJT system.

We introduce a vibrational angular momentum operator $\vec{L}$, the components of which are Hermitean differential operators and are defined (Messiah 1969 p.508) by

$$\vec{L} \equiv \vec{q} \times \vec{p} \tag{7.1}$$

Expressing these components in polar coordinates (q,θ,φ), we can construct a complete and orthonormal set of eigenfunctions of

θ, φ in q-space common to $\vec{L}^2$ and L_z, the spherical harmonics $Y_L^m(\theta,\varphi)$

$$\vec{L}^2 Y_L^m = L(L+1) Y_L^m \tag{7.2}$$

$$L_z Y_L^m = m Y_L^m \tag{7.3}$$

where $L = 0, 1, 2, \ldots, \infty$ and $m = -L, -L+1, \ldots, L$. For the definition of the phase convention and other properties of Y_L^m we refer to Messiah (1969 p.494).

Similarly, we define the electronic orbital angular momentum operator $\vec{\ell}_e$ with components represented within the electronic basis $|2s\rangle$, $|x\rangle$, $|y\rangle$, $|z\rangle$ by

$$\ell_z = -i\,|x\rangle\langle y| + i\,|x\rangle\langle y| \tag{7.4}$$

etc. The electronic eigenstates $|\ell_e(\ell_e)_z\rangle$ of the $\vec{\ell}_e^{\,2}$ and $(\ell_e)_z$ are then given by $|00\rangle = |2s\rangle$ and $|1 \pm 1\rangle = \mp \frac{1}{\sqrt{2}} (|x\rangle \pm i|y\rangle)$, $|10\rangle = |z\rangle$. Now, both $\vec{L}$ and $\vec{\ell}_e$ commute with h_e and h_L of §7, but neither commutes with the vibronic interaction h_{pjT}. However, the total angular momentum operator

$$\vec{J} = \vec{L} + \vec{\ell}_e \tag{7.5}$$

<u>does</u> commute with h_{eL} and thus with the total model Hamiltonian h of (6.11).

Furthermore, we find that the total inversion operator

$$\Lambda = I \rho_o \tag{7.6}$$

also commutes with h and $\vec{J}$, where I is the inversion operator in q-space and defined by

$$I Y_L^m = (-1)^L Y_L^m \tag{7.7}$$

and ρ_o of (6.3) represents the electronic inversion operator. The vibronic eigenstates of h may therefore be classified by the eigenvalues of $\vec{J}^2$ and J_z and also of Λ which will be denoted by

$J(J+1)$, M and Λ', the so-called parity of the state.

We are able to construct eigenfunctions of $\vec{J}^2$ and J_z of the form $|JM, L, \ell_e\rangle$ as linear combinations of the products of Y_L^m with the electronic states $|\ell_e(\ell_e)_z\rangle$ above. For this a table of 3j- symbols is essential (Messiah 1969 p.1054). Then, for the 2s electronic state we simply find

$$|JM, L, s\rangle = Y_L^m |2S\rangle \tag{7.8}$$

where $J = L$, $M = m$, and the function has the parity $(-1)^L$. Similarly, the corresponding eigenfunctions $|JM, L, p\rangle$ are formed from the p states and given in (8.6) in slightly different notation. For a given L their parity is $\Lambda' = (-1)^{L+1}$ where $J = L-1, L, L+1$ (except for $L = 0$ for which $J = 1$ only).

Consequently, any eigenfunction of h which belongs to J, $J_z = M$ and has $\Lambda' = (-1)^J$ can be expressed in the general form

$$\begin{aligned}\Psi_I(JM) = {} & f_1(J,q)\,|JM, J, s\rangle + f_2(J,q)\,|JM, J-1, p\rangle \\ & + f_3(J,q)\,|JM, J+1, p\rangle\end{aligned} \tag{7.9}$$

which we call type I eigenfunction, where the index I denote the parity $(-1)^J$, for convenience. The $f_i(J,q)$ are functions of the radial coordinate q. Note that for $J = 0$ the term in f_2 is absent.

On the other hand eigenfunctions also belonging to J, $J_z = M$ but having parity $\Lambda' = (-1)^{J+1}$ are denoted by the type II wave function

$$\Psi_{II}(JM) = f_4(J,q)\cdot|JM, J, P\rangle \tag{7.10}$$

All eigenfunctions of the model Hamiltonian h belong to one or the other of these two types of vibronic states. In this way we have obtained a means of separating the vibronic wave functions into non-mixing sets.

We now derive coupled differential equations for the $f_i(J,q)$. The vibrational Hamiltonian h_L of (6.12) can be expressed in spherical polar coordinates (q, θ, φ) as

$$h = \mathcal{R}_q + \frac{\vec{L}^2}{2q^2} + \frac{q^2}{2} \tag{7.11}$$

where

$$\mathcal{R}_q \equiv -\frac{\nabla_q}{2} = -\frac{\partial^2}{2\partial q^2} - \frac{\partial}{q\cdot\partial q} \tag{7.12}$$

Furthermore, one can show that the only non-zero matrix elements of h_{pJT} among the "angular" functions $|JM,L,\ell_e\rangle$ are given by

$$\langle JM, J+1, p \mid h_{pJT} \mid JM, J, s\rangle = -\varkappa q \sqrt{\frac{J+1}{2J+1}} \tag{7.13a}$$

$$\langle JM, J-1, p \mid h_{pJT} \mid JM, J, s\rangle = \varkappa q \sqrt{\frac{J}{2J+1}} \tag{7.13b}$$

Let us now substitute the type I wave function (7.9) into the Schrödinger equation for h. The angular functions may be eliminated by using their orthonormality, together with (7.13) and (7.11), and we obtain the three coupled differential equations for the radial functions $f_i(J,q)$ (i = 1,2,3) and the vibronic energy eigenvalue ε:

$$\left[\mathcal{R}_q + \frac{J(J+1)}{2q^2} + \frac{q^2}{2} + \delta - \varepsilon\right] f_1 + \sqrt{2}\varkappa q\left(\frac{J}{2J+1}\right)^{\frac{1}{2}} f_2 - \sqrt{2}\varkappa q\left(\frac{J+1}{2J+1}\right)^{\frac{1}{2}} f_3 = 0 \tag{7.14a}$$

$$\left[\mathcal{R}_q + \frac{J(J-1)}{2q^2} + \frac{q^2}{2} - \delta - \varepsilon\right] f_2 + \sqrt{2}\varkappa q\left(\frac{J}{2J+1}\right)^{\frac{1}{2}} f_1 = 0 \tag{7.14b}$$

$$\left[\mathcal{R}_q + \frac{(J+1)(J+2)}{2q^2} + \frac{q^2}{2} - \delta - \varepsilon\right] f_3 - \sqrt{2}\varkappa q\left(\frac{J+1}{2J+1}\right)^{\frac{1}{2}} f_1 = 0 \tag{7.14c}$$

For the type II state we find in an analogous way,

$$\left[\mathcal{R}_q + \frac{J(J+1)}{2q^2} + \frac{q^2}{2} - \delta - \varepsilon\right] f_4 = 0 \tag{7.15}$$

which is identical to the radial equation for the 3d-simple harmonic oscillator, the energies of which are given in (8.12). As seen from (7.10), a type II vibronic state has parity opposite to that of a type I state belonging to the same J. Furthermore, (7.10) consists purely out of p electronic states and is thus independent of h_{pJT}. Energies of the type II states therefore coincide with

those of the vibrational levels of the p electronic state in the complete absence of s-p vibrational coupling. Note, there are no type II states having J = 0.

(b) The Strong-Coupling Limit

We proceed to seek solutions of (7.14) for the Type I states in the limit of strong coupling. The terms that couple the three differential equations (7.14) for $f_i(J,q)$ result from h_{pJT} and may be represented by the symmetric matrix

$$U = \begin{pmatrix} 0 & \sqrt{2}\,\varkappa q \left(\frac{J}{2J+1}\right)^{\frac{1}{2}} & -\sqrt{2}\,\varkappa q \left(\frac{J+1}{2J+1}\right)^{\frac{1}{2}} \\ \sqrt{2}\,\varkappa q \left(\frac{J}{2J+1}\right)^{\frac{1}{2}} & 0 & 0 \\ -\sqrt{2}\,\varkappa q \left(\frac{J+1}{2J+1}\right)^{\frac{1}{2}} & 0 & 0 \end{pmatrix} \tag{7.16}$$

For strong coupling these terms are large, and we can introduce an orthogonal transformation of the f_i that brings U to diagonal form:

$$F_1 = \frac{1}{\sqrt{2}} f_1 - \left(\frac{J}{2(2J+1)}\right)^{\frac{1}{2}} f_2 + \left(\frac{J+1}{2(2J+1)}\right)^{\frac{1}{2}} f_3 \tag{7.17a}$$

$$F_2 = \frac{1}{\sqrt{2}} f_1 + \left(\frac{J}{2(2J+1)}\right)^{\frac{1}{2}} f_2 - \left(\frac{J+1}{2(2J+1)}\right)^{\frac{1}{2}} f_3 \tag{7.17b}$$

$$F_3 = \left(\frac{J+1}{2J+1}\right)^{\frac{1}{2}} f_2 + \left(\frac{J}{2J+1}\right)^{\frac{1}{2}} f_3 \tag{7.17c}$$

for which we have

$$U F_1 = -\sqrt{2}\,\varkappa q F_1 \tag{7.18a}$$

$$U F_2 = \sqrt{2}\,\varkappa q F_2 \tag{7.18b}$$

$$U F_3 = 0 \tag{7.18c}$$

The coupled differential equations for the F_i follow from (7.17) and (7.14) and are more suitable for calculations in the strong coupling region:

$$\left[\mathcal{R}_q + \frac{1}{2q^2}(J^2+J+1) + \frac{q^2}{2} - \sqrt{2}\,\varkappa q - \varepsilon\right] F_1 + (\delta - \tfrac{1}{2q^2}) F_2 + \tfrac{1}{2q^2}\sqrt{2J(J+1)}\, F_3 = 0 \tag{7.19a}$$

$$\left[\mathcal{R}_q + \frac{1}{2q^2}(J^2+J+1) + \frac{q^2}{2} + \sqrt{2}\,\varkappa q - \varepsilon\right] F_2 + (\delta - \tfrac{1}{2q^2}) F_1 - \tfrac{1}{2q^2}\sqrt{2J(J+1)}\, F_3 = 0 \tag{7.19b}$$

$$\left[\mathcal{R}_q + \frac{1}{2q^2} J(J+1) + \frac{q^2}{2} - \delta - \varepsilon\right] F_3 + \tfrac{1}{2q^2}\sqrt{2J(J+1)}\,(F_1 - F_2) = 0 \tag{7.19c}$$

For $\varkappa > 0$, F_1 has the effective potential energy

$$V_{eff}(F_1) = \frac{q^2}{2} - \sqrt{2}\,\varkappa q \tag{7.20}$$

which has a minimum at $q_0 = \sqrt{2}\,\varkappa = \sqrt{2\varepsilon_G}$ with $V_{eff}^{min} = -\varepsilon_G$. $V_{eff}(F_1)$ is thus identical to the lowest adiabatic energy surface ε_2 of §6 for $\delta = 0$. Similarly,

$$V_{eff}(F_2) = \frac{q^2}{2} + \sqrt{2}\,\varkappa q \tag{7.21}$$

$$V_{eff}(F_3) = \frac{q^2}{2} - \delta \tag{7.22}$$

which can be identified with ε_1 ($\delta = 0$) and ε_3 (δ) of §6, respectively.

For sufficient strong coupling, there will be low-energy solutions of (7.19) having wave functions localized near the potential minimum. For $q \approx q_0 = \sqrt{2\varepsilon_G}$, the difference between the potential energies for F_1, F_2, F_3 is $\sqrt{2}\varkappa q \approx 2\varepsilon_G$, while the terms in (7.19) that couple the different equations are proportional to δ, and in zeroth order to $1/2q^2 \approx \frac{1}{4}\varepsilon_G^{-1}$. Thus if the conditions

$$2\varepsilon_G \gg |\delta| \tag{7.23a}$$

$$\varepsilon_G \gg 1 \tag{7.23b}$$

are fulfilled (we introduce in (7.23a) a factor 2 in accordance with (6.18)), we can drop these coupling terms in good approximation. The term $(J^2 + J + 1)/2q^2$ is approximately constant in the vicinity of the minimum, and the low-energy vibronic states are found by solving the remaining simple differential equation (7.19a) for F_1,

$$\left[R_q + \tfrac{1}{2}(q - q_0)^2 - \varepsilon_G + \tfrac{1}{4\varepsilon_G}(J^2 + J + 1) - \varepsilon \right] F_1(q) = 0 \tag{7.24}$$

with the relative energy of the low-energy states given by

$$\varepsilon_r(\Gamma, J) = J(J+1)/4\varepsilon_G \tag{7.25}$$

In the strong-coupling limt the lowest type I vibronic state is a non-degenerate s-like state ($J = 0, \Lambda' = 1$), while the first excited state is a p-like triplet ($J = 1$, $\Lambda' = -1$), the separation of these levels being given by

$$\varepsilon(\Gamma, 1) - \varepsilon(\Gamma, 0) \equiv \frac{E_{10}}{\hbar\omega} = (2\varepsilon_G)^{-1} \tag{7.26}$$

Since these levels lie lower than the lowest type II state with energies (8.11) by an energy of approximately ε_G, the type I s-like level is the vibronic ground state of the system and the p-like level the first excited state. The order of these levels in the strong coupling limit is therefore independent of the sign of δ, i.e. of the order of the s and p electronic states in the cubic configuration.

Because of our assumption (7.23a), the energy differences of at least the lowest type I states (s, p, d, f ...-like, with $J = 0,1,2,3,\ldots$) as given by (7.26) are $\ll 1$, and F_1 of (7.24) will be approximately the same for these different levels. Since in this

case $F_2 \approx F_3 \approx 0$, we find from (7.17)

$$f_1(J,q) = \frac{1}{\sqrt{2}} F_1 \tag{7.27a}$$

$$f_2(J,q) = -\left(\frac{J}{2(2J+1)}\right)^{\frac{1}{2}} \cdot F_1 \tag{7.27b}$$

$$f_3(J,q) = \left(\frac{J+1}{2(2J+1)}\right)^{\frac{1}{2}} \cdot F_1 \tag{7.27c}$$

where the normalization of the wave function (7.9) requires

$$\int_0^\infty q^2 F_1^2 \, dq = 1 \tag{7.28}$$

From this we find that in the limit of strong coupling the lowest type I vibronic states as given by (7.27) have equal admixtures of electronic 2s and 2p states

$$\int_0^\infty q^2 f_1^2(J,q) \, dq = \frac{1}{2} \tag{7.29a}$$

which is independent of J. Moreover, the proportions of the two p-like states $|JM, J-1, p\rangle$ and $|JM, J+1, p\rangle$ are given respectively by

$$\int_0^\infty q^2 f_2^2(J,q) \, dq = \frac{J}{2(2J+1)} \tag{7.29b}$$

$$\int_0^\infty q^2 f_3^2(J,q) \, dq = \frac{J+1}{2(2J+1)} \tag{7.29c}$$

PART II: Further Investigations of the Ideal (s+p) ⊠ T_{1u} System

§8 Group Theoretical Considerations

The first three paragraphs of part II serve to set up the eigenvalue problem for the energy in matrix form which will then be solved by numerical diagonalization. Our aim now is to construct the vibronic eigenfunctions of the model Hamiltonian with the help of group theory.

Consider the vibrational part H_L of the Hamiltonian. As shown in standard textbooks (Messiah 1969, p. 457, Flügge 1965, p. 99), H_L, $\vec{L}^2$ and L_z constitute a complete set of commuting observables, and the vectors $|n\ L\ m\rangle \equiv |(2N+L)L\ m\rangle$ form a complete orthonormal set of eigenvectors of the Hamiltonian H_L of the 3d-isotropic oscillator with the energies $(n + \frac{3}{2})\hbar\omega \equiv (2N + L + \frac{3}{2})\hbar\omega$, where $n,N = 0,1,2,\ldots$.

According to Wilson et al. (1955, p. 153) the characters of a complete level of degenerate states are in the case of the triply degenerate oscillator given by

$$\chi_n(R) = \sum_{\substack{L=0,2,\ldots \\ \text{or } 1,3,\ldots}}^{n} \chi_L(R) \qquad (8.1)$$

These degenerate states transform according to the symmetrical product D_n of their representations which can be expressed as (Heine 1964, p. 258),

$$D_n \equiv [n] = \sum_{\substack{L=0,2,\ldots \\ \text{or } 1,3,\ldots}}^{n} D_L \qquad (8.2)$$

where L=0,2,4,...,n if n is even, or L=1,3,5,...,n if n is odd. On the other hand the electronic 2s and 2p states

transform under rotation as D_{ℓ_e} ($\ell_e = 0,1$) and the orthonormal eigenvectors common to H_e, $\vec{\ell}_e^{\,2}$ and $(\ell_e)_z$ are given by $|n_e\ \ell_e\ m_e\rangle$,

$$|2\,0\,0\rangle = |2s\rangle \tag{8.3}$$

$$|2\,1\,\pm1\rangle = \mp\frac{1}{\sqrt{2}}\left(|x\rangle \pm i|y\rangle\right) \tag{8.4}$$

$$|2\,1\,0\rangle = |z\rangle$$

The eigenvalue of $h_e \equiv H_e/\hbar\omega$ corresponding to $|200\rangle$ is found from (6.13) and (6.3) to be $+\delta$, whereas the one corresponding to $|2\ 1\ M\rangle$ is $-\delta$.

As the model Hamiltonian H is invariant under a continuous group of simultaneous rotations of the electronic and vibrational coordinates, the total angular momentum operator $\vec{J}$ commutes with H, and the vibronic eigenstates of H may therefore be classified by J and $J_z = M$, as shown in § 7.

Let us construct the vibronic eigenfunctions of H which transform according to D_J. Taking the two sets of basis from above, we can by employing the vector coupling theorem (Heine 1964, p. 69) construct a product space which transforms according to the direct product $D_n \times D_{\ell_e}$, which is reducible into the components $D_{J'}$.

$$D_n \times D_{\ell_e} = \sum_L \left(D_{L+\ell_e} + D_{L+\ell_e-1} + \ldots + D_{|L-\ell_e|} \right) = \sum_{J'} D_{J'} \tag{8.5}$$

From the range of L values given by a certain vibrational quantum number n according to (8.2), we can pick out those values of L whose direct product with ℓ_e leads to a reduction containing D_J. With the vector coupling theorem we find that L can only take the values L = J+1, J, J-1 for $\ell_e = 1$ (and $J \geq 1$; L=1 for J=0) and L=J for $\ell_e = 0$.

The orthonormalized vibronic functions belonging to the component M of the D_J representation can be formed as in § 7 with the help of the Wigner coefficients or the 3j-symbols (Messiah 1969, p. 1054) and are denoted by $|\,JM,(L+2N)L,n_e\ell_e\,\rangle$. They correspond to the symmetry adapted vibronic eigenfunctions used by Englman et al. (1970). In detail,

$$|\,\mathcal{J}M,(\mathcal{J}+2N)\mathcal{J},2s\,\rangle = |(\mathcal{J}+2N)\mathcal{J}\,M\rangle|200\rangle \quad \text{for } \mathcal{J}\geq 0 \tag{8.6a}$$

$$\begin{aligned}|\,\mathcal{J}M,(\mathcal{J}+1+2N)(\mathcal{J}+1),2p\,\rangle &= \\ &= \left(\frac{(\mathcal{J}+1-M)(\mathcal{J}+2-M)}{2(\mathcal{J}+1)(2\mathcal{J}+3)}\right)^{\frac{1}{2}}\cdot|(\mathcal{J}+1+2N)(\mathcal{J}+1)(M-1)\rangle|211\rangle \\ &\quad -\left(\frac{(\mathcal{J}+M+1)(\mathcal{J}-M+1)}{(\mathcal{J}+1)(2\mathcal{J}+3)}\right)^{\frac{1}{2}}\cdot|(\mathcal{J}+1+2N)(\mathcal{J}+1)\;M\;\rangle|210\rangle \\ &\quad +\left(\frac{(\mathcal{J}+M+2)(\mathcal{J}+M+1)}{2(\mathcal{J}+1)(2\mathcal{J}+3)}\right)^{\frac{1}{2}}\cdot|(\mathcal{J}+1+2N)(\mathcal{J}+1)(M+1)\rangle|21\text{-}1\rangle \quad \text{for } \mathcal{J}\geq 0\end{aligned} \tag{8.6b}$$

$$\begin{aligned}|\,\mathcal{J}M,(\mathcal{J}-1+2N)(\mathcal{J}-1),2p\,\rangle &= \\ &= \left(\frac{(\mathcal{J}+M)(\mathcal{J}+M-1)}{2\mathcal{J}(2\mathcal{J}-1)}\right)^{\frac{1}{2}}\cdot|(\mathcal{J}-1+2N)(\mathcal{J}-1)(M-1)\rangle|211\rangle \\ &\quad +\left(\frac{(\mathcal{J}+M)(\mathcal{J}-M)}{\mathcal{J}(2\mathcal{J}-1)}\right)^{\frac{1}{2}}\cdot|(\mathcal{J}-1+2N)(\mathcal{J}-1)\;M\;\rangle|210\rangle \\ &\quad +\left(\frac{(\mathcal{J}-M-1)(\mathcal{J}-M)}{2\mathcal{J}(2\mathcal{J}-1)}\right)^{\frac{1}{2}}\cdot|(\mathcal{J}-1+2N)(\mathcal{J}-1)(M+1)\rangle|21\text{-}1\rangle \quad \text{for } \mathcal{J}\geq 1\end{aligned} \tag{8.6c}$$

$$\begin{aligned}|\,\mathcal{J}M,(\mathcal{J}+2N)\mathcal{J},2p\,\rangle &= \\ &= -\left(\frac{(\mathcal{J}-M+1)(\mathcal{J}+M)}{2\mathcal{J}(\mathcal{J}+1)}\right)^{\frac{1}{2}}\cdot|(\mathcal{J}+2N)\mathcal{J}(M-1)\rangle|211\rangle \\ &\quad +\left(\frac{M^2}{\mathcal{J}(\mathcal{J}+1)}\right)^{\frac{1}{2}}\cdot|(\mathcal{J}+2N)\mathcal{J}\;M\;\rangle|210\rangle \\ &\quad +\left(\frac{(\mathcal{J}-M)(\mathcal{J}+M+1)}{2\mathcal{J}(\mathcal{J}+1)}\right)^{\frac{1}{2}}\cdot|(\mathcal{J}+2N)\mathcal{J}(M+1)\rangle|21\text{-}1\rangle \quad \text{for } \mathcal{J}\geq 1\end{aligned} \tag{8.6d}$$

The unperturbed energy eigenvalues of $(h_L + h_e)$ corresponding to these basis states are given by

$$\varepsilon_1 = \mathcal{J} + 2N + \frac{3}{2} + \delta \qquad \text{for } \mathcal{J}\geq 0 \tag{8.7a}$$

$$\varepsilon_2 = \mathcal{J} + 2N + \frac{5}{2} - \delta \qquad \text{for } \mathcal{J}\geq 0 \tag{8.7b}$$

$$\varepsilon_3 = J + 2N + \frac{1}{2} - \delta, \qquad \text{for } J \geq 1 \tag{8.7c}$$

$$\varepsilon_4 = J + 2N + \frac{3}{2} - \delta \qquad \text{for } J \geq 1 \tag{8.7d}$$

where the degeneracy of the first two ones is (n+1)(n+2)/2, and of the two latter ones n(n+1)/2 with n = J+2N.

Carrying out the construction of the vibronic states (8.6) for the first few specific values of $n \equiv 2N + L$, we obtain the n-D_J - table (Table 3) where sD_J stands for the direct product $D_{\ell_e=0} \times D_{L=J} = D_J$, i.e. for the state (8.6a); similarly, $pD_{J+1} \equiv D_{\ell_e=1} \times D_{L=J+1}$, $pD_{J-1} \equiv D_{\ell_e=1} \times D_{L=J-1}$, $pD_J \equiv D_{\ell_e=1} \times D_{L=J}$, which each contain D_J in its reduction and represent the states (8.6b, c, and d), respectively.

The n-D_J-table gives us the vibronic eigenfunctions of the Hamiltonian H which belong to a specific value of J as the linear combinations of the states (8.6). The simplicity of the problem is that for a given value of n there are never more than two states of (8.6) involved, and it is therefore easy to state a general expansion law.

As we have seen in § 7, the total Hamiltonian commutes with the parity operator, and thus each vibronic eigenstate has definite parity which is determined by its total angular momentum J. This we expect since H_{PJT} has even parity in the combined electronic and vibrational space and can therefore mix only those states of (8.6) to form the vibronic eigenstates transforming as D_J which have the same parity. This then leads us to distinguish between two types of eigenfunctions, corresponding to the ones of § 7. The states (8.6a, b, and c)

TABLE 3 $n - D_J$ - table

n \ D_J	D_0	D_1	D_2	D_3	D_4	D_5	D_6	D_7 . . .
0	sD_0	pD_0						
1	pD_1	sD_1 (pD_1)	pD_1					
2	sD_0	pD_0 pD_2	sD_2 (pD_2)	pD_2				
3	pD_1	sD_1 (pD_1)	pD_1 pD_3	sD_3 (pD_3)	pD_3			
4	sD_0	pD_0 pD_2	sD_2 (pD_2)	pD_2 pD_4	sD_4 (pD_4)	pD_4		
5	pD_1	sD_1 (pD_1)	pD_1 pD_3	sD_3 (pD_3)	pD_3 pD_5	sD_5 (pD_5)	pD_5	
6	sD_0	pD_0 pD_2	sD_2 (pD_2)	pD_2 pD_4	sD_4 (pD_4)	pD_4 pD_6	sD_6 (pD_6)	pD_6
.	.	.	.	.	.	.	.	.
.	.	.	.	.	.	.	.	.
.	.	.	.	.	.	.	.	.

have parity $(-1)^J$ and form the type I vibronic eigenstates of H belonging to J, J_z = M:

$$\Psi^{JM}_{I,j} = \sum_{N=0}^{\infty} \{ b(J,j,J+2N-1)|JM,(J+2N-1)(J-1),2P\rangle + a(J,j,J+2N)\cdot|JM,(J+2N)J,2S\rangle + a(J,j,J+2N+1)|JM,(J+2N+1)(J+1),2P\rangle \} \quad (8.8)$$

where the principle quantum number j = 0,1,2,... classifies states with the same J,M. The (2J+1)-fold degenerate energy eigenstates of h which correspond to (8.8) are denoted by $\varepsilon_j(I,jJ)$. Note, for J=0 the n-D_J-table yields the requirement

$$b(0,j,2N-1) \equiv 0 \quad (8.9)$$

The normalization of $\Psi^{JM}_{I,j}$ reads now,

$$\sum_{N=0}^{\infty} \{ |b(J,j,J+2N-1)|^2 + |a(J,j,J+2N)|^2 + |a(J,j,J+2N+1)|^2 \} = 1 \quad (8.10)$$

Whereas the summation over the second term represents the total admixture of all the s-J-states (8.6a), the summations over the first and third term gives us the total admixtures of the p-(J-1)-states (8.6c) and p-(J+1)-states (8.6b), respectively. In the strong coupling limit these admixtures correspond to the ones of (7.29).

On the other hand we find that the vibronic eigenstates with parity $(-1)^{J+1}$ consist purely out of states (8.6d) and are therefore completely independent of H_{PJT}. Thus, the type II vibronic eigenfunctions of H belonging to J, J_z = M can simply be expressed as

$$\Psi^{JM}_{II,N} = |JM,(J+2N)J,^2\rho\rangle \qquad (8.11)$$

with the corresponding (2J+1)-degenerate energy eigenvalues of h given by (8.7d) to

$$\varepsilon_\delta(II,NJ) = J + 2N + \frac{3}{2} - \delta \qquad (J \geq 1) \qquad (8.12)$$

The states J=0 are excluded by the n-D_J-diagram.

§ 9 Matrix Elements of the Pseudo-Jahn-Teller Interaction.

The matrix elements of h_{PJT} are now calculated by applying the irreducible tensor method and the Wigner-Eckart theorem to the rotation group in three dimensions, R_3. For this purpose it is convenient to introduce the irreducible tensor creation and destruction operators $a^{+(l)}$, $\tilde{a}^{(l)}$ and to calculate their reduced matrix elements.

(a) Introduction of Irreducible Tensors.

By definition, the $(2k + 1)$ operators $T_q^{(k)}$ $(q = -k,\ldots,+k)$ are the standard components of an irreducible tensor operator of order k, $T^{(k)}$, if they satisfy the following commutation relation with $\vec{J}$,

$$\left[J_\pm , T_q^{(k)}\right] = \left[k(k+1) - q(q \pm 1)\right]^{\frac{1}{2}} \cdot T_{q\pm1}^{(k)} \qquad (9.1a)$$

$$\left[J_z , T_q^{(k)}\right] = q\, T_q^{(k)} \qquad (9.1b)$$

In this case the Wigner-Eckart Theorem specializes from (5.1) to

$$\langle \tau J M | T_q^{(k)} | \tau' J' M' \rangle = (-1)^{J-M} \cdot \langle \tau J \| T^{(k)} \| \tau' J' \rangle \cdot \begin{pmatrix} J & k & J' \\ -M & q & M' \end{pmatrix} \qquad (9.2)$$

where the 3j-symbols $\begin{pmatrix} J & k & J' \\ -M & q & M' \end{pmatrix}$ are defined and tabulated in Messiah (1969, p. 1054). The requirements (selection rules) for the non-vanishing of the 3j-symbols are (i) $q + M' = M$ and (ii) $|J' - k| \leq J \leq (J' + k)$.

Consider the vibrational Hamiltonian h_L of § 6. Let us introduce the creation and destruction operators of quanta of the type j(=x,y,z) which are denoted by a_j^+ and a_j

and connected with Q_j, P_j by (Messiah 1969, p. 453),

$$Q_j = \left(\frac{\hbar}{2\mu\omega}\right)^{\frac{1}{2}} \cdot (a_j^+ + a_j) \qquad (9.3)$$

$$(j = x,y,z)$$

$$P_j = i\left(\frac{\mu\hbar\omega}{2}\right)^{\frac{1}{2}} \cdot (a_j^+ - a_j) \qquad (9.4)$$

a_j, a_j^+ are Hermitean conjugates of each other and satisfy the commutation relations

$$[a_j , a_{j'}^+] = \delta_{jj'} \qquad (9.5a)$$

$$(j,j' = x,y,z)$$

$$[a_j , a_{j'}] = [a_j^+ , a_{j'}^+] = 0 \qquad (9.5b)$$

Putting (9.3) and (9.4) into h_L, we obtain

$$h_L = \hat{N} + \frac{3}{2} \qquad (9.6)$$

where $\hat{N}$ is called the total number operator and given by the sum of number operators of quanta of type j:

$$\hat{N} = \sum_{j=x,y,z} a_j^+ a_j \qquad (9.7)$$

Let us now introduce the irreducible tensor $a^{+(1)}$ of rank 1 whose standard components $a_q^{+(1)}$ $(q = 1,0,-1)$ satisfy the relations (9.1) and read

$$a_{+1}^{+(1)} = -\frac{1}{\sqrt{2}} (a_x^+ + i a_y^+) \qquad (9.8a)$$

$$a_0^{+(1)} = a_z^+ \qquad (9.8b)$$

$$a_{-1}^{+(1)} = \frac{1}{\sqrt{2}} (a_x^+ - i a_y^+) \qquad (9.8c)$$

The Hermitean conjugate components of $a_q^{+(1)}$ are

$$a_{+1} = -\frac{1}{\sqrt{2}} (a_x - i a_y) \qquad (9.9a)$$

$$a_0 = a_z \qquad (9.9b)$$

$$a_{-1} = \frac{1}{\sqrt{2}} (a_x + i a_y) \qquad (9.9c)$$

The a_q ($q = 1,0,-1$) do not form the components of an irreducible tensor but together with a_q^+ of (9.8) they do satisfy the necessary commutation relations (9.5) (where we replace $j,j'=x,y,z$ by $q,q' = 1,0,-1$) which define a_q^+, a_q as creation and destruction operators of quanta of type q. Following this interpretation, the operators $\hat{N}_q \equiv a_q^+ a_q$ represent the number of q quanta. The total number operator is now given by

$$\hat{N} = \sum_{q=1,0,-1} a_q^+ a_q = \sum_{j=x,y,z} a_j^+ a_j \qquad (9.10)$$

We define now the Hermitean conjugate tensor $a^{+(1)}$ by

$$\tilde{a}^{(1)} = (a^{+(1)})^+ \qquad (9.11a)$$

where $$\tilde{a}_q^{(1)} = (-1)^{q+1} \cdot (a^{+(1)}_{-q})^+ = (-1)^{q+1} a_{-q} \qquad (q = 1,0,-1) \qquad (9.11b)$$

The phase factor $(-1)^{q+1}$ coincides with the one in Judd (1967, p. 32) and enables $\tilde{a}_q^{(1)}$ to satisfy (9.1), thus being the standard components of the irreducible tensor $\tilde{a}^{(1)}$ of order 1.

Substituting (9.11b) into (9.10), the number operator $\hat{N}$ can be expressed as the scalar product of the two tensors $a^{+(1)}$ and $\tilde{a}^{(1)}$ (Messiah 1969, p. 1076),

$$\hat{N} = -(a^{+(1)} \cdot \tilde{a}^{(1)}) = -\sum_{q=1,0,-1} (-1)^q \cdot a_q^{+(1)} \cdot \tilde{a}_{-q}^{(1)} \qquad (9.12)$$

Furthermore, this scalar product can be related to the tensor product of order 0 by using the definition of (9.18). $\hat{N}$ then reads

$$\hat{N} = \sqrt{3}\,(a^+ a)_0^{(0)} \qquad (9.13)$$

Our next step is to express the vibronic interaction

term H_{PJT} by some convenient irreducible tensors. The electronic operators (6.5) form an irreducible tensor $\rho^{(1)}$ of rank 1 with the following components

$$\rho^{(1)}_{+1} = -\frac{1}{\sqrt{2}} (\rho_x + i \rho_y) \qquad (9.14a)$$

$$\rho^{(1)}_{0} = \rho_z \qquad (9.14b)$$

$$\rho^{(1)}_{-1} = \frac{1}{\sqrt{2}} (\rho_x - i \rho_y) \qquad (9.14c)$$

Similarly, with the help of Q_x, Q_y, Q_z we can construct an irreducible tensor $Q^{(1)}$ of order 1 the components of which have the same phase factors in standard representation as the other irreducible tensor above. H_{PJT} is then expressible as the scalar product of $Q^{(1)}$ and $\rho^{(1)}$:

$$H_{PJT}(T_{1u}) = G \cdot (Q^{(1)} \cdot \rho^{(1)}) = G \sum_{q=1,0,-1} (-1)^q \, Q^{(1)}_q \cdot \rho^{(1)}_{-q} \qquad (9.15)$$

Introducing $a^{+(1)}$, $a^{(1)}$ in $Q^{(1)}$, we find

$$Q^{(1)}_q = \left(\frac{\hbar}{2\mu\omega}\right)^{\frac{1}{2}} \cdot (\alpha^{+(1)}_q - \tilde{\alpha}^{(1)}_q) \qquad (q = 1, 0, -1) \qquad (9.16)$$

We put (9.16) in (9.15) and use (6.10),

$$h_{PJT} = \varkappa \{ (\alpha^{+(1)} \cdot \rho^{(1)}) - (\tilde{\alpha}^{(1)} \cdot \rho^{(1)}) \} \qquad (9.17)$$

We see, h_{PJT} consists out of the two scalar products of the tensors $a^{+(1)}$, $\tilde{a}^{(1)}$ and $\rho^{(1)}$.

(b) Reduced Matrix Elements

In the following we shall make extensive use of tensor products and their reduced matrix elements. Taking the irreducible tensors $a^{+(1)}, \tilde{a}^{(1)}$ from above, we can define a tensor product of order K by (Judd 1963, p. 69, Messiah 1969,

p. 1076),

$$(a^{+}a)^{(K)}_{Q} \equiv [\, a^{+(1)} \boxtimes \tilde{a}^{(1)} \,]^{(K)}_{Q}$$

$$= \sum_{q,q'=1,0,-1} \langle 1\,1\,q\,q' \mid K\,Q \rangle \cdot a^{+(1)}_{q} \cdot \tilde{a}^{(1)}_{q'} \qquad (9.18)$$

where $0 \leq K \leq 2$ and $q+q' = Q$. The $Q = K, K-1, \ldots, -K$ components of the irreducible tensor $(a^{+}a)^{(K)}$ transform according to the I.R. $D^{(K)}$ of R_3 and thus satisfy the commutation relations (9.1) with $\vec{J}$.

Similarly, $a^{+(1)}$ and $\tilde{a}^{(1)}$ can be coupled together to form another tensor product of order K, i.e. the irreducible tensor

$$(a\,a^{+})^{(K)}_{Q} \equiv [\, \tilde{a}^{(1)} \boxtimes a^{+(1)} \,]^{(K)}_{Q}$$

$$= \sum_{q,q'=1,0,-1} \langle 1\,1\,q'\,q \mid K\,Q \rangle \cdot \tilde{a}^{(1)}_{q'}\, a^{+(1)}_{q} \qquad (9.19)$$

where $0 \leq K \leq 2$ and $q+q' = Q$ $(=K, K-1, \ldots, -K)$. In the subsequent treatment the relation

$$(a\,a^{+})^{(K)}_{Q} - (-1)^{K} \cdot (a^{+}a)^{(K)}_{Q} = \delta(K,0) \cdot \sqrt{3} \qquad (9.20)$$

where $0 \leq K \leq 2$, will be quite useful. (9.20) can be proved easily by substituting (9.11) into (9.18) and (9.19) and then employing the commutation relations (9.5) for a^{+}_{q} and $a_{q'}$. To carry out the remaining sum over q, it is convenient to relate the Wigner coefficients in (9.18 and 9.19) to the 3j-symbols which are tabulated for K=0,1,2 in Messiah 1969, p. 1059).

Remark: (9.20) has been generalized by Judd (1967, p.33) to the case of Fermions. When we deal with Bosons, the irreducible tensor operators a^{+}_{nLm} and $\tilde{a}_{nLm}$, of rank L are

coupled together to form $(a^+a)^{(K)}$ and $(aa^+)^{(K)}$, and (9.20) takes the form

$$(a a^+)^{(K)}_Q - (-1)^K (a^+ a)^{(K)}_Q = \delta(K,0)\cdot\sqrt{2L+1} \qquad (9.20a)$$

We consider now the selection rules of $a^{+(1)}_q$ and $\tilde{a}^{(1)}_q$ within the basis states $|n\ L\ m>$ of the 3d-isotropic oscillator discussed in § 8. Matrix elements of the form

$$M_1 = \langle n L m | a^{+(1)}_q | n' L' m' \rangle \qquad (9.21)$$

are non-zero only if the I.R. $D^{(L)}$ is contained in the reduction of the direct product

$$D^{(1)} \times D^{(L')} = D^{(L'+1)} + D^{(L')} + D^{(L'-1)} \qquad (9.22)$$

From the 3-d oscillator we know that if n is even, then L is also an even number (see (8.2), Messiah 1969, p. 456). As seen above, $a^{+(1)}_q$ is a creation operator, and it follows

$$n' = n - 1 \qquad (9.23)$$

thus n' is odd and so is L'.

Similarly, if n and L are odd, n' and L' are even. With (9.22) we find for $M_1 \neq 0$:

$$n = n' + 1 \qquad (9.24a)$$

$$L = L' \pm 1 \qquad (9.24b)$$

In an analog fashion we find the selection rules for

$$M_2 = \langle n L m | \tilde{a}^{(1)}_q | n' L' m' \rangle \qquad (9.25)$$

$M_2 \neq 0$ only if

$$n = n' - 1 \qquad (9.26a)$$

$$L = L' \pm 1 \qquad (9.26b)$$

Thus, L=L' is excluded from (9.24) as well as (9.26).

In our next step we shall carry out the actual calculation of the reduced matrix elements of $a^{+(1)}$ and $\tilde{a}^{(1)}$. Consider the mixed tensors $(a^+a)^{(K)}$ and $(aa^+)^{(K)}$, the components of which act on the same part of the system. Then, the reduced matrix elements of these irreducible tensors are given by using Judd (1963, eqn. 3-39) to

$$\langle n L \| (a^+a)^{(K)} \| n'L' \rangle = [K]^{\frac{1}{2}} \cdot (-1)^{L+L'+K} \cdot \sum_{n''L''} \begin{Bmatrix} 1 & K & 1 \\ L & L'' & L' \end{Bmatrix} \cdot \langle n L \| a^{+(1)} \| n''L'' \rangle \langle n''L'' \| \tilde{a}^{(1)} \| n'L' \rangle \tag{9.27}$$

$$\langle n L \| (aa^+)^{(K)} \| n'L' \rangle = [K]^{\frac{1}{2}} \cdot (-1)^{L+L'+K} \cdot \sum_{n''L''} \begin{Bmatrix} 1 & K & 1 \\ L & L'' & L' \end{Bmatrix} \cdot \langle n L \| \tilde{a}^{(1)} \| n''L'' \rangle \langle n''L'' \| a^{+(1)} \| n'L' \rangle \tag{9.28}$$

where $[K] \equiv 2K+1$ and $\begin{Bmatrix} 1 & K & 1 \\ L & L''L' \end{Bmatrix}$ is the 6j-symbol defined by Judd (1963, p. 57).

Now we put K=0, and obtain for the 6j-symbol

$$\begin{Bmatrix} 1 & 0 & 1 \\ L & L'' & L' \end{Bmatrix} = (-1)^{L+L''+1} \cdot (6L+3)^{-\frac{1}{2}} \cdot \delta_{LL'} \tag{9.29}$$

where $|L-1| \leq L'' \leq (L+1)$. With the selection rules (9.24) and (9.26), we find from (9.27) and (9.28) - considering (9.29),

$$R_1 \equiv \langle n L \| (a^+a)^{(0)} \| n L \rangle = \frac{[L]^{-\frac{1}{2}}}{\sqrt{3}} \cdot \{ \langle n L \| a^+ \| n-1 \; L+1 \rangle \langle n-1 \; L+1 \| \tilde{a} \| n L \rangle + \langle n L \| a^+ \| n-1 \; L-1 \rangle \langle n-1 \; L-1 \| \tilde{a} \| n L \rangle \} \tag{9.30}$$

$$R_2 \equiv \langle n L \| (aa^+)^{(0)} \| n L \rangle$$

$$= \frac{[L]^{-\frac{1}{2}}}{\sqrt{3}} \cdot \{ \langle n L \| \tilde{a} \| n+1 \;\; L-1 \rangle \langle n+1 \;\; L-1 \| a^+ \| n L \rangle$$

$$+ \quad \langle n L \| \tilde{a} \| n+1 \;\; L+1 \rangle \langle n+1 \;\; L+1 \| a^+ \| n L \rangle \; \} \qquad (9.31)$$

where we omitted the indice (1) from $a^{+(1)}$ and $\tilde{a}^{(1)}$ out of convenience. Use of the conjugation relation

$$\langle n'' L'' \| \tilde{a}^{(1)} \| n' L' \rangle = (-1)^{L''+L'+1} \cdot \langle n' L' \| a^{+(1)} \| n'' L'' \rangle^* \qquad (9.32)$$

yields

$$R_1 = \frac{[L]^{-\frac{1}{2}}}{\sqrt{3}} \cdot \{ |\langle n L \| a^+ \| n-1 \;\; L+1 \rangle|^2 + |\langle n L \| a^+ \| n-1 \;\; L-1 \rangle|^2 \} \qquad (9.33)$$

$$R_2 = \frac{[L]^{-\frac{1}{2}}}{\sqrt{3}} \cdot \{ |\langle n+1 \;\; L-1 \| a^+ \| n L \rangle|^2 + |\langle n+1 \;\; L+1 \| a^+ \| n L \rangle|^2 \} \qquad (9.34)$$

Thus, with the last two equations we have a relationship between the reduced matrix elements of $(a^+a)^{(0)}$, $(aa^+)^{(0)}$ and $a^{+(1)}$.

On the other hand we can obtain explicit expressions for the reduced matrix elements of $(a^+a)^{(0)}$ and $(aa^+)^{(0)}$ by applying the Wigner-Eckart Theorem (9.2) and making use of their eigenvalues. As we have seen in (9.13), $(a^+a)^{(0)}$ is related to the number operator $\hat{N}$ with eigenvalue n. From this

$$\langle n L m | (a^+a)^{(0)}_0 | n L m \rangle = \frac{n}{\sqrt{3}} \qquad (9.35)$$

With (9.2) we find

$$\langle n L m | (a^+a)^{(0)}_0 | n L m \rangle = [L]^{-\frac{1}{2}} \cdot \langle n L \| (a^+a)^{(0)} \| n L \rangle \qquad (9.36)$$

This yields,

$$R_1 = n \cdot \frac{[L]^{\frac{1}{2}}}{\sqrt{3}} \qquad (9.37)$$

In an analog way we can proceed for $(aa^+)^{(0)}$. With (9.20) and (9.13), the eigenvalues of $(aa^+)_0^{(0)}$ are given to $(\sqrt{3} + \frac{n}{\sqrt{3}})$. Thus,

$$\langle n\,L\,m|\,(a\,a^+)_0^{(0)}\,|n\,L\,m\rangle \;=\; \sqrt{3} \;+\; \frac{n}{\sqrt{3}} \qquad (9.38)$$

And with the Wigner-Eckart Theorem, we get

$$\langle n\,L\,m|\,(a\,a^+)_0^{(0)}\,|n\,L\,m\rangle \;=\; [L]^{-\frac{1}{2}}\cdot\langle n\,L\,\|\,(a\,a^+)^{(0)}\,\|\,n\,L\rangle \qquad (9.39)$$

(9.38) = (9.39) yields

$$R_2 \;=\; (\sqrt{3} \;+\; \frac{n}{\sqrt{3}}\;)\cdot[\,L\,]^{\frac{1}{2}} \qquad (9.40)$$

The explicit expressions (9.37) and (9.40) for R_1 and R_2 are now substituted into (9.33) and (9.34). In order to relate to each other the reduced matrix elements of $a^{+(1)}$ which occur in (9.33) and (9.34), a change of variable in (9.33) is necessary. We put

$$n' \;= n-1\;, \qquad L' \;= L+1 \qquad (9.41)$$

and after a change of notation we find from (9.33) = (9.37),

$$|\langle n+1\;\;L-1\,\|\;a^+\,\|\;n\,L\rangle|^2 \;= (n+1)(2L-1) - |\langle n+1\;L-1\|\;a^+\|\,n\;L-2\rangle|^2 \qquad (9.42)$$

From (9.34) = (9.40),

$$|\langle n+1\;\;L-1\,\|\;a^+\,\|\;n\,L\rangle|^2 \;= (n+3)(2L+1) - |\langle n+1\;L+1\|\;a^+\|\,n\;L\rangle|^2 \qquad (9.43)$$

With (9.42) and (9.43) we obtain the recurrence formula for the reduced matrix elements of $a^{+(1)}$:

$$|\langle n+1\;\;L+1\,\|\;a^+\,\|\;n\,L\rangle|^2 \;-\; |\langle n+1\;\;L-1\,\|\;a^+\,\|\;n\;L-2\rangle|^2 \;=\; 2\,(n+2L+2) \qquad (9.44)$$

The reduced matrix elements in (9.44) can be regarded as functions of L and L-2, respectively, and we may write

$$f(L) - f(L-s) = 2(n + 2L + 2) \qquad (9.44a)$$

We define f(L-s) in such a way that for negative arguments (L-s) < 0 (s > 0 and integer) we have f(L-s) ≡ 0. This gives us the boundary condition for (9.44a):

$$f(0) = 2(n+2) \qquad (9.45a)$$

$$f(1) = 2(n+4) \qquad (9.45b)$$

(9.44a) and (9.45) yield

$$f(L-2i) - f(L-2i-2) = 2(n+2L+2-4i) \qquad (9.46)$$

where i=0,1,2,..., $\frac{L}{2}$ or $\frac{L-1}{2}$ depending if L even or odd. If L is even, the last term of the expansion will be f(0), if L is odd, we end up with f(1). Because of this we have to distinguish between even and odd values of L. Substituting (9.46) into (9.44a), we are now able to derive explicit expressions for f(2L) and f(2L+1).

Similarly, we can define another function of L:

$$g(L) = |\langle n+1\ L \| a^+ \| n\ L+1\rangle|^2 \qquad \text{for } L \geq 0 \text{ and integer} \qquad (9.47a)$$

$$g(L) \equiv 0 \quad \text{for } L < 0 \qquad (9.47b)$$

Using (9.43) and f(2L) or f(2L+1), we find analog expressions for g(2L-1) and g(2L). However, when we put our obtained expressions into (9.42) and (9.43), we find that only those corresponding to odd values of L are solutions of (9.42) and (9.43). Furthermore, we see that these solutions are valid for any value of L, and therefore we can forget again about the separation into even and odd L made above.

Thus, with the conjugation relation (9.32) the reduced

matrix elements of $a^{+(1)}$ and $\tilde{a}^{(1)}$ are given by

$$\langle n+1\ L+1 \| a^{+(1)} \| n\ L \rangle = \langle n\,L \| \tilde{a}^{(1)} \| n+1\ L+1 \rangle = \pm (L+1)^{\frac{1}{2}} \cdot (n+L+3)^{\frac{1}{2}} \tag{9.48a}$$

$$\langle n+1\ L-1 \| a^{+(1)} \| n\ L \rangle = \langle n\,L \| \tilde{a}^{(1)} \| n+1\ L-1 \rangle = \pm L^{\frac{1}{2}} \cdot (n+2-L)^{\frac{1}{2}} \tag{9.48b}$$

or

$$\langle n\,L \| a^{+(1)} \| n-1\ L-1 \rangle = \langle n-1\ L-1 \| \tilde{a}^{(1)} \| n\,L \rangle = \pm L^{\frac{1}{2}} \cdot (n+L+1)^{\frac{1}{2}} \tag{9.49a}$$

$$\langle n\,L \| a^{+(1)} \| n-1\ L+1 \rangle = \langle n-1\ L+1 \| \tilde{a}^{(1)} \| n\,L \rangle = \pm (L+1)^{\frac{1}{2}} \cdot (n-L)^{\frac{1}{2}} \tag{9.49b}$$

We note that (9.48) and (9.49) satisfy the relation (9.20) also for K=1 and K=2 which can be shown - analog to above - by applying the Wigner-Eckart Theorem to $(a^{+}a)^{(K)}$ and $(aa^{+})^{(K)}$ and making use of their reduced matrix elements (9.27) and (9.28). (9.20) gives us the reduced matrix elements of $a^{+(1)}$ and $\tilde{a}^{(1)}$ only up to a relative sign which is all what is required for the matrix diagonalization in § 10. In the following we shall, however, employ the positive sign which is in agreement with O'Brien's results who also derived these reduced matrix elements by making use of an approach involving the coefficients of fractional parentage (O'Brien 1972b).

We proceed to calculate the reduced matrix elements of the irreducible tensor $\rho^{(1)}$, the components of which are given in standard representation in (9.14). Its matrix elements within the electronic states (8.3) and (8.4) have the form $\langle 2\ell_e m_e | \rho_q^{(1)} | 2\ell'_e m'_e \rangle$ and can be

calculated explicitely:

$$\langle 211 \mid \rho^{(1)}_{+1} \mid 200 \rangle = -\langle 200 \mid \rho^{(1)}_{+1} \mid 21\text{-}1 \rangle =$$
$$= \langle 21\text{-}1 \mid \rho^{(1)}_{-1} \mid 200 \rangle = -\langle 200 \mid \rho^{(1)}_{-1} \mid 211 \rangle =$$
$$= \langle 210 \mid \rho^{(1)}_{0} \mid 200 \rangle = \langle 200 \mid \rho^{(1)}_{0} \mid 210 \rangle = 1$$

The application of the Wigner-Eckart Theorem yields then the non-vanishing reduced matrix elements of $\rho^{(1)}$:

$$\langle 21 \| \rho^{(1)} \| 20 \rangle = -\langle 20 \| \rho^{(1)} \| 21 \rangle = \sqrt{3} \qquad (9.50)$$

(c) Matrix Elements of H_{PJT}

The non-vanishing matrix elements of h_{pJT} within the space of the vibronic basis states $|JM,nL,2\ell_e\rangle$ of § 8 can now be calculated using the results above. We denote

$$\langle JM,nL,2\ell_e \mid h_{PJT} \mid J'M',n'L',2\ell_e' \rangle =$$
$$= \varkappa \cdot (A - B) \qquad (9.51)$$

where

$$A = \langle \mathcal{J}M, nL, 2\ell_e \mid (a^{+(1)} \cdot \rho^{(1)}) \mid \mathcal{J}'M', n'L', 2\ell_e' \rangle$$
$$B = \langle \mathcal{J}M, nL, 2\ell_e \mid (\tilde{a}^{(1)} \cdot \rho^{(1)}) \mid \mathcal{J}'M', n'L', 2\ell_e' \rangle$$

In contrast to (9.18 and 9.19) the scalar products above consist out of irreducible tensors, $a^{+(1)}$ or $a^{(1)}$ and $\rho^{(1)}$, operating respectively on different parts of the total system, namely on the lattice and on the electron. With Judd (1963, eqn. 3-36) or Messiah (1969, eqn. C.91) we find

$$A = \delta(\mathcal{J},\mathcal{J}') \cdot \delta(M,M') \cdot (-1)^{\mathcal{J}+\ell_e+L'} \cdot \begin{Bmatrix} L & 1 & L' \\ \ell_e' & \mathcal{J} & \ell_e \end{Bmatrix} \cdot$$
$$\cdot \langle nL \| a^{+(1)} \| n'L' \rangle \langle 2\ell_e \| \rho^{(1)} \| 2\ell_e' \rangle \qquad (9.52)$$

where $\{\ \}$ denotes the 6j-symbol of Messiah 1969, p. 1061).

Similarly, B is given by

$$B = \delta(J,J')\cdot\delta(M,M')\cdot(-1)^{J+\ell_e+L'}\begin{Bmatrix} L & 1 & L' \\ \ell_e' & J & \ell_e \end{Bmatrix}\cdot$$

$$\cdot\langle n L \| \tilde{a}^{(1)} \| n' L'\rangle\cdot\langle 2\ell_e \| \rho^{(1)} \| 2\ell_e'\rangle \qquad (9.53)$$

Using the solutions (9.48), (9.49) and (9.50) for the reduced matrix elements of $a^{+(1)}$, $\tilde{a}^{(1)}$ and $\rho^{(1)}$, we find that the 6j-symbols relate L to J. We arrive at four different non-zero expressions for A and also for B. After changing the notation in A and B we are able to relate A and B to each other and the four matrix elements (9.51) of h_{PJT} are then, in general, given by

$$C = \langle J M, (n+1)L, 2\ell_e \mid h_{PJT} \mid J M, n L', 2\ell_e' \rangle =$$

$$= \langle J M, n L', 2\ell_e' \mid h_{PJT} \mid J M, (n+1)L, 2\ell_e\rangle = -\varkappa B \qquad (9.54)$$

Within the vibronic states (8.6), C takes the following form:

$$C_1 = C_1^* = \langle J M, (J+2N-1)(J-1), 2p \mid h_{PJT} \mid J M, (J+2N)J, 2s\rangle$$

$$= \varkappa\cdot\sqrt{\frac{J(2J+1+2N)}{2J+1}} \qquad (9.54a)$$

$$C_2 = C_2^* = \langle J M, (J+2N+1)(J+1), 2p \mid h_{PJT} \mid J M, (J+2N)J, 2s\rangle$$

$$= -\varkappa\cdot\sqrt{\frac{(J+1)(2J+3+2N)}{2J+1}} \qquad (9.54b)$$

$$C_3 = C_3^* = \langle J M, (J+2N-1)(J+1), 2p \mid h_{pJT} \mid J M, (J+2N) J, 2s \rangle$$

$$= \varkappa \cdot \sqrt{\frac{(J+1)2N}{2J+1}} \qquad (9.54c)$$

$$C_4 = C_4^* = \langle J M, (J+2N+1)(J-1), 2p \mid h_{pJT} \mid J M, (J+2N) J, 2s \rangle$$

$$= -\varkappa \cdot \sqrt{\frac{2J(N+1)}{2J+1}} \qquad (9.54d)$$

The matrix elements above correspond, of course, to the ones of (7.13). As expected from the previous discussion, the type II states (8.10) or (8.6d) are not connected to the other states of (8.6) by the interaction term.

§ 10 Numerical Diagonalization of the Energy Matrix

With the results obtained in the two previous paragraphs we are now able to set up the matrix for the energy. Our eigenvalue equation for the type I states (8.8) reads

$$(h - \varepsilon(I,jJ))\, \Psi^{JM}_{I,j} = 0 \qquad (10.1)$$

Multiplication from the left with $\langle JM,(J+2N-1)(J-1),2p|$, $\langle JM,(J+2N)J,2s|$, and $\langle JM,(J+2N+1)(J+1),2p|$, respectively, where $N=0,1,2,\ldots,\infty$, yields with (8.7) and (9.54) an infinite set of equations which are coupled by the coefficients a and b of the eigenvector. It is convenient to express these equations in matrix form, and the energy eigenvalues $\varepsilon(I,jJ)$ are the solutions of the corresponding secular equation.

Table 4 shows the first five of these coupled equations. As expected from (9.54), the energy matrix is real and symmetrical. Furthermore, it is a symmetrical band matrix where in general only the two off-diagonal elements immediately next to the diagonal element on either side in a row are non-zero whereas all the others vanish. Table 4 is also valid for the case J=0 when we introduce the requirement (8.9),

$$b(0,j,2N-1) \equiv 0 \qquad (10.2)$$

The energy matrix reduces then to real symmetric tri-diagonal form. We solve the eigenvalue problem (10.1) by numerical diagonalization of the energy matrix. The computations were carried out on the Oxford ICL 1906A computer by making use of various library programs of

TABLE 4

ENERGY MATRIX

$$
\begin{bmatrix}
(J+\frac{1}{2}-\delta-\varepsilon) & \varkappa\sqrt{J} & 0 & 0 & 0 & 0\cdots \\
\varkappa\sqrt{J} & (J+\frac{3}{2}+\delta-\varepsilon) & -\varkappa\cdot\sqrt{\frac{(J+1)(2J+3)}{2J+1}} & -\varkappa\sqrt{\frac{2J}{2J+1}} & 0 & 0\cdots \\
0 & -\varkappa\cdot\sqrt{\frac{(J+1)(2J+3)}{2J+1}} & (J+\frac{5}{2}-\delta-\varepsilon) & 0 & \varkappa\cdot\sqrt{\frac{(J+1)\cdot 2}{2J+1}} & 0\cdots \\
0 & -\varkappa\sqrt{\frac{2J}{2J+1}} & 0 & (J+\frac{5}{2}-\delta-\varepsilon) & \varkappa\sqrt{\frac{J\cdot(2J+3)}{2J+1}} & 0\cdots \\
0 & 0 & \varkappa\cdot\sqrt{\frac{(J+1)\cdot 2}{2J+1}} & \varkappa\cdot\sqrt{\frac{J\cdot(2J+3)}{2J+1}} & (J+\frac{7}{2}+\delta-\varepsilon) & \cdots \\
\vdots & \vdots & \vdots & \vdots & \vdots & \ddots
\end{bmatrix}
\begin{bmatrix}
b\,(J,j,J-1) \\
a\,(J,j,J) \\
a\,(J,j,J+1) \\
b\,(J,j,J+1) \\
a\,(J,j,J+2) \\
\vdots
\end{bmatrix}
= 0
$$

with the requirement $b(0,j,2N-1)=0$

the Nottingham Algorithms Group, the choice of which depended mainly on the amount of eigenvalues and eigenvectors required for a particular calculation. In the N.A.G. Library Manual these subroutines carry the notations F02AAF, F02ABF, F02AMF, F02AVF, F02ACF, F02ASF.

The mathematical procedure of these subroutines is essentially the same for all of them. The original real symmetric matrix A is transformed into a real symmetric tridiagonal matrix T by Householder's method (for details we refer to Martin et al. 1968). Either selected or all the eigenvalues and eigenvectors are then calculated using the QL algorithm (Bowdler et al. 1968). The eigenvectors are normalised to unity and are always accurately orthogonal. However, according to the library manuals, there is no guarantee that the eigenvalues and eigenvectors are correct solutions of the original matrix as this depends on the sensitivity of the matrix to the rounding errors produced in tridiagonalisation. Furthermore, the accuracy of the calculated eigenvalues of T decreases with increasing number of iterations.

The computations also imply several problems of convergence arising from the finite dimension of A. Since, of course, one is not able to set up an infinite large energy matrix, we approximate this circumstance by setting up a square matrix A with the finite dimension D and take only the ℓ lowest eigensolutions of A, where $\ell << D$. A simple and easy way of checking that these ℓ solutions are sufficiently accurate is by increasing the dimension of A to D_1, where D_1

has to be substantially larger than D. The new ℓ_1 solutions are then compared with the previous ones.

Difficulties of convergence are mainly determined by the size of the off-diagonal elements, the orders of which depend on the product of the coupling constant $\varkappa$ and the square root of J but not on δ. Concerning the high lying energy levels and absorption spectra (T = 0), we are primarily interested in the states with J=1, thus the convergence depends only on $\varkappa$.

For $\varkappa \leq 1$ convergence is obtained quite easily. We find that at least the $\ell = D/2$ lowest eigenvalues are correct. On the other hand for $\varkappa > 1$ only the first few eigensolutions are correct and convergence decreases rapidly for increasing values of $\varkappa$. As regards to the temperature dependent emission spectra, eigenstates with $J \gg 1$ are also required, which limit our calculations to not too strong coupling strengths and not too high temperatures.

Furthermore, the available core size limits the dimension D to about 250 for J=0 and 180 for $J \geq 1$, which in return puts an upper limit on $\varkappa$. Reasonably accurate results for the low energy diagrams in § 11 were obtained by putting $D \approx 50$ for $\varkappa \leq 1$ and $D \approx 100$ for $\varkappa \leq 5$, whereas for the high energy eigenvalues for J=1 we chose $D \approx 100$ for $\varkappa \leq 1$ and $D \approx 180$ for $\varkappa \leq 5$. For the absorption spectra in § 14 we chose $D \approx 180$ for $\varkappa \leq 4$ and for the ($T \neq 0$)-emission spectra in § 13 $D \approx 150$ for $\beta \leq 2$.

The job time required to calculate one of the high (J=1)-energy graphs (8 to 10) was in the order of 5 minutes, the one for a (T=0)-absorption spectrum (Graphs 35 to 39) at

Ξ_G = 16 was about 1-2 minutes, whereas the job time involving the (T > 0)-emission spectra (Graphs 18 to 21) reached 10-15 minutes.

§ 11 Energy Levels and Vibronic Wave Functions

(a) Weak Coupling - Perturbation Approach

As long as we deal only with the model Hamiltonian (6.11) without considering any external field or spin-orbit coupling, it is convenient to make use of the full-rotational symmetry, also then when we calculate the perturbational effect of h_{PJT} (6.14) on the angular states (8.6). We can again employ the matrix elements C_i of (9.54) in order to calculate the perturbed wave functions and energy corrections. Of course, the type II states (8.6d) need not be considered at all, as explained above.

A perturbation approach for $|\delta| \neq 0.5$ reveals that in general the following conditions have to be satisfied:

$$\left|\frac{\varkappa\sqrt{N}}{2(\delta \pm \frac{1}{2})}\right| \ll 1 , \quad \left|\frac{\varkappa\sqrt{J}}{2(\delta \pm \frac{1}{2})}\right| \ll 1 , \quad \left|\frac{\varkappa\sqrt{J+N}}{2(\delta \pm \frac{1}{2})}\right| \ll 1 . \qquad (11.1)$$

where $|\delta| = 0.5$ corresponds to an electronic energy separation of one phonon quantum (see eqn. 6.9). For a given value of and δ ($\neq \pm 0.5$) the condition (11.1) cannot be fulfilled for very large values of J and/or N, i.e. for the energetically high lying states, which suggests that the perturbational approach is only justified for the low lying states.

Furthermore, it is clear that $|\delta| \gg 0.5$, or even $|\delta| \ll 0.5$, in order that the denominator of (11.1) is reasonably large. In the case $|\delta| \gg 0.5$ we find from (11.1) the simplified perturbation condition

$$\left|\frac{\varkappa}{2\delta}\right| \ll 1 \qquad (11.2a)$$

and for $|\delta| \approx 0$:

$$|\varkappa| \ll 1 \qquad (11.2b)$$

which explains why the perturbation treatment for $|\delta| \gg 0.5$ yields better result than for $|\delta| \approx 0$.

For $\delta = \pm 0.5$ we find perturbation conditions which are similar to (11.1) but with denominators now being equal to 2. The arguments above apply also here.

As seen from (8.7), the positions of the unperturbed energy levels depend on the parameter δ of the electronic 2s-2p-spacing. Let us state now nonzero energy corrections to lowest order for different δ. As all the corrections belong to type I states, we omit the index I. In contrast to the notation of (8.8) we are now able to classify the vibronic eigenstates by indices referring to the unperturbed wave function(s) involved.

In the general case $|\delta| \neq 0.5$ non-degenerate perturbation theory applies to all (J=0)-states as well as to all the 2s-states arising from (8.6a), furthermore to the lowest state coming from (8.6c). No energy corrections occur to first order in $\varkappa$, but to second order we find:

For (8.6a): $$\mathcal{E}_1^{(2)}(J,N) = \frac{\mathcal{E}_G}{2(2J+1)\cdot(\delta^2-\frac{1}{4})} \cdot \left\{\delta\cdot\left[4J(J+2+2N)+3+4N\right] + \frac{3}{2}\cdot(2J+1)\right\} \quad \text{for } J \geq 0 \qquad (11.3a)$$

For (8.6b): $$\mathcal{E}_2^{(2)}(J=0,N) = -\frac{\mathcal{E}_G}{2\cdot(\delta^2-\frac{1}{4})}\cdot\left\{\delta(4N+5)+\frac{1}{2}\right\} \quad \text{for } J = 0 \qquad (11.3b)$$

For (8.6c): $$\mathcal{E}_3^{(2)}(J,N=0) = -\frac{\mathcal{E}_G\cdot J}{2\cdot(\delta+\frac{1}{2})} \quad \text{for } J \geq 1 \qquad (11.3c)$$

The remaining states for $J \geq 1$ arising from (8.6b,c) are doubly degenerate. Degenerate perturbation theory applies, and the degeneracy is lifted to second order in $\varkappa$:

$$\mathcal{E}^2_{I/II}(J,N) = (A \pm \sqrt{B^2+4C^2})/2 \quad \text{for } J \geq 1 \qquad (11.3d)$$

where $$A = \frac{\varepsilon_G}{(1-4\delta^2)} \cdot \left\{ 1 + 2\delta\,(2J+4N+5) \right\} \qquad (11.4a)$$

$$B = \frac{\varepsilon_G}{(1-4\delta^2)} \left\{ 2J+1+2\delta\left(1 + \frac{4(N+1)}{(2J+1)}\right) \right\} \qquad (11.4b)$$

$$C = \frac{\varepsilon_G\, 4\delta}{(2J+1)(1-4\delta^2)} \cdot \sqrt{2J(J+1)(2J+3+2N)(N+1)} \qquad (11.4c)$$

Note that these considerations apply also to the accidental degeneracies which occur for $\delta = \pm (2m+1)/2$, $m=1,2,3,\ldots$.

In the special case of electronic degeneracy $\delta = 0$ the treatment above simplifies considerably and non-degenerate perturbation theory applies throughout. The cross term C above vanishes now which arises from the circumstance that the energy differences between the 'p-states' (8.6b,c) and the two linking 's-states' (8.6a) are $\Delta\varepsilon = \pm 1$ and also that (9.54) yields the relation

$$C_2(N)\; C_4(N) = C_1(N+1) \cdot C_3(N+1) \qquad (11.5)$$

The energy corrections above reduce now to:

For (8.6a): $\varepsilon_1^{(2)}(J) = -3\,\varepsilon_G$ for $J \geq 0$ (11.6a)

For (8.6b): $\varepsilon_2^{(2)}(J) = (J+1)\,\varepsilon_G$ for $J \geq 0$ (11.6b)

For (8.6c): $\varepsilon_3^{(2)} = -J\cdot\varepsilon_G$ for $J \geq 1$ (11.6c)

These energy corrections are independent of N in contrast to (11.3). Moreover, (11.6a) does not depend on J.

In the special cases $\delta = \pm 0.5$ degenerate perturbation treatment yields a linear splitting of the degeneracies involved. For the singlet states non-degenerate perturbation theory applies of course and gives a quadratic energy correction. For $\delta = +0.5$ we find the lowest singlet states (8.6c):

$$\varepsilon_3^{(2)}(J, N=0) = -J\cdot\varepsilon_G/2 \qquad \text{for } J \geq 1 \qquad (11.7a)$$

The doublet state (8.6a,b) and the triplet state arising from (8.6a,b,c) are listed to first order in $\varkappa$:

$$\varepsilon^{(1)}_{I/II}\ (J, N') = \pm\, \varkappa \sqrt{J + 2N' + 3} \qquad \text{for } J \geq 0 \quad (11.7b)$$

$$\varepsilon^{(1)}_{III}\ (J, N') = 0 \qquad \text{for } J \geq 1 \quad (11.7c)$$

where $N' = 0,1,2,\ldots$.

Similarly, we obtain for $\delta = -0.5$:

For (8.6a): $\varepsilon^{(2)}_{1}\ (J = N = 0) = -3\,\epsilon_G/2$ for $J=N=0$ (11.8a)

For (8.6a,b,c):

$$\varepsilon^{(1)}_{I/II}\ (J, N') = \pm\, \varkappa \sqrt{J + 2N'} \qquad \text{for } J=0,\ N' \geq 1, \text{ and } J \geq 1,\ N' \geq 0 \quad (11.8b)$$

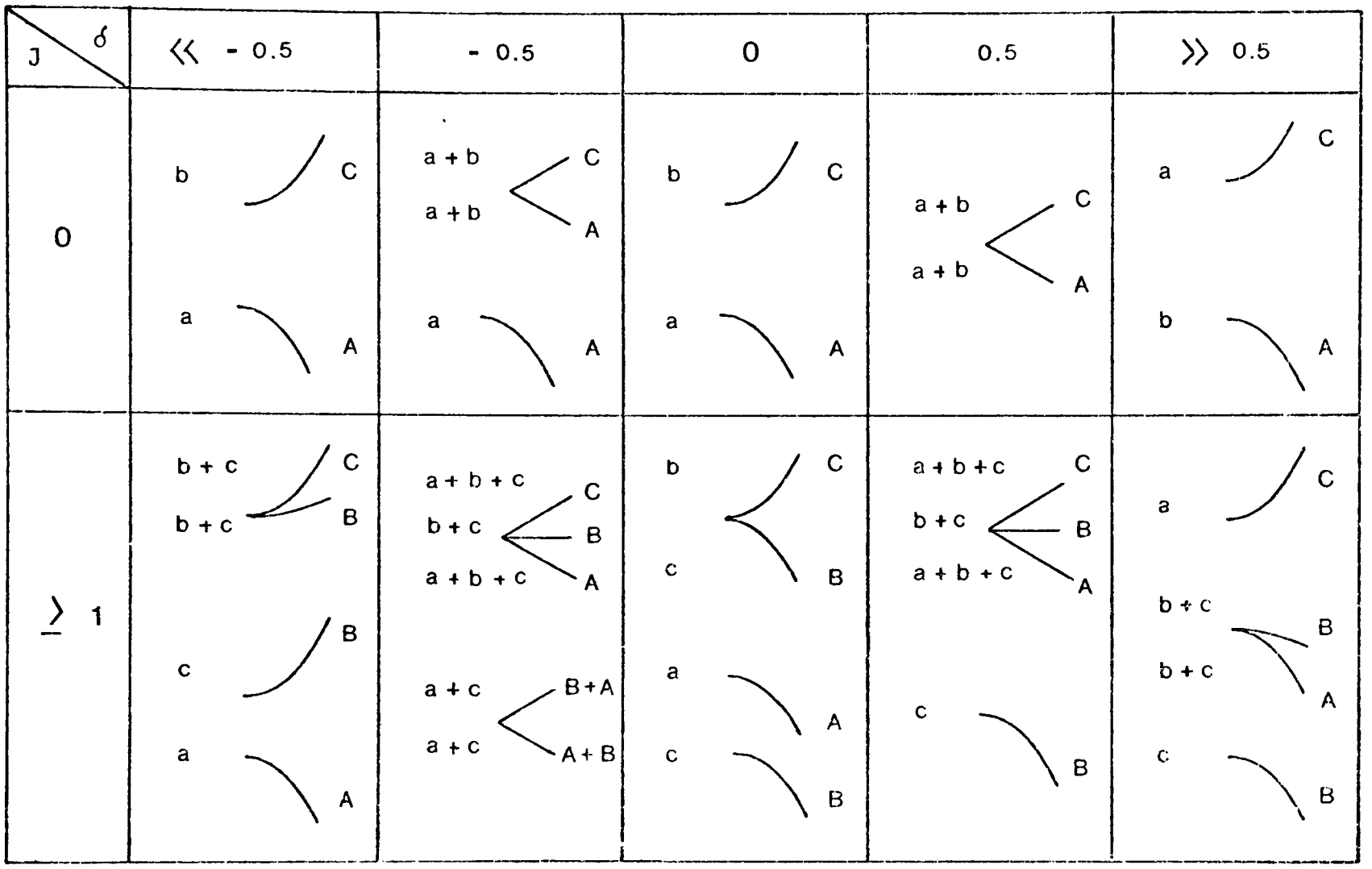
$$\varepsilon^{(1)}_{III}\ (J, N') = 0 \qquad \text{for } J \geq 1,\ N' \geq 1 \quad (11.8c)$$

The energy corrections (11.3 to 11.8) are schematically represented in Fig. 6 together with the appropriate zero-order wave functions, abbreviated as a,b,c.

In the considerations below we shall be interested in the energy difference of the two lowest states, i.e. the difference between the lowest J=0 and J=1 state. As for all states, the parameter δ determines which of the states (8.6) contribute to the lowest pair. For zero coupling we find in the case of $\delta > 0$ that the state (8.6c) with J=1, N=0 is lowest and the first excited state is (8.6a) with J=N=0 for $\delta < 0.5$ or (8.6b) with J=N=0 for $\delta > 0.5$. For $\delta = 0.5$ the first excited state is (8.6a and b). Similarly, in the case of $\delta \leq 0$ the state (8.6a) with J=N=0 is lowest and the next higher state is (8.6c) with J=1,N=0 for $\delta > -0.5$ or (8.6a) for J=1,N=0 with $\delta < -0.5$. For $\delta = -0.5$ it is (8.6a and c).

FIG. 6

Schematic representation of the type I states (8. 6a, b, c), abbreviated as a, b, c in weak coupling for various values of δ.



The zeroth order wave functions of degenerate or non-degenerate perturbation theory are given schematically as sums of a, b, c together with the associated type A, B, C states in order of increasing energy where the reoccuring states are omitted. The nonzero energy corrections are given to lowest order in $\varkappa$. Note that the zero- and one-phonon absorption lines are connected to the lowest (8. 6c)- and (8. 6a)- state with J = 1, respectively.

The energy difference for weak coupling between the two lowest levels for each of these cases is then obtained with the appropriate energy corrections above.

(b) The Strong Coupling Limit

For the following discussion it will be of advantage to rewrite some of the results derived in § 7. It was shown there that the transformed differential equations (7.19) decouple for large values of q, and low energy solutions can be found which serve the following second-order linear differential equation

$$\left[\mathcal{R}_q + \tfrac{1}{2}(q-q_0)^2 - \mathcal{E}_G + \frac{1}{4\mathcal{E}_G}\left(J^2+J+1\right) - \mathcal{E}\right] F_1(q) = 0 \qquad (11.9)$$

where we use the notation of § 7. It is convenient to put

$$G_1(q) = q\, F_1(q) \qquad (11.10)$$

and to replace (11.9) by the equivalent radial equation

$$\frac{d^2G_1(q)}{dq^2} + \left[2\mathcal{E} - (q-q_0)^2 + 2\mathcal{E}_G - \frac{1}{2\mathcal{E}_G}\cdot\left(J^2+J+1\right)\right] G_1(q) = 0 \qquad (11.11a)$$

In order that the solutions $G_1(q)$ are regular, the following condition has to be satisfied:

$$G_1(q=0) = 0 \qquad (11.11b)$$

If we limit ourselves to values of q in the vicinity of $q_0 >> 1$, i.e. to energetically low-lying eigensolutions, and introduce the new variable $x = q-q_0$, (11.11a) takes the form

$$\frac{d^2G_1(x)}{dx^2} + \left[2\mathcal{E} - x^2 + 2\mathcal{E} - \frac{1}{2\mathcal{E}_G}\left(J^2+J+1\right)\right] G_1(x) = 0 \qquad (11.12)$$

$G_1(x)$ exists only in the interval $-q_0 \leq x < \infty$. For $q_0 \gg 1$ it is at least for the low-lying solutions a good approximation

to extend this interval to $-\infty < x < \infty$. (11.12) becomes then the radial equation for the linear harmonic oscillator with the energy eigenvalues

$$\varepsilon(I, j\,J) = j + \tfrac{1}{2} - \varepsilon_G + \left(J^2 + J + 1\right) / 4\,\varepsilon_G \qquad (11.13)$$

and the normalised eigenfunctions

$$G_1^{(j)}(x) = \left(\sqrt{\pi}\; 2^j\, j!\right)^{-\frac{1}{2}} \cdot \exp\left(-x^2/2\right) \cdot H_j(x) \qquad (11.14)$$

with $j, J = 0, 1, 2, \ldots$ but not too large. $H_j(x)$ are the Hermite Polynominals defined by Messiah (1969, p. 491). The ground state $j=0$ reads

$$G_1^{(o)}(q - q_o) = \pi^{-\frac{1}{4}} \cdot \exp\left\{-(q - q_o)^2/2\right\} \qquad (11.15)$$

As $q_o \gg 1$ we find $G_1^{(j)}(x = -q_o) \approx 0$ in accordance with condition (11.11b), which justifies our approximation. We see also from (11.9 and 11.12) that the term in J is a constant and $G_1^{(n)}$ of (11.14) is thus independent of J. Obviously (7.25) and(7.26) follow from (11.13).

(c) Computational Results

The numerical calculations outlined in § 10 serve to link up the weak and strong coupling regions and provide solutions for intermediate coupling strengths.

(i) Low-Lying Energy Levels

Graphs 1 to 5 show some of the energetically low-lying eigenvalues of the model Hamiltonian h (6.11), which are associated with type I and II states of § 8. The energy levels are plotted as functions of the coupling coefficient $\varkappa = (\varepsilon_G)^{\frac{1}{2}}$ for representative values of δ. It is convenient to add the stabilization energy ε_G to the vibronic energies in order to

be able to draw the type I energy levels up to strong coupling. The type II energy eigenvalues are of course independent of $\varkappa$.

The type I energy levels can exhibit several extrema before approaching asymptotically the constant values of the strong coupling limit where we find a strict ordering of the levels with different values of J but all belonging to the same quantum number j (see 11.13).

The first order perturbation treatment above proves useful for the identification of the levels in weak coupling and provides reasonably correct solution for $\varkappa \lesssim 0.5$ when j and J are small. As expected, the accuracy is better for $|\delta| >> 0.5$ than for $\delta = 0$, but decreases rapidly for increasing values of j and J.

We are again interested in the two lowest states: the J=0 and J=1 type I states belonging to j=0. Whenever the J=0 state is lowest in the weak coupling region, i.e. for $\delta \leq 0$, it will stay lowest for all coupling strengths (because of the ordering in strong coupling). If, however, the J=1 state is lowest for weak coupling, which can occur for $\delta > 0$, a crossing of the levels will take place. This point, which has been suggested by Ham (1973a) merely from an examination of the coupled differential equations (7.19), is also confirmed by our computational results. In particular, the two lowest levels for $\delta = 0.5$ cross at $\varkappa \approx 0.642$ (Graph 3) and for $\delta = 2.5$ at $\varkappa \approx 1.227$ (Graph 5).

Graph 6 shows the absolute value of the energy difference ε_{10} between the two lowest levels, as a function of ε_G for various parameters δ. The strong coupling approximation is given by (7.26) to $1/2\,\varepsilon_G$, which appears as a straight line in

the graph, and approximates the curves well for strong coupling, even when there is a level crossing.

In the strong coupling limit the energies of the lowest type I levels are given by (11.13). As this expression was obtained using the conditions (7.23) of strong coupling, we expect best agreement with our computational results for $\delta = 0$. Indeed, eqn. (11.13) yields in this case also a good approximation for intermediate coupling strengths. As (11.13) does not contain the parameter δ, it is desirable to extend this formula to general δ. Taking the results obtained from Graph 6 into account and being inspired by the neglected terms of the differential eqns. (7.19), we make the following Ansatz:

$$\varepsilon_G(I, jJ) = j + \tfrac{1}{2} - \varepsilon_G + \left(J^2 + J + \alpha(\delta)\right) / 4\varepsilon_G \qquad (11.16a)$$

where $j, J = 0, 1, 2, \ldots$ but not too large. A straight forward investigation of the behaviour of the lowest $J=0$ level reveals the simple formula

$$\alpha(\delta) = 1 - \delta^2 \qquad (11.16b)$$

which holds surprisingly well for at least the range $|\delta| \lesssim 5$. For $j=0$, the accuracy of (11.16) is of the order 0.01 for $\varkappa \approx 2$, 0.001 for $\varkappa \approx 3$ and improves for larger values of $\varkappa$, but decreases for increasing j. Moreover, (11.16) will be a reasonable approximation as long as J is not too large. The validity of (11.16) for various values of j in the case of $J \leq 1$, $\varepsilon_G \leq 4$, $|\delta| \leq 2.5$ can be seen from the Graphs 11,12.

For $\delta = 0$, expression (11.16) is identical to (11.13). For $J=0$ and 1, (11.16) yields the difference (7.26). Furthermore, in the case of $|\delta| = 1$ and $J = 0$ the last term of (11.16a) disappears and the energies take a particularly simple form.

It is interesting to note that the eigenvalues for $\delta = -1$, $j=0$

$$\varepsilon_{-1}(I, 00) = 1/2 - \varepsilon_G \qquad (11.17)$$

appears to be the <u>exact</u> expression for all coupling strengths; (11.17) has been tested for $0 \leq \varepsilon_G \leq 64$. This cannot of course apply to $\delta=1$, $j=0$ as in this case the energy at $\varepsilon_G = 0$ is 3/2.

(ii) Electronic Admixtures in the Vibronic States

At this point it is instructive to consider the admixtures of the three states (8.6a-c), and thus of the electronic 2s and 2p states, in the vibronic type I states (8.8). Graph 7 shows the total admixtures of the s-J-states (8.6a) as a function of the coupling strength for the four lowest J=0 states in the case of $\delta=0$. As the J=0 states contain no admixtures of p-(J-1)-states (8.6c), the normalization (8.10) reduces to

$$\sum_{N=0}^{\infty} \left\{ \left| a(0, j, 2N) \right|^2 + \left| a(0, j, 2N+1) \right|^2 \right\} = 1 \qquad (11.18)$$

where the summation over the first and second term represent the total admixtures of the s-(J=0)-states (8.6a) and p-1-states (8.6b), respectively.

For zero coupling strength, the states of this graph belonging to j=0 and 2 are pure s-states, whereas the j=1 and 3 states are pure p-states. As the coupling strength increases, the 2s- and 2p-admixtures of the states decrease rapidly. The lines may exhibit several extrema, the form of which is similar to that of a damped oscillation, until they approach the asymptotic value 1/2 of strong coupling. This value has been predicted by Ham (1973a), see (7.29a), and is a very good approximation for the few lowest J=0 states for $\varkappa \gtrsim 2$. As expected, the accuracy decreases for increasing values of j.

TABLE 5 s - J - and p -(J+1) -Admixtures in Type I States with j = 0 for $\delta = 0$.

The upper and lower values belonging to a given J correspond to the s - J - and p -(J+1) -admixtures, respectively.

J \ $\varkappa$	0	0.5	1	2	3	4	5	∞
0	1	0.70996	0.56592	0.50580	0.50092	0.50027	0.50011	$\frac{1}{2}$
	0	0.29004	0.43408	0.49420	0.49908	0.49973	0.49989	$\frac{1}{2}$
1	0	0.25656	0.48828	0.50410	0.50088	0.50027	0.50011	$\frac{1}{2}$
	0	0.04678	0.21555	0.31758	0.33036	0.33244	0.33298	$\frac{1}{3}$
2	0	0.32475	0.48391	0.50271	0.50081	0.50026	0.50010	$\frac{1}{2}$
	0	0.06133	0.19192	0.27949	0.29542	0.29858	0.29943	$\frac{3}{10}$
3	0	0.36021	0.48405	0.50175	0.50072	0.50025	0.50010	$\frac{1}{2}$
	0	0.07175	0.18550	0.26269	0.27981	0.28380	0.28494	$\frac{2}{7}$
4	0	0.38269	0.48495	0.50110	0.50063	0.50024	0.50010	$\frac{1}{2}$
	0	0.08014	0.18371	0.25340	0.27080	0.27541	0.27680	$\frac{5}{18}$
5	0	0.39846	0.48569	0.50065	0.50055	0.50023	0.50010	$\frac{1}{2}$
	0	0.08720	0.18362	0.24764	0.26489	0.26994	0.27156	$\frac{3}{11}$

TABLE 6 s-J-ADMIXTURES in TYPE I STATES with $j = J = 0$

δ \ $\varkappa$	0	0.5	1	2	3	4	5	∞
2.5	0	0.05355	0.16151	0.34697	0.42979	0.46063	0.47486	$\frac{1}{2}$
1.0	0	0.24994	0.35840	0.44120	0.47245	0.48441	0.49001	$\frac{1}{2}$
0.5	0 and 1	0.46343	0.45747	0.47338	0.48668	0.49234	0.49506	$\frac{1}{2}$
- 0.5	1	0.85736	0.67157	0.53842	0.51516	0.50820	0.50516	$\frac{1}{2}$
- 1.0	1	0.92337	0.76159	0.57121	0.52941	0.51613	0.51020	$\frac{1}{2}$
- 2.5	1	0.97873	0.90978	0.67018	0.57220	0.53992	0.52535	$\frac{1}{2}$

In a similar fashion we have investigated in the case of $\delta = 0$ the s-J- and p-(J+1)-admixtures for the type I states with j=0 and $0 \leq J \leq 5$. Table 5 shows the computed admixtures for various values of $\varkappa$. The strong coupling limit is indicated by $\varkappa = \infty$ with results taken from (7.29), which approximate well the computed figures for $\varkappa \gtrsim 2$. The total admixture of the p-(J-1)-states (8.6c) can be obtained with the normalization condition (8.10) or (11.18).

Finally, in Table 6 we consider the s-J-admixtures of the lowest J=0 states for various values of δ and $\varkappa$. Comparing these values with the corresponding ones belonging to δ=0 of Table 5, we find that the strong coupling value approximates the computed figures best when $|\delta|$ is small, as expected from (7.23).

(iii) High-Lying Energy Levels - Type A,B, and C States

The final part of this paragraph deals with a further classification of the type I levels which proves particularly useful for large values of the electronic 2s-2p-spacing $|\delta|$ and which provides a link with the adiabatic energy surfaces.

Graphs 8 to 10 show the type I and II energy levels for J=1 (without adding ε_G) v.s. coupling strength for δ=0, $\pm$ 2.5, respectively. These graphs are crucial for the understanding of other cases with different J and δ and for the interpretation of the absorption spectra in § 14. With these and similar (not shown) graphs we come to the following conclusions:

(α) The type I energy levels with given J exhibit a tendency to cross which appears to be strongest at higher energies and for larger values of $|\delta|$. Although the levels with

the same J actually never cross, as the wave functions of the diagonalized matrix do not factorize, it is reasonable to regard them as crossed when the tendency is strong and to investigate the behaviour and properties of these new states. For general δ and J, the type I levels may then be divided into the three groups A, B, and C, each of which carried its own set of principle quantum numbers in place of j. Type A energy levels exhibit a parabolic tendency to decrease for increasing values of $\varkappa$, i.e. $\varepsilon' \leq 0$, $\varepsilon'' < 0$, where $\varepsilon' \equiv \partial\varepsilon/\partial\varkappa$ and $\varepsilon'' \equiv \partial^2\varepsilon/\partial\varkappa^2$. The lowest lying ones of these levels are described reasonably well by expression (11.16) for intermediate and strong coupling and have been the subject of the discussion above. On the other hand, type B levels show only little dependence upon $\varkappa$ with either $\varepsilon' \leq 0$ or $\varepsilon' \geq 0$ and ε'' >/< 0. Finally, type C levels exhibit a parabolically increasing behaviour with $\varepsilon' \geq 0$ and $\varepsilon'' > 0$.

(β) Comparing the type I levels belonging to fixed δ but various values of J (not shown), we find that no type B levels occur for J=0. Furthermore, there is an energy shift between the corresponding type A, B, or C levels belonging to different J in analogy to the energy eigenvalues (8.7) for zero coupling. As this shift is nearly constant for all coupling strengths, the lowest lying energy levels of each of the three sets A, B, and C show a qualitative similar behaviour for different values of J. Moreover, it appears that for each set the energy levels with large main quantum numbers exhibit an identical

behaviour which does not depend significantly upon J. Because of these reasons it is sufficient for at least the qualitative understanding of the $\varkappa$-dependence to consider only the levels with $J=1$ (see Graphs 8 to 10).

(γ) The highest lying type A, B, C levels with fixed J but varying δ exhibit a $\varkappa$-dependence which does not appear to be significantly dependent on the sign of δ, although there is again a constant shift in the absolute values of the corresponding energy levels (the type C levels for $\delta < -\frac{1}{2}$ lie by the amount $\Delta\mathcal{E} = 1$ higher than the ones for $\delta > \frac{1}{2}$).

We proceed to discuss in detail the dependence of the type A, B, C energy levels on $\varkappa$ and δ. For this purpose we shall take already into account some of the results of § 14 but shall leave their discussion until later. Strong tendency of levels crossing is found up to strong coupling in the case of $\delta << -0.5$ for all energy levels involved and in the case of $\delta >> 0.5$ for the energetically high lying levels. For $|\delta| \lesssim 1$ and for the lowest lying levels of $\delta > 1$, this tendency becomes very small, and it is impossible to identify the type A, B, C levels purely by inspecting the behaviour of the energy levels. However, by analysing the properties of the type I states we may associate a series of points on the levels with one of the type A, B, or C levels (see § 14). The connection between the zero-order wave functions (8.6a-c) of perturbation theory and the type A, B, C levels of weak coupling is schematically shown in Fig. 6.

An analogous expression to (11.13) and (11.16) has been

given by O'Brien (1973) for the higher energy levels (we now replace j by A),

$$\varepsilon\,(I, A) \;=\; A + 1/2 \;-\; \varepsilon_G \qquad (11.19a)$$

with A = 0,1,2,..., and the condition

$$\varepsilon \;\gg\; 2\,\delta \qquad (11.19b)$$

These solutions are independent of J and δ and have been obtained from an extension of the WKB method to the case where several wave functions depend on the same independent variable through a system of coupled differential equations (see Appendix). Our computed results reveal that (11.19) holds reasonably well for $\delta \approx 0$, $\varepsilon_G > 1$, and energies $\varepsilon > 6$, as expected. However, for $|\delta| \gg 0.5$ we find little quantitative agreement with (11.19) in the investigated intervals $0 \leq \varepsilon_G \leq 25$ and $\varepsilon < 13$, as the spacings of the levels appear to be larger than the ones predicted by this formula. Nevertheless, (11.19) appears to provide a better approximation for very large coupling strengths and very high energies.

For sufficiently large principle numbers B, type B levels are independent of ε_G and given by

$$\varepsilon_\delta\,(I, BJ) \;=\; J + 2B + 1/2 \;-\; \delta \qquad (J \geq 1) \qquad (11.20a)$$

where B = 0,1,2,...,J=1,2,3,.. . This expression is identical to the eigenvalues (8.7c) of the vibronic angular p-(J-1)-states (8.6c), which exist only for $J \geq 1$. As there are no type B levels for J=0, the existence of these levels is thought to be due to the influence of the (8.6c)-states. (11.20a) has also been obtained by O'Brien (1973) as a high energy solution from her WKB calculation with the following condition

$$\varepsilon + \delta \;\gg\; 1 \qquad (11.20b)$$

which is clearly demonstrated in the Graphs 8 to 10 (type B levels are indicated by arrows pointing to the energies (11.20a)). The lowest lying type B levels follow expression (11.20a) reasonably well only in the weak coupling region where their curvature is positive for $\delta < -0.5$ and negative for $\delta > -0.5$.

When the tendency of levels crossing is strong (see Graph 9), type B levels deviate increasingly from expression (11.20a) for increasing coupling strengths. For fixed ε_G, the deviation is larger for the lower lying levels, each of which appears to approach the nearest higher lying type II level in the strong coupling limit. All type B levels can be traced up to strong coupling purely by inspection of the energy graphs. For $\delta << -0.5$ the relative energies of the type B levels appear to follow the approx. expression $a\left\{1 - \exp(-b\,\varepsilon_G)\right\}$ where a,b, are positive constants for given δ, J, B. In the case $\delta = -2.5$, J=1 we find for B=0 and $0 \leq \varepsilon_G \leq 25$: $a \approx 1$, $b \approx 0.15$. As B increases, a or b or both decrease. Note that the energy separation between the type B levels is 2 for $\varepsilon_G = 0$ and decreases for increasing ε_G but appears to be always larger than 1.5.

When the tendency of levels crossing is weak (see Graphs 8, 10), type B levels are formed only in the weak coupling region. The 'existence' of these levels for stronger coupling can only be detected by analysing the properties of all the states (see § 14).

Finally, type C levels exhibit an ascending tendency for increasing coupling strength. At $\varepsilon_G = 0$ the energies of these levels are given for $\delta \geq 0.5$ by (8.7a) and for $\delta \leq 0.5$

by (8.7b). In the weak coupling region the energy corrections are of course given by the appropriate expressions of § 11 (a). Note that these levels exist up to strongest coupling only in the case $|\delta| > 0.5$ where they are approximately given by the upper branch of the hyperbola

$$\varepsilon_\delta(I,CJ) = \sqrt{1 + \left(J + 2C - \tfrac{3}{5}|\delta| + 3 + \gamma_1\right)\varepsilon_G} + J + 2C + |\delta| + \tfrac{1}{2} + \gamma_2 \qquad (11.21)$$

where $\gamma_1 = \begin{cases} 0 \\ \frac{1}{2} \end{cases}$ and $\gamma_2 = \begin{cases} 0 \\ 1 \end{cases}$ for $\begin{matrix} \delta > 0.5 \\ \delta < -0.5 \end{matrix}$

with C, J=0,1,2,... . This expression has been found essentially by trial and error and has been investigated for $\varepsilon_G \leq 16$ and $|\delta| \leq 5$, $0 \leq J \leq 2$, $0 \leq C \leq 4$. Very good agreement with the computed results is found in most cases. The accuracy increases as N becomes larger but decreases when $|\delta|$ either approaches 0.5 or becomes $>> 0.5$. In weak coupling (11.21) is equal to the weak coupling formulae of § 11(a) for some values of δ, J, and C but not for all. As expected from these results, the energy separation between the type C levels is equal to 2 for $\varepsilon_G = 0$ and increases as ε_G becomes larger.

For $|\delta| \lesssim 0.5$, type C levels can only be found in the weak coupling region. For $\delta = \pm 0.5$ the dependence on $\varkappa$ is then primarily linear and given by (11.7b and 11.8b), for $\delta=0$ the second order energy corrections are given by (11.6b). As with the type B levels, we may formally extend the type C levels up to strongest coupling by analysing the properties of all the j-energy levels with given J (see § 14).

Note that type C levels do not appear in O'Brien's WKB calculation (1973). This has to be expected as this calculation incorporates the conditions of the strong coupling limit (7.23)

which is in agreement with the computational results obtained for $\delta \approx 0$.

The emphasis up to now has been on the ε_G-dependence of the energy levels for given δ. It is instructive to look also at their dependence on δ for given ε_G. This has been done for J=0 and 1 in the Graphs 11 and 12, respectively. At zero coupling strength the states and energies are of course given by (8.6a-d) and (8.7a-d). Note the double J-degeneracy of the (8.6b and c) states for $J \geq 1$ (Graph 12). At $\varepsilon_G = 0$ the crossing points of the levels have double and triple J-degeneracies. However, all J-degeneracies are lifted at $\varepsilon_G > 0$, and no crossings can occur.

The graphs exhibit at low energies a set of energy levels with approximate parabolically decreasing behaviour and at high energies a set of levels with oscillatory δ-dependence. As ε_G increases the low lying levels increase in number and appear to decouple from the upper ones. As we have seen, the few lowest ones of these levels are described by (11.16). The graphs also indicate the regions of δ and ε_G where there is strong tendency of level crossing and where type A, B, and C energy levels can be defined. The results from above, especially (11.20) and (11.21), are confirmed.

The results of this section, together with the ones of § 14, reveal that the type A, B, and C energy levels can be associated with the lowest, middle and highest adiabatic energy surface of Fig. 5, respectively. As we have seen in § 6, there are two degenerate middle surfaces, one of which belongs to the type II energy levels.

As the coupling strength increases, and $2\varepsilon_G > |\delta|$, the

well of the lower energy surface becomes deeper and contains more type A levels, the energies of which are given by (11.16). Simultaneously, the highest energy surface becomes increasingly steeper with the effect that the type C levels are shifted towards higher energies and that the spacing between the levels increases. The middle surface is of course not affected by ε_G but depends on δ. Consequently, the type B levels do not depend significantly upon ε_G but show a δ-dependent behaviour.

The strong and weak tendencies to form type A, B, C energy levels can be regarded as an intrinsic feature of this PJT system. Whenever the lowest energy surface lies close to the middle one, as for $\delta > 0$, or close to the middle and upper surfaces, as for $|\delta| \lesssim 0.5$, the tendency to form type B, or B and C levels appears to be weak.

§ 12 Optical Emission and Absorption

(a) General Expressions

In discussing the optical properties of atomic systems we make use of the approximation which is based on the correspondence principle and in which the atomic system is treated quantum mechanically and the radiation field classically. When localized optical centres interact with light of wave lengths which are large compared to the linear dimension of the centre, we can employ the electric dipole approximation (Heitler 1954). For optical centres in crystals we assume that the centres are separated enough so that the interactions between them can be neglected (Dexter 1958).

Suppose, an optical centre like the F centre has an electronic ground state a and an excited state b. The corresponding vibronic states and energies are denoted by $\Psi_k^{(a)}(\underset{\sim}{q},\underset{\sim}{Q})$ with $E_k^{(a)}$ and $\Psi_\ell^{(b)}(\underset{\sim}{q},\underset{\sim}{Q})$ with $E_\ell^{(b)}$, where $\underset{\sim}{q},\underset{\sim}{Q}$ are the same as in § 2. The rate of spontaneous emission of light of energy E and polarization η resulting from a transition from $\Psi_\ell^{(b)}$ to $\Psi_k^{(b)}$ is given by (Dexter 1958, Fowler 1968, p. 61):

$$i_\eta(b,E) = C_1 \cdot Av_\ell \sum_k |\langle \Psi_\ell^{(b)} | D_\eta | \Psi_k^{(a)} \rangle|^2 \cdot \delta\left(E_\ell^{(b)} - E_k^{(a)} - E\right) \tag{12.1}$$

where $$C_1 = \frac{4n E^3}{3\hbar^4 \cdot C^3} \left(\frac{F_{eff}}{F_o}\right)^2 \tag{12.2}$$

n is the refractive index of the medium, C the speed of light in vacuum. The factor $(F_{eff}/F_o)^2$ describes the fact that the electron in question is located at a centre in a

crystal at which the effective electric field F_{eff} may differ from the average macroscopic electric field F_o. Furthermore, we ignore the variation of C_1 over the energy range of the states $\Psi_k^{(a)}$ to which the transitions occur, on the assumption that the width of the emission band is small compared with its mean energy. The average $A\nu_\ell$ is understood to be a thermal average over the initial states weighting each with the customary Boltzmann factor $\exp(-E_\ell^{(b)}/kT)$ whereas the sum is carried out over the final states $\Psi_k^{(a)}$.

The electric dipole moment operator $\vec{D}$ is for linearly polarized light given by

$$D_\eta = e\eta \qquad (\eta = x,y,z) \tag{12.3}$$

and its matrix elements between the electronic $|1s\rangle$- and $|2p\rangle$-states are denoted by

$$D = \langle 1s \mid D_\eta \mid \eta \rangle \tag{12.4}$$

where $\eta = x,y,z$.

The arguments which led to (12.1) can also be applied to the absorption case. An absorption cross section can be defined as the transition probability which is multiplied with the energy absorbed in a transition and divided by the incident energy flux associated with one photon per unit volume. It is given by (Dexter 1958, Lax 1952):

$$\delta(a,E) = C_2 \cdot A\nu_k \sum_\ell \left| \langle \Psi_k^{(a)} \mid D_\eta \mid \Psi_\ell^{(b)} \rangle \right| \cdot \delta\left(E_\ell^{(b)} - E_k^{(a)} - E\right) \tag{12.5}$$

where

$$C_2 = \frac{n}{\varepsilon} \cdot \left(\frac{F_{eff}}{F_o}\right)^2 \cdot \frac{4\pi^2 E}{3\hbar C} \tag{12.6}$$

In analogy to C_1, C_2 essentially describes the macroscopic

effect of the dielectric medium on the absorption centre. ε is the dielectric constant at the optical frequency involved. We note that the operations of summation and averaging in (12.5) are interchanged in comparison to (12.1).

(b) Weak Coupling - Perturbation Approach

Let us now state the results of the first order perturbation calculation of the emission and absorption spectra for zero temperature. Suppose the electronic 2s state lies below or is degenerate with 2p, i.e. $\delta \leq 0$. Then, as outlined in § 11, a type I state (8.8) with $j = J = 0$ is lowest for all ε_G. For weak coupling the lowest state arising from the s-J-substate (8.6a) with $J = N = 0$, has in first order of $\varkappa$ an admixture of the p-(J+1)-substate (8.6b) with $J = N = 0$ due to the vibronic coupling. This p-admixture is responsible for an electronic dipole transition to the vibronic states $\Psi_{N'J'M'}(1s)$ of (13.1) with $N' = 0$, $J' = 1$.

The resulting emission spectrum (12.1) merely consists of a single line, the one-phonon line, and is given by

$$i_{\eta,\delta}(I00,\varepsilon) = \frac{C_1 D^2}{3} M_\delta^{(e)}(1) \cdot \delta\left(\varepsilon_0 + \delta - 1 - \frac{3\varepsilon_G}{1-2\delta} - \varepsilon\right) \qquad (12.7)$$

with $\eta = x,y,z$ and the strength of the one-phonon line is

$$M_\delta^{(e)}(1) = \frac{3\varepsilon_G}{(1-2\delta)^2} \qquad (12.8)$$

For $\delta > 0$ and sufficiently weak coupling, a type I state with $j=0, J=1$ is lowest and arises from a p-(J-1)-substate (8.6c) with $N=0$, $J=1$. In first order of $\varkappa$ the vibronic coupling mixes a s-J-substate (8.6a) with $N=0, J=1$ with the effect of creating a $\varkappa$ dependent normalization factor for

$|1M,00,2p>$. An electronic dipole transition occurs to the vibronic ground state $\Psi_{000}(1s)$. The resulting zero-phonon line has the strength

$$M_\delta^{(e)}(0) = 1 - \frac{\varepsilon_G}{(1+2\delta)^2} \tag{12.9}$$

and the position is given by

$$i_{\eta,\delta}(I01,\varepsilon) = \frac{C_1 D^2}{3} M_\delta^{(e)}(0) \cdot \delta\left(\varepsilon_0 - \delta - \frac{\varepsilon_G}{1+2\delta} - \varepsilon\right) \tag{12.10}$$

When calculating the absorption spectrum at T=0, i.e. from the ground state $\Psi_{000}(1s)$ of (13.1), we find that the only non-vanishing matrix elements of the electric dipole operator are the ones which involve the p-(J-1)-substates (8.6c) with J=1,N=0. The first order perturbation treatment of § 11(a) reveals that in the case of $\delta \neq -0.5$, and $\eta = z$, the state arising from $|10,00,2p>$ carries the main contribution of the electric dipole transition and gives the zero-phonon line. Similarly, the state arising from $|10,11,2s>$ of (8.6a) gives the one-phonon line as this state contains $|10,00,2p>$ in first order of $\varkappa$.

For $|\delta| \neq 0.5$ the normalised absorption spectrum defined by (12.5) and (14.1) is given by

$$I_\delta^{(a)}(oo,\varepsilon) = M_\delta^{(a)}(o)\,\delta\left(\varepsilon_o - \delta - \frac{\varepsilon_G}{1+2\delta} - \varepsilon\right) + M_\delta^{(a)}(1)\,\delta\left(\varepsilon_o + \delta + 1 - \frac{\varepsilon_G(10\delta+3)}{(1-4\delta^2)}\,\varepsilon\right) \tag{12.11}$$

where the position and strength of the zero-phonon line $M_\delta^{(a)}(o)$ is the same as for emission and given by (12.9). The strength of the one-phonon line is

$$M_\delta^{(a)}(1) = \frac{\varepsilon_G}{(1+2\delta)^2} \tag{12.12}$$

In the case of $|\delta| = 0.5$ the above formulae have to be modified because of the degeneracies involved, as outlined in § 11(a). For $\delta = 0.5$, the zero-phonon line is identical to the one in (12.11) as the lowest singlet state arises from $|10,00,2p>$. A diagonalization of the matrices belonging to the triple degeneracies occurring for J=1 yields zero order states, one of which is a mixture of the p-states (8.6b and c) involved and two of which contain the corresponding s-state (8.6a) as well. Because of this two one-phonon lines occur with half of the expected strengths.

The absorption spectrum is given by

$$I^{(a)}_{0\cdot5}(00,\varepsilon) = M^{(a)}_{0\cdot5}(0)\cdot\delta\left(\varepsilon_0 - \tfrac{1}{2} - \tfrac{\varepsilon_G}{2} - \varepsilon\right) + \tfrac{1}{2} M^{(a)}_{0\cdot5}(1)\cdot\left\{\delta\left(\varepsilon_0 + \tfrac{3}{2} + 2\varkappa + \tfrac{\varepsilon_G}{4} - \varepsilon\right) + \delta\left(\varepsilon_0 + \tfrac{3}{2} - 2\varkappa + \tfrac{\varepsilon_G}{4} - \varepsilon\right)\right\} \tag{12.13}$$

For $\delta = -0.5$, the states (8.6a and c) with J=1,N=0 are degenerate for $\varkappa = 0$ and as the mutual matrix elements are non-vanishing, no distinction can be made between the zero- and one-phonon lines. The strengths of the absorption lines show now a linear dependence of $\varkappa$, and the spectrum is given by

$$I^{(a)}_{-0\cdot5}(00,\varepsilon) = \tfrac{1}{2}\cdot(1+\varkappa)\cdot\delta\left(\varepsilon_0 + \tfrac{1}{2} + \varkappa - \varepsilon_G - \varepsilon\right) + \tfrac{1}{2}\cdot(1-\varkappa)\cdot\delta\left(\varepsilon_0 + \tfrac{1}{2} - \varkappa - \varepsilon_G - \varepsilon\right) \tag{12.14}$$

§ 13 Numerical Calculation of the Emission Spectrum

(a) At zero temperature

The above considerations revealed that the lowest energy level consists for all coupling strengths only out of type I states (8.8) with j=0 and either J=0 or J=1. Spontaneous emission for T=0 can therefore only occur from one of these states.

Let us first calculate the spontaneous emission spectrum (12.1) for the general (2J+1)-fold degenerate state $\Psi^{JM}_{I,j}$ with energies $\mathcal{E}(I,jJ)$. We assume that the vibronic states $\Psi_{N'J'M'}(1s)$ associated with the electronic 1s ground state have the simple product form

$$\Psi_{N'J'M'}(1s) = |(2N'+J')J'M'\rangle \cdot |1s0\rangle \qquad (13.1a)$$

with the energies

$$\varepsilon(N'J',1s) = -\varepsilon_0 + 2N' + J' + \frac{3}{2} \qquad (13.1b)$$

where $N', J' = 0,1,2,\ldots$. Note that the electronic 1s-state lies lower than the zero point of energy (chosen between the excited electronic states, see § 6) by the energy $\varepsilon_0 = E_0/\hbar\omega$, which is assumed to be very much larger than δ and ε_G. The vibrational functions $|(2N'+J')J'M'\rangle$ are discussed in § 8. From (12.1) we find for T=0:

$$i_\eta(IjJ,\varepsilon) = \frac{C_1}{2J+1} \sum_{M=J,J-1,\ldots,-J} \sum_{N'J'M'} \left| \langle \Psi^{JM}_{I,j} | D_\eta | \Psi_{N'J'M'}(1s) \rangle \right|^2 \cdot \delta(\varepsilon(I,jJ) - \varepsilon(N'J',1s) - \varepsilon) \qquad (13.2)$$

Carrying out the calculation for $\eta = z$ we find for the matrix element involved:

$$\langle {}^{2}\Phi^{JM}_{I,j} \mid D_z \mid {}^{2}\Phi_{N'J'M'}(1S) \rangle =$$

$$= D \cdot \sum_{N=0}^{\infty} \Big\{ b(J,j,J+2N-1) \cdot \left(\frac{(J+M)(J-M)}{J(2J-1)} \right)^{\frac{1}{2}} \cdot \delta_{N',N} \cdot \delta_{J',J-1} \cdot \delta_{M',M}$$

$$- a(J,j,J+2N+1) \cdot \left(\frac{(J+M+1)(J-M+1)}{(J+1)(2J+3)} \right)^{\frac{1}{2}} \delta_{N',N} \cdot \delta_{J',J+1} \cdot \delta_{M',M} \Big\} \qquad (13.3)$$

where $b \equiv 0$ for J=0 (see (8.9). Substituting expression (13.3) into (13.2) leaves us with a sum over M(= J,J-1,..,-J) which can easily be carried out since the energies in the delta-functions do not depend on M. With the sums

$$Q_1 \equiv \sum_{M} \frac{(J+M)(J-M)}{J(2J-1)} = \frac{1}{3}(2J+1) \qquad (13.4a)$$

$$Q_2 \equiv \sum_{M} \frac{(J+M+1)(J+1-M)}{(J+1)(2J+3)} = Q_1 \qquad (13.4b)$$

we find for the emission spectrum from the state ${}^{2}\Phi^{JM}_{I,j}$:

$$i_\eta(IjJ,\varepsilon) = \frac{C_1 D^2}{3} \Big\{ |b(J,j,J-1)|^2 \cdot \delta(\varepsilon(I,jJ) - \varepsilon(0(J-1),1s) - \varepsilon)$$

$$+ \sum_{N=0}^{\infty} \Big[|a(J,j,J+2N+1)|^2 + |b(J,j,J+2N+1)|^2 \Big] \cdot$$

$$\cdot \delta(\varepsilon(I,jJ) - \varepsilon(N(J+1),1s) - \varepsilon) \Big\} \qquad (13.5)$$

Again, b is taken to be identical to zero for J=0. In the following we omit the index η and put for convenience:

$$I^{(e)}(IjJ,\varepsilon) = \frac{3}{C_1 D^2} \cdot i(IjJ,\varepsilon) \qquad (13.6)$$

By integrating the emission spectrum (13.5) over the energy we find the total probability per unit time of the emission of a photon of polarization η. Summing the result over all polarizations yields the reciprocal of the radiative lifetime $\tau_r(jJ)$ of the state $\Psi^{JM}_{I,j}$,

$$\tau_r^{-1}(jJ,\varkappa) = C_1 D^2 \cdot N_\delta(jJ,\varkappa) \tag{13.7}$$

where

$$N_\delta(jJ,\varkappa) = 1 - \sum_{N=0}^{\infty} |a(J,j,J+2N)|^2 \tag{13.8}$$

N_δ^{-1} can be regarded as the normalization constant of (13.6) and was obtained in analogy to Ham's treatment (1973a, eqn. 5.8b). $\sum_N |a(J,j,J+2N)|^2$ is the admixture of the s-J-states (8.6a) and has been discussed for various values of $\varkappa$ and δ in § 11. From (8.10) we note that N_δ represents the total p-admixture of the states (8.6b and c), which reduces for J=0 to the admixture of the p-(J+1)-states (see (11.18)). In the case of zero coupling strength N_δ will either be equal to 1 for a pure p-state (8.6b) and (8.6c) or equal to zero for an s-state (8.6a). The radiative lifetime of a 2p electronic state is given by $\tau_r(p) = [C_1 D^2]^{-1}$, and $N_\delta(j,J,\varkappa)$ is thus equal to the ratio of the radiative lifetime of a pure p-state to that of a type I vibronic state $\Psi^{JM}_{I,j}$. As Ham (1973a) has shown for the strong coupling limit (see § 7), the energetically low lying type I vibronic states have equal admixtures of 2s and 2p electronic states and in this case we find $N_\delta = 0.5$, independent of the electronic 2s-2p spacing and independent of j and J.

At zero temperature three cases occur:

(α) A type I state with j=J=0 is lowest. As seen in § 11, for $\delta \leq 0$ this is the case for all ε_G. For $\delta > 0$, however, this state is lowest only for stronger coupling. With (13.5 and 13.6) we find:

$$I_\delta^{(e)}(I00,\varepsilon) = \sum_{N=0}^{\infty} M_\delta^{(e)}(2N+1)\cdot\delta\left(\varepsilon(I,00)-\varepsilon(N1,1s)-\varepsilon\right) \tag{13.9}$$

where the strengths of the odd (2N+1)-phonons lines (N=0,1,2,...) are given by .

$$M_\delta^{(e)}(2N+1) = \left|a(0.0,2N+1)\right|^2 \tag{13.10}$$

(β) A type I state with j=0,J=1 is lowest. Complementary to (α), this situation occurs only for $\delta > 0$ and for weaker coupling:

$$I_\delta^{(e)}(I01,\varepsilon) = M_\delta^{(e)}(0)\cdot\delta\left(\varepsilon(I,01)-\varepsilon(00,1s)-\varepsilon\right) + \sum_{N=0}^{\infty} M_\delta^{(e)}(2N+2)\cdot\delta\left(\varepsilon(I,01)-\varepsilon(N2,1s)-\varepsilon\right) \tag{13.11}$$

where the even zero-phonon and (2N+2)-phonons lines (N=0,1,2,...) are given by

$$\begin{aligned} M_\delta^{(e)}(0) &= \left|b(1.0,0)\right|^2 \\ M_\delta^{(e)}(2N+2) &= \left|a(1,0,2N+2)\right|^2+\left|b(1,0,2N+2)\right|^2 \end{aligned} \tag{13.12}$$

(γ) As a consequence of the behaviour of the two lowest levels outlined in (α) and (β), see § 11, we expect a levels crossing for $\delta > 0$ at some definite value of ε_G, and emission at T=0 will occur from both states j=0,J=0 and J=1:

$$I_\delta^{(e)}\left(\begin{matrix}I00\\I01\end{matrix}\middle|\,\varepsilon\right) = \frac{1}{4}\left\{I_\delta^{(e)}(I00,\varepsilon)+3I_\delta^{(e)}(I01,\varepsilon)\right\} \tag{13.13}$$

As a consequence of the energies (13.1b), the lines of the spectra have uniform spacings which are independent of ε_G. However, the positions of the total emission spectra depend on the coupling strength.

Using the expressions (13.9 to 13.13), the emission spectra have been given for representative values of δ and α in the Graphs 13 to 16. In the case of $\delta = 0$ the spectra belonging to the $(j = 0, J = 1)$-level are also shown (Graph 14). The positions of the delta-functions from a $(j = J = 0)$-level are given by $\varepsilon''_o - (2N+1)$ with $\varepsilon''_o = \varepsilon(I,00) + \varepsilon_o - 3/2$, and from a $(j = 0, J = 1)$- level by $\varepsilon'_o - 2N$ with $\varepsilon'_o = \varepsilon(I,01) + \varepsilon_o - 3/2$, where $N = 0,1,2,\ldots$, ε_o is taken as a given constant and $\varepsilon(I,00)$, $\varepsilon(I,01)$ follow from the computations of § 11. Of course, $\varepsilon'_o = \varepsilon''_o$ for $\varepsilon(I,00) = \varepsilon(I,01)$. Values for $N_\delta(jJ,\alpha)$ have also been included in the graphs and were obtained from the Tables 5, 6, and (13.8). $N_\delta(jJ,\alpha)$ represents the total 2p-admixture and is therefore given by the sum of the strengths of all the delta-functions of a spectrum.

For weak coupling the overlap integrals between the type I vibronic states (8.8) with $j = 0$, $J = 0$, or 1 and the states $\Psi_{N'J'M'}(1s)$ with small N' are largest and the few-phonon lines dominate. The emission spectra are now strongly affected by the kind of state which is lowest at $\varepsilon_G = 0$. When the coupling strength increases, the influence of the many-phonons lines becomes appreciably prominent, as expected from the semi-classical theory of Toyozawa and Inoue (1966), and the spectra resemble Poisson-distributions. In strong coupling the 2s- and total 2p-admixtures of the vibronic states, and

also $N_\delta(jJ,\varkappa)$, each approach the value $\frac{1}{2}$. For given coupling strength we note that as δ decreases from positive to negative values, N_δ decreases and so do the strengths of the individual phonons lines. Moreover, the positions of the maxima in the spectra do not depend significantly on the ordering of the electronic states. Note also the crossing of the two lowest levels in Graph 16 at $\varkappa \approx 1.227$.

A more detailed analysis of the spectra can be achieved by plotting the strengths of the individual phonons lines (13.10 and 13.12) v.s. coupling strength. This has been done for $\delta = 0$ in Graph 17 where the odd- and even-phonons lines correspond to Graphs 13 and 14, respectively. The $(\varkappa, M^{(e)})$-coordinates of the maxima of the 1-, 3-, 5-phonons lines are approximately given by (0.97,0.383), (1.90,0.208), (2.41,0.165), and for the 0-, 2-, 4-phonons lines by (0,1), (1.30,0.305), (2.10,0.192), respectively. The lines do not follow exactly a Poisson-distribution.

(b) At Higher Temperatures

The emission spectrum for temperatures greater than zero consists out of two contributions, one of them comes from the type I vibronic states (8.8), the other one from the type II states (8.11). Using the general expression for the emission (12.1), we can write in analogy to above

$$i_{\eta T} = \frac{1}{A} \cdot \left\{ A_I \, i_{\eta T}(I) + A_{II} \, i_{\eta T}(II) \right\} \qquad (13.14)$$

where the emission spectrum for the type I states is given by

$$i_{\eta T}(I) = \frac{C_1}{A_I} \cdot \sum_{jJM} \exp\{-\varepsilon(I,jJ)/\beta\} \cdot \sum_{N'J'M'} \left| \langle \Psi^{JM}_{I,j} | D_\eta | \Psi_{N'J'M'}(1s) \rangle \right|^2 \cdot \delta\left(\varepsilon(I,jJ) - \varepsilon(N'J',1s) - \varepsilon \right) \qquad (13.15)$$

with

$$A_I = \sum_{jJ} (2J+1)\cdot \exp\{-\varepsilon(I,jJ)/\beta\} \tag{13.16}$$

Similarly, the emission spectrum for the type II states reads with (10.11 and 10.12)

$$i_{\eta\tau}(II) = \frac{C_2}{A_{II}} \cdot \sum_{NJM} \exp\{-\varepsilon(II,NJ)/\beta\} \cdot \sum_{N'J'M'} \left| \langle \Psi^{JM}_{II,N} \mid D_\eta \mid \Psi_{N'J'M'}(1s) \rangle \right|^2 \cdot$$

$$\cdot \delta(\varepsilon(II,NJ) - \varepsilon(N'J',1s) - \varepsilon) \tag{13.17}$$

with

$$A_{II} = \sum_{NJ} (2J+1)\cdot \exp\{-\varepsilon(II,NJ)/\beta\} \tag{13.18}$$

and

$$\beta = \frac{kT}{\hbar\omega} \tag{13.19}$$

where k is the Boltzmann Constant and T the absolute temperature. Furthermore,

$$A = A_I + A_{II} \tag{13.20}$$

We recall $\varepsilon(N'J',1s)$ is given by (13.1b). Note that we again ignore the variation of C_1 over the energy range of the vibronic states.

The emission spectrum for the type I states can now be expressed in terms of the coefficients a,b of the linear combinations (8.8). Taking again $\eta = z$, the calculation of the matrix element in (13.15) and the summations over M,N',J',M' are identical to the ones in § 13(a). Omitting again η, we find with (13.3, 13.4):

$$I^{(e)}_\tau(I) = A_I^{-1} \cdot \sum_{jJ} (2J+1)\cdot \exp\{-\varepsilon(I,jJ)/\beta\} \cdot I^{(e)}(IjJ,\varepsilon) \tag{13.21}$$

where $I^{(e)}(IjJ,\varepsilon)$ is given by (13.5 and 13.6).

Since the type II states do not depend on the coupling

constant, we also expect their contribution to the emission spectra to be independent of ε_G. Using (8.6d) and $\eta = z$, the matrix elements in (13.17) are given by

$$\langle \Xi^{JM}_{II,N} \mid D_z \mid \Xi_{N'J'M'}(1s) \rangle = \frac{D \cdot M}{\sqrt{J(J+1)}} \cdot \delta_{N',N} \cdot \delta_{J',J} \cdot \delta_{M',M} \qquad \text{for } J \geq 1 \tag{13.22}$$

The energy difference between all the states involved in part (13.17) of the emission spectrum is thus independent of N and J and given by $\mathcal{E}(II,NJ) - \mathcal{E}(NJ,1s) = \varepsilon_o - \delta$. Part (II) of the spectrum therefore consists only out of a single line, the position of which depends only on the electronic 2s-2p-spacing but not on ε_G or T.

With (13.6) we find

$$I^{(e)}_T(II) = A^{-1}_{II} \sum_{NJ} (2J+1) \cdot \exp\{-\varepsilon(II,NJ)/\beta\} \cdot \delta(\varepsilon_o - \delta - \varepsilon) \tag{13.23}$$

$$= \delta(\varepsilon_o - \delta - \varepsilon)$$

The strength of this line is according to (13.14) given by A_{II} which depends on δ and β but not on ε_G. Using the general relation

$$\sum_{k=0}^{\infty} a^{kx} = \frac{1}{1 - a^x} \qquad (a > 1,\ x < 0) \tag{13.24}$$

we find with (13.18),

$$A_{II} = \frac{e^{(\delta - \frac{5}{2})/\beta} \cdot (3 - e^{-1/\beta})}{(1 - e^{-2/\beta})(1 - e^{-1/\beta})^2} \tag{13.25}$$

At very small temperatures A_{II} is approximately given by $3 \cdot \exp\{(\delta - 5/2)/\beta\}$.

The total emission spectrum for $T > 0$ is thus given by

$$I_T^{(e)} = \frac{1}{A} \left\{ A_I I_T^{(e)} (I) + A_{II} I_T^{(e)} (II) \right\} \qquad (13.26)$$

Taking into account all significant contributions up to $J = 30$, (13.26) has been computed for several values of δ, ε_G and β (Graphs 18 to 21). In this calculation we replace the delta-functions by Gaussians with areas equal to 1. This imposes some requirements on the magnitude and width of the Gaussians. Denoting the strength and position of a delta-function by M and L, the corresponding Gaussian then reads

$$\frac{2M}{H\sqrt{2\pi}} \cdot \exp \left\{ -\frac{2}{H^2} \cdot (\varepsilon - L)^2 \right\} \qquad (13.27)$$

where H is the width of the function. The factor $\frac{2}{H\sqrt{2\pi}}$ ensures that the integration over all ε yields M. However, the magnitude is in general altered by the same factor, unless we choose $H = \frac{2}{\sqrt{2\pi}}$ in the computation we put $H = 0.5$.

As the temperature increases, the spectra are smoothed and shift towards lower energies. As δ increases, the areas under the bands become larger as well. The contribution of the type II states increase with β and δ but decrease for increasing ε_G. Note that the structure of the bands (apart from the type II peak) does not appear to depend significantly on δ.

§ 14 Numerical Calculation of the Absorption Spectrum at Zero Temperature

Taking into account that transitions take place only from the vibronic ground state (13.1) with $N' = J' = M' = 0$, the matrix elements (13.3 and 13.22) reveal which of the excited vibronic states are connected by the electric dipole operator. We find that transitions can occur only to vibronic type I states (8.8) with J=1, j=0,1,2,..., but not to type II states since the latter exist only for total angular momentum J greater than zero. Omitting again the index η as the spectrum is isotropic, we are able to define the normalised absorption spectrum for T = 0 and given δ and ε_G by

$$I_\delta^{(a)}(00,\varepsilon) = \frac{1}{c_2 D^2} \cdot \sigma(00,\varepsilon) \qquad (14.1)$$

where the absorption cross section is given by (12.5). With (8.8) and (13.3) we find

$$I_\delta^{(a)}(00,\varepsilon) = \sum_{j=0}^{\infty} M_\delta^{(a)}(j) \cdot \delta\left(\varepsilon(1,j1) - \varepsilon(00,1s) - \varepsilon\right) \qquad (14.2)$$

where the j-absorption line is by definition given by

$$M_\delta^{(a)}(j) = \left|b(1,j,0)\right|^2 \qquad (j=0,1,2,\ldots) \qquad (14.3)$$

and $\varepsilon(00,1s)$ is found from (13.1b).

(a) Absorption Lines

As seen in § 13, the definition of the 'n-phonons line' is quite unique for emission at T = 0 as the final states of the transitions have simple product wave functions with definite numbers of vibrational quanta. In absorption we can still use the same definition in the weak coupling region

simply by saying that the zero-phonon line is the one which links the state arising from $|1M,00,2p>$, (8.6c), with the ground state $\overset{+}{\downarrow}_{ooo}(1s)$. Accordingly, the one-phonon line in absorption occurs for a transition to a state arising from $|1M,11,2s>$, (8.6a), as this state contains $|1M,00,2p>$ to first order in $\varkappa$; and so on (see § 12). However, for stronger coupling the type I states consist of a large number of product states with different vibrational numbers due to the matrix elements (9.54), and the original definition of a n-phonons line does not make sense. It is then appropriate to associate an absorption line with a certain (J=1)-energy level with quantum number j in the fashion (14.3).

Graphs 22 to 25 show the absorption lines associated with some of the lowest (J=1)-energy levels v.s. coupling strength and give a representative picture for the whole range of δ. Note that $\delta = -0.5$ can at least for weak coupling be regarded as a reference point for the spectra as in this case the lowest (J=1)-states at $\varepsilon_G = 0$ are the degenerate substates (8.6a and c) with $N = 0$. In general, each absorption line may exhibit several relative or absolute extrema. There are several groups of absorption peaks which may be associated with the type A, B, and C energy levels of § 11.

Two situations arise. When the tendency of energy levels crossing is strong (see § 11), a group of absorption peaks can in good approximation be replaced by an envelope line which is a smooth and continuous function and is the sum of mainly one or two intensity contributions. In particular, this can be done for the type B and C absorption lines for $\delta << -0.5$ (Graph 22) and for the type C lines for $\delta >> 0.5$

(Graph 25). Points on an absorption line correspond to points on the associated type B or C energy level. (Note to Graph 22: the introduction of a type (B = 0)-line makes compensational corrections of the type A lines necessary.)

Alternatively, when the tendency of energy levels crossing is weak (see § 11), the intensity overlap consists mainly of two or more absorption lines and does not show a simple functional dependence on ε_G. It is then impractical to introduce envelope lines in the above manner. However, the maxima of a certain group of absorption lines correspond to points on the j-energy levels which lie on lines equivalent to the type B or C levels and with similar ε_G-dependence. An identification of these levels is therefore also possible for weak tendency of crossing and has been indicated in the Graphs 8 and 10. This is the case for the lowest lying type B levels and for all the type C levels for $|\delta| \lesssim 0.5$. In particular, we may formally extend the range of validity of expression (11.21) for the type C levels to $-0.5 < \delta < 0.5$, where $\gamma_1 = 0$, $\gamma_2 = 1$ yields a reasonably good approximation. For $\delta = \pm 0.5$ the dependence of the type C levels on the coupling strength is for all ε_G approx. given by the linear energy corrections (11.7b and 11.8b).

Similarly, we may look for the δ-dependence of the type B and C levels. This has been done in Graph 12 where the major contributions to the intensity of the type B=0 and C=0 absorption lines have been indicated. For strong tendency of levels crossing these contributions arise only either from one or two closely lying levels, as expected. However, for weak tendency two or more energy levels contribute, and the

resulting spread in energy can be large. The existence of type B and C levels can now be seen as a mean position for the various contributions. Expressions (11.20 and 11.21) are then good approximations for all values of δ.

The zero- and one-phonon lines of § 12 (b) provide good approximations for $|\delta| \gg 0.5$ with $\alpha \lesssim 0.75$ and for $\delta \approx -0.5$ with $\alpha \lesssim 0.5$. The zero-phonon line is associated with the lowest type B level in weak coupling for all values of $\delta \neq -0.5$ (see Fig. 6, Graphs 12, 22 to 25). The one-phonon line belongs in weak coupling to the lowest type A level for $\delta < -0.5$ and $-0.5 < \delta \leq 0.5$ and to the lowest type C level for $\delta \geq 0.5$. For $\delta = -0.5$ the distinction between zero- and one-phonon lines becomes impossible and so does the association of the absorption lines in weak coupling to either a type A or B level. Note that the two one-phonon lines for $\delta = 0.5$ belong to a type A and C level, respectively.

Looking now at the functional dependence of the type A, B, C absorption lines, we find that for strong tendency of energy levels crossing the intensities of these lines take approximately the forms:

$$P_A(\varepsilon_G) = \alpha_1 \cdot \varepsilon_G^{A+1} \cdot \exp(-\beta_2 \varepsilon_G) \qquad (A = 0,1,2,..) \qquad (14.4a)$$

$$P_{B,0}(\varepsilon_G) = (1-\alpha_2) \exp(-\beta_2 \varepsilon_G) + \alpha_2 \qquad (14.4b)$$

$$\underset{\alpha_B \geq 1}{P_C}(\varepsilon_G) = \alpha_3 \cdot \left(1 - \exp(-\beta_3 \varepsilon_G)\right) \qquad (14.4c)$$

where α_i, β_i $(i=1,2,3)$ are positive constants for given δ. (14.4a) is appropriate for all type A absorption lines. For $\delta = -2.5$ we find $\alpha_1 = 1/16$, $\beta_1 = 0.64$, where the accuracy decreases for increasing ε_G. For $\delta \ll -0.5$ the points on the

energy levels corresponding to maxima of the type A absorption lines lie approximately on the straight line

$$\varepsilon^{A}_{max} \approx 2.5 + \delta - \varkappa \qquad (\delta << -0.5,\ \varkappa > 0) \qquad (14.5)$$

The envelope line belonging to the lowest type B energy level is approximately given by (14.4b). For $\delta = -2.5$ and $0 \leq \varepsilon_G \leq 16$: $\alpha_2 = 0.7$, $\beta_2 = 0.2$. All further type B and C lines follows approx. (14.4c). For C = 0 we find for $-2.5 \leq \delta \leq 2.5$ and $0 \leq \varepsilon_G \leq 16$; $\alpha_3 \approx 0.05$; and for $\delta = 2.5$: $\beta_3 = 0.5$. For increasing δ, β_3 becomes larger as well. When the tendency of levels crossing is weak, the maxima of the type B and C absorption lines follow approx. (14.4b and c).

(b) Absorption Spectra

The absorption spectra are in general characterised by three different parts originating from the type A, B, and C energy levels with J=1 and their associated absorption lines. The discussion above revealed that each of the type B or C levels belongs in general to a group of lines and that the intensity of a single absorption line with given ε_G can, especially for weak coupling, contain contributions from all three type A,B,C levels. The spread in energy of an absorption peak in a spectrum may thus be taken as a characteristic for the tendency to form a particular type B or C energy level. The introduction of an absorption envelope line means for the spectra that a group of lines is replaced by a single absorption line with some intermediate position.

The Graphs 26 to 39 show the absorption spectra for

representative values of δ and ε_G. The normalization of the spectra has been used as a check that all significant intensity contributions have been taken into account. At low energies the spectra of particularly the intermediate and strong coupling region are characterised by evenly spaced type A absorption lines. At a certain energy the spectra show an absolute maxima associated with the lowest type B level after which the spectra exhibit irregularly spaced lines of different intensities. The spectra at highest energies are featured by a high intensity peak belonging to the type C=O energy level.

It is useful to introduce the sum of the intensities associated with the type A or a particular type B or C absorption peak which is the area under the corresponding part of the line shape function and provides a zeroth moment description of the spectra. This sum is together with the maximal intensity an indication of the spread in energy of a particular peak and has been given in Table 7 for various values of δ and ε_G. It can be seen that the type (B=O)-absorption peak carries about 99 to 70% of the total intensity and the type A peak up to 10 or 20%. All other peaks have lower intensities which increase for increasing coupling strength but decrease for increasing values of $\delta > 0$. Note that in weak coupling and for $\delta << -0.5$ the type A contribution is larger than the type C=O one, but vice versa for $\delta >> 0.5$.

Whenever the lowest adiabatic energy surface of Fig. 5 is far away from the two upper ones, type A absorption lines appear at the low energy end of the spectra. This is certainly the case for $\delta << -0.5$ at all coupling strengths. The type A

TABLE 7

The Table shows the order of the maximal intensities of the type A and the first few type B and C absorption lines for typical values of δ and ξ_G. In the strong coupling limit asymptotic values of the intensities have been stated for some of the lines.

The figures in brackets are the sums of the intensities of a particular type of absorption lines, usually linked with some peak in the spectra when ξ_G takes the specific values 0.25, 1, 4 and 16. In the cases of no entry the contributions are less than 0.005.

When the type A and (B=0) -absorption lines overlap, it is impossible to state the intensities or their sums for either the type A or (B=0) -lines, apart from an estimate at strong coupling. However, the total sum of the intensities of the type A and (B=0) -lines can always be given.

δ / ξ_G / Absorpt. Peak	-2.5				0				2.5			
	$\ll \frac{\lvert\delta\rvert}{2}$ (0.25)	$\leq \frac{\lvert\delta\rvert}{2}$ (1)	$> \frac{\lvert\delta\rvert}{2}$ (4)	$\gg \frac{\lvert\delta\rvert}{2}, \gg 1$ (16)	$\ll 1$ (0.25)	≤ 1 (1)	> 1 (4)	$\gg 1$ (16)	$\ll \frac{\lvert\delta\rvert}{2}$ (0.25)	$\leq \frac{\lvert\delta\rvert}{2}$ (1)	$> \frac{\lvert\delta\rvert}{2}$ (4)	$\gg \frac{\lvert\delta\rvert}{2}, \gg 1$ (16)
A $\sum$ A	$\leq 10^{-2}$ (o.o1)	10^{-2} (o.o4)	10^{-2} (o.10)	2.10^{-2} (o.14)	$\leq 10^{-2}$ (?)	Overlap with (B=0)-abs.peak (?)	(?)	3.10^{-2} ($\approx$o.2)	$\leq 10^{-3}$ (o.oo)	Overlap with (B=0)-abs.peak (?)	(?)	4.10^{-2} ($\approx$o.2)
B = 0 $\sum$ (B=0)	1 (o.99)	1 (o.95)	1 (o.86)	7.10^{-1} (o.75)	1 (?)	10^{-1} (?)	10^{-1} (?)	3.10^{-1} ($\approx$o.7)	1 (o.99)	1 (?)	10^{-1} (?)	2.10^{-1} ($\approx$o.7)
$\sum$(A+(B=0))	(1.00)	(o.99)	(o.96)	(o.89)	(o.99)	(o.97)	(o.93)	(o.88)	(o.99)	(o.98)	(o.95)	(o.91)
B = 1 $\sum$ (B=1)	$\leq 10^{-4}$	10^{-3}	10^{-2} (o.o1)	4.10^{-2} (o.o3)	$\leq 10^{-2}$	10^{-2} (o.o1)	10^{-2} (o.o2)	3.10^{-2} (o.o3)	$\leq 10^{-4}$	10^{-3}	10^{-2} (o.o1)	2.10^{-2} (o.o2)
B = 2 $\sum$ (B=2)	$\leq 10^{-8}$	10^{-5}	10^{-3}	10^{-3} (o.o1)	$\leq 10^{-5}$	10^{-3}	10^{-2} (o.o1)	10^{-2} (o.o1)	$\leq 10^{-7}$	10^{-5}	10^{-3}	10^{-3}
B = 3 $\sum$ (B=3)	$\leq 10^{-9}$	10^{-7}	10^{-4}	10^{-3} (o.o1)	$\leq 10^{-8}$	10^{-4}	10^{-3}	10^{-2} (o.o1)	$\leq 10^{-7}$	10^{-6}	10^{-4}	10^{-3}
C = 0 $\sum$ (C=0)	$\leq 10^{-3}$	10^{-2} (o.o1)	10^{-2} (o.o3)	5.10^{-2} (o.o5)	$\leq 10^{-2}$	10^{-2} (o.o2)	10^{-2} (o.o4)	5.10^{-2} (o.o5)	$\leq 10^{-2}$ (o.o1)	10^{-2} (o.o2)	10^{-2} (o.o4)	5.10^{-2} (o.o5)
C = 1 $\sum$ (C=1)	$\leq 10^{-6}$	10^{-5}	10^{-3}	10^{-3} (o.o1)	$\leq 10^{-5}$	10^{-4}	10^{-3}	10^{-2} (o.o1)	$\leq 10^{-5}$	10^{-4}	10^{-3}	10^{-2} (o.o1)

lines exhibit a distribution, the maximum of which is shifted towards lower energies and larger values of quantum number A as ε_G and the adiabatic well becomes deeper (fixed δ). The width of this distribution increases for increasing coupling strength. In the strong coupling region the distribution resembles a Poisson-distribution with approximately equidistant lines of energy separation 1.

For $\delta \geq -0.5$ type A absorption lines are only then sufficiently separated from the type B lines when the coupling is sufficiently strong and δ sufficiently small (see Graph 37). The maximal intensities and the associated sums of the type A intensities are about 0.01 to 0.05 and 0.1 to 0.3, respectively, for $\varepsilon_G = 16$ and $|\delta| \leq 5$ and decrease for decreasing values of δ. For $\delta < -0.5$ the positions of the maxima are approximately given by (14.5).

The type B states with J=1, and the middle energy surface, can be associated with a series of absorption peaks, the positions of which are given by the energies of these states. Because of the nature of the type B levels, the relative positions of these peaks do not change significantly with ε_G, and the separation of the peaks is approximately equal to 2. However, according to (11.20) the absolute positions of the peaks depend on $(-\delta)$. Because of this circumstance the lowest type B absorption peaks can overlap the type A lines in such a way that, even in strong coupling, a type A absorption peak is not visible in the spectra, which is the case when the lowest and middle adiabatic energy surfaces lie close together.

In the interval $-5 \leq \delta \leq 5$, the maximal intensities and

'areas' associated with the type (B=0)-peaks range from about 0.8 to 0.2 and from about 0.84 to ≈ 0.7, respectively. (We note that the total intensity sum of type A lines and (B=0)-peak at $\varepsilon_G = 16$ is approx. 0.91 and 0.94 for $\delta = -5$ and 5, respectively, and approaches 1 as $|\delta|$ becomes very large.) The magnitudes of the type B peaks with $B \geq 1$ increase for increasing coupling strengths but descend for increasing quantum numbers B.

The high energy end of the spectra is characterised by absorption peaks which can be associated with type C states with J=1 and the upper adiabatic energy surface. The positions of these peaks are of course given by the type C energy levels which are shifted towards higher energies as ε_G and $|\delta|$ increases (see 11.21). The separations of the peaks are $\gtrsim 2$ and approximately constant for given ε_G but increase for increasing values of ε_G. Whereas in the strong coupling limit the maximal intensities and the associated intensity sums of the type (C=0)-peaks are approximately independent of δ for $|\delta| \lesssim 2.5$ and are each about 0.05 for $\varepsilon_G = 16$, these quantities increase for decreasing δ and decrease for increasing δ (i.e. for $\varepsilon_G = 16$, $\delta = -5$ and 5, each of them are about 0.06 and 0.04, respectively). All higher type C peaks have lower intensities.

Note that at $\delta \gg 0.5$ and strong coupling, i.e. when the lowest and middle energy surfaces are far away from the highest one, the spectra are characterised by an 'energy gap' of extremely low intensity (Graph 39).

§ 15 Emission and Absorption Lines in the Strong Coupling Limit

We make use now of explicit expressions for the vibronic type I eigenstates and for the 3-d harmonic oscillator eigenfunctions and are able to state the one- and zero-phonon lines of emission in closed form.

The lowest lying excited eigenstates are in the strong coupling limit given by (7.9 and 7.27). The radial functions $F_l^{(j)}(q)$ in (7.27) are obtained from (11.10 and 11.14), with the energy eigenstates given by (11.13). Emission occurs again to the states $\Psi_{N'J'M'}(1s)$ of (13.1). Now, however, we require these states as explicit functions of the polar coordinates (q, θ, φ). With Flügge (1965) we find the wave functions of the 3-d harmonic oscillator with energies $\varepsilon = 2n + \ell + \frac{3}{2}$ to

$$\Psi_{n\ell m}(q,\theta,\varphi) = c_{n\ell}\, q^{\ell} e^{-\frac{q^2}{2}} F\left(-n, \ell+\tfrac{3}{2}; q^2\right) \cdot Y_{\ell}^{m}(\theta,\varphi) \tag{15.1}$$

where $C_{n\ell}$ denotes the normalisation constant and Y_ℓ^m the spherical harmonics defined by Messiah (1969, p. 494). The confluent hypergeometric series $F(\alpha,\beta;z)$ is for $\alpha = -n$ given by a polynominal of n-th power

$$F\left(-n,\beta,z\right) = \sum_{s=0}^{n} (-1)^s \frac{\Gamma(n+1)\cdot\Gamma(\beta)}{\Gamma(n-s+1)\cdot\Gamma(\beta+s)} \cdot \frac{z^s}{s!} \tag{15.2}$$

where the gamma function is defined by $\Gamma(X+1) = X!$ with X being any real number. For n=0: $F(0,\beta,z) = 1$.

The transition matrix elements may be calculated in analogy to (13.3). The emission spectrum at zero temperature occurs from a type I state with j=J=M=0 and is then found

from (13.6):

$$I^{(e)}(I00,\varepsilon) = \frac{1}{2} \sum_{N'=0}^{\infty} \left| X^{(j=0)}_{N',j'=1} \right|^2 \delta\left(\varepsilon(I,00) - \varepsilon(N'1,1s) - \varepsilon \right) \tag{15.3}$$

where

$$X^{(0)}_{N',j'=1} = \int_0^{\infty} q^2 \cdot f_{N',j'=1}(q) \cdot F_1^{(0)}(q)\, dq \tag{15.4}$$

and

$$f_{N',j'=1}(q) = C_{N',j'=1} \cdot q \cdot \exp\left(-\frac{q^2}{2}\right) \cdot F\left(-N', \frac{5}{2}; q^2\right) \tag{15.5}$$

Transitions occur only to the states (13.1) with J'=1, and the spectrum consists purely of odd-phonons lines.

Putting N'=0, the strength of the one-phonon line in the strong coupling limit is then given by

$$M^{(e)}_{SCL}(1) = \frac{1}{2} \cdot \left| X^{(0)}_{01} \right|^2 = \frac{4}{3\pi} \cdot \exp(-2\varepsilon_G) \cdot |z_1| \tag{15.6}$$

where we used $q_0 = \sqrt{2\varepsilon_G}$ of § 6 and 7. z_1 denotes the definite integral

$$z_1 = \int_0^{\infty} q^2 \exp\left(-q^2 + \sqrt{2\varepsilon_G}\, q\right) dq \tag{15.7}$$

Introducing

$$\exp\left(\sqrt{2\varepsilon_G}\, q\right) = \sum_{t=0}^{\infty} \frac{\left(\sqrt{2\varepsilon_G}\, q\right)^t}{t!} \tag{15.8}$$

the integration over q can be carried out (Bronstein et al. 1967, p. 350):

$$z_1 = \sum_{t=0}^{\infty} \frac{(2\varepsilon_G)^{\frac{t}{2}}}{2\, t!} \cdot \Gamma\left(\frac{t+3}{2}\right) \tag{15.9}$$

It is now convenient to introduce the error function defined by Gradshteyn et al. (1965) as

$$\operatorname{erf}(x) = \frac{2}{\sqrt{\pi}} \int_0^x e^{-t^2} dt = \frac{2}{\sqrt{2\pi}} \cdot e^{-x^2} \cdot \sum_{K=0}^{\infty} \frac{\left(\sqrt{2}\, x\right)^{2K+1}}{(2K+1)!!} \tag{15.10}$$

where $(2K+1)!! = 1\cdot3\cdot5\cdot\ldots\cdot(2K+1)$. Making use of the properties of the gamma function, we arrive after some tedious manipulation at

$$M^{(e)}_{scL}(1) = \frac{1}{6\pi}\cdot e^{-2\varepsilon_G}\cdot\left|\frac{\sqrt{2\pi}}{2}(\varepsilon_G+1)\cdot e^{\frac{\varepsilon_G}{2}}\cdot\left\{1+\operatorname{erf}\left(\sqrt{\frac{\varepsilon_G}{2}}\right)\right\} + \sqrt{\varepsilon_G}\right|^2 \tag{15.11}$$

Since $\varepsilon_G \gg 1$ we may write in very good approximation $\operatorname{erf}\left(\sqrt{\frac{\varepsilon_G}{2}}\right) \approx 1$ and find

$$M^{(e)}_{scL}(1) = \frac{1}{3}\cdot(\varepsilon_G+1)^2\cdot\exp(-\varepsilon_G) \tag{15.12}$$

Similarly, we can calculate the emission spectrum from the type I state with j=0, J=1, only. The transitions to the ground state (13.1) with N'=J'=0 then define a zero-phonon line, the strength of which is in the strong coupling limit given by

$$M^{(e)}_{scL}(0) = \frac{1}{6}\cdot\left|X^{(0)}_{00}\right|^2 = \frac{2}{3\pi}\cdot\exp(-2\varepsilon_G)\cdot|z_2|^2 \tag{15.13}$$

where

$$z_2 = \int_0^\infty q\,\exp\left(-q^2+\sqrt{2\varepsilon_G}\,q\right)dq \tag{15.14}$$

can be calculated in the same way as above. We find

$$M^{(e)}_{scL}(0) = \frac{1}{6\pi}\cdot e^{-2\varepsilon_G}\cdot\left|1+\frac{\sqrt{2\pi\,\varepsilon_G}}{2}\cdot\exp\left(\frac{\varepsilon_G}{2}\right)\cdot\left\{1+\operatorname{erf}\left(\sqrt{\frac{\varepsilon_G}{2}}\right)\right\}\right|^2 \tag{15.15}$$

Again we put $\operatorname{erf}\left(\sqrt{\frac{\varepsilon_G}{2}}\right) \approx 1$ for $\varepsilon_G \gg 1$ and obtain

$$M^{(e)}_{scL}(0) = \frac{1}{3}\,\varepsilon_G\,\exp(-\varepsilon_G) \tag{15.16}$$

Using (15.11 and 15.15) the strengths of the one- and zero-phonon lines have been plotted v.s. $\varkappa$ for $\delta = 0$ in the

Graphs 41 and 42, together with the computed values of § 13 and the weak coupling results of § 12(b). As seen, the strong coupling expressions approximate the computed lines well for intermediate and strong coupling. We have also computed the emission spectrum (15.3) which is a good approximation of the spectra in the Graphs 13, 15, 16 for strong coupling. However, we were not able to find a closed expression similar to (15.11).

The absorption lines from the ground state (13.1) with $N'=J'=0$ to the lowest lying type I states of strong coupling can be calculated in a similar manner. Of course, the $(j=0)$-absorption line is identical to the zero-phonon emission line. The strength of the $(j=1)$-absorption line is defined by the transition probability to the type I state with $j=J=1$ and found to be

$$M^{(a)}_{SCL}(1) = \frac{1}{6}\cdot\left|\chi^{(1)}_{00}\right|^2 = \frac{4}{3\pi}\cdot\exp(-2\varepsilon_G)\cdot\left|z_1 - \sqrt{2\varepsilon_G}\cdot z_2\right|^2 \qquad (15.17)$$

where z_1, z_2 are given by (15.7 and 15.14), respectively. We obtain

$$M^{(a)}_{SCL}(1) = \frac{1}{6\pi}\cdot e^{-2\varepsilon_G}\cdot\left|\frac{\sqrt{2\pi}}{2}\cdot(\varepsilon_G-1)\cdot e^{\frac{\varepsilon_G}{2}}\cdot\left\{1+\operatorname{erf}\left(\sqrt{\frac{\varepsilon_G}{2}}\right)\right\} + \sqrt{\varepsilon_G}\right|^2 \qquad (15.18)$$

With the strong coupling condition $\varepsilon_G \gg 1$ this expression reduces to

$$M^{(a)}_{SCL}(1) = \frac{1}{3}\cdot(\varepsilon_G-1)^2\cdot\exp(-\varepsilon_G) \qquad (15.19)$$

Graph 43 shows the strength of the $(j=1)$-absorption line v.s. $\varkappa$ for $\delta = 0$. Expression (15.18) and the results of § 12(b) approximate well the computed line of § 14 in strong and weak coupling, respectively. For the absorption spectrum we refer to § 16.

§ 16 Absorption Line Shape in Semi-Classical Approximation

The explicit calculation of the absorption spectrum for stronger coupling presents a problem in so far as the differential equations (7.19) do not decouple for small q, and it is in this region where we expect from the Frank-Condon approximation the transition intensities to have maxima.

In the following we shall calculate the line shape function in semi-classical approximation by essentially the same method which has been used by Toyozawa and Inoue (1966) to investigate the absorption bands of ideal Jahn-Teller systems. However, whereas they used the high temperature Boltzmann distribution, we shall employ the proper quantum-statistical probability distribution.

Assuming non-degenerate electronic states we can utilize the Born-Oppenheimer approximation of § 2. We then employ the semi-classical Franck-Condon principle in which the nuclei are regarded as standing still during the optical transition (Lax 1952).

After an optical transition, the heavy particles, subject to a new potential, will not be in equilibrium with the latter. Hence, the important final states for the transition will be excited states with large quantum numbers which, according to the Bohr correspondence principle, can be treated as approximately classical. Thus the final vibrational state $\chi_{nm}(\underset{\sim}{Q})$ will oscillate rapidly except near the classical turning points. A good approximation to the sum over the final states ℓ of the absorption cross section (12.5) can therefore be obtained by replacing $E_\ell^{(b)}$ in the delta-function

by the effective Born-Oppenheimer potential $E^{(b)}(\underset{\sim}{Q})$ for the heavy particles when the electron is in the excited state b which is nothing but a mean value independent of ℓ. Similarly, if many initial states k are involved, it is convenient to use a corresponding mean-value approximation $\bar{E}^{(a)} = E^{(a)}(\underset{\sim}{Q})$.

Furthermore, we shall make use of the Condon approximation in which the dependence of the electric dipole matrix element on nuclear positions $\underset{\sim}{Q}$ is either neglected or averaged over (Dexter 1958). The transition probability can then be written as a product of an electronic factor and a line shape function which depends on the vibrational motion only.

The normalized absorption line shape function in the approximation of the semi-classical Franck-Condon principle is given by

$$I^{(a)}(\omega) = \frac{1}{r} \cdot \sum_{f=1}^{r} \int \cdots \int \prod_{n} dQ_n \cdot P_i(\underset{\sim}{Q}) \cdot \delta\left(E_f(\underset{\sim}{Q}) - E_i(\underset{\sim}{Q}) - \hbar\omega\right) \quad (16.1)$$

where $P_i(\underset{\sim}{Q})$ is the quantum-statistical probability distribution for the heavy particles in the initial state. $E_i(\underset{\sim}{Q})$ and $E_f(\underset{\sim}{Q})$ are the energies of the initial and final states. We assume that E_f, being the solution of the static JT problem, is a multi-valued function of $\underset{\sim}{Q}$ and has a r-fold (electronic) degeneracy for $\underset{\sim}{Q}=0$. In the product n runs over all vibrational coordinates. Similarly, the sum is carried out over all r energy surfaces.

As seen from § 6, the energy solutions of the static problem of the (s+p) ⊠ T_{1u}-system depend only on the radial coordinate q as a direct result of the spherical symmetry of the model Hamiltonian. It is therefore of advantage to

introduce the polar coordinates (q, θ, φ) also for the probability distribution P_i.

The vibronic states associated with the electronic ground state have the simple product form (13.1), where the wave functions of the 3-d oscillator are given by (15.1). P_i is thus the probability distribution for the 3-d-isotropic oscillator. Landau and Lifschitz (1967) derived the quantum mechanical probability for the 1-d harmonic oscillator. It is easy to extend these formulae to the 3-d case. The quantum mechanical probability that when the system is in the initial electronic ground state it will be found in the volume element $d\Omega = d\varphi\, d\vartheta \sin\vartheta\, dq q^2$ of phase space is represented by

$$dw_\Omega = P_i\, d\Omega \tag{16.2}$$

The probability distribution function P_i is given by

$$P_i = \left(\frac{b}{\pi}\right)^{\frac{3}{2}} \cdot \exp(-bq^2) \tag{16.3}$$

with the parameter $b = \tanh\frac{1}{2\beta}$ (16.4)

where $\beta = \frac{kT}{\hbar\omega}$ (16.5)

At high temperatures, $\beta \gg 1$, we find $b \approx \frac{1}{2\beta}$. The quantisation ceases to have any effect, and P_i is the classical Boltzmann-distribution within the energy continuum of the initial electronic state. At low temperatures, $\beta \ll 1$, i.e. $b \approx 1$. P_i takes the form of the purely quantum probability distribution for the coordinate in the ground state of the oscillator; this is the square of the modulus of its ground state wave function. It corresponds to the fact that when $kT \ll \hbar\omega$ the oscillations of the oscillator are practically

unexcited.

We again use the notation employed in § 6 and 7. The expression for the normalized absorption function in the general case of non-zero electronic 2s-2p splitting is given by

$$I^{(a)}(\varepsilon) = \frac{1}{4} \cdot \sum_{i=1}^{4} \int_0^{2\pi} d\varphi \int_0^{\pi} d\theta \sin\theta \int_0^{\infty} dq\, q^2 \cdot \left(\frac{b}{\pi}\right)^{\frac{3}{2}} \cdot \exp(-b q^2) \cdot \delta\left(\varepsilon_i(q) - \varepsilon_a(q) - \varepsilon\right) \tag{16.6}$$

where the adiabatic energy surfaces $\varepsilon_i(q)$ are given by (6.15 and 6.16) and $\varepsilon_a(q)$ by $-\varepsilon_o + \frac{q^2}{2}$. As these energies do not depend on any angular coordinates, the integrals can easily be calculated by making use of the following principle property of the delta-function δ (Messiah 1969, p. 469),

$$\delta\left[g(q)\right] = \sum_n \frac{1}{|g'(q_n)|} \cdot \delta(q - q_n) \tag{16.7}$$

where $g(q_n) = 0$, $g'(q_n) \neq 0$. We arrive at

$$I^{(a)}(\varepsilon) = \mathcal{J}_1^{(a)}(\varepsilon) + \mathcal{J}_2^{(a)}(\varepsilon) \tag{16.8a}$$

where

$$\mathcal{J}_1^{(a)}(\varepsilon) = \pi^{-\frac{1}{2}} \cdot \left(\frac{b}{2\varepsilon_G}\right)^{\frac{3}{2}} \cdot \sqrt{(\varepsilon - \varepsilon_o)^2 - \delta^2} \cdot |\varepsilon - \varepsilon_o| \cdot \exp\left\{-\frac{b}{2\varepsilon_G}\left[(\varepsilon - \varepsilon_o)^2 - \delta^2\right]\right\} \tag{16.8b}$$

$$\text{for } |\varepsilon - \varepsilon_o| \geq |\delta|$$

$$\mathcal{J}_2^{(a)}(\varepsilon) = \frac{1}{2} \cdot \delta(\varepsilon - \varepsilon_o + \delta) \tag{16.8c}$$

$$\text{for } -\infty < \varepsilon < +\infty \ .$$

The spectrum consists of three parts in accordance with

the three different adiabatic energy surfaces: a delta-function with constant strength and δ-dependent position, and two wings the shape, maxima and positions of which depend on δ^2, ε_G, and b (or T). The wings have reflection symmetry to each other, and there is a gap of $2|\delta|$ between them where the absorption intensity is zero. The intensity contribution of each wing is for all values of δ, ε_G and b 25% of the total intensity.

For $b\delta^2/4\varepsilon_G \ll 1$, i.e. for strong coupling and/or high temperatures, the positions, magnitude of the maxima of the wings, and width at half maximum are given by

$$\varepsilon_{max\ 1/2} = \varepsilon_o \pm \sqrt{\frac{2\varepsilon_G}{b}\cdot\left(1 + \frac{b\delta^2}{4\varepsilon_G}\right)} \qquad (16.9)$$

$$I^{(a)}_{max} = \frac{1}{e}\cdot\sqrt{\frac{b}{2\pi\varepsilon_G}}\cdot\left(1 + \frac{b\delta^2}{4\varepsilon_G}\right) \qquad (16.10)$$

$$\Delta = \frac{7}{6}\cdot\sqrt{\frac{2\varepsilon_G}{b}}\cdot\left(1 - \frac{b\delta^2}{6\varepsilon_G}\right) \qquad (16.11)$$

Note that for $\delta=0$ expressions (16.9 and 16.10) are exact for all ε_G and b.

In order to compare the semi-classical spectra with each other, it is convenient to introduce the new variable $x = (\varepsilon - \varepsilon_o)/\sqrt{2\varepsilon_G}$. The corresponding normalised line shape function $I^{(a)}_{sc}(x)$ is then defined by $I^{(a)}(\varepsilon)d\varepsilon = I^{(a)}_{sc}(x)dx$ where $\varepsilon = \varphi(x)$ and $I^{(a)}_{sc}(x) = I^{(a)}(\varphi(x)) \cdot \varphi'(x)$. It has been drawn in Graph 44 for $\delta=0$ and b=1, $\frac{1}{2}$, $1/4$, (i.e. β=0, 0.91,2) and $\delta/\sqrt{\varepsilon_G} = 5/8, 5/4$ with b=1. For $\delta=0$, $I^{(a)}_{sc}$ is independent of ε_G and can be taken as a reference to the other cases.

We now compare (16.8) with the results of § 14. As expected, best agreement is found for strong coupling where the energy surfaces of Fig. 5 are far apart from each other. A direct comparison has been made in the Graphs 35 to 39. In the same way as the lowest, middle and upper energy surfaces could be associated with the type A, B, and C absorption peaks, respectively, the three semi-classical contributions correspond to these peaks and may be denoted accordingly.

Turning first to the low-energy type A wing, we find good agreement with the computed spectra as regards to the position of the maximum, where the accuracy improves as $|\delta|$ becomes smaller. However, the magnitude of the maximum, the width and the area of the wing are given in good approximation only for $\delta > 0$. The delta-function (16.8c), which corresponds to all of the type B absorption peaks, is placed close to the centre of gravity of the type (B=0)-peak, particularly in the case of $\delta \gtrsim -0.5$. Table 7 shows that (18.8c) takes into account only some fixed part of the total type B intensity with best agreement reached for $\delta \gtrsim 0$. Finally we find that the high-energy type C wing is only roughly related to the type C peaks. In particular, the maximum of the wing occurs at lower energies than the type (C=0)-peak. However, the gap between the type A and B wings (for $\delta \neq 0$) exhibits itself in the spectra as a drop in intensity, especially for large δ.

17 Reduction Factors

In § 5 we examined the properties of the electronic 2p-states and found that their threefold degeneracy can only be lifted by a perturbation of symmetry E_g, T_{2g} or T_{1g}. It is of considerable interest to investigate how the properties of these states compare with those of the lowest type I vibronic states with J=1, which transform in cubic symmetry O_h as T_{1u}.

For the JT-problem this was first done by Ham (1965) who introduced reduction factors by relating the matrix elements of the perturbation within a given vibronic level to the electronic interaction. Whereas the form which this interaction takes within the vibronic level is determined by symmetry, the size of the matrix elements and thus the magnitude of the initial linear splitting of the level are proportional to the appropriate reduction factor, which itself depends only on the strength of the JT-interaction. A good summary and discussion of Ham's methods have been provided by Abragam and Bleaney (1970).

In a similar way we can define reduction factors K for the (s+p) ⊗ T_{1u} system as the ratio of the response of the lowest triplet vibronic state and that of the electronic 2p-state for an external field of E_g, T_{2g} or T_{1g} symmetry. For any electronic operator $O^{\Gamma\gamma}$ transforming as the γ-component of the I.R. Γ we define

$$\langle \Psi^{1M}_{I,0} \mid O^{\Gamma\gamma} \mid \Psi^{1M}_{I,0} \rangle = K^{j=1}_{j=0}(\Gamma) \cdot \langle 21M \mid O^{\Gamma\gamma} \mid 21M' \rangle \qquad (17.1)$$

provided the last factor is non-zero.

We may define representative electronic operators of symmetry E_g, T_{2g} and T_{1g} in terms of the orbital angular momentum given by (7.4), as done by Ham (1973a). The components of this electronic orbital angular momentum transform as T_{1g} and are within the electronic eigenstates (8.4) given by

$$\ell^{T_{1g},x} = \ell_x = \frac{1}{\sqrt{2}} \cdot \{ (|211\rangle + |21\text{-}1\rangle) \cdot \langle 210| + |210\rangle \cdot (\langle 211| + \langle 21\text{-}1|) \} \quad (17.2a)$$

$$\ell^{T_{1g},y} = \ell_y = \frac{i}{\sqrt{2}} \cdot \{ -|210\rangle \cdot (\langle 21\text{-}1| - \langle 211|) + (|21\text{-}1\rangle - |211\rangle) \cdot \langle 210| \} \quad (17.2b)$$

$$\ell^{T_{1g},z} = \ell_z = |211\rangle\langle 211| - |21\text{-}1\rangle\langle 21\text{-}1| \quad (17.2c)$$

For E_g we may use

$$\ell^{E_g,\theta} = \ell_z^2 - \frac{1}{2}(\ell_x^2 + \ell_y^2) \quad (17.3a)$$

$$\ell^{E_g,\epsilon} = \frac{\sqrt{3}}{2} \cdot (\ell_x^2 - \ell_y^2) \quad (17.3b)$$

Similarly for T_{2g},

$$\ell^{T_{2g},\xi} = \frac{\sqrt{3}}{2} \cdot (\ell_y \ell_z + \ell_z \ell_y) \quad (17.4a)$$

$$\ell^{T_{2g},\eta} = \frac{\sqrt{3}}{2} \cdot (\ell_z \ell_x + \ell_x \ell_z) \quad (17.4b)$$

$$\ell^{T_{2g},\zeta} = \frac{\sqrt{3}}{2} (\ell_x \ell_y + \ell_y \ell_x) \quad (17.4c)$$

The only non-zero matrix elements of $\ell^{T_{1g}}$ within the lowest type I vibronic level with J=1 are then given by

$$\langle \Psi_{I,0}^{1M} | \ell_x | \Psi_{I,0}^{1(M-1)} \rangle = \langle \Psi_{I,0}^{1(M-1)} | \ell_x | \Psi_{I,0}^{1M} \rangle =$$

$$= \frac{1}{2} \sqrt{(1+M)(2-M)} \cdot K_0^1(T_{1g}) \quad (17.5a)$$

$$\langle \Psi^{1M}_{I,0} | \ell_y | \Psi^{1(M-1)}_{I,0} \rangle = -\langle \Psi^{1(M-1)}_{I,0} | \ell_y | \Psi^{1M}_{I,0} \rangle =$$

$$= \frac{i}{2} \cdot \sqrt{(1+M)(2-M)} \cdot K^1_0(T_{1g}) \qquad (17.5b)$$

$$\langle \Psi^{1M}_{I,0} | \ell_z | \Psi^{1M}_{I,0} \rangle = M \cdot K^1_0(T_{1g}) \qquad (17.5c)$$

where M or M-1 takes -1, 0, 1. The reduction factor $K^1_0(T_{1g})$ may be expressed in terms of the coefficients a and b of (8.8) by employing the eigenstates (8.8) and making use of one of these relations. Non-zero matrix elements within the vibronic functions (8.6b and c) occur which in the case of ℓ_z have the general form

$$\langle JM, (J+1+2N)(J+1), 2p | \ell_z | JM, (J+1+2N)(J+1), 2p \rangle = -\frac{M}{J+1} \qquad (17.6a)$$

$$\langle JM, (J-1+2N)(J-1), 2p | \ell_z | JM, (J-1+2N)(J-1), 2p \rangle = \frac{M}{J} \qquad (17.6b)$$

We find

$$K^1_0(T_{1g}) = \sum_{N=0}^{\infty} \left\{ |b(1,0,2N)|^2 - \frac{1}{2} \cdot |a(1,0,2N+2)|^2 \right\} \qquad (17.7)$$

For ℓ^{Eg} and ℓ^{T2g} we can proceed in a similar fashion.

Non-zero matrix elements analog to (17.6) are in the case of $\ell^{Eg,\theta}$ given by

$$\langle JM, (J+1+2N)(J+1), 2p | \ell^{Eg,\theta} | JM, (J+1+2N)(J+1), 2p \rangle =$$

$$= -\frac{J(J+1) - 3M^2}{2(J+1)(2J+3)} \qquad (17.8a)$$

$$\langle JM, (J-1+2N)(J-1), 2p | \ell^{Eg,\theta} | JM, (J-1+2N)(J-1), 2p \rangle =$$

$$= -\frac{J(J+1) - 3M^2}{2J \cdot (2J-1)} \qquad (17.8b)$$

Furthermore, we realize that the electronic operators transform in the full rotational symmetry of our vibronic model, i.e. in the combined space of electronic and vibrational coordinates, as a set of functions belonging to J=2 with parity $\wedge' = +1$. The reduction factors for operators of E_g and T_{2g} symmetry are therefore the same as long as we limit ourselves to linear PJT-coupling. However, when including for instance quadratic coupling terms the symmetry of the system reduces to the site-symmetry O_h and then the reduction factors $K(E_g)$ and $K(T_{2g})$ are independent parameters. For full rotational symmetry we therefore find

$$K_0^1(E_g) \equiv K_0^1(T_{2g}) = \sum_{N=0}^{\infty} \left\{ \left| b(1,0,2N) \right|^2 + \frac{1}{10} \cdot \left| a(1,0,2N+2) \right|^2 \right\} \tag{17.9}$$

The definition of the reduction factors above can easily be generalized to any j and J. Of course, expression (17.1) holds for any j and J=1 when we apply the wave functions $\mathcal{Y}_{I,j}^{1M}$ in the matrix element on the left-hand side. However, when we generalized to any J, the electronic 2p-states in the right-hand matrix element of (17.1) have to be replaced by any one state of the two sets of vibronic 'angular' functions (8.6b or c) with the same J. We then employ also the property that the components of $\ell^{T_{1g}}$ transform as J=1 and $\wedge' = +1$ and the ones of both ℓ^{E_g} and $\ell^{T_{2g}}$ as J=2 and $\wedge' = +1$. This has been done by Ham (1973a) in terms of the $f_{2/3}$-coefficients of § 7. Making use of the integrals (7.29b and c), which correspond to the sums of $|a(1,0,2N+2)|^2$ and $|b(1,0,2N)|^2$ over N in (17.7 and 17.9), he was able to predict for the strong coupling limit :

$$K_0^1(T_{1g}) = 0 \qquad (17.10a)$$

$$K_0^1(E_g) \equiv K_0^1(T_{2g}) = \frac{1}{5} \qquad (17.10b)$$

This means that in the strong coupling limit the magnetic splitting of the lowest type I vibronic state with J=1 is completely quenched, whereas the effect of applied strain is not. The strain splitting of this level is reduced by 80% compared to the splitting of the electronic 2p-states.

For weak coupling we may apply the same perturbation treatment as in § 11(a). There we have seen that the lowest vibronic triplet state for $\delta < -0.5$ is predominantly the s-J-state (8.6a) with J=1, N=0, whereas for $\delta > -0.5$ it is the p-(J-1)-state (8.6c) with J=1, N=0. For $\delta = -0.5$ and $\varkappa = 0$ these states are degenerate and split linearly in first order of $\varkappa$. Making again use of (17.6 and 17.8) we find for

$\delta < -0.5$

$$K_0^1(T_{1g}) = \frac{|\delta| \cdot \varepsilon_G}{2 \cdot (\delta^2 - \frac{1}{4})^2} \qquad (17.11a)$$

$$K_0^1(E_g) \equiv K_0^1(T_{2g}) = \frac{(\delta^2 + \frac{1}{4}) \cdot \varepsilon_G}{2 \cdot (\delta^2 - \frac{1}{4})^2} \qquad (17.11b)$$

thus

$$K_0^1(E_g) = \left\{ |\delta| + \frac{1}{4|\delta|} \right\} \cdot K_0^1(T_{1g}) \qquad (17.11c)$$

and for $\delta > -0.5$

$$K_0^1(T_{1g}) = K_0^1(E_g) \equiv K_0^1(T_{2g}) = 1 - \frac{\varepsilon_G}{4(\delta + \frac{1}{2})^2} \qquad (17.12)$$

and for $\delta = -0.5$

$$K_0^1(T_{1g}) = K_0^1(E_g) \equiv K_0^1(T_{2g}) = \frac{1}{2} \cdot (1 - \varkappa) \qquad (17.13)$$

It is now easy to state simple extrapolation formulae for the different values of δ which link the weak and strong coupling regions, as has been done by Ham (1965, 1968) for the E-E- and T-T-JT cases. However, neither from the computational results, nor from the general expressions (17.7 and 17.9), have we been able to find a unique expression for each of the reduction factors and a relation between them analogous to the ones in the JT-cases which hold for all values of δ and ε_G.

The reduction factors are depicted in the Graphs 45 to 47 as a function of ε_G for representative values of δ. Note the double logarithmic scale. As can be seen, the weak and strong coupling expressions hold reasonably well. The overall dependence of the reduction factors on ε_G depends crucially on δ, i.e. on the type of state at zero coupling strength. For $\delta << -0.5$, K (T_{1g}) becomes very small also in the intermediate coupling region and decreases as $|\delta|$ increases.

Note for $\delta < 0$, $K(E_g)$ is <u>less than $1/5$</u> as this asymptotic value is approached. In the inteval $-1 < \delta < 0$, $K(E_g)$ exhibits a slight 'dip' at intermediate and strong coupling strengths which is reflected in a reduction of the total p-(J-1)-admixture of the state. In all cases where $K(E_g) > 1/5$ goes into $K(E_g) < 1/5$, we find that $\sum_N |b(1,0,2N)|^2$ tends from $> 1/6$ to $< 1/6$ where $\sum_N |a(1,0,2N)|^2 < 1/3$, although the values of ε_G at which this occurs do not coincide (for the p-(J-1)-admixture this 'crossing' occurs at slightly larger ε_G). Within the dip and at strongest coupling strengths the total 2p-admixture of the state, i.e. the sum of all the p-(J-1)- and p-(J+1)-contributions, is therefore $< 1/2$, which is

equivalent to $\int_0^\infty dqq^2 F_1^2 < 1$ in the notation of § 7. For $\delta \lesssim -1$ the total 2p-admixture is $\leq 1/2$ for all values of ε_G.

§ 18 Summary and Discussion

An intrinsic feature of the (s+p) ⊠ T_{1u}-system, and probably of all PJT systems, is that the energy levels belonging to type I vibronic states with the same total angular momentum J exhibit a certain tendency to cross as the coupling strength is varied which depends on the magnitude and sign of the electronic 2s-2p spacing. When the tendency of levels crossing is strong, it is useful to classify the type I vibronic states into the three further types A, B, and C, which can be associated with the lowest, middle and upper energy surface of § 6, respectively.

Moreover, the analysis of the individual absorption lines v.s. coupling strength reveals that, in general, a group of absorption peaks can be associated with either one of the type B or C energy levels, or with all the type A levels, with J=1. This circumstance makes the introduction of type A, B, C levels also useful for weak tendency of levels crossing, enabling a unified description of the absorption spectra for all values of δ and ε_G.

The computational results of § 11 and 14 suggest that a factorization of the type I vibronic states does not only occur for the lowest lying states (of type A) in the strong coupling limit (see § 7 and Graphs 11, 12), but also in good approximation for the higher lying ones whenever the energy levels with the same J show strong tendencies to cross. The coupled differential equations (7.14), or their transformed equivalents, are then expected to decouple partially or completely in good approximation for all coupling strengths. The search for a suitable transformation which can perform

this is left to further study.

Using the WKB approximation, an analytical treatment for the higher energy eigenstates of certain dynamically coupled JT-systems has been performed by O'Brien (see Appendix). She anticipated that the higher energy levels and wave functions can successfully be calculated by neglecting the centrifugal terms in the coupled differential equations which arise by taking full account of the kinetic energy. When applying her method to the $(s+p) \otimes T_{1u}$-system, she employed eqn. (7.14 and 7.19) for the inner and outer solution, respectively. However, by taking into account the conditions of the strong coupling limit (7.23), the results apply only to relatively small $|\delta|$, and it is not surprising that only solutions for type A and B states could be found but not for type C (see § 11). Even when extending this method to larger values of $|\delta|$, we expect better results for $\delta < 0$ than for $\delta > 0$, as the WKB approximation does not give good results when the energy surfaces lie close. This is also in agreement with our comments of § 11 on the strong/weak tendencies of energy levels crossings.

The absorption lines show a pronounced resonance structure as the coupling strength is varied. In general, resonance points of zero intensity occur between type B absorption lines which correspond in good approximation to the constant resonance energies

$$\mathcal{E}^{B}_{res} = \frac{7}{2} + 2B - \sigma \qquad (18.1)$$

where B=0,1,2,... . Thus, whenever a type I state has an energy equal to (18.1), its associated absorption line has

zero absorption intensity. These energies coincide with the ones for the higher lying type B levels for J=1, see eqn. (11.20). This circumstance is not surprising as the intensities of the type B states decrease with increasing quantum number B, and the points of zero intensity are expected to lie closer to a peak of lower than of higher energy. However, whenever type C and B levels lie very close, we expect some interference between their associated absorption lines, and the minimal points may only be relative. For the type C absorption lines themselves absolute minima with a ε_G-dependence similar to (11.21) are expected.

For $\delta << -0.5$, the absorption lines exhibit pronounced relative minima when changing from a type B=0 to a type A behaviour (Graph 22). The associated resonance energies show a dependence on the coupling strength similar to the one of the type A maxima, eqn. (14.6), and are approximately given by

$$\varepsilon^{A}_{res} = 2 - \delta - \varkappa \qquad (\delta << -0.5) \qquad (18.2)$$

The resonance structure is thought to be a direct consequence of the dynamic PJT effect and reflects the fact that the effective splitting of the purely electronic levels can be of the same order of magnitude as the elementary phonon excitations. In particular, at the resonance points energy may be exchanged between the electronic and nuclear system which will affect the transition probabilities. When both systems are completely in resonance, we expect the absorption intensity to drop to zero at the frequency which corresponds to the exchange (resonance) energy. Note that for strong tendency of energy levels crossing, i.e. when the

energy surfaces are far apart, the absorption lines may be replaced by envelope lines, and the resonance effect may then be neglected (Graph 22, 25).

The optical resonance effect has also been studied for the dynamic JT problem. The author and Wagner (1971, 1973) have applied a non-linear canonical transformation to the $T \otimes T_2$ system in cubic symmetry where an electronic triplet state is coupled to a T_2 vibrational mode. The transformation diagonalises the total Hamiltonian exactly in the weak coupling region and factorises the wave functions. However, it was assumed that in accordance with equivalent calculations in the E-E case (Sigmund and Wagner 1973), the neglected higher-order terms in the Hamiltonian do not play any decisive role and that the transformation is a good approximation also for intermediate and strong coupling. The strengths of the zero- and one-phonon lines are investigated as functions of the coupling strength. The lines show a series of resonance points and explain the variations in the absorption spectra.

The drawback of these calculations is however that no measure for the reliability of the single phonon lines is given which could have been provided by a matrix diagonalization, such as the one of Englman et al. (1970). Because of this it would appear challenging to apply the method of the non-linear canonical transformation also to the $(s+p) \otimes T_{1u}$-system and to make a quantitative comparison with the computed results. In fact, the paper by the author and Wagner (1973) mentioned that the one-phonon line appears to have minimal points for those values of the coupling strength where the zero-phonon line has maxima. It is surprising that a similar

statement holds for the (s+p) ⊠ T_{1u}-system when the electronic 2s- and 2p-states are degenerate. We find that the absorption line associated with the (J=1)-energy level of main quantum number j = v+2 (v = 1,2,3,...) appears to have zero absorption strength for the same coupling strengths where the (j=v)-absorption line shows an absolute maximum (Graph 24).

The matrix diagonalization of § 10 has made use of the full rotational symmetry of the model Hamiltonian and has been a most convenient way to calculate the energy eigenvalues and wave functions. Alternatively, the eigenvalue problem can be set up in cubic symmetry and a matrix diagonalization may then be performed. Using this line, Englman (1972b, 1972a, p. 73) has calculated the energy levels and reduction factors for some low-lying states as functions of the linear coupling strength for δ = -2.5 and 2/3 and has also investigated the effect of quadratic coupling. Whenever comparable, our results agree exactly with his. However, because of the cubic symmetry employed the computational difficulties as regards to convergence are more severe than with our band matrices. The dimensions of his matrices never exceed 100 x 100, and the lowest energy levels are given reliably only for $\epsilon_G \lesssim 8$. Furthermore, for intermediate and strong coupling only energy levels not exceeding $2\hbar\omega$ above the lowest level have been given, and a calculation of the absorption spectra was apparently not feasible.

Numerical calculations of the above kind have of course been used for a number of years. As regards to the dynamic JT problem, it was first Longuet-Higgins et al. (1958) who

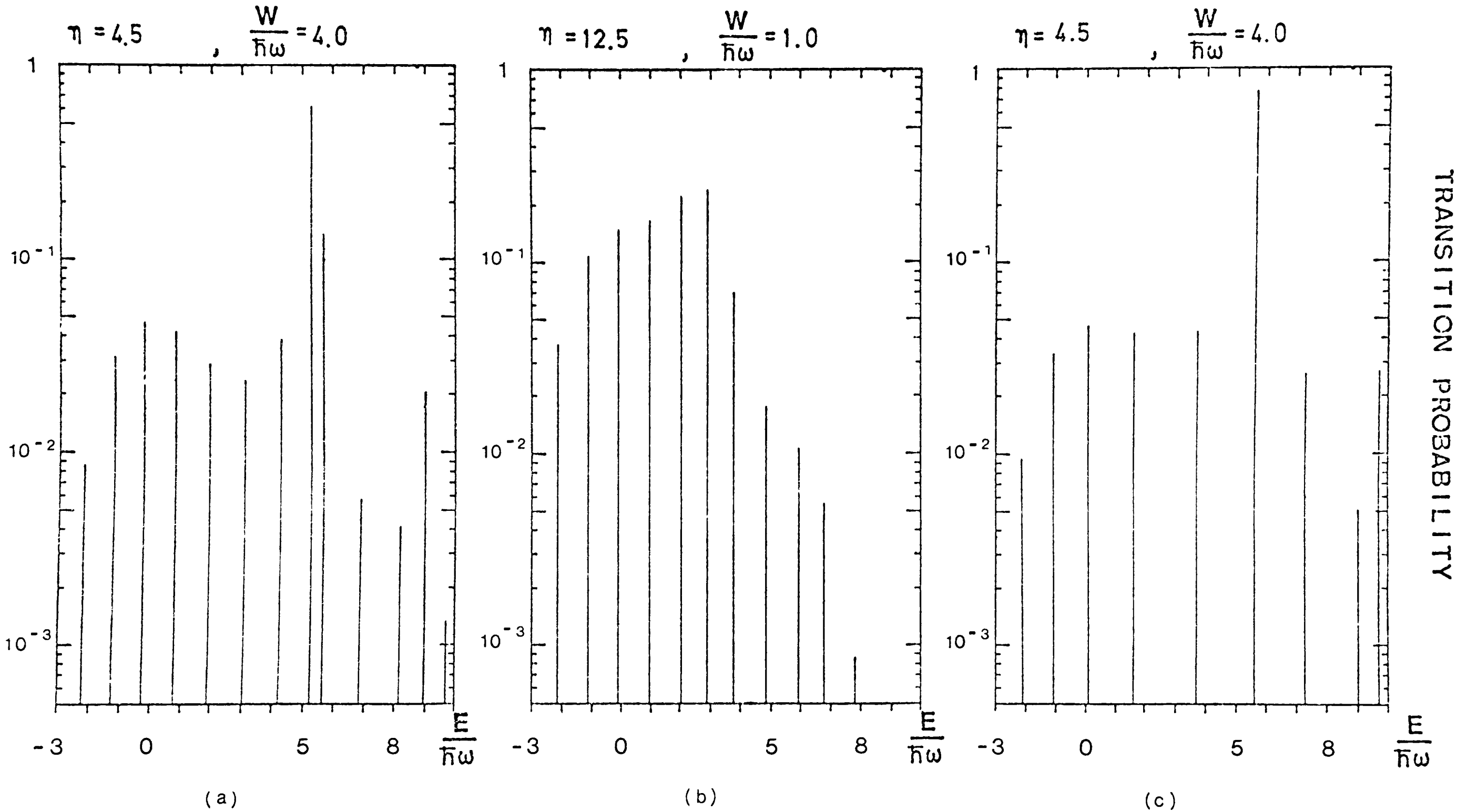
carried out a numerical diagonalization of band matrices for the E-E system to investigate emission and absorption spectra. Similar calculations have also been made by O'Brien (1971c, see Englman 1972a, p. 50) who included a Gaussian broadening of the lines to simulate experimental curves, and also by Englman et al. (1970) for the $T\text{-}T_2$ case.

In more recent time the method has also been applied by Matsume (1974) to the non-degenerate and doubly degenerate pseudo-JT systems. In accordance with our triply degenerate PJT system studied above, it was assumed that the excited electronic states consist out of an 'allowed state' with I.R. Γ_a, i.e. a state which is allowed for electronic-dipole transitions from the electronic ground state (Γ_g), and a closely lying 'forbidden state' (Γ_f) both of which are coupled by a vibrational mode (Γ_{ph}) referred to as 'trigger phonons'. A system of a certain symmetry group can thus be abbreviated by $(\Gamma_f + \Gamma_a) \boxtimes \Gamma_{ph}$ where Γ_{ph} has to be contained in the direct product $\Gamma_a \times \Gamma_f$. Examples of the non- and doubly degenerate PJT systems are $(A_{1g} + B_{1u}) \boxtimes B_{1u}$ in D_{2h} symmetry and $(B_{1u} + E_{1u}) \boxtimes E_{2g}$ of D_{6h} where in each case the electronic ground state has I.R. A_{1g}. It is seen that our $(A_{1g} + T_{1u}) \boxtimes T_{1u}$ system of O_h is a natural extension of these systems.

It is instructive to compare the three PJT systems with each other. In all cases the adiabatic energy surfaces show a qualitative similar behaviour with varying coupling strength but differ of course as regards to their number and dimensionality. Whereas the 1-d non-degenerate PJT system has two energy surfaces (corresponding to the lowest and upper ones of Fig. 5), the doubly degenerate PJT system has three which show circular

ABSORPTION SPECTRA (Natsume 1974)

FIG. 7



symmetry in a two-dimensional q-space. The middle energy surface of the doubly degenerate system is a paraboloid and does not vary with coupling strength. As we have seen, the triply degenerate PJT system has spherical symmetry and four energy surfaces, two of which are degenerate and independent of ε_G. It is remarkable that the conditions of forming the lowest minimum are the same in all three cases and given by (6.18).

As regards to the absorption spectra at zero temperature, comparison with the $(s+p) \otimes T_{1u}$ system is unfortunately only possible for $\delta < 0$, i.e. for cases where the forbidden state lies below the allowed one, as Natsume has studied only these cases. Figure 7 shows two representative spectra (a),(b) for the non-degenerate system and one spectrum (c) for the doubly-degenerate case, where (a) and (c) correspond roughly to Graph 28 and (b) to Graph 31. Note that $\eta = \frac{2\varepsilon_G}{|\delta|}$, $\frac{W}{\hbar\omega} = -2\delta$.

It is remarkable how the spectra for the three PJT systems with the same parameters resemble each other. Best agreement in respect of intensity and relative position is found for the lowest lying lines, particularly when the lowest adiabatic energy surface is far away from the higher one(s), i.e. for sufficiently large $|\delta|$ and/or strong coupling. However, marked differences exist between the spectra for small $|\delta|$ and for higher energies which is due to the influence of the middle and upper adiabatic energy surfaces. Because of the same reasons we also expect less agreement for all cases with $\delta > 0$.

In the case of non-zero temperature the type II states will give us a contribution with no correspondence in the

other cases. As in § 13 this contribution consists only out of a single line where the position depends on δ but not on ε_G and T but where the intensity depends now only on T but not on δ or ε_G. Following the notation of § 14 the total absorption spectrum is given by

$$I_T^{(a)} = I_T^{(a)}(I) + I_T^{(a)}(II) \quad \text{where}$$

$$I_T^{(a)}(II) = \frac{e^{-1/\beta} \cdot (3 - e^{-1/\beta})}{3 \cdot (1 + e^{-1/\beta})} \cdot \delta(\varepsilon_o - \delta - \varepsilon) \qquad (18.3)$$

As T becomes large, $I_T^{(a)}(II)$ tends to 1/3. The calculation of $I_T^{(a)}$ is left to further investigation.

PART III : Vibronic Model for the Relaxed Excited State of the F Centre

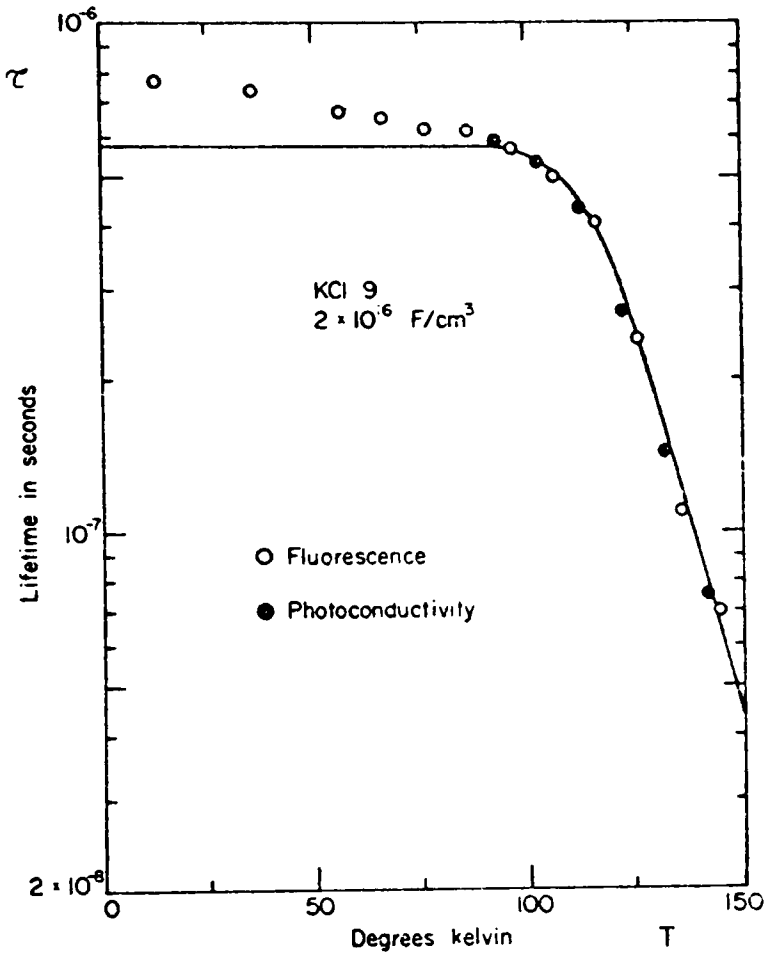
§ 19 Experimental Evidence and Theoretical Background

F centre luminescence was first observed in 1954 (see Fowler 1968, p. 97), and since then its properties have been studied extensively. It was found that the luminescence band is Stokes-shifted by a large amount from the absorption band, and has a bell-like shape similar to that of the absorption band. The luminescence is unpolarized, even when the exciting light is polarized. The observation of the radiative lifetime by Swank and Brown (1963) has probably created the most stimulating discussion concerning F centre luminescence. By measuring the time dependence of both luminescence and photo-conductivity after excitation as a function of temperature (Fig. 8), they found that the radiative lifetime in KCl, KBr, KI, and NaCl is in the order of 10^{-6} sec and about 10 to 100 times longer than one expects from the oscillator strengths in absorption. They assumed that all the excited F centres decay through the lowest relaxed state, whose lifetime determines the decay time of the emission. Furthermore, they postulated that only two decay channels were available: radiative emission and thermal ionization. The decay probability may thus be written as

$$1/\tau = 1/\tau_r + 1/\tau_o \cdot e^{-\Delta E/kT} \qquad (19.1)$$

where τ and τ_r are the observed and radiative lifetime, respectively. The last term is the probability of thermal

FIG. 8



OBSERVED LIFETIME OF THE EXCITED F CENTER IN KCl

(after Swank and Brown, 1963)

ionization into the conduction band with activation energy ΔE and ionization attempt frequency $1/\tau_o$. The fluorescent yield from the RES is defined as

$$\eta_r = \tau/\tau_r \qquad (19.2)$$

These expressions were satisfactorily tested for the four alkali halides. The solid line in Fig. 8 indicates a 'best fit' of (19.1) for KCl, with the resulting parameters $\Delta E = 0.14$ eV, $\tau_r = 0.58 \cdot 10^{-6}$ sec, $\tau_o^{-1} = 1.2 \cdot 10^{12}$ sec^{-1} (Fowler 1968, p. 98).

More recent studies, however, have shown that the decay can involve other non-radiative decay channels. Podini (1966) found in NaF, for instance, a third nonradiative non-photoconductive decay mode. Moreover, in studies of electric field effects on the F centre emission several researchers (Spinolo and Fowler 1965, Bogan and Fitchen 1970) have observed that ionization may occur during relaxation. This means, as Stiles et al. (1970) have pointed out, that in general η_r will not be a readily measurable quantity. However, the quantum efficiency η_e defined by

$$\eta_e = \frac{\text{number of photons emitted}}{\text{number of photons absorbed}} \qquad (19.3)$$

can always be measured. Furthermore, if η_o is defined as the probability for an excited F electron to reach the RES, then $\eta_e = \eta_o \eta_r$. This means that in order to obtain a value for τ_r from lifetime and quantum yield measurements, care must be taken to see whether or not $\eta_o = 1$. In particular, if there is a channel available for the excited electron to escape to the ground state, this expression might not hold.

In the following we shall give a brief discussion of the results of some of the more recent experiments on the F centre luminescence. However, we shall state mostly those data which are relevant to our later calculation and discussion.

Stiles et al. (1970) investigated the effect of temperature and applied electric field on the radiative lifetime τ_r of the F centre in KCl, KF and NaF. By measuring the luminescent decay time τ and the relative luminescent yield η, they were able to determine τ_r. They found that $\eta_o = 1$ for KCl and KF but not for NaF. In the latter case they used additional data (Podini 1966) to determine τ_r. In all three alkali halides the radiative lifetime decreases as the temperature increases. The electric-field induced change in τ_r was found to be proportional to the square of the applied electric field.

Bogan and Fitchen (1970) measured the Stark effect in F centre emission for six alkali halides. The changes induced by the field are quadratic in the field strength and isotropic with respect to the crystalline axes. At low temperatures an enhancement of the emission polarized parallel to the field direction is found together with a compensating decrease of the emission polarized perpendicular to the field; furthermore, a red-shift of the band in both polarizations, and a broadening in certain cases.

The temperature dependence of the radiative lifetime and of the electric-field-induced polarization of the luminescence enable us to determine the energy separation E_{10} between the two lowest vibronic levels of the excited electronic state in the relaxed configuration. As the transition probability is not only proportional to the transition dipole moment, but

also to the cube of the emission energy, an extra field and temperature dependence of the lifetime due to the shift or temperature change through the factor E^3 has to be expected. This correction of the experimental data has to be made before comparison with the theoretical expressions of § 20 can take place. Stiles et al. (1970) took the change in the cube of the experimentally determined emission energy E, averaged over the whole band, as a rough measure of how such changes affect the radiative lifetime. Defining the quantity

$$M^2 = (\tau_r < E^3 >)^{-1} \qquad (19.4)$$

they found that the temperature dependence of M^2 below $\sim 100^o$ K is well described for KCl, KF, and NaF by

$$\frac{M^2(T)}{M^2(o)} = \frac{1 + 3R \cdot \exp(-E_{10}/kT)}{1 + 3\exp(-E_{10}/kT)} \qquad (19.5)$$

As we shall see in the next paragraph, this expression is appropriate if the lowest level is s-like and the excited state a p-like triplet, and R is then the ratio of the lifetimes of these levels

$$R = \tau_r(0)/\tau_r(1) \qquad (19.6)$$

The temperature dependence of the electric-field-induced polarization below $\sim 100^o$ K was found by Bogan and Fitchen (1970) to be given by

$$\frac{P(o)}{P(T)} - 1 = 3Re^{-E_{10}/kT} \qquad (19.7)$$

where R is again given by (19.6) if the lowest level is s-like and the next excited one a p-like state (§ 20).

Using (19.5 and 19.7), values for E_{10} and R could be obtained from the experimental data for various alkali halides

(Table 8). Ohkura et al. (1974) carried out a similar analysis to Bogan and Fitchen and their results, together with the ones of Ruedin et al. (1973) who measured the temperature dependence of the spin-lattice relaxation time (Orbach process) in the RES, have also been included in Table 8, as well as the energies of the LO lattice phonons (at $\vec{q}=0$) for comparison. There is some discrepancy between Ruedin's values and those of the other researchers, which is not understood. We have chosen to use the values obtained from the data on the Stark effect and radiative lifetime. Note also the large uncertainty in the results obtained from the electric-field-induced polarization.

Table 9 shows the dependence of the linear polarization, of the change in the radiative lifetime and of the first moment on the square of the applied electric field. M^2 is again related to τ_r through (19.4). Note that $\langle \Delta E_x \rangle = \langle \Delta E_z \rangle = \langle \Delta E \rangle$.

Hetrick and Compton (1967) have measured the stress-induced linear polarization of the F-band luminescence in KCl, NaCl, NaF, and RbCl for uniaxial stress X along the [001] and [110] directions. They found that the induced polarization P depends linearly on the applied stress X along the [001] direction (Table 10) and is completely independent of temperature between 20 and 140° K, for all of the crystals studied. In the case of a stress along [110] and light viewed along [001], no induced polarization was observed.

The observation of a magnetic-field-indiced circular polarization of the emission of the F centre was first reported for KF and KCl by Fontana and Fitchen (1969, 1970b). The

effects were found to be small compared to the ones of absorption and independent of temperature. It was concluded that the emitting level is not split by the field and is separated significantly from higher lying ones, and that the spin-orbit contribution is negligible. Indeed, Fontana (1970a) could show that the F-electron spin polarization had been completely quenched by the intense optical pumping used in the experiments, and that absence of a spin-orbit contribution was to be expected. More recently, Baldacchini and Mollenauer succeeded in measuring also the paramagnetic part of the circular polarization for KBr and KI, as well as the diamagnetic one, although the signs were not established (Table 12).

The g factor in the RES has also been determined by Mollenauer et al. (1969, 1971, 1972a,b), using a method of optical detection of spin resonance, and by a different method by Ruedin et al. (1972). For all crystals the observed g shift is negative (Table 12).

The long radiative lifetime of the F centre luminescence could be explained by Fowler (1964, 1968) with a semicontinuum model for NaCl by assuming that the electronic 2p state in the relaxed configuration is very much more diffuse spatially than in the unrelaxed configuration, as a result of the ions adjusting themselves to the change in charge distribution following the optical excitation, and this would strongly reduce the matrix element for emission to the 1s ground state.

Alternatively, Swank and Brown (1963) suggested that the longer lifetime might result because the lowest level of the excited state in the relaxed configuration is a state of

even parity, such as the 2s state. Indeed, both Fowler et al. (1967) and Wood and Öpik (1969) have found that after relaxation the 2s and 2p states may lie very close. For KCl, Wood and Öpik found that the 2s state crosses the 2p state and ends up ~ 0.08 eV lower in energy.

A model, with a nondegenerate state being lowest, is favoured by the evidence that this lowest state is not split by stress or by an electric or magnetic field and that the ESR g factor is isotropic (Mollenauer et al. 1969, Ruedin 1972). The suggestion that this lowest state is an s-like level of even parity is supported by the fact that its radiative lifetime decreases in an electric field, presumably because the field mixed this state with an excited odd-parity p-like state having a shorter lifetime. Although neither Fowler et al. or Wood and Öpik actually considered 2s-2p mixing in their calculations, it is clear that such mixing will play a decisive role if these levels lie very close. Bogan and Fitchen (1970) have developed a semi-classical model along these lines which assumes that the F electron responds adiabatically to the fluctuating internal electric field due to odd-parity LO phonons, resulting in a strong mixing of the electronic 2s and 2p states (internal Stark effect). This view does not of course preclude the possibility that the 2p state is spatially diffuse, even though it is not the lowest level in the relaxed configuration. Indeed, Wood and Öpik's calculation indicates that the 2p state expands substantially as a result of the symmetric lattice relaxation associated with the large Stokes shift.

As was shown in Part I, Ham (1973a) has given a general

solution of the vibronic problem posed by this model where the electronic 2s and 2p states interact in cubic symmetry via a T_{1u} vibrational mode. Using the exact wave functions for the resulting vibronic states, he was able to derive general expressions for various quantities that have been measured in recent experiments.

Moreover, Ham has given a detailed comparison of the experimental data with his results for strong coupling. Following his arguments, we may compare the values for E_{10} of Table 8 with the separation (7.26) of the two lowest vibronic levels in strong coupling. Since $E_G \gg \hbar\omega$ it follows from (7.26) that E_{10} should be very much smaller than one-half the energy of the effective vibrational mode which best represents the coupling of the F centre with the T_{1u} modes of its environment. This is clearly not the case. For KI and KBr an optically active T_{1u} mode of the F centre has been identified lying within the gap between the acoustic and optical phonon branches of the perfect crystal (Table 8). However, for most other alkali halides experimental data like these are not available, and it is then convenient to use the LO lattice phonon (at $\vec{q} = 0$) which has the highest energy of all phonons of the perfect lattice. With Table 8 we find that the strong-coupling model is not consistent with the experimental values of E_{10} for the listed alkali halides.

The strong-coupling model also predicts radiative lifetimes which are the same for the different low-energy levels and are equal to $2\tau_r(p)$ (see § 13). The fairly large values for the lifetime ratio R in Table 8 are therefore also inconsistent with this model. Furthermore, according to Ham

the electric-field-induced change in the radiative lifetime of the lowest level should approach zero in the strong coupling limit, and we would then expect $\Delta M^2(o)/M^2(o)$, obtained from $\Delta\tau_r(o)/\tau_r(o)$ by (19.4), to be much smaller than the induced polarization P(o). In fact Table 9 shows that these quantities differ by less than a factor of 2.

One can therefore conclude from the experimental data that the system cannot be strongly coupled to the T_{1u} modes, and that an interpretation of these results must be sought in the regime of weaker coupling strength. This view is in contrast to the semi-classical Bogan-Fitchen model (1970) which assumes that the electronic 2s and 2p states are strongly mixed by a fluctuating electric field due to LO phonons. Indeed, Ham (1973a) could show that the states of this model can be identified with different groups of the exact vibronic states in the strong coupling limit associated with the three energy surfaces of Fig. 5.

Finally, from a moment analysis (Henry et al. 1965, Loader 1969) of the vibrational broadening of the F band in absorption and of the stress-induced linear dichroism (Hetrick 1969), Ham could obtain an estimate for the JT energies and E_G for KCl in the unrelaxed configuration:

$$E_A = 0.17 \text{ eV}, \quad (E_{JT})_E \leq 0.07 \text{ eV},$$
$$0.04 \leq (E_{JT})_T \leq 0.06 \text{ eV}, \quad E_G \leq 0.5 \text{ eV} . \tag{19.8}$$

It was argued that E_G is probably no more than 0.1 to 0.2 eV. However, these values may be changed significantly in the relaxed configuration because of the large relaxation of the totally symmetric mode. Moreover, with Table 2 it was

concluded that the experimental situation requires the following conditions to be satisfied

$$E_{sp} < 0,\ (E_{JT})_E < |E_{sp}|,\ (E_{JT})_T < |E_{sp}|,\ E_G < \tfrac{1}{4}\,|E_{sp}| \qquad (19.9)$$

With (19.8) we find now $|E_{sp}| \gtrsim 0.06$ eV for KCl.

TABLE 8: Parameters for the temperature dependence of radiative lifetime, electric-field-induced linear polarization and spin-lattice relaxation time of F-band emission, and energies of LO mode at ($\vec{q} = 0$) and optically active T_{1u} mode.

alkali halide	E_{10} (meV)				R			$\hbar\omega_{LO}$	$\hbar\omega_{T_{1u}}$
	(a)	(b) (±2)	(c) (±2)	(d)	(a)	(b)	(c)	(meV)	(meV)
KF	17	16.5		7.1	2.75	4.3 ± 1.3		40.1 [e]	
KCl	18	18		14.2	2.75	3.3 ± 1.3		26.7 [f]	
KBr			12	9.4			4.9 ± 1.2	21.1 [e]	12.3 [g]
KI			11	6.5			3.0 ± 1.0	17.8 [e]	10.2 [g]
NaF	17	12			5.6	1 ± 1		52.5 [h]	
NaCl				9.4				32.8 [i]	
RbCl		15.5				2 ± 1		21.4 [k]	
RbBr				7				16.1 [e]	
RbI				7.2				13.4 [e]	

[a] Stiles *et al.* (1970), [b] Bogan and Fitchen (1970), [c] Ohkura *et al.* (1974), [d] Ruedin *et al.* (1973), [e] Fowler (1968, p. 627), [f] Raunio and Almquist (1969a), [g] Bäuerle and Hübner (1970), [h] Buyers (1967), [i] Raunio *et al.* (1969b), [k] Raunio and Rolandson (1970).

TABLE 9: Electric-field-induced linear polarization of F-band emission, red shift and change in radiative lifetime. The radiative lifetime is related to M^2 by (19.4) of the text.

alkali halide	$\Delta M^2/M^2F^2$ [10^{-6} (kV/cm)$^{-2}$]	$P(0)/F^2$ [10^{-6} (kV/cm)$^{-2}$]			$\langle \Delta E \rangle / F^2$ [10^{-7} (eV) (kV/cm)$^{-2}$]		
	(a)	(b)	(c)	(d)	(b)	(c)	(d)
KF	4.2 ± 0.6	8 ± 3			-1.6 ± 0.3		
KCl	6.0 ± 1.0	10 ± 3		13	-2.0 ± 0.5		-1.7
KBr			33 ± 2			-5.4 ± 0.4	
KI			13 ± 1			-6.0 ± 0.3	
NaF	3.0 ± 0.5	4 ± 1			-1.4 ± 0.5		
NaCl		7 ± 2			-3.0 ± 0.8		
RbCl		6 ± 2			-1.6 ± 0.3		
CsF		0.2 ± 0.1					

(a) Stiles et al. (1970), (b) Bogan and Fitchen (1970), (c) Ohkura et al. (1974), (d) Kühnert (1967).

TABLE 10: Stress-induced linear polarization of F-band emission for uniaxial stress X along [001]

alkali halide	P/X $[10^{-3}\ (kg/mm^2)^{-1}]$
KCl	9.9
RbCl	11.1
NaCl	3.9
NaF	3.1

These data are taken from the slopes of the lines in Fig. 1 of the paper by Hetrick and Compton (1967).

TABLE 11: Stress-coupling coefficients for the 2p electronic states in the unrelaxed configuration, obtained from stress-induced linear dichroism data in F-band absorption

alkali halide	A_3 [10^{-4} eV $(kg/mm^2)^{-1}$]	A_5 [10^{-4} eV $(kg/mm^2)^{-1}$]
KCl	6.1 ± 0.9 a)	8.8 ± 1.2 a)
	5.9 ± 0.8 b)	8.0 ± 1.1 b)
KBr	4.4 ± 0.6 a)	6.3 ± 0.9 a)
KI	6.2 ± 0.9 a)	9.8 ± 1.4 a)
NaCl	2.4 ± 0.4 a)	6.7 ± 1.0 a)
RbCl	7.0 ± 1.0 a)	5.8 ± 0.8 a)

A_3 and A_5 are defined by (21.10 and 21.12) of the text.

a) Schnatterly (1965): data at 80° K

b) Hetrick (1969): data at 7° K

TABLE 12: Diamagnetic and paramagnetic part of the circular polarization of the emission induced by a magnetic field, and electron g factors in ground state and RES of the F centre.

alkali halide	$\Delta_d(o)/H$ [10^{-8} Gauss]	$\Delta_p(o)$ [10^{-3}]	Electron g factors in relaxed excited state (d)	(e)	ls ground state (f)
KF	-6 ± 1 a)			1.993	1.996
KCl	-9 ± 1 b)		1.976 ± 0.001	1.981	1.995
KBr	16.3 ± 1.7 c)	1.27 c)	1.862 ± 0.002	1.873	1.982
KI	18.5 ± 1.2 c)	2.16 c)	1.627 ± 0.002	1.630	1.964
NaCl				1.973	1.997
RbBr				1.845	1.967
RbI				1.634	1.949

a) Fontana and Fitchen (1969), b) Fontana (1970b), c) Baldacchini and Mollenauer: in this measurement the signs of Δ_d and Δ_p were not established, d) Mollenauer and Pan (1972b), e) Ruedin (1972), f) Seidel and Wolf.

§ 20 Weak Coupling Limit - Perturbation Treatment

The previous comments have made clear that a strong-coupling model for the RES of the F centre cannot explain the available experimental data. Indeed, Ham's paper (1973a) called for a weak coupling analysis of the coupling to the T_{1u} mode.

In the following we shall first briefly state the results of first-order perturbation theory of the vibronic coupling (in cubic symmetry) and then include the effects of electric and magnetic fields and applied uniaxial stresses. In treating external perturbations like these, it is of advantage to solve the electronic problem first and treat then the vibronic coupling as a perturbation. Alternatively, we have taken the vibronic interaction and each of the external fields as simultaneous perturbations which provided a useful check on our calculations.

(a) Low-energy vibronic states with no external perturbation

Essentially, we consider the same model as in § 6. However, we now take the 2s electronic state to be <u>below</u> the 2p state in the cubic configuration ($Q_x = Q_y = Q_z = 0$) by an energy difference $|E_{sp}|$ appreciably larger than the quantum $\hbar\omega$ of the vibrational T_{1u}-mode. Furthermore, the zero of energy is taken to coincide with the 2s state. In the model Hamiltonian H_L and H_{PJT} therefore read the same but the electronic part takes the form,

$$H_e' = \tfrac{1}{2} \cdot |E_{sp}| \cdot (1 - \rho_o) \qquad (20.1)$$

In analogy to § 11(a) perturbation theory of the low-energy vibronic states requires that G is sufficiently small,

$$E_G = \frac{G^2}{2\mu\omega^2} \lesssim \frac{1}{4}|E_{sp}| \qquad (20.2a)$$

and that

$$|E_{sp}| \gg \hbar\omega \qquad (20.2b)$$

Note that (20.2a) is the condition (6.22) for the minimum energy of the static problem to occur for the 2s state in the cubic configuration. We also assume that $|E_o| \gg |E_{sp}|$, i.e. the electronic 1s-ground state lies very much below the excited states and its influence can be neglected.

The vibrational Hamiltonian (6.1) has in cubic symmetry the eigenfunctions

$$|n_x n_y n_z\rangle = F_{n_x}(Q_x) \cdot F_{n_y}(Q_y) \cdot F_{n_z}(Q_z) \qquad (20.3)$$

where $F_n(Q)$ is the n^{th} eigenfunction of the 1-d simple harmonic oscillator, and the energies $(n + \frac{3}{2})\hbar\omega$ where $n = n_x + n_y + n_z$.

We now calculate the matrix elements of H_{PJT}. The following relation holds for any vibrational coordinate Q (see Messiah 1965, p. 492),

$$Q|n\rangle = \left(\frac{\hbar}{2\mu\omega}\right)^{\frac{1}{2}} \cdot \left\{ \sqrt{n+1}\,|n+1\rangle + \sqrt{n}\,|n-1\rangle \right\} \qquad (20.4)$$

The only non-vanishing matrix elements between vibrational states are given by

$$\langle n|Q|n+1\rangle = \langle n+1|Q|n\rangle = \left(\frac{\hbar}{2\mu\omega}\right)^{\frac{1}{2}} \cdot \sqrt{n+1} \qquad (20.5)$$

The non-zero matrix elements between the electronic states are found with (6.5) to be

$$\langle i | \rho_j | 2s \rangle = \langle 2s | \rho_j | i \rangle = \delta_{ij} \quad (i,j = x,y,z) \qquad (20.6)$$

In the following we will be particularly interested in the properties of the two lowest vibronic states. The discussion of § 11 has made clear in general that whenever the electronic 2s state is below the 2p state or equal in energy, i.e. for $\delta \leq 0$, the lowest vibronic state is a 's-like' state and transforms as J=0 and the first excited state is a 'p-like' triplet state and transforms as J=1 for all coupling strengths. Of course, here we are only concerned with the cases $\delta \ll -\frac{1}{2}$.

The wavefunctions and energies of the lowest and first excited vibronic states are denoted by $^2\Gamma_I(o)$, $E_I(o)$ and $^2\Gamma_I(1)$, $E_I(1)$, respectively, and the other quantities accordingly. We put for convenience,

$$G_o = G \cdot \sqrt{\frac{\hbar}{2\mu\omega}} \qquad (20.7)$$

The perturbed wavefunction for the vibronic ground state is then given to first order in G by

$$^2\Gamma_I(o) = b_o \cdot |000\rangle|2S\rangle + b_1 \cdot \left(|100\rangle|x\rangle + |010\rangle|y\rangle + |001\rangle|z\rangle \right) \qquad (20.8a)$$

where

$$b_1 = - G_o \left(|E_{sp}| + \hbar\omega \right)^{-1} \qquad (20.8b)$$

and $b_o = 1 - \frac{3}{2} \cdot b_1^2$ gives the normalization correct to order G^2. The energy of this level to order G^2 is found to be

$$E_I(o) = \frac{3}{2}\hbar\omega - 3E_G\hbar\omega \left(|E_{sp}| + \hbar\omega \right)^{-1} \qquad (20.9)$$

in accordance with (11.3a).

Similarly, we find for the p-like triplet state for the wave function to first order in G

$$^{2}\Gamma_{IX}(1) = C_0|100\rangle|2s\rangle + C_1|000\rangle|x\rangle + C_2|200\rangle|x\rangle + b_1(|110\rangle|y\rangle + |101\rangle|z\rangle) \quad (20.10a)$$

where

$$C_1 = -G_0(|E_{sp}| - \hbar\omega)^{-1}, \quad C_2 = \sqrt{2}\, b_1 \quad (20.10b)$$

and $C_0 = 1 - (C_1^2 + C_2^2 - 2b_1^2)/2$,

and similar expressions for $^{2}\Gamma_{Iy}(0)$ and $^{2}\Gamma_{Iz}(0)$. The energy difference between the two lowest vibronic levels is then

$$E_{10} = E_I(1) - E_I(0) = \hbar\omega\left\{1 - 2E_G|E_{sp}|\cdot[E_{sp}^2 - (\hbar\omega)^2]^{-1}\right\} \quad (20.11)$$

(For specific examples of $|E_{10}| = |\mathcal{E}_{10}|\cdot\hbar\omega$ see Graph 6.)

The probability per unit time that the vibronic ground state in weak coupling will decay radiatively to the 1s electronic ground state with emission of a photon of polarization η is found from § 12 to be

$$\Gamma_\eta(0) = \frac{E_G\,\hbar\omega}{\tau_r(p)\cdot(|E_{sp}| + \hbar\omega)^2} \quad (20.12)$$

where $\tau_r(p) = [C_1\ D^2]^{-1}$ is the radiative lifetime of the 2p electronic state. Accordingly the ratio of the radiative lifetime of the vibronic ground state to $\tau_r(p)$ is given by

$$\frac{\tau_r(0)}{\tau_r(p)} = \frac{(|E_{sp}| + \hbar\omega)^2}{3\,E_G\,\hbar\omega} \quad (20.13)$$

We note that this ratio is equal to $N_\delta^{-1}(0)$ of (13.7 - 8).

The ratio R of the radiative lifetime $\tau_r(0)$ to $\tau_r(1)$ is then

$$R = \frac{\tau_r(0)}{\tau_r(1)} = \frac{4}{3}\left\{1 + \left(\frac{|E_{sp}| + \hbar\omega}{2(|E_{sp}| - \hbar\omega)}\right)^2\right\} \quad (20.14)$$

which is approximately 5/3 for $|E_{sp}| \gg \hbar\omega$. Again from § 13 R is found to be equal $N_\delta(1)/N_\delta(0)$.

With (12.1) we calculate the temperature dependence of the radiative lifetime

$$\tau_r^{-1}(T) = \tau_r^{-1}(0) \cdot \frac{1 + 3R \cdot \exp(-E_{10}/kT)}{1 + 3 \cdot \exp(-E_{10}/kT)} \qquad (20.15)$$

where the temperature is sufficiently low so that only the two lowest vibronic states are appreciably populated.

(b) Stark Effects in Emission

If a uniform electric field F is applied to the crystal along the z direction, the perturbation of the defect is given by

$$\mathcal{H}_F = - D_z \cdot F_e \qquad (20.16)$$

where F_e is the local effective field and the electric dipole moment operator $\vec{D}$ is given by (12.3). For simplicity we neglect any lattice polarization and assume that the coupling to the field is due solely to the electrons.

As the components of $\vec{D}$ transform like x,y,z, the perturbation $\mathcal{H}_F$ can have nonzero matrix elements only between vibronic states of opposite parity Λ', thus giving the selection rules $\Delta J=0, \pm 1$. In addition we find $\Delta M=0$ for a field in the z direction. When calculating the perturbed vibronic ground state with J=0, no coupling to the type II states is possible as the latter exist only for $J \geq 1$. The matrix elements between the electronic 2s- and 2p-states are given by

$$d = \langle 2s | D_\eta | \eta \rangle \qquad (20.17)$$

where η = x,y,z. Again, we neglect the influence of the 1s-electronic ground state.

Disregarding the vibronic coupling for the moment and considering only the effect of $\mathcal{H}_F$ on the excited electronic states, we find that the applied electric field leads to a direct mixing of the 2s and $2p_z$ electronic states and then to an induced polarized luminescence from the 2s level. When we take the vibronic coupling into account, the ground state wave function is given to first order in F_e and G,

$$\begin{aligned} \Psi^F(0) = \; & b_o^F \cdot |000\rangle|2S\rangle \; + \; b_2 \cdot |000\rangle|z\rangle \\ & + \; b_1 \cdot \left(|100\rangle|x\rangle \; + |010\rangle|y\rangle \; + |001\rangle|z\rangle \right) \end{aligned} \tag{20.18}$$

where

$$b_2 = d F_e / |E_{sp}| \tag{20.18a}$$

with

$$b_o^F = 1 - \tfrac{3}{2} b_1^2 - \tfrac{1}{2} b_2^2 \tag{20.18b}$$

and b_1 is given by (20. 8b). The field-induced change in energy is

$$\Delta E(0) \equiv E_I^F(0) - E_I(0) = - \frac{d^2 F_e^2}{|E_{sp}|} \tag{20.19}$$

In second order, the perturbed state contains 2s-terms of orders $GF_e(\hbar\omega \cdot |E_{sp}|)^{-1}$ and $E_G(\hbar\omega \cdot |E_{sp} + \hbar\omega|)^{-1}$, which do not contribute to the transition probabilities.

When calculating $I_z(o)$ in analogy to (20.12), we note that there is no interference between the total transition probability resulting from the field-induced term and the vibrationally induced term in (20.18), because of the orthogonality of $|000\rangle$ and $|001\rangle$. We find to order F_e^2,

$$I_z(0) = \tau_r^{-1}(p) \cdot \left\{ \frac{d^2 F_e^2}{|E_{sp}|^2} + \frac{E_G \hbar\omega}{(|E_{sp}| + \hbar\omega)^2} \right. \tag{20.20}$$

while $I_x(o)$ and $I_y(o)$ are of course given by (20.12). The induced polarization is then

$$P(0) = \frac{I_z(0) - I_x(0)}{I_z(0) + I_x(0)} = \frac{d^2 F_e^2}{2 E_G \hbar\omega}\left(\frac{|E_{sp}| + \hbar\omega}{E_{sp}}\right)^2 \qquad (20.21)$$

The change in radiative lifetime is

$$\Delta[\ \tau_r^{-1}(0)] = \tau_r^{-1}(\rho)\cdot\left(\frac{d F_e}{E_{sp}}\right)^2 \qquad (20.22)$$

With (20.13) we find now

$$P(0) = -\frac{3}{2}\cdot\frac{\Delta\tau_r(0)}{\tau_r(0)} \qquad (20.23)$$

Assuming a negligible field-induced shift in the 1s electronic state, we expect the field-induced change of the first moment of the F-band emission at 0^o K, for light polarized perpendicular to the field, to be simply

$$\langle \Delta E_x^1(0)\rangle \equiv E_x^1(0^F) - E_x^1(0) = \langle \Delta E_y^1(0)\rangle = \Delta E(0) \qquad (20.24)$$

For light polarized parallel to the field the perturbation in (20.18) induces a transition to the no-phonon level of the 1s state, and we find

$$\langle \Delta E_z^1(0)\rangle = -\Delta E(0)\cdot\left\{\frac{(|E_{sp}| + \hbar\omega)^2}{|E_{sp}|\cdot E_G} - 1\right\} \qquad (20.25)$$

Since the assumption of weak coupling is $E_G < \frac{1}{4}\cdot|E_{sp}|$, we see that $\langle \Delta E_z^1(0)\rangle$ should be positive and larger in magnitude than $\langle \Delta E_x^1(0)\rangle$ and $\langle \Delta E_y^1(0)\rangle$, which are negative as $\Delta E(0)$.

The calculation for the first excited state proceeds in the same way as above. In this approximation the energy difference between the ground and first excited state does not change with F_e and is given by (20.11). We find that $[I_z(1) - I_x(1)]$ has the same value as $[I_z(0) - I_x(0)]$. However, $[I_z(1) + I_x(1)]$ is not equal to $[I_z(0) + I_x(0)]$ because of the lifetime ratio R of (20.14), and we therefore

obtain

$$\frac{P(1)}{P(0)} = \frac{\tau_r(1)}{\tau_r(0)} = R^{-1} \qquad (20.26)$$

For temperatures at which only the two lowest vibronic states are significantly populated, the temperature dependence of the polarization is given by

$$P(T) = \frac{P(0) + 3R\,P(1)\cdot\exp(-E_{10}/kT)}{1 + 3R\cdot\exp(-E_{10}/kT)} \qquad (20.27)$$

Similarly, we may calculate the temperature dependence of the radiative lifetime τ_r^F for an applied electric field

$$\frac{\tau_r^F(T)}{\tau_r^F(0)} = \frac{P(T)}{P(0)} = \frac{1 + 3\cdot\exp(-E_{10}/kT)}{1 + 3R\cdot\exp(-E_{10}/kT)} \qquad (20.28)$$

(c) Stress-Induced Polarization of Emission

The coupling of the electronic 2p states to a uniform strain introduced in the crystal by an applied stress may be expressed in a standard form for an orbital triplet state in cubic symmetry as (Ham 1972a)

$$\mathcal{H}_S = V_2\cdot(e_\theta\, l^{E_g,\theta} + e_\epsilon\, l^{E_g,\epsilon}) + V_3\cdot(e_{yz}\, l^{T_{2g},\xi} + e_{zx}\, l^{T_{2g},\eta} + e_{xy}\, l^{T_{2g},\zeta}) \qquad (20.29)$$

where the electronic operators l^{E_g} and $l^{T_{2g}}$ are defined by (17.3 and 17.4). V_2 and V_3 are appropriate strain coupling coefficients and e_{ij} is a component of the strain tensor

$$e_{ij} = e_{ji} = \tfrac{1}{2}\cdot\left(\frac{\partial u_i}{\partial x_j} + \frac{\partial u_j}{\partial x_i}\right) \qquad (20.30)$$

and we define

$$e_\theta = e_{zz} - \tfrac{1}{2}(e_{xx} + e_{yy})$$
$$e_\epsilon = \tfrac{\sqrt{3}}{2}(e_{xx} - e_{yy}) \qquad (20.31)$$

The electronic operators of (20.29) transform as J=2 (see § 17) and their matrix elements with respect to the vibronic states must obey the selection rules $\Delta J \geq 2$ and $\Delta \Lambda' = 0$. In particular, the only states admixed in first order with a type I vibronic state with J=0 are the d-like type I states with J=2, $\Lambda' = +1$.

For uniaxial stress X along[001], the only nonzero component of the strain is $e_\theta = X/(C_{11} - C_{12})$, and we find that the electronic state $|z\rangle$ has the energy $|E_{sp}| - V_2 e_\theta$, while $|x\rangle$ and $|y\rangle$ have $|E_{sp}| + V_2 e_\theta / 2$. The perturbed vibronic ground-state wave function is then given by (20.8) but with the strain splitting included in the energy denominator of the first-order terms. Expanding the resulting polarized emission probabilities, as given by (20.12), to first order in $V_2 e_\theta$, we obtain for the linear polarization

$$P(0) = \frac{3 V_2 e_\theta}{2\cdot(|E_{sp}| + \hbar\omega)} \quad . \tag{20.32}$$

In a similar fashion we calculate the polarization P(1) for the first excited triplet level by modifying the wave functions (20.10) to include the strain splitting of the 2p states in the energy denominator.

$$P(1) = \frac{I_z(1) - I_x(1)}{I_z(1) + I_x(1)} = \frac{3 V_2 e_\theta}{2\cdot(|E_{sp}| + \hbar\omega)} \cdot u \tag{20.33a}$$

where

$$u = \frac{4 + \left[(|E_{sp}| + \hbar\omega)/(|E_{sp}| - \hbar\omega)\right]^3}{4 + \left[(|E_{sp}| + \hbar\omega)/(|E_{sp}| - \hbar\omega)\right]^2} \tag{20.33b}$$

For $|E_{sp}| \gg \hbar\omega$, $u \approx 1$. P(1) is then equal to P(0) to a good approximation, so that the stress-induced polarization should be independent of temperature even up to temperatures at which

the first excited vibronic triplet level is appreciably populated. Whether this temperature independence persists to even higher temperatures has not been investigated, but presumably it does not persist to temperatures at which the electronic 2p states are appreciably populated, $kT \sim |E_{sp}|$.

The calculation of (20.33) has ignored any Boltzmann-factor population difference between the three states of the triplet, because the strain splitting of this triplet is reduced by a factor $\sim(2E_G\hbar\omega/E_{sp}^2)$ compared to the splitting of the 2p electronic state. The additional contribution to P due to this splitting is smaller than P(1) in (20.33) by a factor $\sim(E_G\hbar\omega/2kT|E_{sp}|)$, which is small under our assumption $E_G < |E_{sp}|/4$ at temperatures at which the excited level is appreciably populated.

For a stress X along [110] we have $e_\theta = -X/2(C_{11}-C_{12})$ and $e_{xy} = X/4C_{44}$. The 2p strain eigenstates are now $|x'\rangle = (|x\rangle + |y\rangle)/\sqrt{2}$, $|y'\rangle = (|x\rangle - |y\rangle)/\sqrt{2}$, and $|z\rangle$ with energies $V_2e_\theta/2 - V_3e_{xy}$, $V_2e_\theta/2 + V_3e_{xy}$, and $-V_2e_\theta$, respectively. The resulting polarization as viewed along [001] is given by

$$P_z(0) = \frac{I_{x'}(0) - I_{y'}(0)}{I_{x'}(0) + I_{y'}(0)} = \frac{2V_3 e_{xy}}{|E_{sp}| + \hbar\omega} \qquad (20.34)$$

where x' denotes polarization along [110] and y' that along $[1\bar{1}0]$. For the polarization as viewed along $[1\bar{1}0]$, we obtain

$$P_{y'}(0) = \frac{I_{x'}(0) - I_z(0)}{I_{x'}(0) + I_z(0)} = \frac{2V_3 e_{xy} - 3V_2 e_\theta}{2(|E_{sp}| + \hbar\omega)} \qquad (20.35)$$

For [110] stress we also find a temperature independence of P similar to the one for [001], with the ratio P(1)/P(0)

given again by the same factor u of (20.33b).

(d) Magnetic Circular Polarization of Emission

A magnetic field H applied in the z-direction gives rise to the orbital Zeeman interaction

$$\mathcal{H}_H^{orb} = g_L \mu_B H \ell_z \qquad (20.36)$$

where $\mu_B = \frac{e\hbar}{2mc}$ is the Bohr magneton and g_L is the orbital g factor of the electronic p-states. ℓ_z is given by (17.2c). As $\vec{\ell}$ transforms as J=1, the non-zero matrix elements of its components must obey the selection rules ΔJ=0 or 1 and cannot connect two vibronic states with J=0. Furthermore, $\vec{\ell}$ commutes with ρ_o of § 6 and therefore with Λ and can only couple states of the same parity Λ' (Ham 1973a). Equation (20.36) can therefore mix only type II states with J=1, $\Lambda' = +1$ into an s-like type I state (J=0, $\Lambda' = +1$).

When treating the problem by simple perturbation theory it is convenient to apply the magnetic field first and then to include the vibronic coupling. $\mathcal{H}_H^{orb}$ leaves the 2s electronic state of course unaffected but splits linearly the 2p states. The perturbed energies are $|E_{sp}| + g_L\mu_B H$, $|E_{sp}|$, and $|E_{sp}| - g_L\mu_B H$, belonging to $|211\rangle$, $|210\rangle$, and $|21\text{-}1\rangle$ of (8.4), respectively. Treating now H_{PJT} of (6.4) by perturbation theory, the ground-state wave function is to first order in G given by

$$\Psi_I(o) = b_{000}|000\rangle|2s\rangle + \{c^+_{100}|100\rangle + c^+_{010}|010\rangle\}|211\rangle + \{c^-_{100}|100\rangle + c^-_{010}|010\rangle\}|21\text{-}1\rangle + c^z_{001}|001\rangle|210\rangle \qquad (20.37)$$

where

$$C^{+}_{100} = iC^{+}_{010} = \frac{G_o}{\sqrt{2}}\left(|E_{sp}| + \hbar\omega + g_L\mu_B H \right)^{-1}$$

$$C^{-}_{100} = -iC^{-}_{010} = -\frac{G_o}{\sqrt{2}}\left(|E_{sp}| + \hbar\omega - g_L\mu_B H \right)^{-1} \qquad (20.38)$$

$$C^{z}_{001} = -G_o\left(|E_{sp}| + \hbar\omega \right)^{-1}$$

$$b_{ooo} = 1 - \frac{1}{2}\left\{ |C^{+}_{100}|^2 + |C^{+}_{010}|^2 + |C^{z}_{001}|^2 + |C^{-}_{100}|^2 + |C^{-}_{010}|^2 \right\}$$

As in the case of the applied stress, the polarization induced in the luminescence from the vibronic ground state results also here from the splitting of the 2p electronic states, through the change in the amount by which these states are mixed into the ground state by the vibronic coupling. The emission probabilities $I_+(o)$ and $I_-(o)$ for light with left- and right-handed circular polarization along the magnetic field, where the electric dipole moment is given by $D_{\pm} = e(x \mp iy)/\sqrt{2}$, are obtained in a similar fashion as above,

$$I_+(o) = \tau_r^{-1}(p)\cdot\left(|C^{+}_{100}|^2 + |C^{+}_{010}|^2 \right)$$
$$I_-(o) = \tau_r^{-1}(p)\cdot\left(|C^{-}_{100}|^2 + |C^{-}_{010}|^2 \right) \qquad (20.39)$$

We expand these results to first order in H and obtain for the diamagnetic part of the circular polarization,

$$\Delta_d(o) \equiv \frac{I_+(o) - I_-(o)}{I_+(o) + I_-(o)} = -\frac{2g_L\mu_B H}{|E_{sp}| + \hbar\omega} \qquad (20.40)$$

The negative sign of $\Delta_d(o)$ thus favours emission of light right circularly polarized when the propagation vector is in the direction of the magnetic field.

When taking into account the electron spin we have to include the spin-orbit interaction

$$\mathcal{H}_{so} = \lambda \vec{l}\,\vec{S} \qquad (20.41)$$

where λ is the spin-orbit parameter and the components of $\vec{\ell}$ are given by (17.2). The spin vector operator $\vec{S}$ is equal to $\frac{1}{2}\vec{\sigma}$ with the Pauli matrices $\vec{\sigma} \equiv (\sigma_x, \sigma_y, \sigma_z)$ defined in Messiah (1965, p. 545). The spin states may be chosen to be quantized with respect to the z-direction and are given by $|+\rangle \equiv |\tfrac{1}{2}, +\tfrac{1}{2}\rangle$ and $|-\rangle \equiv |\tfrac{1}{2}, -\tfrac{1}{2}\rangle$. With $\mathcal{H}_{so}$ as a small correction, the perturbed vibronic ground states ${}^2\Gamma_I'(0\,\pm)$ contain λ-dependent terms with equal and opposite spin directions. While the first ones induce circular polarization in the luminescence, the latter ones lead to a small probability of spin flip in the optical transition to the electronic ground state.

The induced circular polarization from a net spin polarization, defined as

$$\langle S_z \rangle = \tfrac{1}{2} \cdot (p_+ - p_-), \tag{20.42}$$

can now be calculated, where p_+ and p_- denote respectively the probabilities that the spin has values $S_z = +\frac{1}{2}$ and $-\frac{1}{2}$ in the lowest type I vibronic state. Because of the Pauli principle we have $p_+ + p_- = 1$. Neglecting the terms with opposite spin, the perturbed vibronic ground states ${}^2\Gamma_I'(0\,+)$ and ${}^2\Gamma_I'(0\,-)$ are regarded as the states with p_+ and p_-, respectively. The actual calculation proceeds along the same lines as before, and we arrive at

$$\Delta(0) = -\frac{2(g_L \mu_B H + \lambda \langle S_z \rangle)}{|E_{sp}| + \hbar\omega} \tag{20.43}$$

Finally, we can calculate the change δg in the g factor of the s-like ground states, which results from the vibronic mixing of the 2s and 2p electronic states. δg is defined

by the relation

$$\delta g = \langle \Psi_I'(0\pm)| g_L \ell_z | \Psi_I'(0\pm)\rangle / (\pm \tfrac{1}{2}) \qquad (20.44)$$

and we obtain

$$\delta g = -\frac{4}{3} \cdot \frac{\lambda g_L}{(|E_{sp}| + \hbar\omega)} \cdot \frac{\tau_r(p)}{\tau_r(0)} \qquad (20.45)$$

§ 21 Comparison with Experiment

Turning now to a weak-coupling analysis of the experimental data, we postulate that the principle coupling between the 2s and 2p states is with a vibrational mode having a frequency near that of the LO lattice phonons. In particular, we would expect coupling with the long-wavelength LO phonons to predominate if the 2s and 2p states are diffuse and if their interaction occurs primarily via the electric field associated with these vibrational modes.

Ham (1973a) has shown that if 2s lies below 2p in the cubic configuration, the separation $|E_{sp}|$ may be found in the weak-coupling case from the diamagnetic part of the magnetic-field-induced polarization of the emission. As regards to the g_L value we use the one obtained for the unrelaxed configuration from the circular dichroism of the optical absorption which we assume approximates that for the relaxed configuration as well: $g_L = 0.95 \pm 0.1$ for KCl (Margerie 1967) and $g_L \sim 1$ for KF (Fontana 1970a) and also for KBr and KI. These values were obtained from the change in the first moment of the F band, using the method of Henry et al. (1965). Substituting the experimental values $\Delta_d(o)/H$ for these alkali halides of Table 12 (we assume that the sign of $\Delta_d(o)$ is negative in all cases)into (20.40), we find

$$\begin{aligned} (|E_{sp}| + \hbar\omega) \sim\ & 0.19 \text{ eV} \quad (KF) \\ & 0.12 \text{ eV} \quad (KCl) \\ & 0.07 \text{ eV} \quad (KBr) \\ & 0.06 \text{ eV} \quad (KI) \end{aligned} \tag{21.1}$$

The energy difference $|E_{sp}|$ of the electronic states in the

relaxed cubic configuration is therefore smaller than (21.1) by one vibrational quantum, which should lie in the range 0.01 - 0.04 (Table 8).

There are several alternative ways in which we may interpret the data to obtain a value for the coupling strength, and we shall consider these in turn. If we take again the LO lattice phonon as the principle coupling between the 2s and 2p states, and use (20.11) together with the observed values for E_{1O} of Table 8 to estimate the coupling energy E_G from the ratio $E_G/\hbar\omega$, we would expect this estimate of E_G to be an upper bound, since the LO phonon has the highest energy of all phonons of the perfect lattice. Similarly, this estimate will give us a lower bound for the lifetime ratio $\tau_r(o)/\tau_r(p)$.

With (21.1) and $\hbar\omega = \hbar\omega_{LO}$ of Table 8 we find

$$\begin{array}{lllll} |E_{sp}| \sim & 0.15 & & eV & (KF) \\ & 0.09 & & eV & (KCl) \\ & 0.05 & (0.06) & eV & (KBr) \\ & 0.04 & (0.05) & eV & (KI) \end{array} \qquad (21.2)$$

The numbers in brackets were obtained by using $\hbar\omega = \hbar\omega_{T_{1u}}$ of Table 8. Substituting (21.2) and the corresponding values for E_{1O} of Table 8 into (20.11), we obtain an estimate of the coupling energy,

$$\begin{array}{lllll} E_G \sim & 0.040 & eV & (KF) \\ & 0.014 & eV & (KCl) \\ & 0.009 & eV & (KBr) \\ & 0.006 & eV & (KI) \end{array} \qquad (21.3)$$

Alternatively, if we put again $\hbar\omega = \hbar\omega_{T_{1u}}$, we find for both

KBr and KI that within the limits of experimental uncertainty E_{10} has the same value as $\hbar\omega_{T_{1u}}$. We conclude that E_G is very small and may be in the order of 1 meV for both KBr and KI. All these values are consistent with Ham's conclusion above that the coupling to the T_{1u} modes is weak. The radiative lifetime is now obtained from (20.13):

$$\begin{aligned} \tau_r(o)/\tau_r(p) \quad \sim \quad & 7.5 && \text{(KF)} \\ & 12 && \text{(KCl)} \\ & 9 && \text{(KBr)} \\ & 11 && \text{(KI)} \end{aligned} \tag{21.4}$$

This ratio gives the factor by which the radiative lifetime is enhanced at the lowest temperatures, relative to that of the 2p state, as a result of the 2s state being below 2p. The low-temperature radiative lifetime has been measured to 380 nsec in KF, 717 nsec in KCl, 1.1 μsec in KBr, and 3.2 μsec in KI (Stiles et al.1970, Swank and Brown 1963, Fröhlich and Mahr 1966). Using these values, $\tau_r(p)$ is calculated to 51, 60, 122, and 291 nsec for KF, KCl, KBr, and KI, respectively.

Similarly, from (20.14) we obtain values of the ratio R,

$$\begin{aligned} R \quad \sim \quad & 2.3 && && \text{(KF)} \\ & 2.4 && && \text{(KCl)} \\ & 3.4 && (2.1) && \text{(KBr)} \\ & 3.4 && (2.1) && \text{(KI)} \end{aligned} \tag{21.5}$$

where the numbers in brackets correspond again to $\hbar\omega = \hbar\omega_{T_{1u}}$ of Table 14. We may compare (21.5) with the observed ratios of Table 8. Note that 3.4 for KBr and KI agrees better with the experimental data. Note also that the large values for

R favour the weak-coupling model since R becomes smaller as the coupling strength increases and approaches unity in the strong-coupling limit, as we have seen above.

There are two other ways to estimate $\tau_r(o)/\tau_r(p)$ and E_G from the Stark effect data. Firstly, we may combine (20.13) with (20.21) and obtain

$$P(o) = \frac{3\,\tau_r(o)\,d^2F_e^2}{2\,\tau_r(p)\cdot|E_{sp}|^2} \qquad (21.6)$$

Employing the measured values for P(o) of Table 9 and using (21.2), we can evaluate $\tau_r(o)/\tau_r(p)$ once we have determined $d^2F_e^2$. Henry et al. (1965) have shown for the unrelaxed configuration that this last quantity is given by the change in the second moment of the F absorption band for light polarized parallel to the applied field: $\langle \Delta E_z^2 \rangle = d^2F_e^2$. The experimental value for this quantity presumably provides a lower bound for the value of $d^2F_e^2$ that should be used in (21.6), since the calculations of Wood and Öpik (1969) show that the 2s and 2p states should both become more diffuse in the relaxed configuration. Chiarotti et al. (1969) have measured $\langle \Delta E_z^2 \rangle$ for KCl and obtained the value 4.8×10^{-7} eV^2 (by integrating over the region of the F band alone) for an applied field F = 40 kV/cm (where F denotes the applied field, F_e the local field, in our notation). Substituting this value for $d^2F_e^2$ in (21.6), together with the appropriate value for $P(o)/F^2$ from Table 9, we find

$$\tau_r(o) \;/\; \tau_r(p) \sim 180 \quad (KCl) \qquad (21.7)$$

With (20.13) and (21.1) we obtain now $E_G \sim 1$ meV. This estimate will therefore be a lower bound for E_G and an upper

bound for $\tau_r(o)/\tau_r(p)$. As the lifetime ratio seems unreasonably large, we could bring (21.7) into agreement with (21.4) by increasing $d^2F_e^2$ for the relaxed configuration by a factor ~ 15 compared with the experimental value obtained from the absorption data. Such a large change in this quantity due to lattice relaxation can be expected. Wood and Öpik (1969) have indeed found an increase by a factor ~ 3 in the dipole matrix element d from their theoretical wave functions. In any case the correct value of $\tau_r(o)/\tau_r(p)$ should be intermediate between (21.4 and 7).

The other way to find an estimate for the radiative lifetime and E_G is to combine the induced polarization P(o) of (21.6) with the induced shift of the F emission band for light polarized perpendicular to the applied electric field. From (20.19 and 20.24):

$$\frac{P(o)}{\langle E_x \rangle} = - \frac{3\,\tau_r(o)}{2\,\tau_r(p)\cdot|Esp|} \qquad (21.8)$$

With Table 9 we obtain now $\tau_r(o)/\tau_r(p) \sim 5$ for KF, ~ 3 for KCl, ~ 2 for KBr, and ~ 0.6 for KI, and from (20.13) $E_G \sim 0.06$ eV for both KF and KCl, ~ 0.04 eV for KBr, and ~ 0.11 eV for KI. The results for KF, which correspond to $\tau_r(p) \sim 76$, are not seriously in disagreement with the values (21.3 and 21.4), but for the other alkali halides they are and must be regarded as an upper bound for E_G in view of the observed values of E_{10}. This is in clear disagreement with our model: the measured values for $\langle \Delta E_x \rangle / F^2$ for KCl and KBr are about 4 times larger, the one for KI about 19 times larger than it should be in order to be consistent with the other data on the basis of our weak coupling model.

A further discrepancy is found in the induced shift $\langle \Delta E_z \rangle$ for light polarized parallel to the applied electric field. According to (20.25) this shift should be to higher energy, in contrast to the smaller red shift predicted for $\langle \Delta E_x \rangle$ by (20.24). However, the Stark effect measurements revealed the same red shift for both signs of polarization in all of the investigated crystals.

Expression (20.23) predicts a definite value for the ratio of the electric-field-induced polarization P(0) to the change in radiative lifetime. Correcting the lifetime change data for the field induced shift of the emission by (19.4), the ratio of P(0) to $\Delta M^2/M^2$ then equals +3/2 in the weak-coupling model which is consistent with the data for KF, KCl, NaF of Table 9.

Turning now to Hetrick and Compton's measurements (1967), we find that their results are consistent with (20.32, 20.34, 20.35) if we have for the strain-coupling coefficients $V_2 \gg V_3 \sim 0$. We can therefore obtain an independent estimate of $|E_{sp}| + \hbar\omega$ from (20.32) if we assume that V_2 is the same as in the unrelaxed configuration, for which it may be obtained from the stress-induced change in the first moment of the F-band absorption (see Table 11). Taking a uniaxial stress X along [001], we have for the difference in the first moment change for light polarized parallel and perpendicular to the stress axis (Fowler 1968, p. 406),

$$\langle \Delta E_z \rangle - \langle \Delta E_x \rangle = -\frac{3}{2} V_2 e_\theta = -A_3 X \qquad (21.9)$$

We express (20.32) in terms of the stress-coupling coefficient A_3,

$$P(0)/X = A_3 / (|E_{sp}| + \hbar\omega) \qquad (21.10)$$

Combining the data of Table 10 with the value of A_3 obtained by Schnatterly (1965) and Hetrick (1969) (Table 11), we obtain from (21.10) a value ($|E_{sp}| + \hbar\omega$) $\sim$ 0.06 eV for KCl, NaCl, and RbCl. For KCl this is only half the value given by (21.1). As the value of A_3 that should be used in (21.10) may differ substantially from that measured in absorption because of the large symmetric-mode relaxation, we regard (21.1) as more reliable.

A large change in the coupling coefficient accompanying the relaxation seems to be the only plausible explanation for the complete absence of induced polarization for [110] stress and light viewed along [001]. From (20.34) we conclude that V_3 is zero in the relaxed configuration. This result contrasts with Schnatterly's absorption measurements (1965), which show that in the unrelaxed configuration the coupling to the shear e_{xy} is as strong as that to e_θ in all of the crystals measured. For [110] uniaxial stress and light incident along [001] the relation analogous to (21.9) is

$$\langle \Delta E_{x'} \rangle - \langle \Delta E_{y'} \rangle = -2V_3 e_{xy} = -A_5 X \qquad (21.11)$$

where x', y' are denoted by [110],[1$\bar{1}$0], respectively, and A_5 is given in Table 11.

The temperature independence of the induced polarization (Hetrick and Compton 1967) would be consistent with the weak-coupling model if we had $|E_{sp}| \gg \hbar\omega$, since the ratio P(1)/P(0) = u is then unity (see 20.32, 20.33). If we take $|E_{sp}|$ = 0.09 eV, $\hbar\omega$ = 26.7 meV for KCl, we obtain u = 1.39, from which we would expect an increase in polarization by $\sim$ 15% as the temperature is raised to 140° K. No such change was observed. The stress results therefore require that on the basis of the weak-coupling

model $|E_{sp}|$ is not smaller than ~ 0.10 eV for any of the crystals in Table 10.

On the other hand the radiative lifetime and the electric-field-induced polarization depend strongly on the temperature. We see that by defining M^2 through (19.4) expressions (20.15) and (19.5) are identical and (20.28) agrees with (19.7) for sufficiently low temperatures. Moreover, our model predicts that $P(T)/P(0) \equiv M^2(0)/M^2(T)$ which is at least approximately satisfied by the results of Table 8.

The results (21.1) agree quite well with the findings of Park and Faust (1966) and the more recent ones of Kondo and Kanzaki (1974) that strong optical absorption from the relaxed excited state (the 2s state in our model) occurs to another state (the 2p state) lying for KCl, KBr, and KI about 0.1065, 0.0870, and 0.0775 eV, respectively, higher in energy.

Baldacchini and Mollenauer determined the paramagnetic component of the magnetic circular polarization for emission (Table 12), corresponding to spin polarization $P' = 2 < S_z >$ in the excited state of 0.14 and 0.21 for KBr and KI, respectively. Combining these results with (21.1) and (20.43) we obtain for the spin-orbit parameter λ of the 2p states in the relaxed configuration the result

$$|\lambda| \sim 0.6 \text{ meV} \qquad (21.12)$$

for both KBr and KI. This result contrasts with the values $\lambda = -15$ meV for KBr and $\lambda = -26$ meV for KI in the unrelaxed configuration as determined from the magnetic circular dichroism of the absorption (Margerie 1967) although one would expect some reduction in $|\lambda|$ as a result of a more diffuse 2p wave function in the relaxed configuration.

Assuming that λ is negative as in the unrelaxed configuration, we expect δg of (20.45) to be positive in contrast with the results of Table 12. Moreover, if we calculate δg for our alkali halides by employing (21.1 and 21.4) and the values found for λ in the unrelaxed configuration, we obtain a vibronic g shift which is about 5 times smaller in magnitude than the experimental shift.

There is of course a significant negative g shift in the 1s ground state which has been explained by Adrian (1957) as resulting from the spatial variation of the 1s F centre wave function near the neighbouring ions due to the orthogonality requirement to their p core states. The spin-orbit interaction due to the nuclear potential of these ions couples the F centre wave function to excited states, thereby causing a negative g shift. We may therefore assume that the dominant component of the negative g shift in the RES originates from the same mechanism and overrides the influence of the vibronic coupling.

§ 22 Discussion

We have shown that the weak-coupling model is able to account quantitatively for most of the available experimental data for KF, KCl, KBr, and KI, if the 2s electronic state is about 0.05 to 0.15 eV below 2p in the relaxed configuration. There is, however, one major discrepancy which we have been unable to explain: the red-shift of the emission band in both polarizations induced by an applied electric field. Moreover, agreement with the model appears a little forced when we try to fit simultaneously all the various data. It is therefore tempting to speculate that a better explanation of the data could be obtained if we consider the JT coupling of the 2p states to the E_g and T_{2g} modes as well.

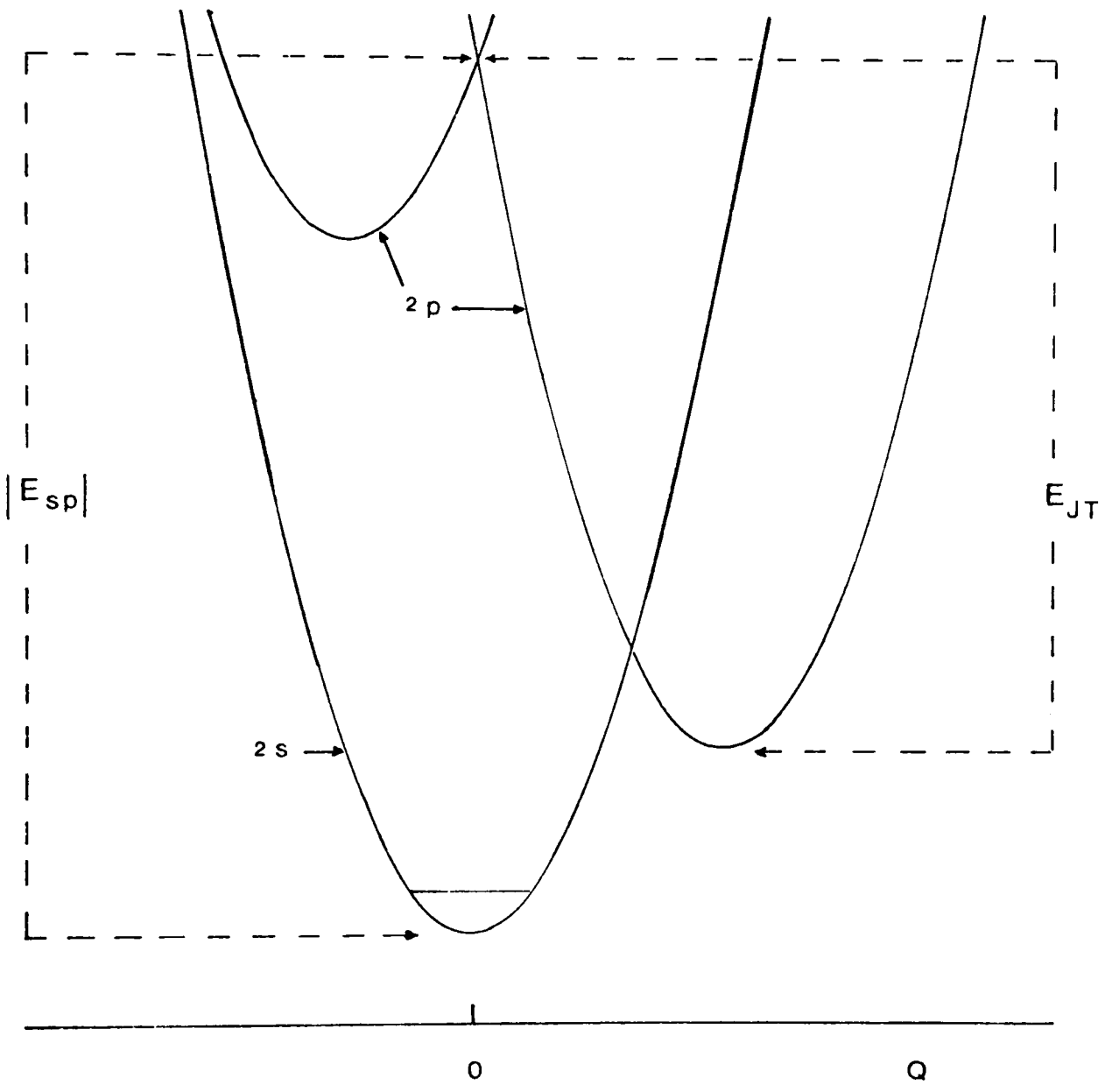
The estimates (19.8) for KCl indicate a fairly large JT coupling compared to E_G of (21.3). However, we can rule out the possibility that the JT coupling is strong enough to bring the energy minimum of the JT-distorted 2p states below that of the 2s state, since it follows from Table 2 that the vibronic ground state should then be degenerate. Similarly, we can disregard the possibility that the ground state is one of a number of closely spaced tunnelling levels of the 's-p mixed type' resulting from strong coupling both to the T_{1u} and E_g or T_{2g} modes. Either of these situations should cause the polarization of the emission produced by an applied electric or magnetic field, or stress to be strongly temperature dependent at low temperatures, contrary to observation. Finally, we have the situation where the JT coupling significantly affects the 2p states but where the minimum in the adiabatic energy surfaces for these states remains above the

energy of the 2s state in cubic configuration, as in Fig. 9. This is the only situation in which the ground state is non-degenerate, and where the conditions (19.9) apply. Moreover, we expect the estimates (19.8) to be reduced for the relaxed configuration as the 2p wave functions are probably much more diffuse there than in absorption. Indeed, Hetrick and Compton's data (1967) show that the stress-coupling coefficient A_5 is very small in the relaxed configuration, so that coupling with long-wavelength T_{2g} phonons should be negligible.

Nevertheless, an appreciable JT coupling of the 2p states will not greatly change the results of § 21, as long as the JT energy is significantly smaller than $|E_{sp}|$, as in Fig. 9. As the E_g and T_{2g} modes do not directly affect the 2s state, the JT coupling affects the vibronic ground state only through the 2p states which are mixed with 2s by the T_{1u} coupling or by an applied electric field. From Fig. 9 it is clear that mixing of the 2p states into the lowest vibrational state of 2s occurs only near Q = 0, where this state has appreciable amplitude, and that the average separation of the 2s and 2p energy surfaces in this region is the cubic energy difference $|E_{sp}|$. The properties of the lowest vibrational states of the 2p energy surfaces, which would show such effects of the JT coupling as the quenching of orbital angular momentum (Ham 1965), are thus not relevant in determining the properties of the perturbed vibronic ground state, and we can neglect the JT coupling in good approximation.

Indeed, when carrying out a perturbation treatment of both T_{1u} and E_g modes, it is convenient to treat the coupling of the electronic system to the E_g mode first, as the problem

FIG. 9



ADIABATIC ENERGY SURFACES FOR ELECTRONIC 2s AND 2p STATES AS FUNCTIONS OF A E_g OR T_{2g} DISTORTION MODE Q

may then be solved exactly since the interaction (5.16) is diagonal within the electronic space, and then to include the coupling to the T_{1u} mode and external fields as simultaneous perturbations. Sums over the vibronic states of the E_g mode may be eliminated by replacing energy differences between vibronic levels by an average approximately equal to $(|E_{sp}| - (E_{JT})_E) \gg \hbar\omega_E$ and employing their closure relations. The resulting expressions for the radiative lifetimes, polarizations, etc. are independent of $\hbar\omega_E$ and identical to the ones of § 20 when we replace $|E_{sp}|$ by $|E_{sp}| - (E_{JT})_E$.

Our conclusions contrast with the work of Iida et al. (1972), who attributed the small value of the circular polarization $\Delta_d(o)$ to the partial quenching of the orbital angular momentum by the coupling to the E_g mode. Their work is not directly comparable with our work, since they took the 2s-2p mixing to result from an internal field which they treated adiabatically. However, it appears they interpreted the numerical results wrongly and that the small value of $\Delta_d(o)$ is caused also in their model by the 2s state being significantly below 2p in the relaxed cubic configuration.

Mollenauer and Baldacchini (1972a) have proposed an interpretation for the optically detected ENDOR spectrum of KI and KBr in the RES, in terms of the radial distribution expected for a pure 2p wave function with no 2s admixture. They suggested that a suitable nondegenerate state comprising equal admixtures only to the 2p orbitals $|211\rangle$, $|21\text{-}1\rangle$, and $|210\rangle$ may result from a dynamic treatment of the vibronic T_{1u} coupling. Ham (1973a) has shown, however, that the 2p admixture into the lowest type I ground state with J=0 is only

50% in the strong coupling limit (§ 7). The only situation in which the ground state is made up predominantly from the 2p states is when 2p is below 2s ($E_{sp} > 0$) and the vibronic coupling is weak. The ground state is then triply degenerate, and a dynamic JT effect will be expected as a result of the coupling to E_g and T_{2g} modes which will not lift the degeneracy of the ground state. However, the degeneracy will be removed partially by the spin-orbit interaction, but with λ negative the $J = \frac{3}{2}$ state should be below $J = \frac{1}{2}$. In any case, the observation that the excited-state g factor in KI is isotropic is itself evidence that the vibronic ground state has no orbital degeneracy.

Recently, Wang et al.(1973) formulated a method of calculating the nearly degenerate states of a bound lattice polaron and applied it to study the RES of the F centre in KCl. Their results imply that the lowest excited state contains ~ 70% 2s and ~ 30% 2p character and that the mixing of the 2s and 2p electronic states due to electron-phonon interaction is not in the strong-coupling regime where an approx. equal mixing of these states occurs. This weak-coupling interpretation is qualitatively consistent with our previous results. However, from (21.4) we find that the lowest vibronic state for KCl has 2s- and 2p-admixtures of ~ 92% and ~ 8%, respectively. According to Tables 5 and 6, their conclusions correspond therefore either a somewhat stronger coupling or a smaller value of $|E_{sp}|$, with $E_{sp} < 0$, than our results.

Our treatment has ignored the coupling to the totally symmetric A_{1g} modes on the assumption that the 2s and 2p states

have the same coupling strength to these modes. Kayanuma and Toyozawa (1974) considered the possibility that each of these states have somewhat different coupling strengths to an A_{1g} mode. Including an interaction of the form (5.15), they investigated the vibronic problem composed of T_{1u} and A_{1g} modes and claimed on this basis to be able to remove the discrepancies of our model which involve the Stark effect shifts of the emission band. Carrying out an analysis for KCl, they found $E_{sp}/\hbar\omega \approx 1.0 - 1.5$, $E_G/\hbar\omega \approx 0.3 - 0.5$, $E_A/\hbar\omega \approx 1.5$, where E_A is the stabilization energy of the A_{1g} mode. The value for E_{sp} is about 3 times smaller than our estimate (21.2) but $E_{sp} + E_A$ agrees well, and so does E_G with (21.3). Furthermore, it appears from their diagrams that the quantities E_{10}, R, and $\Delta [\tau_r^{-1}(0)]$ of § 20 are not appreciably affected by the strong coupling to the A_{1g} mode. However, a reduction of the effective orbital g-value is found: $g_L \approx 0.6 - 0.7$. It will be interesting to read their conclusions in a more detailed publication.

In our treatment we have taken the vibronic coupling to be with a single T_{1u} mode. This is a good approximation if this coupling is with the LO phonons since we can then form a linear combination of these modes, all having roughly the same frequency, such that the coupling is only with this effective mode. If, on the other hand, the coupling is with a number of modes of different frequencies, our perturbation results need only be modified by summing the effects of the various modes. In the case of stronger coupling a good approximation could then be obtained using a single suitably averaged T_{1u} mode chosen in the manner described

by O'Brien (1972a).

Some years ago Tomura et al. (1967) pointed out that the temperature dependence of the F centre radiative lifetime in KCl below $\sim 120^{o}$ K could be fitted to the expression $\tau_r^{-1}(T) = \tau_r^{-1}(0) \cdot \coth(\hbar\omega/2kT)$ resulting from a forbidden 2s to 1s transition made allowed by coupling to an odd-parity phonon of energy $\hbar\omega$. This expression agrees with (20.15) if the coupling is sufficiently weak so that E_{10} of (20.11) is not appreciably smaller than $\hbar\omega \ll |E_{sp}|$ and terms of order $\exp(-2\hbar\omega/kT)$ may be neglected. Our weak-coupling model may therefore be regarded as an extension of this suggestion.

§ 23 Final Comments

In this thesis we investigated the ideal (s+p) ⊠ T_{1u} pseudo-Jahn-Teller system with emphasis on energy levels and optical properties. Useful in itself, such a study gives us also more insight into other PJT systems and throws new light on the JT problem as the electronic 2s-2p degeneracy is now only one particular case.

Our study has by no means been exhaustive, and we have hinted already further lines of interest in § 18. A comprehensive treatment including quadratic coupling and JT modes is certainly desirable. In general, this will of course lower the symmetry of the problem to cubic symmetry, thus shifting all vibronic levels and splitting those with $J \geq 2$ as well as differentiating between the reduction factors $K(E_g)$ and $K(T_{2g})$. However, there are special cases where the rotational symmetry is preserved, and approaches similar to those of O'Brien (1971b, 1969) and of Judd (1974) should prove useful.

We have shown that our vibronic model, with a 2s electronic state lying below 2p, provides a realistic picture for the F centre in KF, KCl, KBr, and KI. If it applies also to other alkali halides is another matter which has to be clarified by further measurements. Presumably it is not appropriate for CsF for which a very small electric-field-induced polarization (Bogan-Fitchen 1970) and a short radiative lifetime (Fulton-Fitchen 1970) have been measured.

Finally, we may look for other systems where this model is applicable. Ham (1972c) has pointed out that it should be appropriate for the U-centre. This topic is also left to future study.

REFERENCES

Abragam A Bleaney B (1970) Electron Paramagnetic Resonance of Transition Metal Ions, Oxford Clarendon Press

Adrian F J (1957) Phys Rev 107, 488

Baldacchini G Mollenauer L F to be published

Bäuerle D Hübner R (1970) Phys Rev B2, 4252

Bogan L D Fitchen D B (1970) Phys Rev B1, 4122; Bogan L D Stiles L F Fitchen D B (1969) Phys Rev Lett 23, 1495

Born M Huang K (1954) Dynamical Theory of Crystal Lattices, Oxford Clarendon Press

Born M Oppenheimer J R (1927) Ann Phys 84, 457

Bowdler H Martin R S Reinsch C Wilkinson J H (1968) Num Math 11, 293

Bronstein I N Semendjajew K A (1967) Taschenbuch der Mathematik, Harri Deutsch Zürich

Buyers W J L (1967) Phys Rev 153, 923

Chiarotti G Grassano U Rosei R(1966) Phys Rev Lett 17, 1043; Chiarotti G Grassano U M Margaritondo G Rosei R (1969) Nuovo Cimento B64, 159

Dexter D L (1958) Sol St Phys 6, 352

Englman R Caner M Toaff S (1970) J Phys Soc Japan 29, 306

Englman R (1972a) The Jahn-Teller Effect in Molecules and Crystals, Wiley Interscience London

Englman R (1972b) unpublished calculations

Fano U Racah G (1959) Irreducible Tensorial Sets, Academic Press

Flügge S (1965) Rechenmethoden der Quantentheorie, Springer Verlag Berlin

Fontana M P Fitchen D B (1969) Phys Rev Lett 23, 1497

Fontana M P (1970a) Phys Rev B2, 1107

Fontana M P (1970b) Phys Rev B2, 4304, (1972) Phys Rev B5, 759

Fowler W B (1964) Phys Rev 135, A1725

Fowler W B Calabrese E Smith D Y (1967) Sol St Comm 5, 569

Fowler W B (1968) Physics of Color Centers, Academic Press

Frŏhlich D Mahr H (1966) Phys Rev 141, 692

Fulton T A Fitchen D B (1970) Phys Rev B1, 4011

Gradshteyn I S Ryzhik I M (1965) Table of Integrals, Series and Products, Academic Press

Grevsmŭhl U Wagner M (1973) Phys Stat Sol (b) 58, 139; Grevsmŭhl U (1971) Diplomarbeit, Universität Stuttgart

Griffith J S (1962) The Irreducible Tensor Method for Molecular Symmetry Groups, Prentice-Hall International, London

Ham F S (1965) Phys Rev 138, A1727

Ham F S (1968) Phys Rev 166, 307

Ham F S Schwarz W M O'Brien M C M (1969) Phys Rev 185, 548

Ham F S (1972a) in Electron Paramagnetic Resonance ed S Geschwind, Plenum Press

Ham F S (1972b) Phys Rev Lett 28, 1048; (1972c) Seminar held in the Clarendon Laboratory, Oxford University

Ham F S (1973a) Phys Rev B8, 2926

Ham F S Grevsmŭhl U (1973b) Phys Rev B8, 2945

Heitler W (1954) Quantum Theory of Radiation, Oxford University Press

Henry C H Schnatterly S E Slichter CP (1965) Phys Rev 137, A583; Henry C H Slichter C P in Fowler (1968)

Hetrick R E Compton W D (1967) Phys Rev 155, 649

Hetrick R E (1969) Phys Rev 188, 1392

Iida T Kurata K Muramatsu S (1972) J Phys Chem Solids 33, 1225

International Conference in Color Centers in Ionic Crystals, (1974) Sendai Japan, Tohoku University

Jahn H A Teller E (1936) Phys Rev 49, 874; (1937) Proc Roy Soc A161, 220

Jahn H A (1938) Proc Roy Soc A164, 117

Judd B R (1963) Operator Techniques in Atomic Spectroscopy, McGraw Hill; (1967) Second Quantization and Atomic Spectroscopy, The Johns Hopkins Press, Baltimore

Judd B R (1974) Can J Phys 52, 999

Kayanuma Y Toyozawa Y in Int Conf Color Centers (1974)

Kondo Y Kanzaki H in Int Conf Color Centers (1974), (1975) Phys Rev Lett 34, 664

Kühnert H (1967) Phys Stat Sol 21, K171

Landau L D Lifschitz E M (1967) Statistical Physics § 28, 30, Pergamon Press

Lax M (1952) J Chem Phys 20, 1752

Liehr A D (1963) J Phys Chem 67, 389 and 471

Loader R J (1969) Ph D thesis, Reading University

Longuet-Higgins H C Öpik U Pryce M H L Sack R A (1958) Proc Roy Soc A244, 1; Longuet-Higgins H C (1961) Adv in Spectr 2, 429

Margerie J (1967) J Phys (Paris) Suppl 28, C4-103

Markham J J (1966) F-Centers in Alkali Halides, Solid State Physics Suppl 8, Academic Press

Martin R S Reinsch C Wilkinson J H (1968) Num Math 11, 181

Messiah A (1969) Quantum Mechanics, Vol I and II, North-Holland

Moffitt W Thorson W (1957) Phys Rev 108, 1251

Mollenauer L F Pan S Yngvesson S (1969) Phys Rev Lett 23, 683; Mollenauer L F Pan S Winnaker A (1971) Phys Rev Lett 26, 1643; Mollenauer L F Pan S (1972b) Phys Rev B6, 772

Mollenauer L F Baldacchini G (1972a) Phys Rev Lett 29, 465

O'Brien M C M (1969) Phys Rev 187, 407

O'Brien M C M (1971b) J Phys C: Solid State Phys 4, 2524

O'Brien M C M (1971c) in Englman (1972a) p.50

O'Brien M C M (1972a) J Phys C: Solid State Phys 5, 2045

O'Brien M C M (1972b),(1973) unpublished calculations

Ohkura H Iida T Mori Y Kamada O in Int Conf Color Centers (1974)

Ö̈pik U Pryce M H L (1957) Proc Roy Soc A238, 425

Park K Faust W L (1966) Phys Rev Lett 17, 137

Podini P (1966) Phys Rev 141, 572

Raunio G Almiquist L (1969a) phys stat sol 33, 209; Raunio G Almiquist L Stedman R (1969b) Phys Rev 178, 1496; Raunio G Rolandson S (1970) J Phys C3, 1013

Ruedin Y Schnegg P-A Jaccard C Aegerter M A (1972) phys stat sol (b) 54, 565; (1973) phys stat sol (b) 55, 215

Schnatterly S E (1965) Phys Rev 140, A1364

Seidel H Wolf H C in Fowler (1968) p. 537

Sigmund E Wagner M (1973) phys stat sol (b) 57, 635

Spinolo G Fowler W B (1965) Phys Rev 138, A661

Stiles L F Jr Fontana M P Fitchen D B (1970) Phys Rev B2, 2077; (1969) Sol State Comm 7, 681

Sturge M D (1967) Sol State Phys 20, 91

Swank R K Brown F C (1963) Phys Rev 130, 34; (1962) Phys Rev Lett 8, 10

Tinkham M (1964) Group Theory and Quantum Mechanics, McGraw Hill

Tomura M Kitada T Honda S (1967) J Phys Soc Jap 23, 454

Toyozawa Y Inoue M (1965) J Phys Soc Jap 20, 1289; (1966) J Phys Soc Jap 21, 1663

Van Vleck J H (1939) J Chem Phys 7, 72

Wang S Matsuura M Wong C C Inoue M (1973) Phys Rev B7, 1695

Wigner E P (1959) Group Theory and its Application to the Quantum Mechanics of Atomic Spectra, Academic Press

Wilson E B Decius J C Cross P C (1955) Molecular Vibrations, McGraw Hill

Wood R F Ö̈pik U (1969) Phys Rev 179, 783

GRAPH INDEX

Graphs 1 to 5: Lowest vibronic energy levels v.s. $\sqrt{\varepsilon_G}$ for $J \leq 2$ or 3, $j \leq 2$ or 3 and $\delta = 0, \pm 0.5, \pm 2.5$. δ denotes the parameter of the electronic 2s-2p spacing and is defined by (6.9). The stabilization energy $\varepsilon_G = \varkappa^2$ is added to the energies of the levels for convenience. The type I levels are labelled by the main quantum number j and their total angular momentum J. Note the ordering for strong coupling. On the left, all possible occurring states at zero coupling strength are denoted by a(J+2N,J), b(J+1+2N,J+1), c(J-1+2N,J-1) and d(J+2N,J) which refer to the vibronic states (8.6a,b,c, and d), respectively. Note that not all of the corresponding levels are drawn.

Graph 6: Energy difference between the two lowest vibronic type I levels v.s. ε_G for various values of δ: $|\varepsilon_{10}| \equiv |\varepsilon(I,00) - \varepsilon(I,01)|$. Note the double logarithmic scale. In the limit of strong coupling the dependence is $(2\varepsilon_G)^{-1}$.

Graph 7: Total admixtures of the s-J-states (8.6a) in the four lowest type I states with J = 0 and $\delta = 0$:
$\sum_{N=0}^{\infty} |a(0,j,2N)|^2$ v.s. $\sqrt{\varepsilon_G}$.

Graphs 8 to 10: Vibronic energy levels with J=1 v.s. $\sqrt{\varepsilon_G}$ for $\delta = 0, \pm 2.5$. In contrast to the Graphs 1 to 5, ε_G has not been added. Note that the type II levels are independent of ε_G. The numbers in the graphs refer to the j-values of the levels. The arrows on the right-hand side and top indicate type B and C levels and are denoted with the appropriate quantum numbers. The crosses on some of the levels in the Graphs 8 and 10 refer to maxima of the type B absorption lines, the circles in Graph 8 to maxima of the type C absorption lines with C=0 (see § 14 and Graphs 22 to 25).

Graphs 11 to 12: Vibronic energy levels with J=0 and 1 for fixed ε_G v.s. δ. For $\varepsilon_G = 0$ the states and corresponding energies are given by (8.6a-d) and (8.7a-d), respectively, which are referred to in the graphs as a,b,c,d. Note the doubly J-degenerate states in Graph 12, arising from (8.6b and c). For clarity, type II states are drawn only for $\varepsilon_G = 0$ (Graph 12). The crosses and circles in Graph 12 indicate the major intensity contributions of the lowest lying type B and C absorption peaks, respectively (for B=0 only intensities greater than 0.1 are represented). Note that for $\varepsilon_G = 0$ the lowest type B level is given by (8.7c) with J=1,N=0. Similarly, the lowest type C level is given by (8.7a) for $\delta \geq 0.5$ and (8.7b) for $\delta \leq 0.5$ with J=1,N=0.

Graphs 13 to 16: Emission spectra from the lowest type I state with J=0 for δ=0 (G.13), J=1 for δ=0 (G. 14), J=0 for $\delta = -2.5$ (G.15), J=0 and/or 1 for $\delta = 2.5$ (G.16). The spectra are given

for representative values of $\varkappa = \sqrt{\varepsilon_G}$ and are drawn v.s. $\varepsilon - \varepsilon'_o$ or $\varepsilon - \varepsilon''_o$ where $\varepsilon'_o = \varepsilon(I,01) + \varepsilon_o - 1.5$ and $\varepsilon''_o = \varepsilon(I,00) + \varepsilon_o - 1.5$, so that the n^{th}-phonons line has the position $(-n)$ in the graphs. $\varepsilon(I,00)$ or $\varepsilon(I,01)$ has been stated in each case together with the total 2p-admixtures $N(jJ)$ at given δ and $\varkappa$.

Graph 17: Strengths of the (2N)- and (2N+1)-phonons emission lines for $\delta=0$ with $N=0,1,2$ v.s. $\sqrt{\varepsilon_G}$, which correspond to the Graphs 14 and 13, respectively.

Graphs 18 to 21: Emission spectra at non-zero temperatures for $\delta=0$ and $\varepsilon_G=1$ and for $\delta=0,\pm2.5$ and $\varepsilon_G = 4$. The broadening parameter is denoted by H, and β is defined by $kT/\hbar\omega$.

Graphs 22 to 25: Strengths of absorption lines v.s. $\sqrt{\varepsilon_G}$ for representative values of δ. The numbers in the graphs denote the j-values of the corresponding type I states with J=1. The arrows on the right-hand side indicate type A, B, and C absorption lines. The type B and C lines with given quantum numbers each refer to a group of absorption maxima; for strong tendency of energy levels crossing the associated envelope absorption lines are drawn (dashed lines).

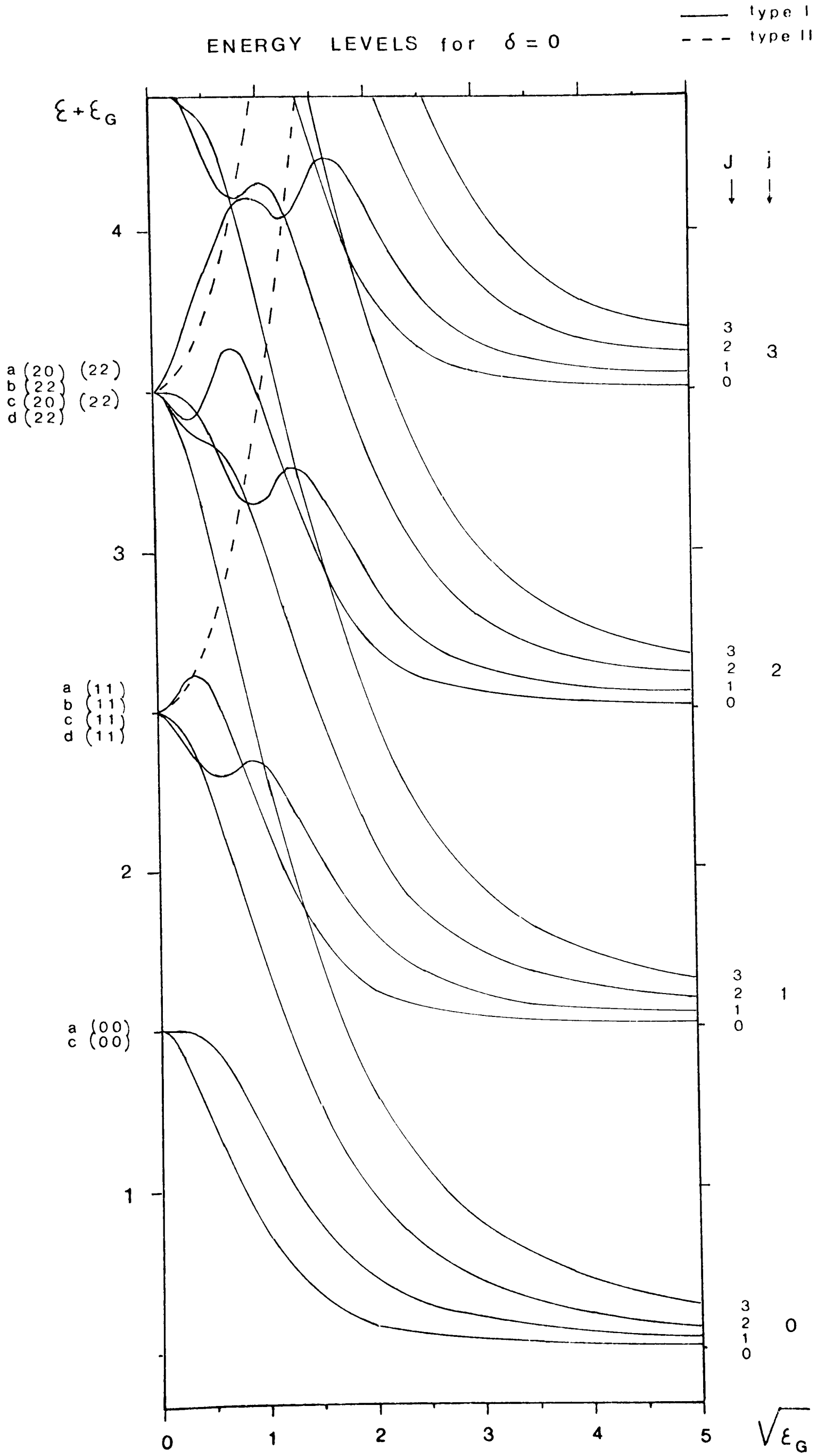
Graphs 26 to 39: Normalised absorption spectra at zero temperature for representative values of δ and ε_G. $I^{(a)}(00,\varepsilon)$ of (14.2) is drawn on logarithmic scale v.s. $\varepsilon - \varepsilon_o + 3/2$. Each absorption line is associated with a type I energy level with j and J=1. The letters and numbers in the graphs indicate type A,B,C absorption peaks. Whereas each quantum number A refers to an absorption line of predominantly type A character, each B or C belongs in general to a group of lines associated with a type B or C energy level with J=1. Whenever possible, absorption peaks with B = 0,1,2,3 and C =0,1 have been indicated. Similarly, type A lines have been denoted whenever identified. The notation in Graph 35, for instance, means that all lines at the low-energy end of the spectrum up to and including j=A=19 have predominantly type A character. The dashed lines in the Graphs 35 to 39 represent the semiclassical absorption line shape function (16.13).

Graphs 41 to 43: Strengths of one-phonon emission line, zero-phonon line and (j=1)-absorption line for $\delta=0$ v.s. $\sqrt{\varepsilon_G}$. The computed lines of § 13 and 14 are compared with the weak coupling approximation of § 12 and the strong coupling expressions (15.11, 15, and 18), respectively.

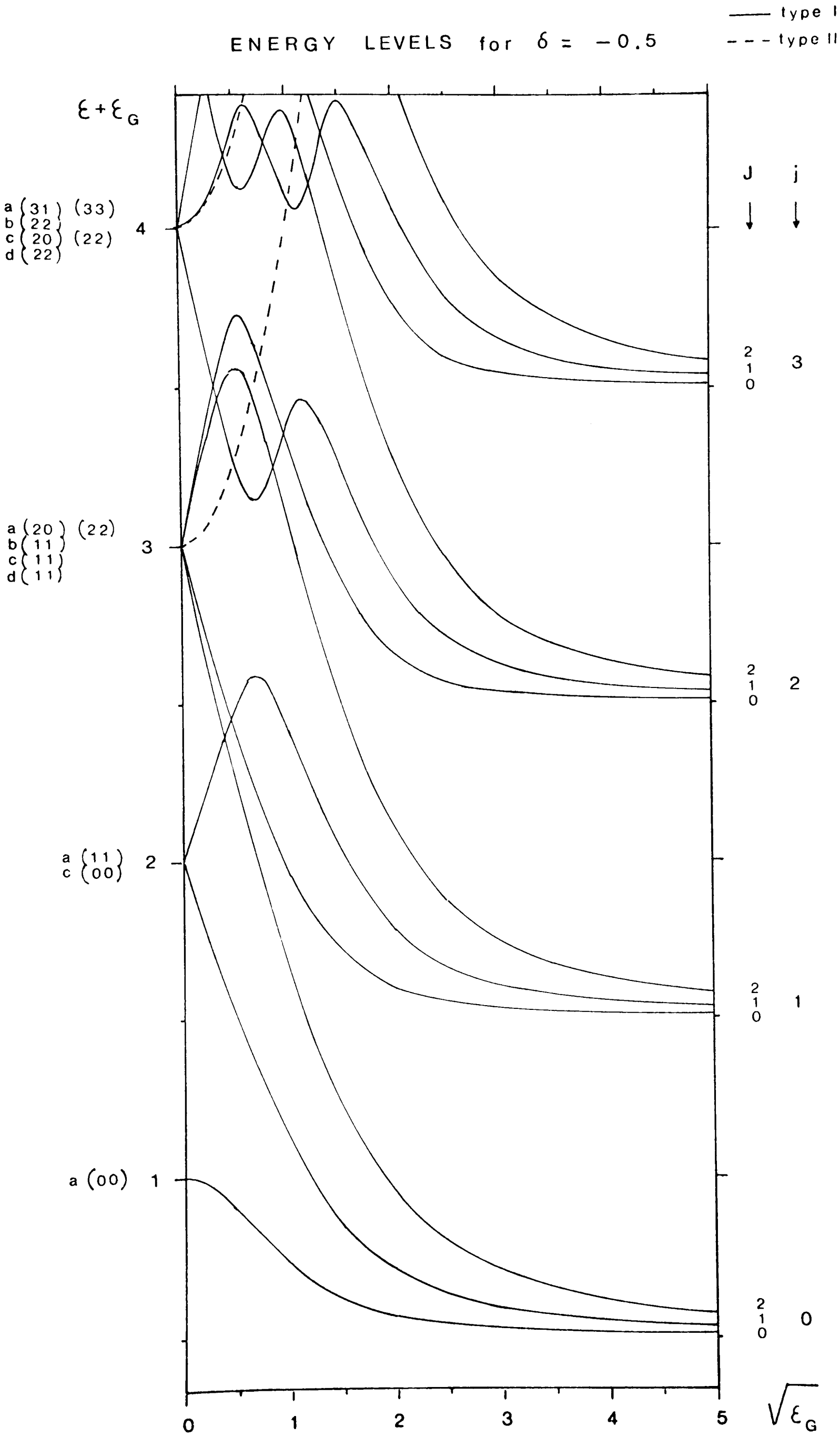
Graph 44: Semi-classical absorption bands v.s. $X = (\varepsilon - \varepsilon_o)/\sqrt{2\varepsilon_G}$ for representative values of δ and b. Note that $b = \tanh(\frac{1}{2}\beta)$ with $\beta = kT/\hbar\omega$. $b=1,\frac{1}{2},1/4$ correspond to $\beta=0,0.91,2$, respectively. The wings belonging to the same parameters have reflexion symmetry as regards to X=0, they are independent of the sign of δ. Whereas the strengths of the delta-functions are equal to 0.5 for all parameters, their positions depend only on $\delta/\sqrt{2\varepsilon_G}$, with dashed lines corresponding to positive values of δ.

Graphs 45 to 47: Reduction factors $K(\varepsilon)$ and $K(T_1)$ v.s. ε_G for representative values of δ. Note the double logarithmic scale.

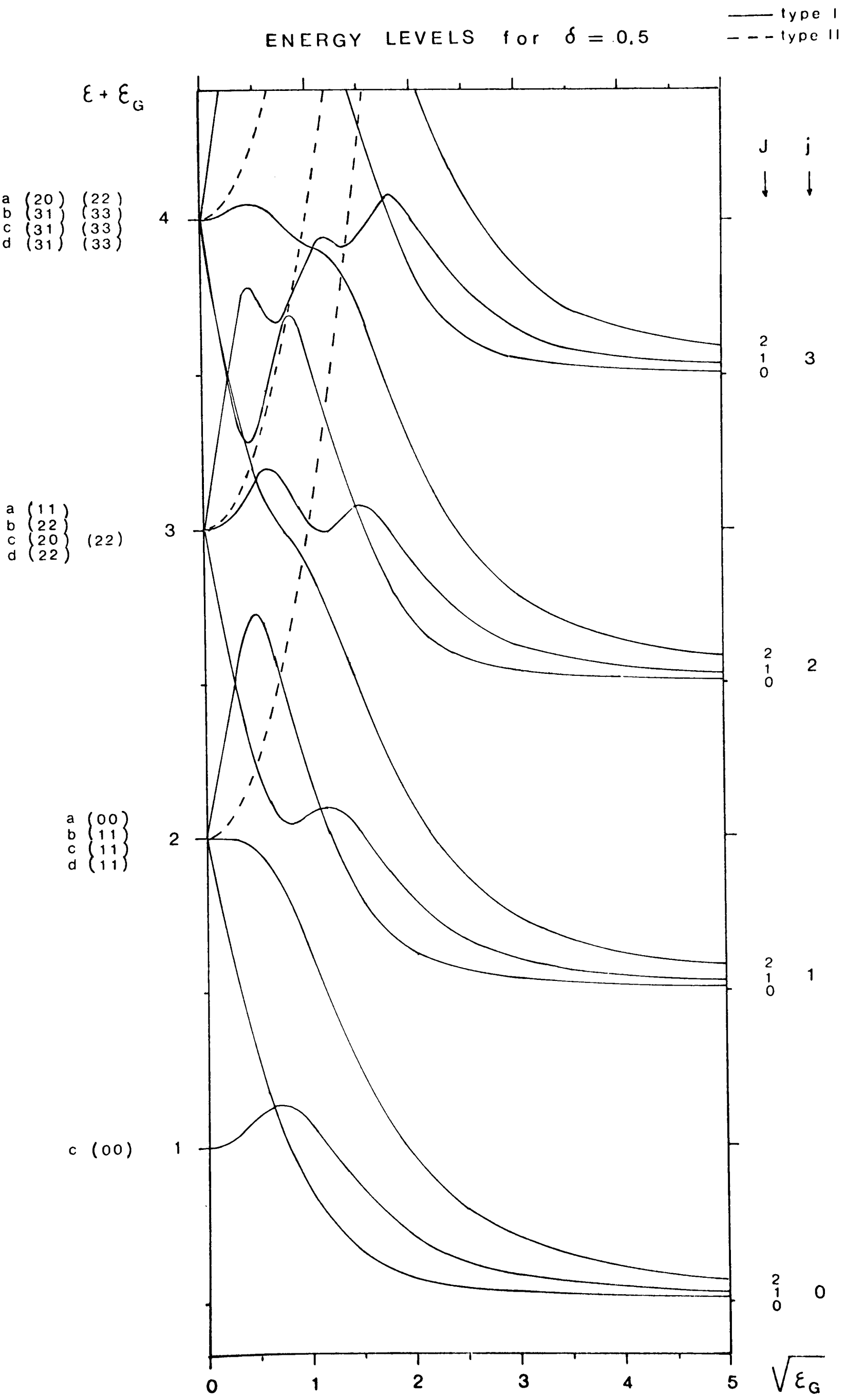
GRAPH 1


type I
type II
ENERGY LEVELS for δ = 0
ε + ε_G
J j
4
3
2
1
a (20) (22)
b (22)
c (20) (22)
d (22)
a (11)
b (11)
c (11)
d (11)
a (00)
c (00)
3 2 1 0
3
2
1
0
0 1 2 3 4 5
√ε_G

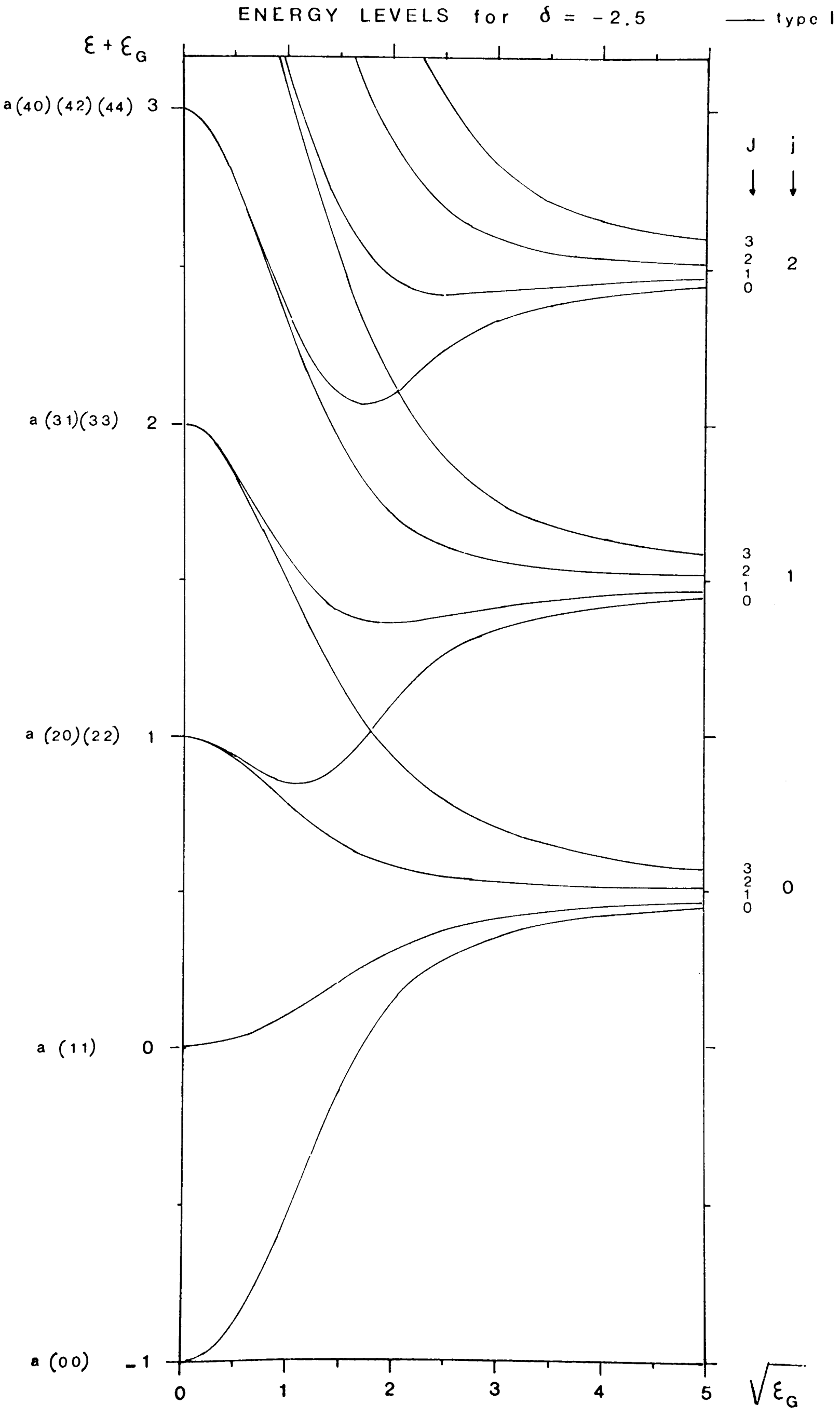
GRAPH 2


type I
type II
ENERGY LEVELS for δ = −0.5
ε + ε_G
J j
a (31) (33)
b (22)
c (20) (22)
d (22)
4
2 1 0 3
a (20) (22)
b (11)
c (11)
d (11)
3
2 1 0 2
a (11)
c (00)
2
2 1 0 1
a (00)
1
2 1 0 0
0 1 2 3 4 5
√ε_G

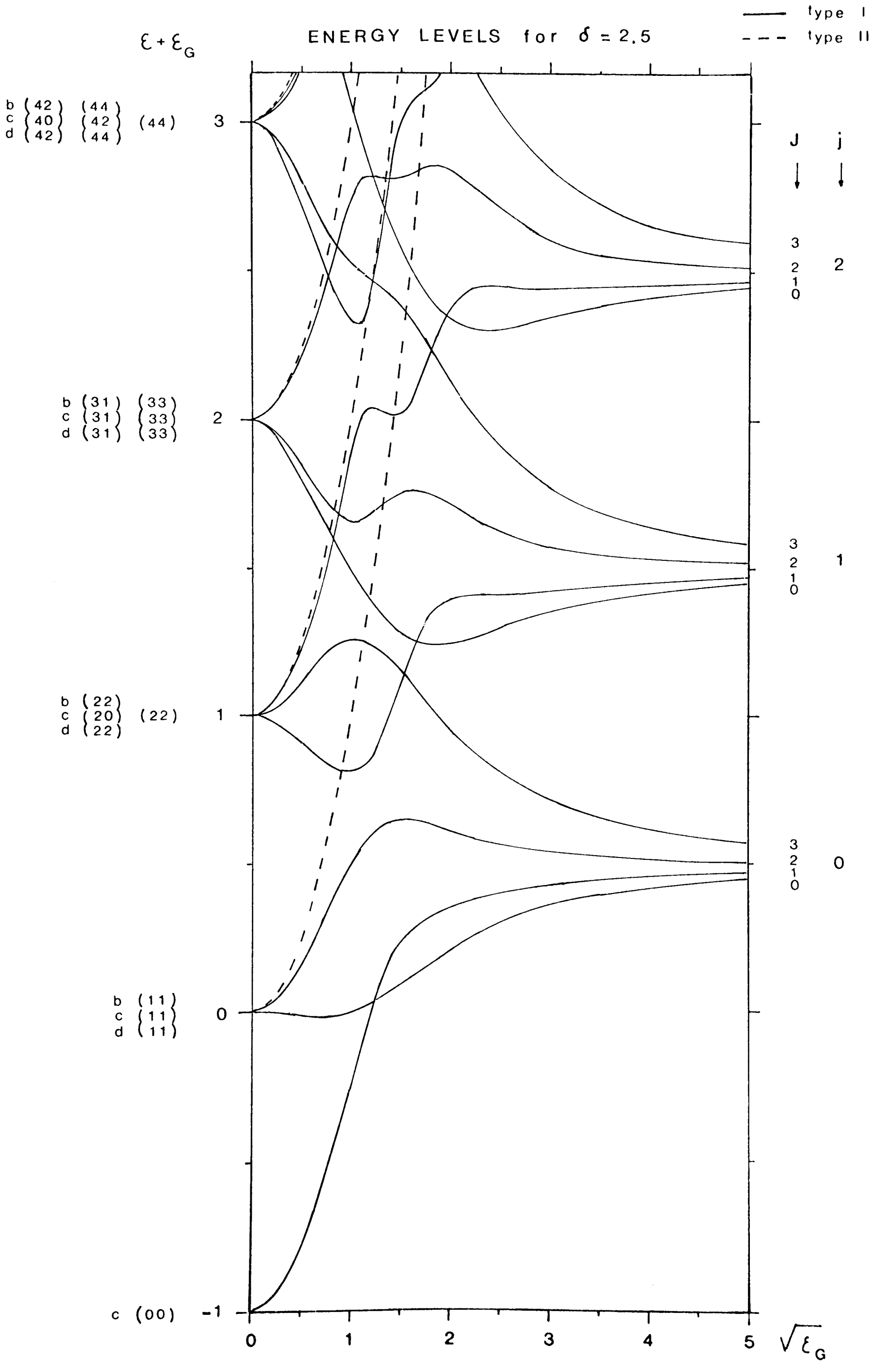
GRAPH 3


type I
type II
ENERGY LEVELS for δ = 0.5
ε + ε_G
J j
a (20) (22)
b (31) (33)
c (31) (33)
d (31) (33)
4
2 1 0 3
a (11)
b (22)
c (20) (22)
d (22)
3
2 1 0 2
a (00)
b (11)
c (11)
d (11)
2
2 1 0 1
c (00)
1
2 1 0 0
0 1 2 3 4 5
√ε_G

GRAPH 4

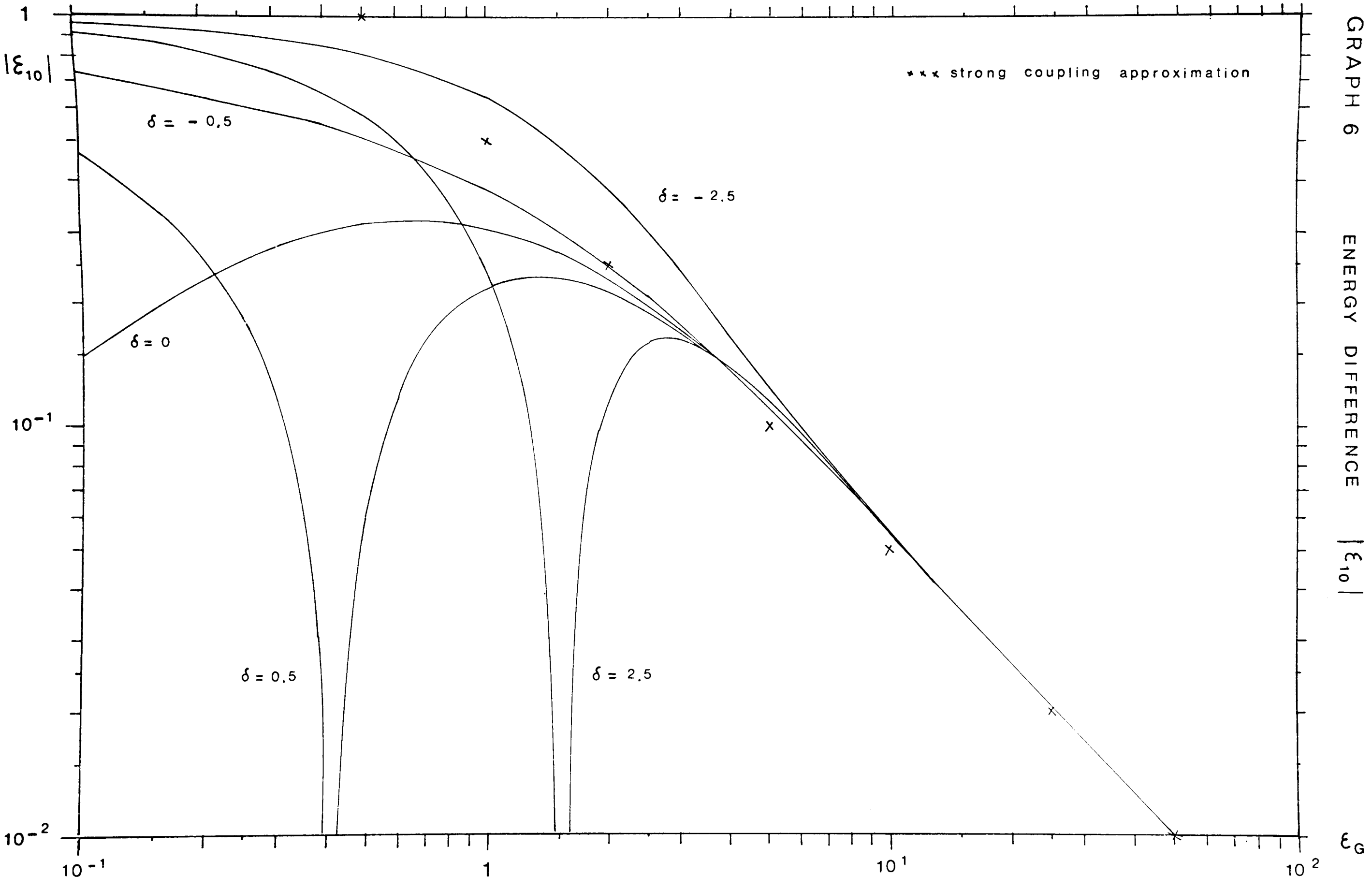

ENERGY LEVELS for δ = -2.5
type I
ε + ε_G
a(40)(42)(44) 3
a(31)(33) 2
a(20)(22) 1
a(11) 0
a(00) -1
J j
3 2 1 0 2
3 2 1 0 1
3 2 1 0 0
0 1 2 3 4 5
√ε_G

GRAPH 5


type I
type II
ENERGY LEVELS for δ = 2.5
ε + ε_G
b (42) (44)
c (40) (42) (44)
d (42) (44)
3
b (31) (33)
c (31) (33)
d (31) (33)
2
b (22)
c (20) (22)
d (22)
1
b (11)
c (11)
d (11)
0
c (00)
-1
J
j
3
2
1
0
2
3
2
1
0
1
3
2
1
0
0
0
1
2
3
4
5
√ε_G

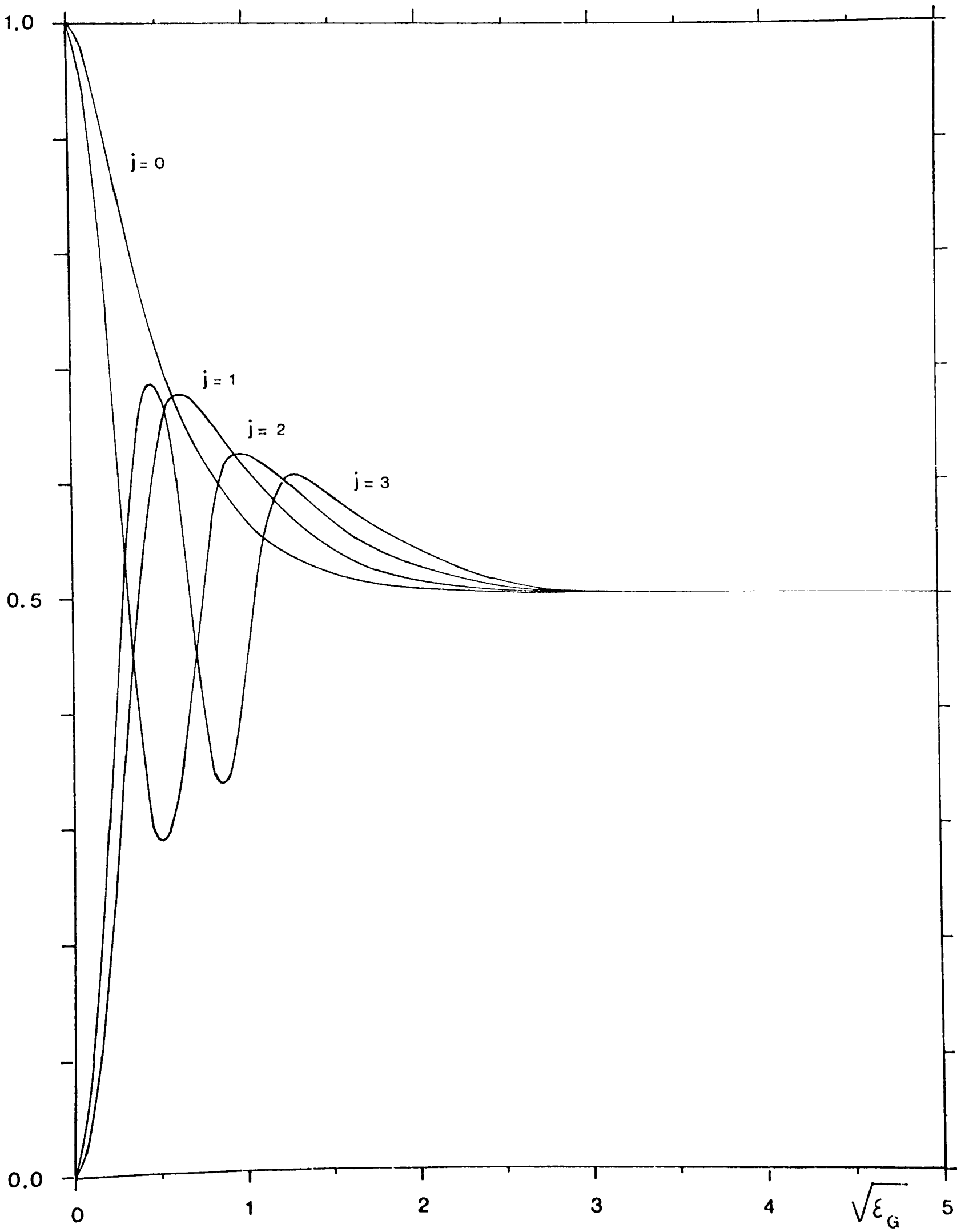
GRAPH 6

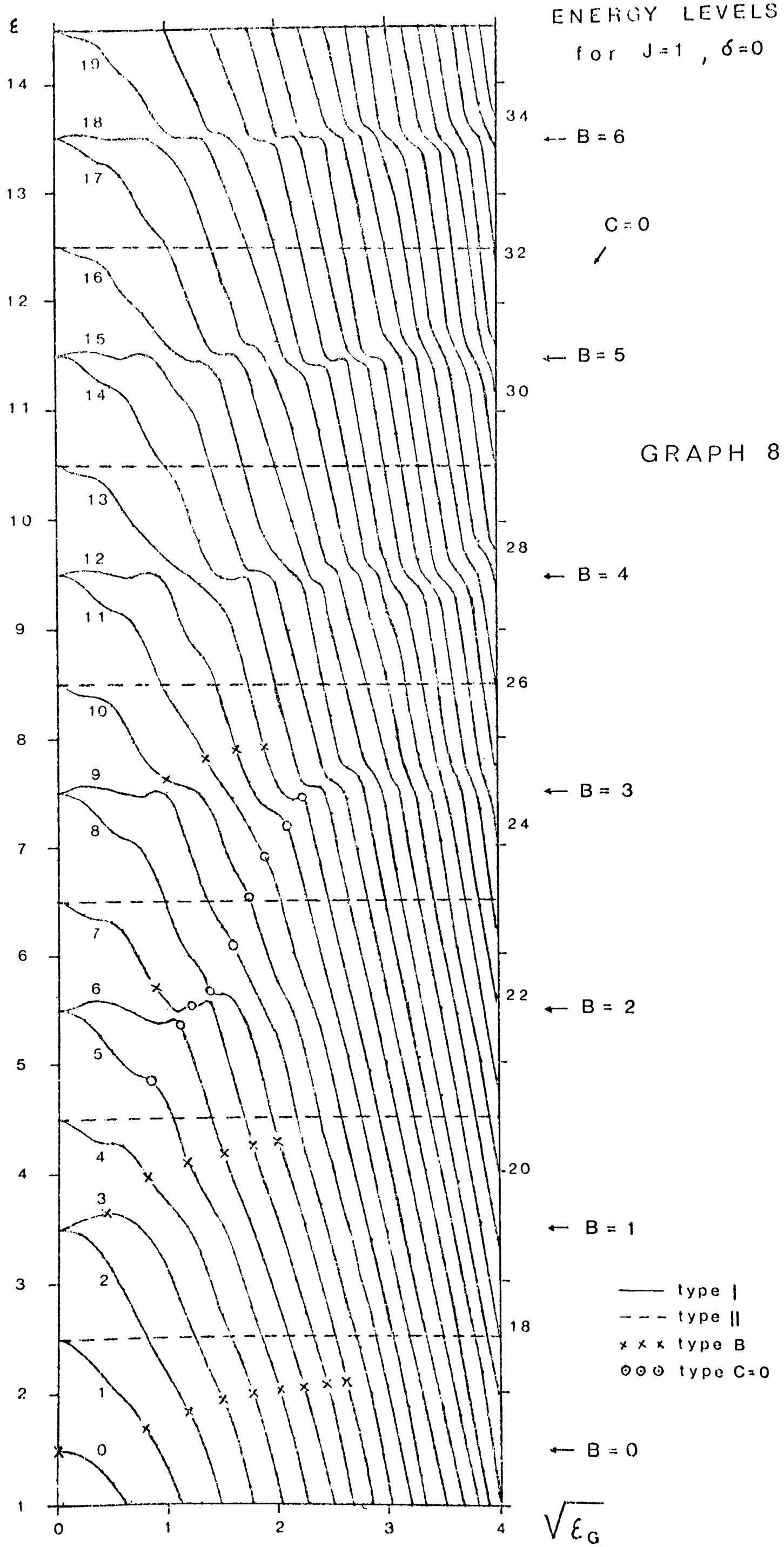
ENERGY DIFFERENCE $|\varepsilon_{10}|$



GRAPH 7

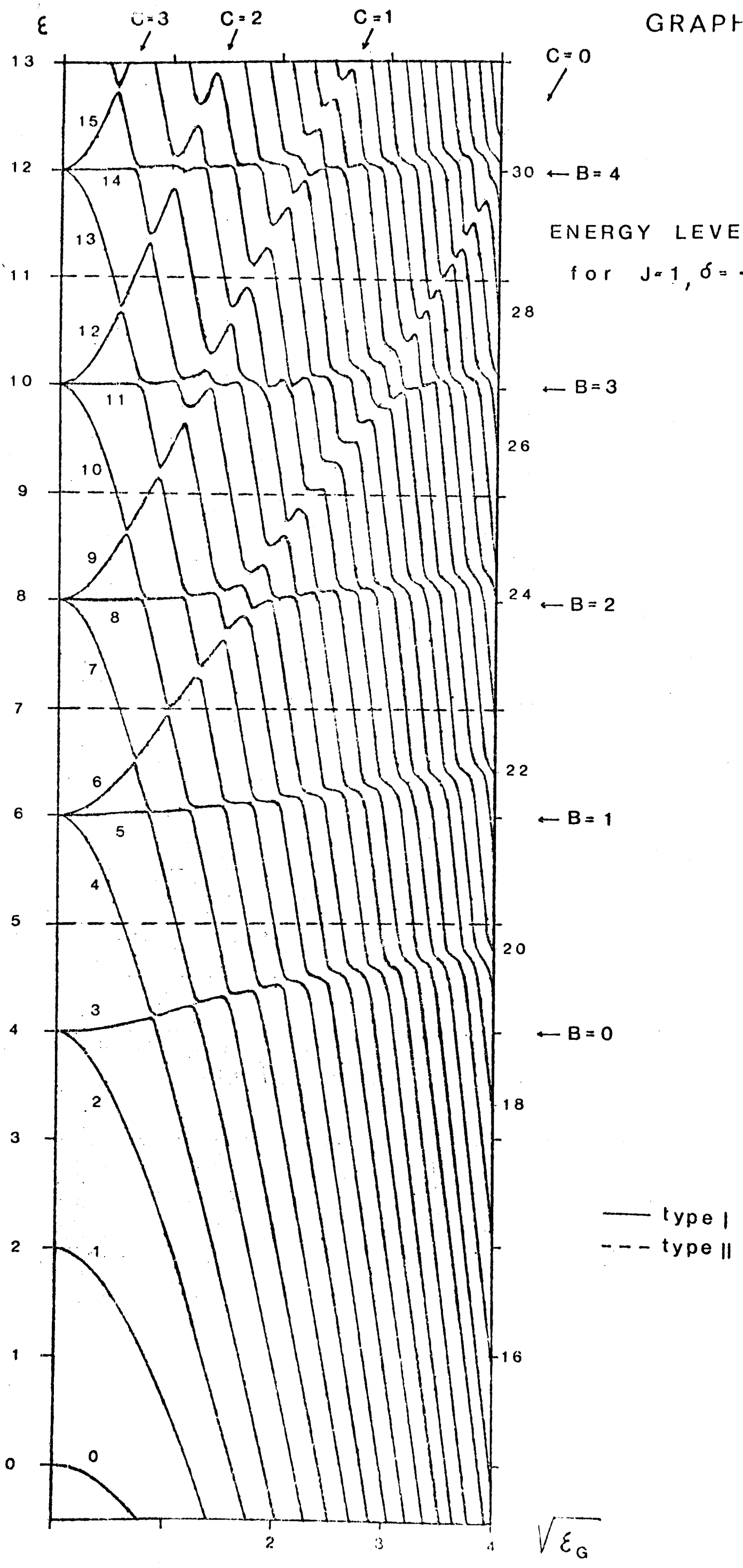
s-J-ADMIXTURES of type $\bar{I}$ states with $J=0$ for $\delta=0$



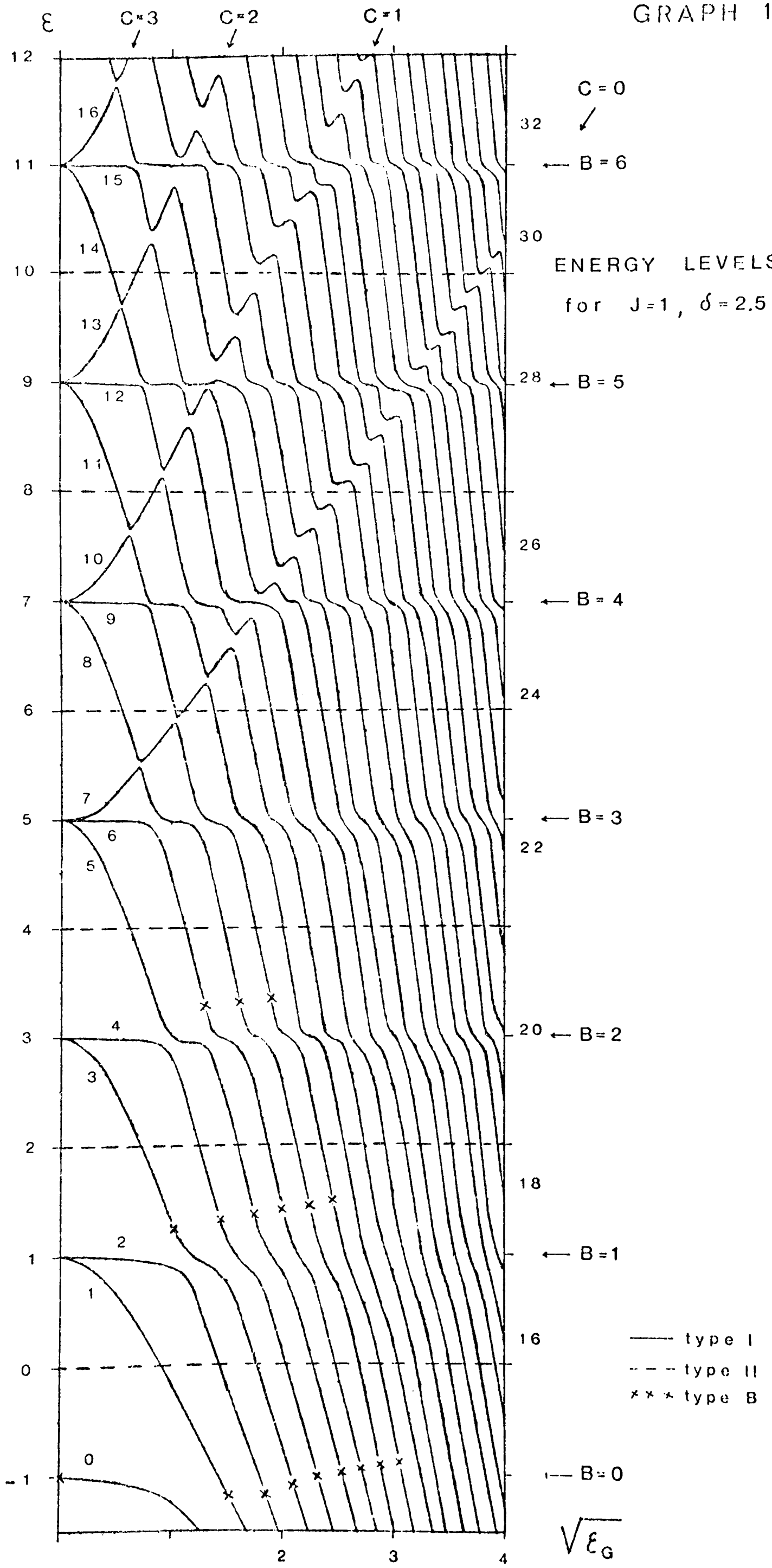

ENERGY LEVELS
for J=1 , δ=0
ε
14
13
12
11
10
9
8
7
6
5
4
3
2
1
0
1
2
3
4
19
18
17
16
15
14
13
12
11
10
9
8
7
6
5
4
3
2
1
0
34
32
30
28
26
24
22
20
18
← B = 6
C = 0
← B = 5
← B = 4
← B = 3
← B = 2
← B = 1
← B = 0
type I
type II
type B
type C=0
$\sqrt{\varepsilon_G}$

GRAPH 8

GRAPH 9

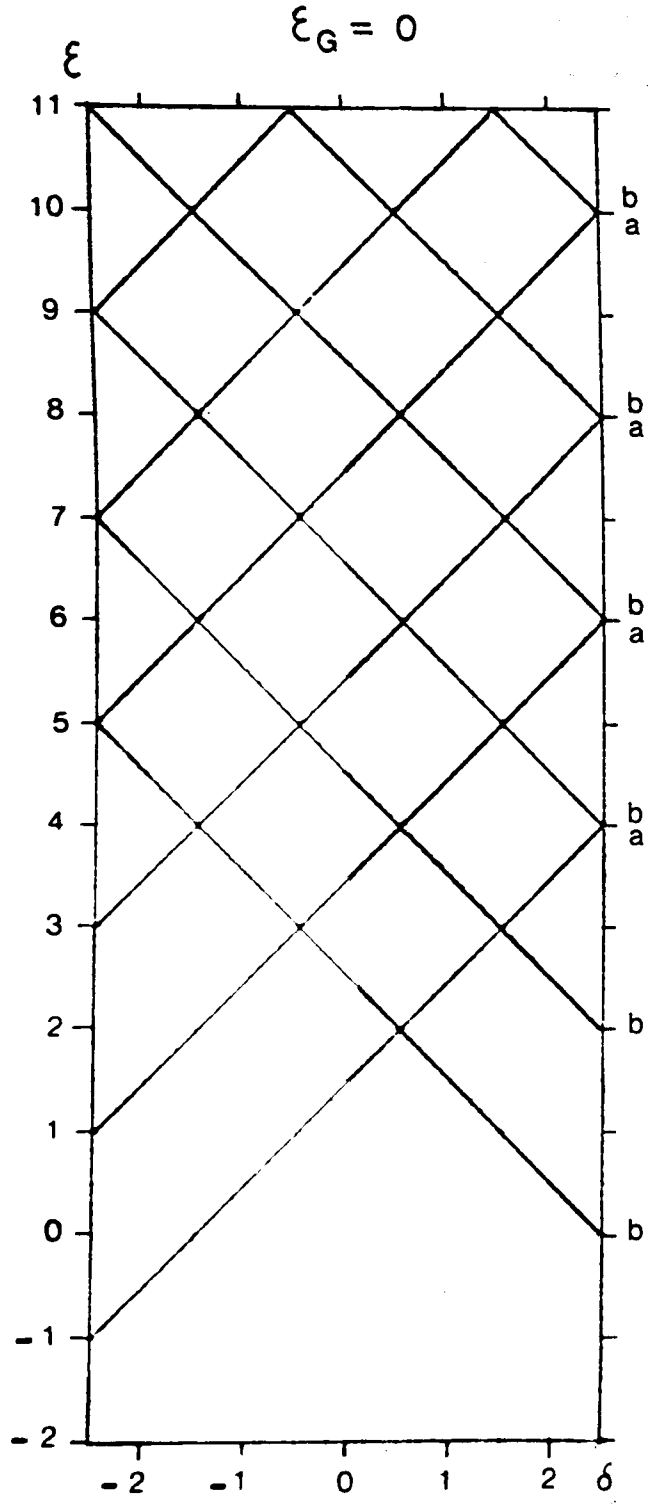

ε
C=3
C=2
C=1
C=0
13
12
11
10
9
8
7
6
5
4
3
2
1
0
15
14
13
12
11
10
9
8
7
6
5
4
3
2
1
0
30
28
26
24
22
20
18
16
← B=4
← B=3
← B=2
← B=1
← B=0
ENERGY LEVELS
for J=1, δ=-2.5
type I
type II
2
3
4
√ε_G

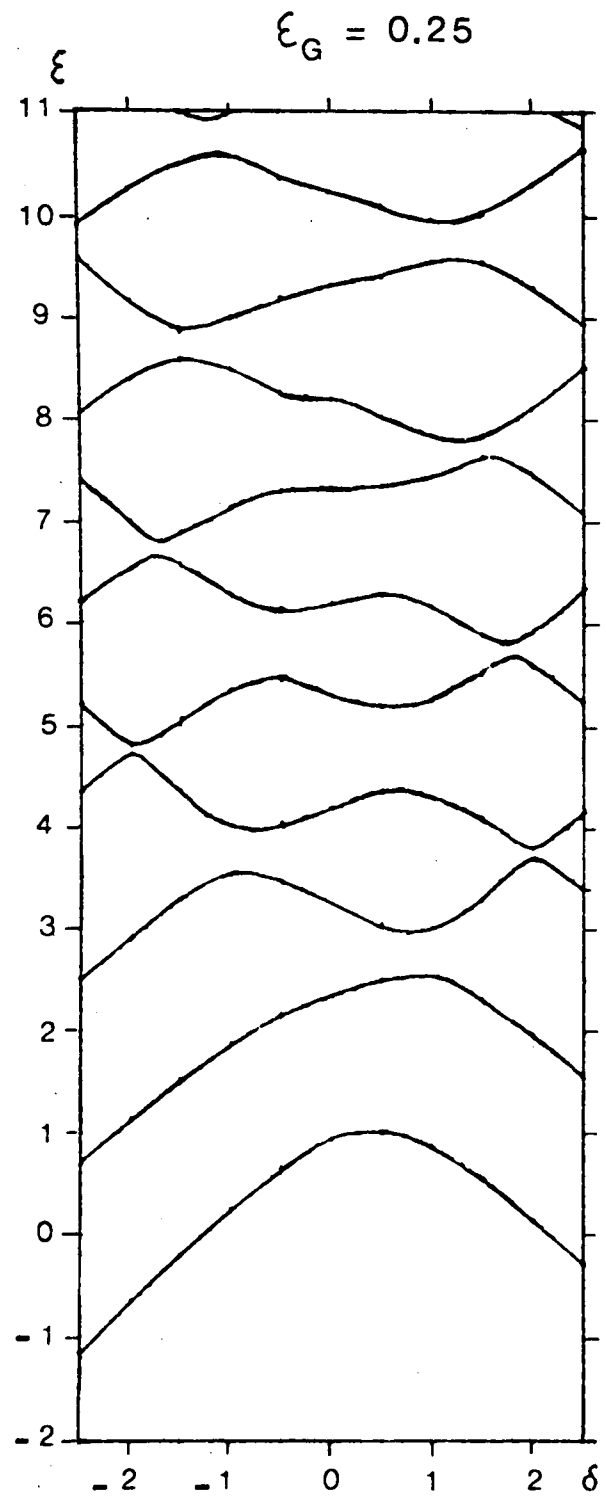
GRAPH 10

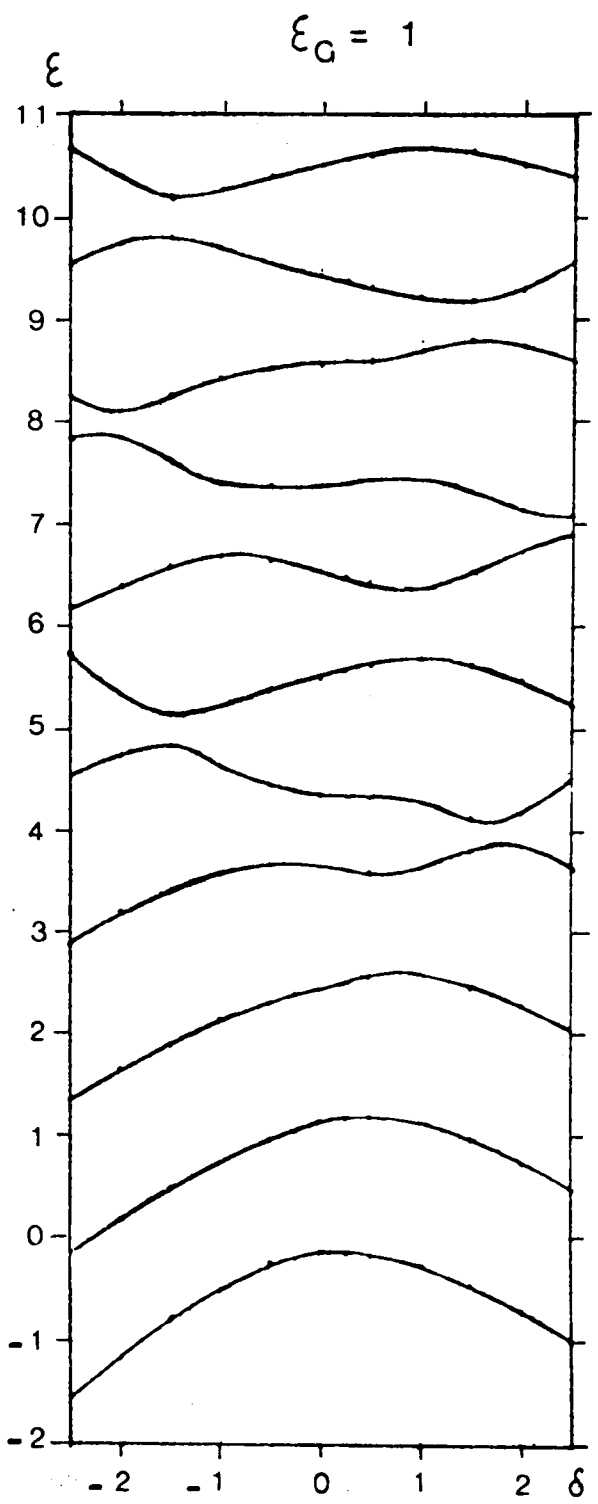

ε
C=3
C=2
C=1
C = 0
12
11
10
9
8
7
6
5
4
3
2
1
0
-1
16
15
14
13
12
11
10
9
8
7
6
5
4
3
2
1
0
32
30
28
26
24
22
20
18
16
B = 6
B = 5
B = 4
B = 3
B = 2
B = 1
B = 0
ENERGY LEVELS
for J = 1 , δ = 2.5
type I
type II
type B
2
3
4
$\sqrt{\varepsilon_G}$

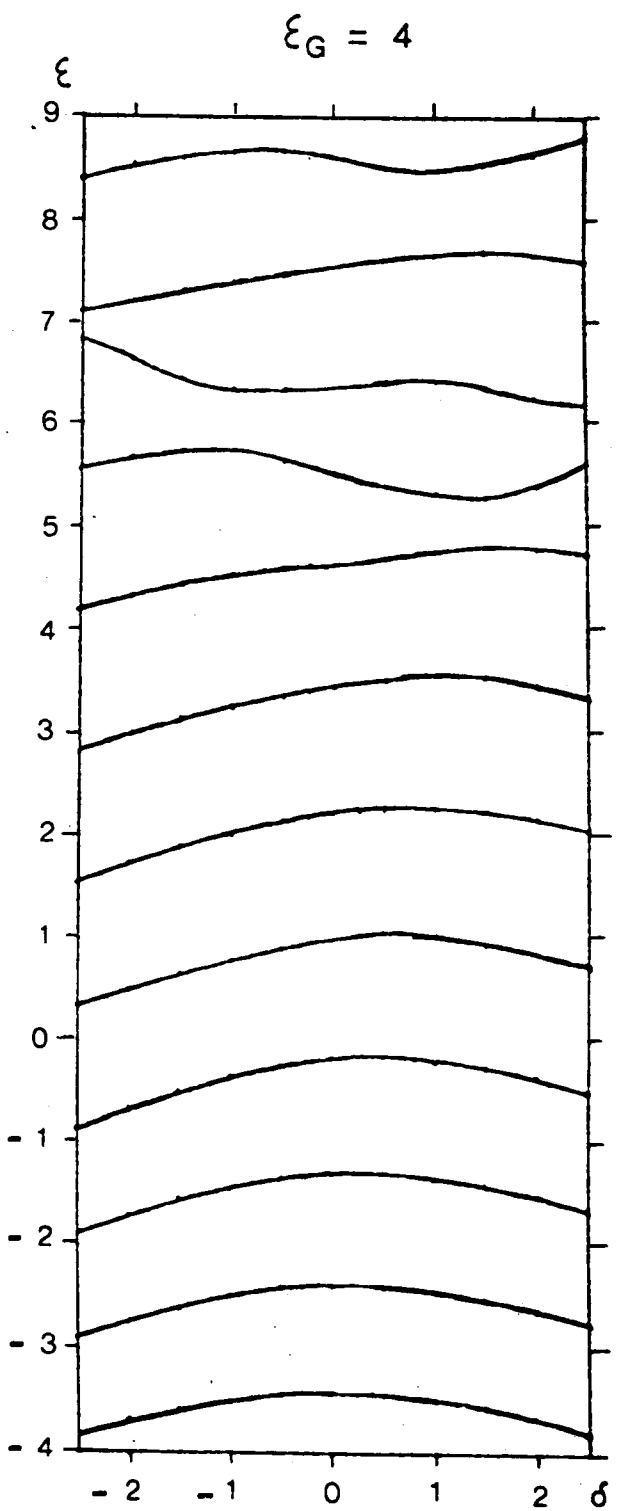
ENERGY LEVELS for J=0 and given ε_G

GRAPH 11







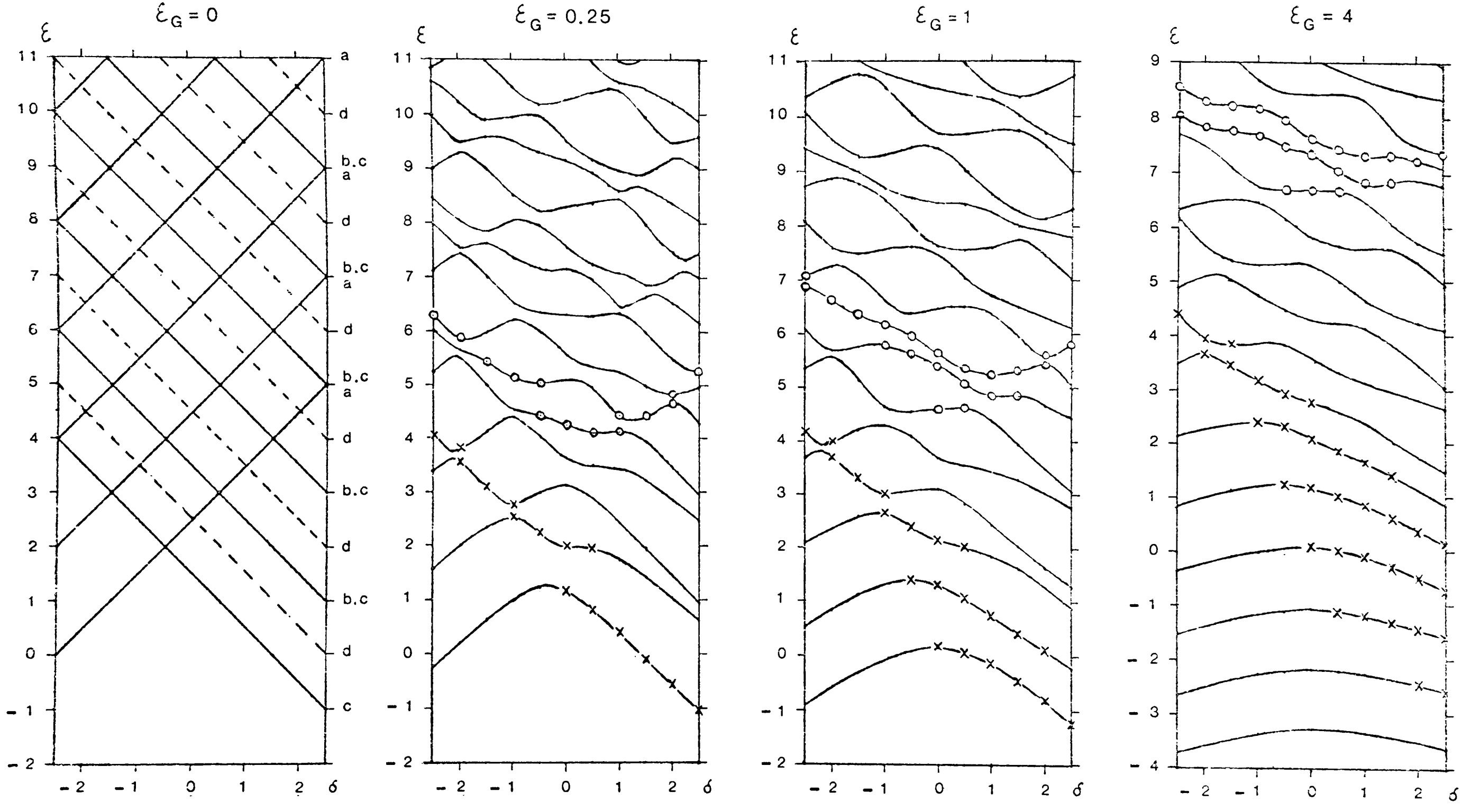


GRAPH 12

ENERGY LEVELS for J = 1 and given ε_G

—— type I ××× type B=0

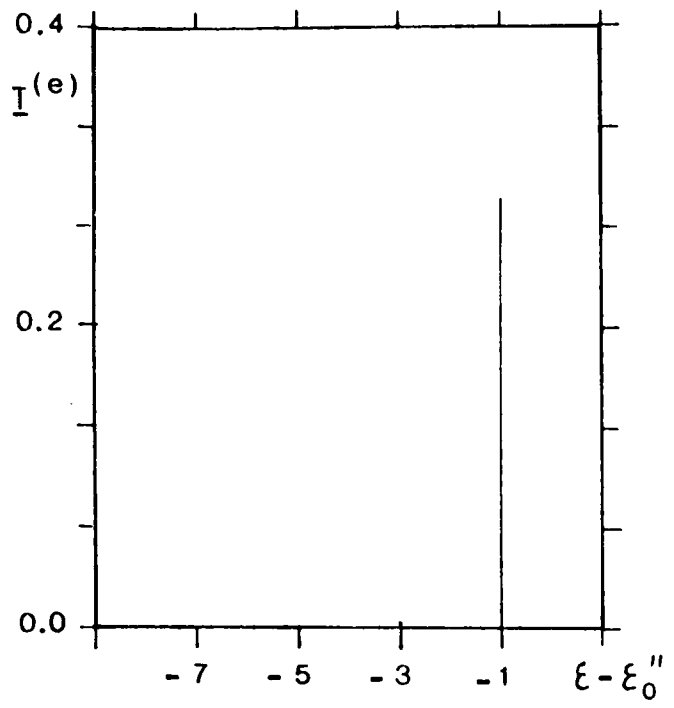
– – – type II ooo type C=0



EMISSION SPECTRA at T=0 for $\delta = 0$

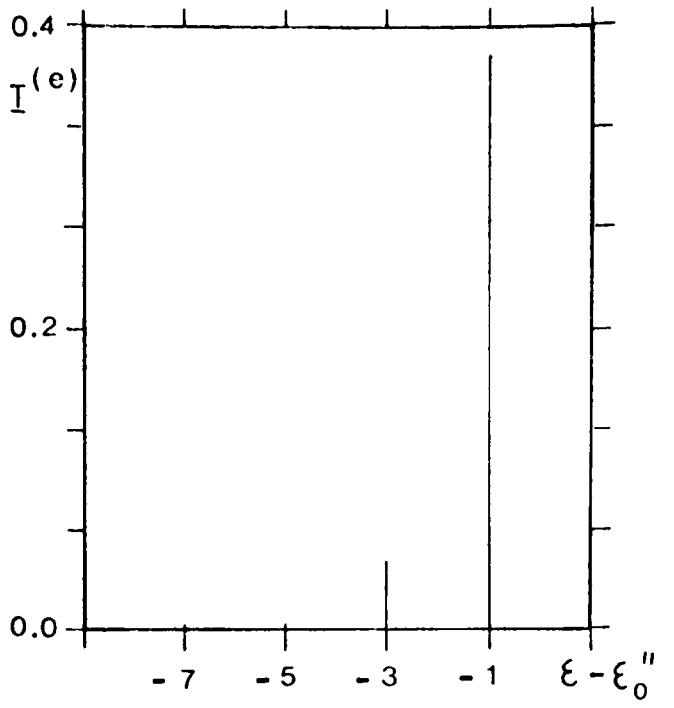
$\varepsilon(00) = 0.93765$

$\varkappa = 0.5$, $N(00) = 0.29004$

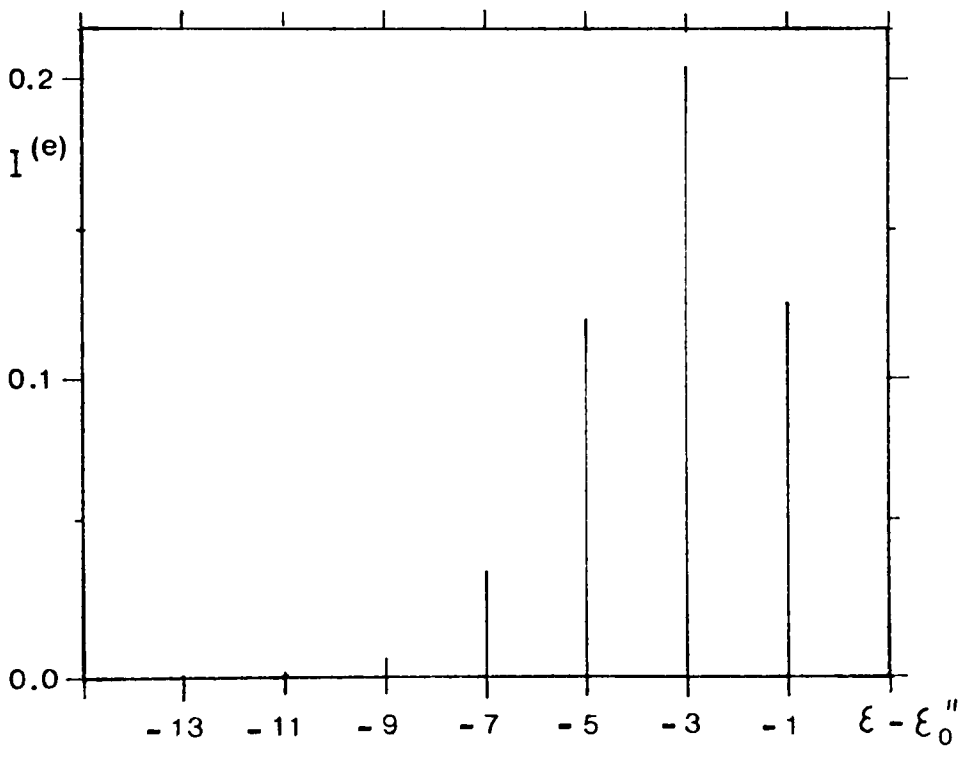


$\varepsilon(00) = -0.16216$

$\varkappa = 1$, $N(00) = 0.43408$

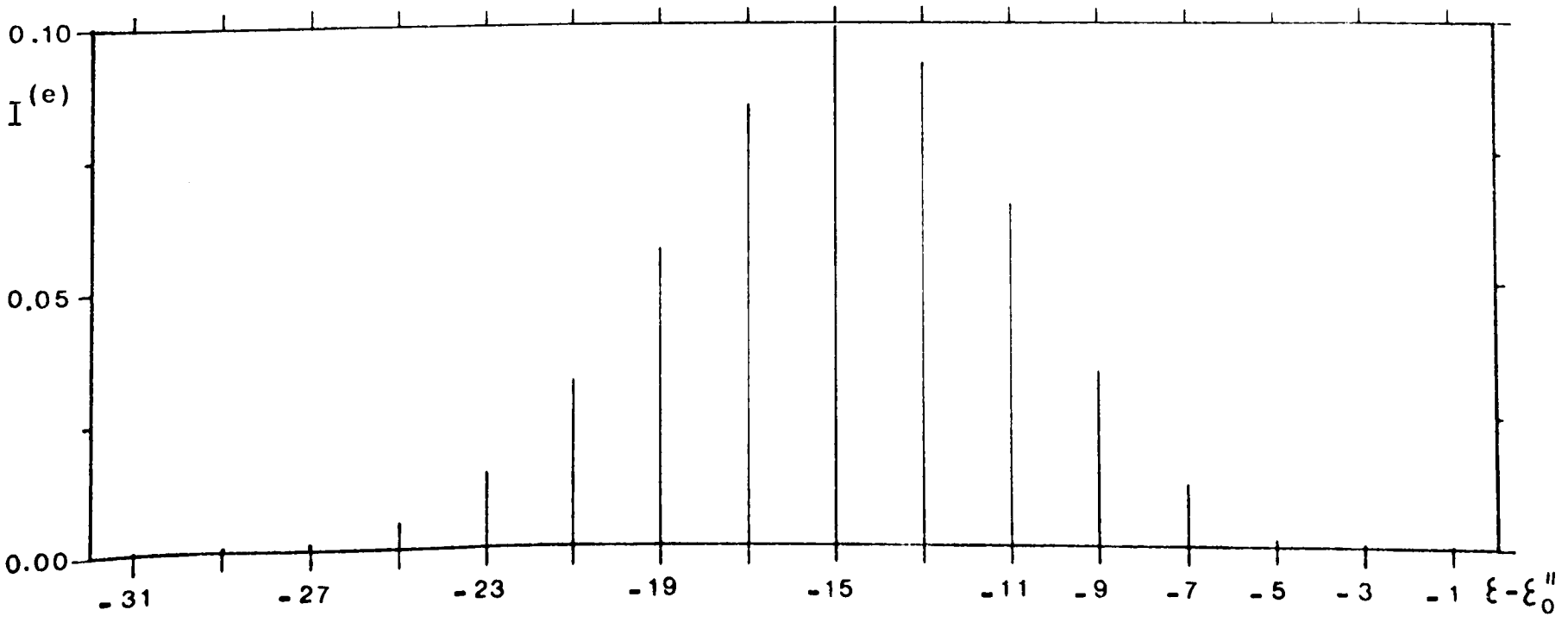


$\varkappa = 2$, $\varepsilon(00) = -3.42301$, $N(00) = 0.49420$



GRAPH 13

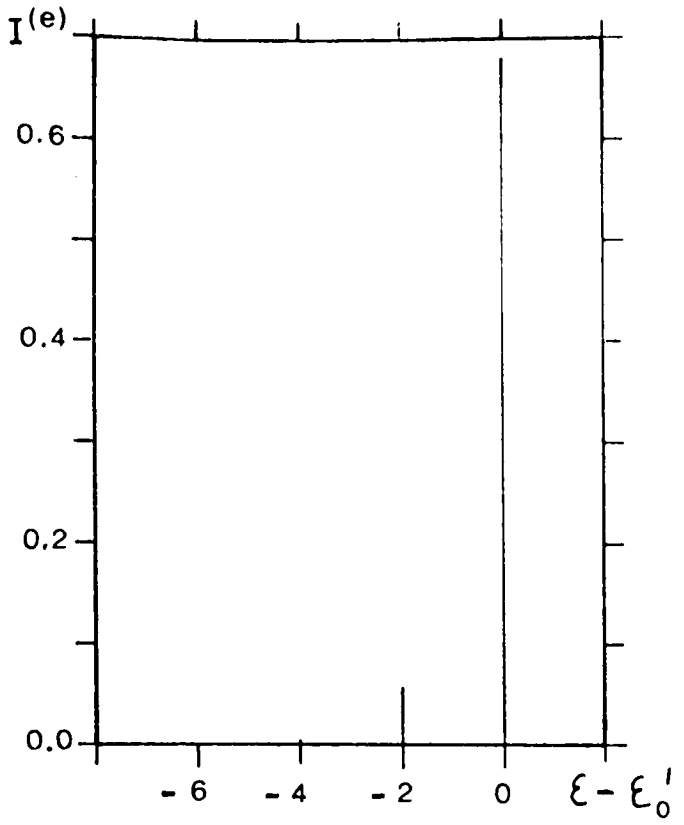
$\varkappa = 4$, $\varepsilon(00) = -15.48360$, $N(00) = 0.49973$



EMISSION SPECTRA from j = 0, J = 1 -state for $\delta = 0$

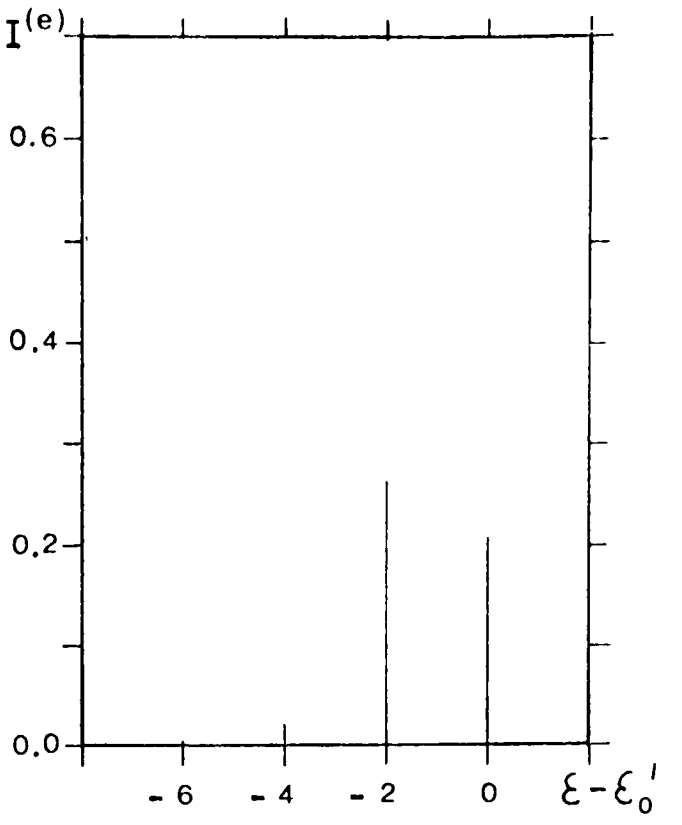
$\xi(01) = 1.19663$

$\varkappa = 0.5$, $N(01) = 0.74344$

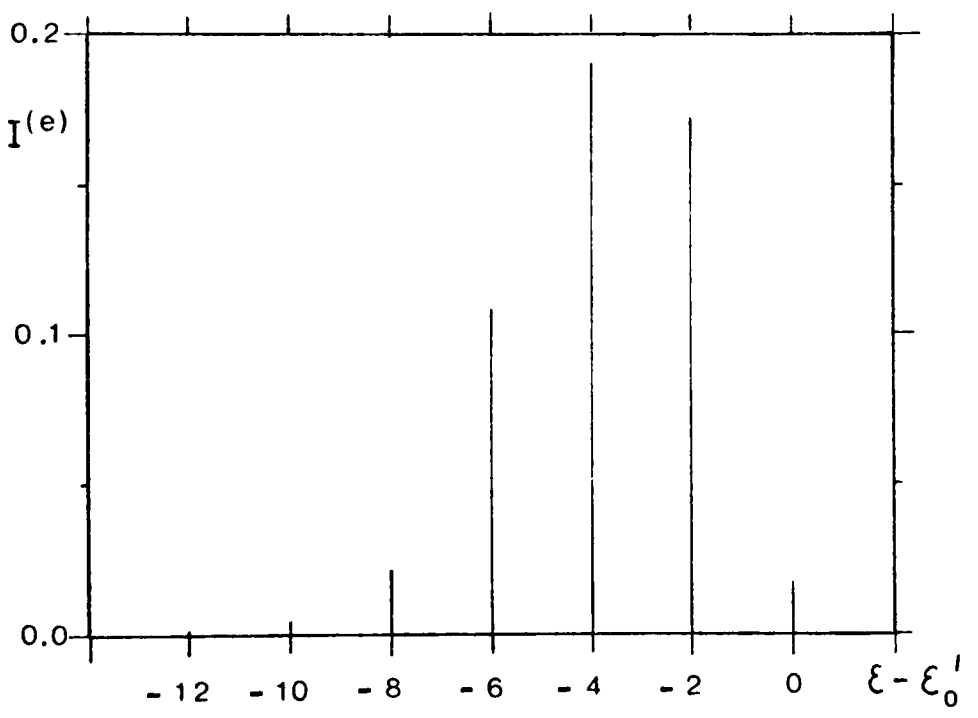


$\xi(01) = 0.14620$

$\varkappa = 1$, $N(01) = 0.51172$

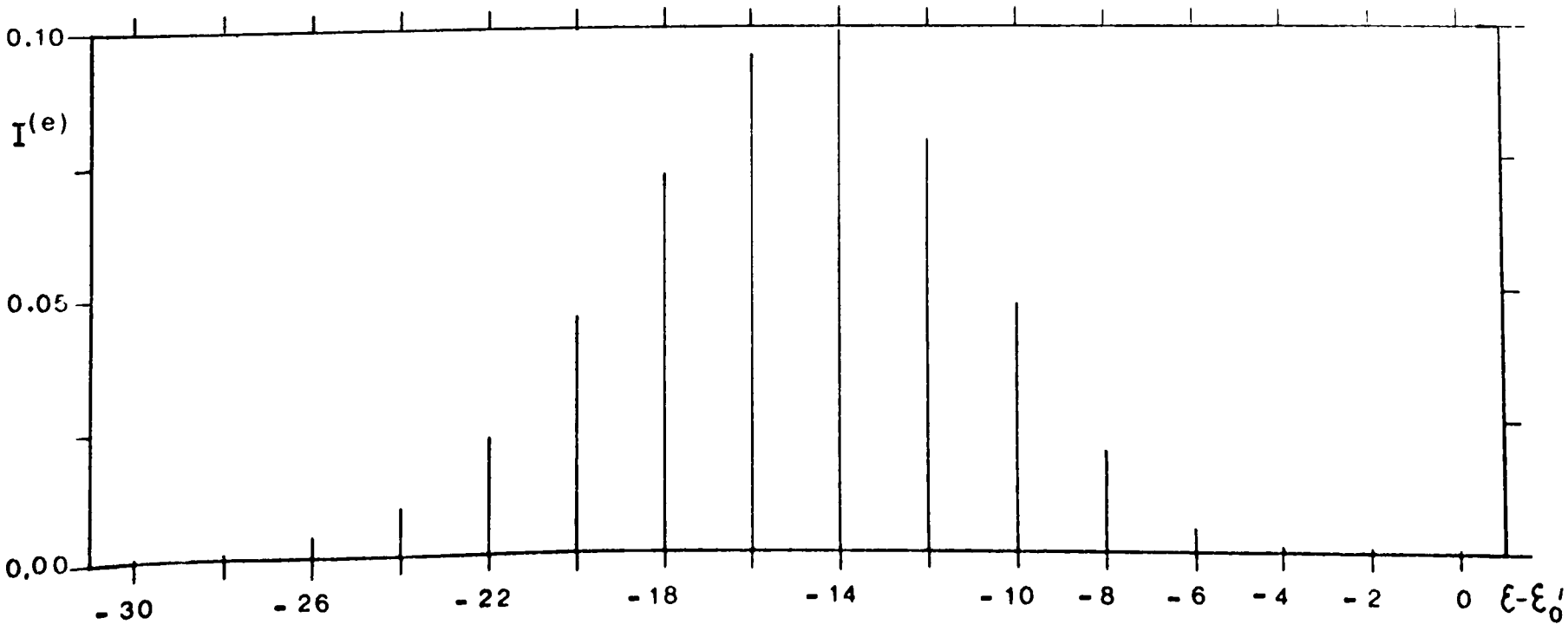


$\varkappa = 2$, $\xi(01) = -3,28612$, $N(01) = 0,49590$



GRAPH 14

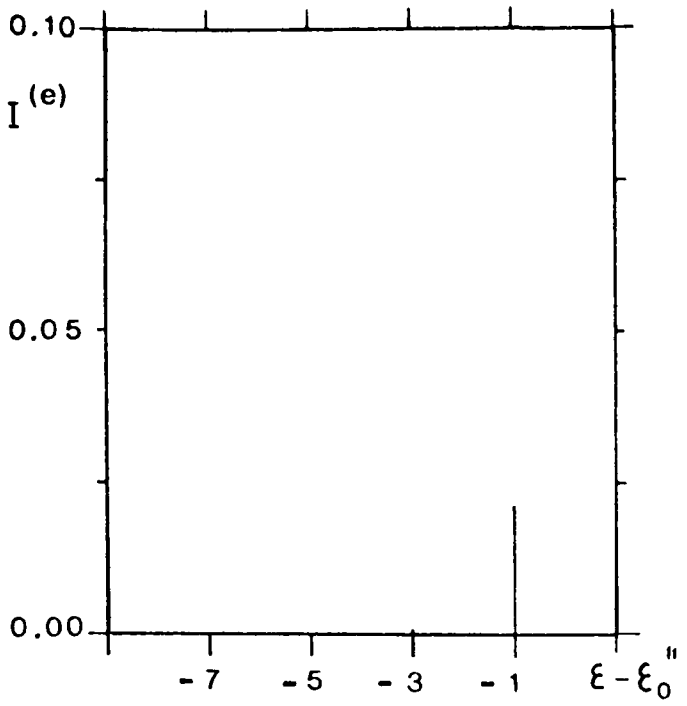
$\varkappa = 4$, $\xi(01) = -15.45095$, $N(01) = 0.49973$



EMISSION SPECTRA at T=0 for $\delta = -2.5$

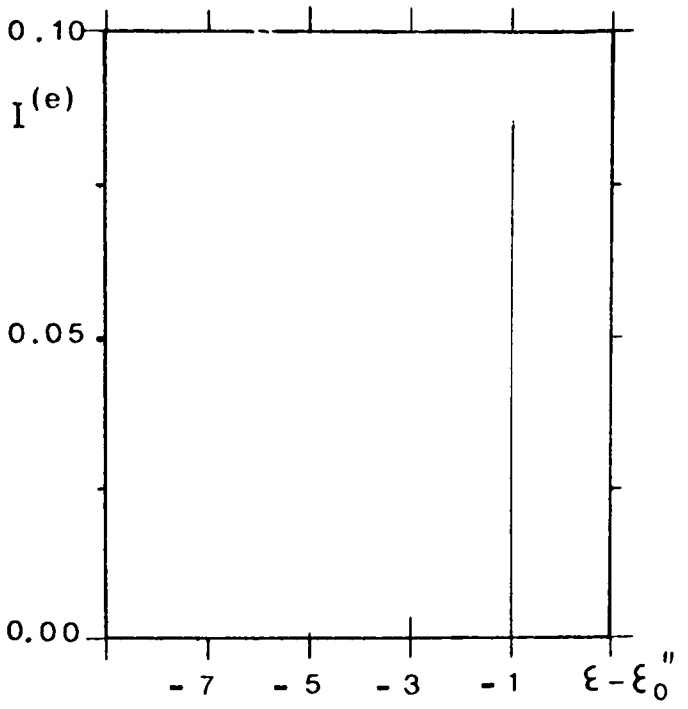
$\varepsilon(00) = -1.12769$

$\varkappa = 0.5$, $N(00) = 0.02127$



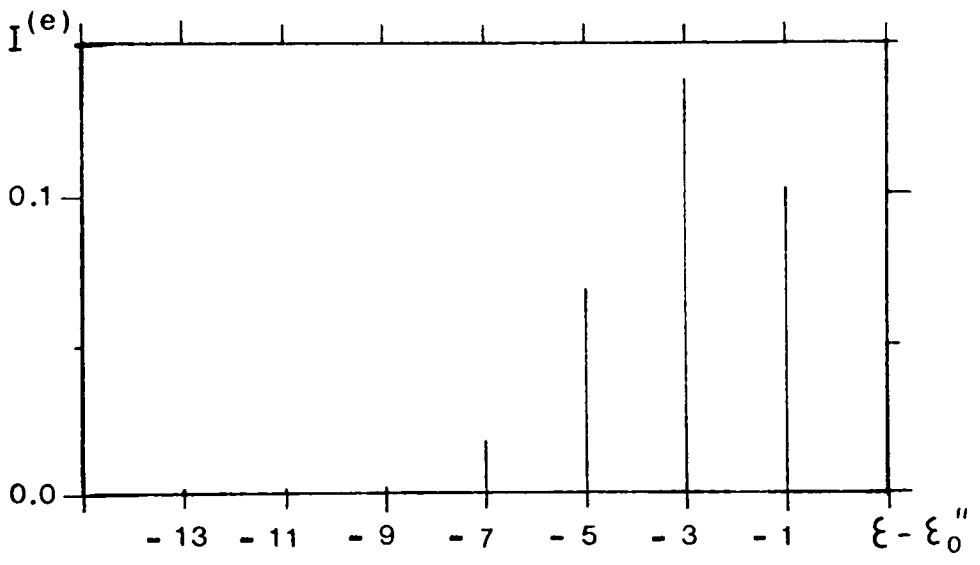
$\varepsilon(00) = -1.54711$

$\varkappa = 1$, $N(00) = 0.09022$



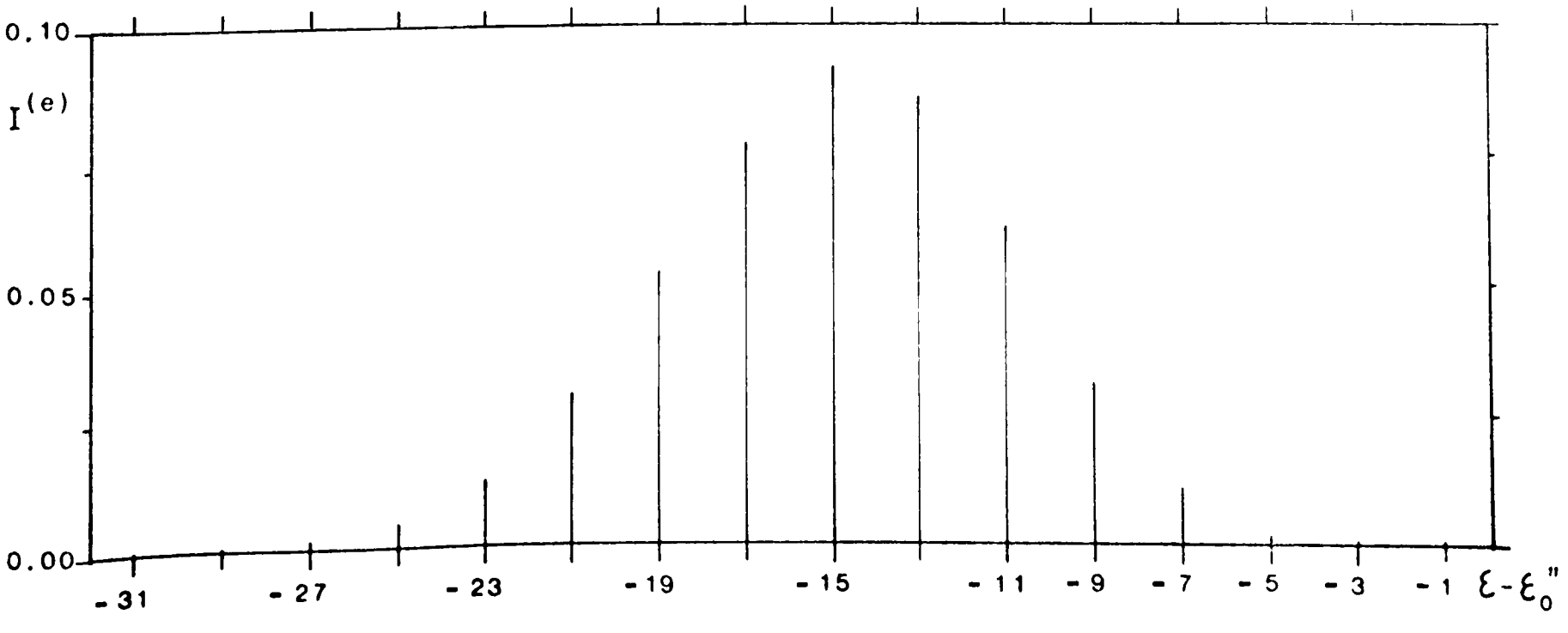
$\varepsilon(00) = -3.86198$

$\varkappa = 2$, $N(00) = 0.32982$



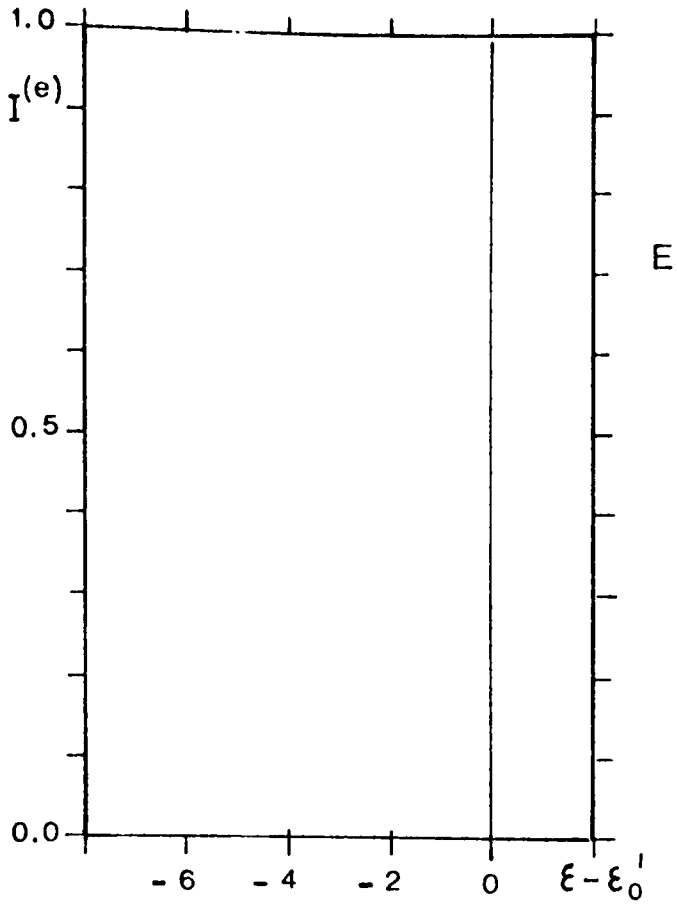
GRAPH 15

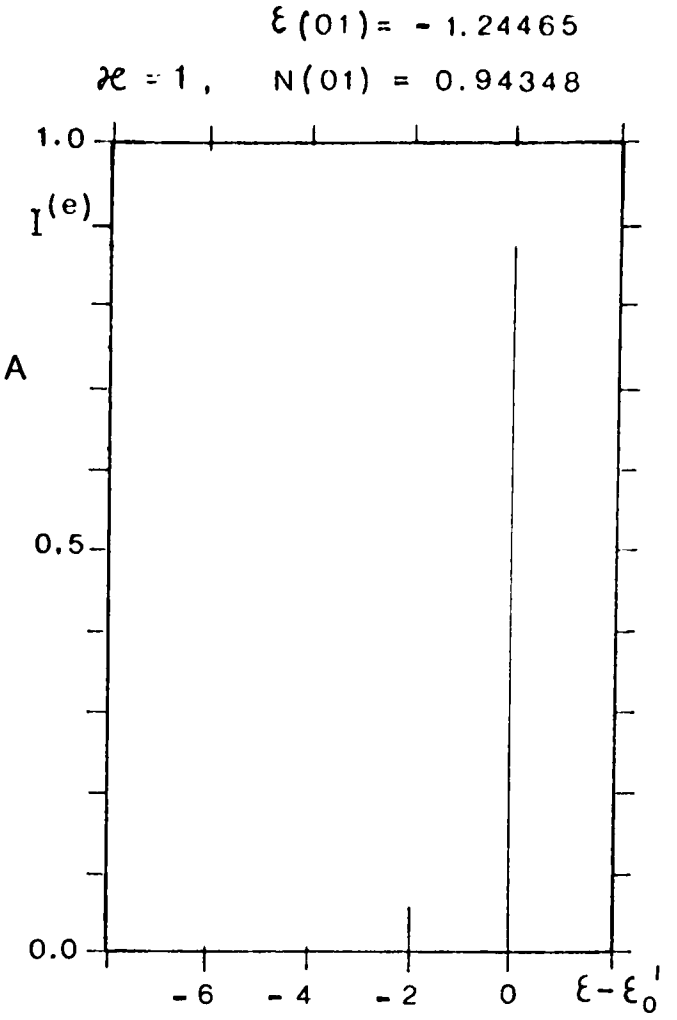
$\varkappa = 4$, $\varepsilon(00) = -15.58408$, $N(00) = 0.46008$

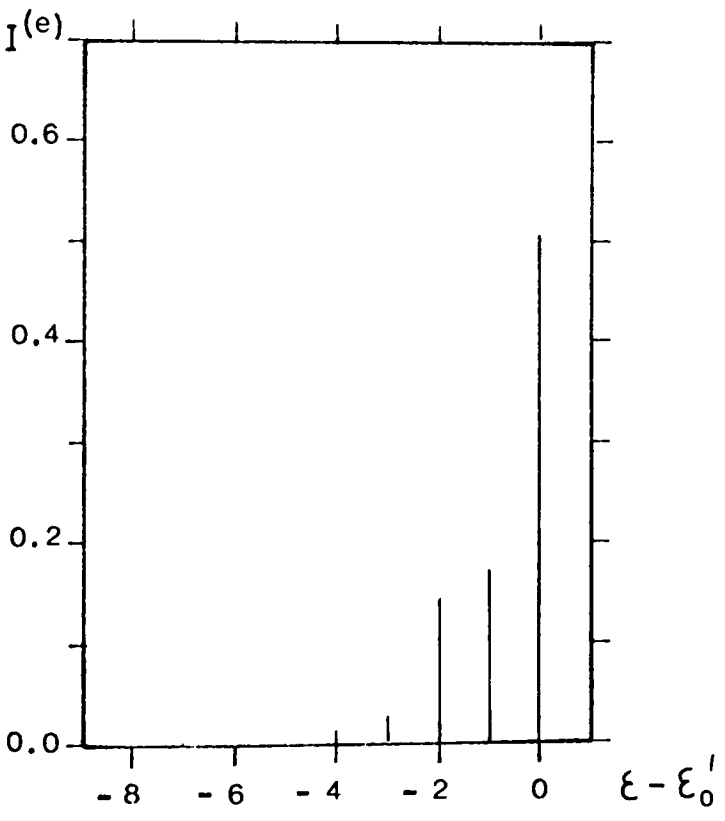


EMISSION SPECTRA

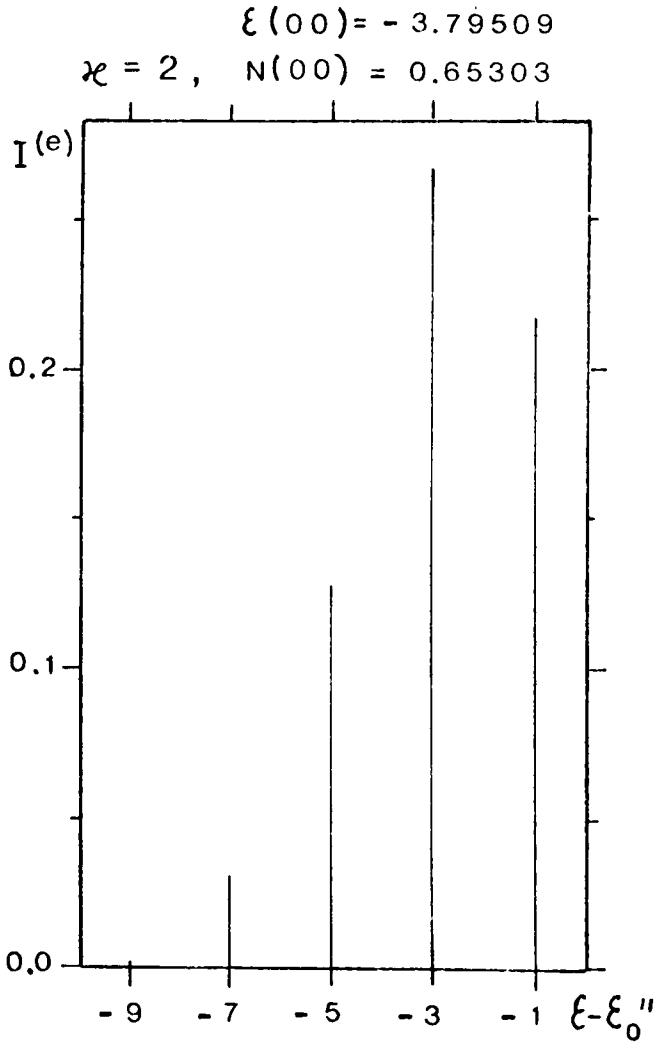
at T=0 for $\delta = 2.5$

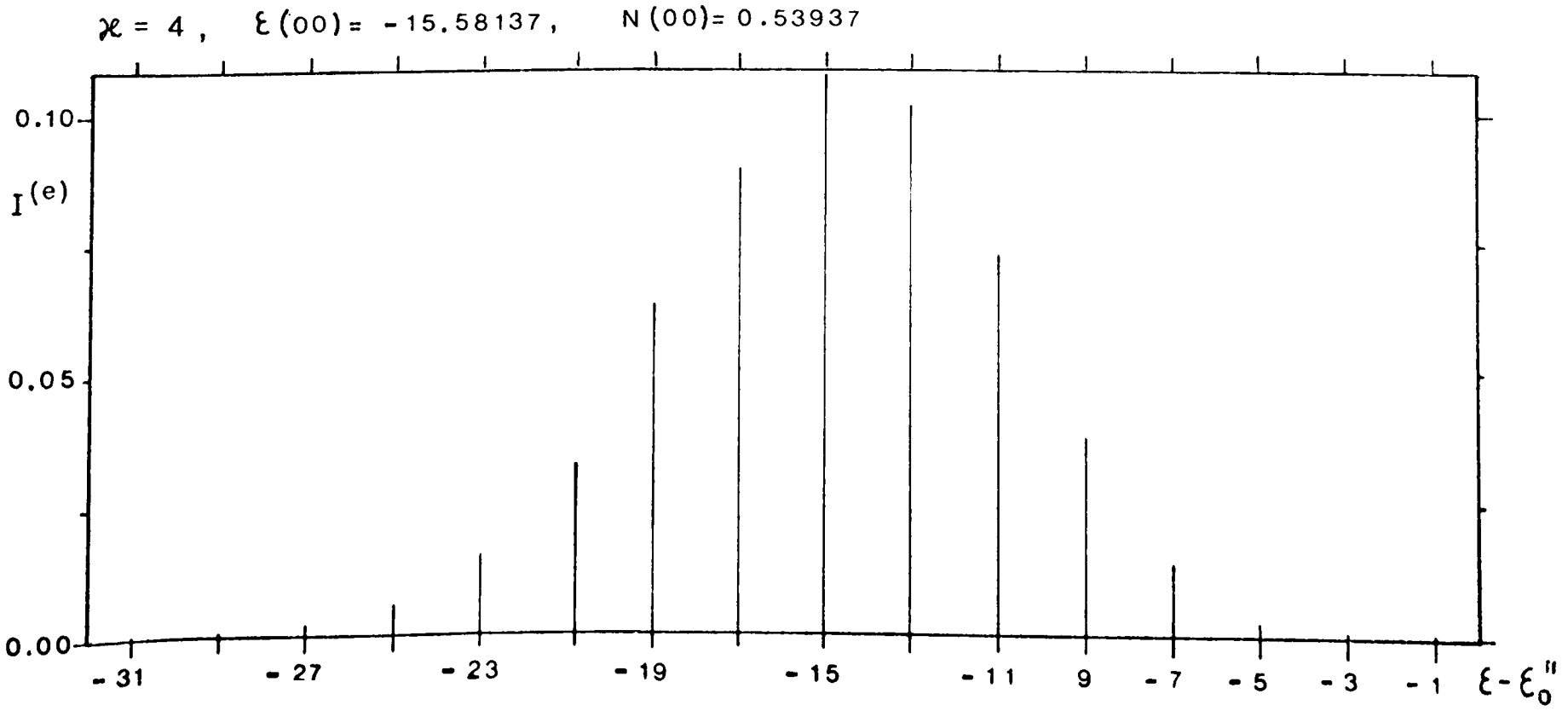






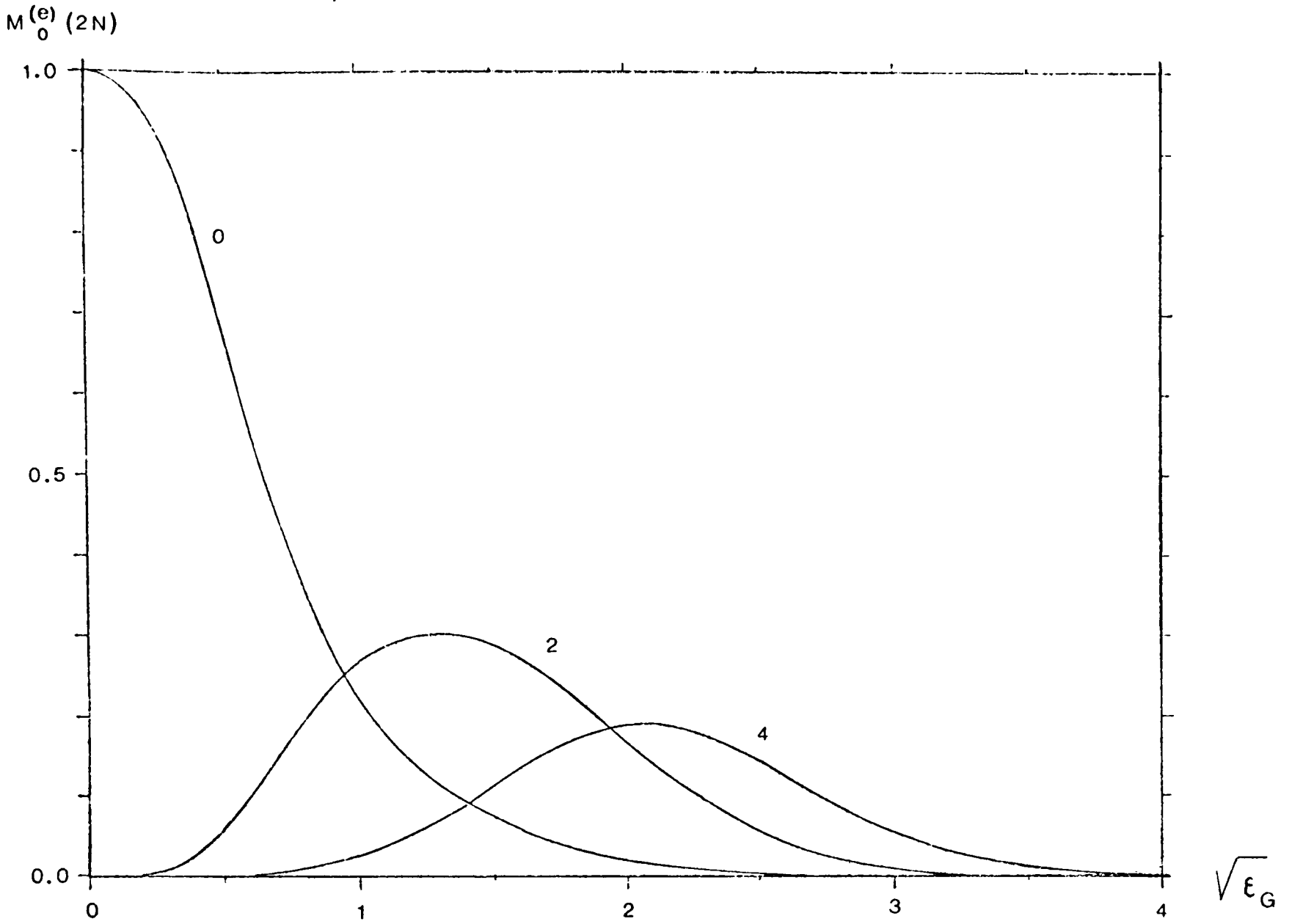
GRAPH 16



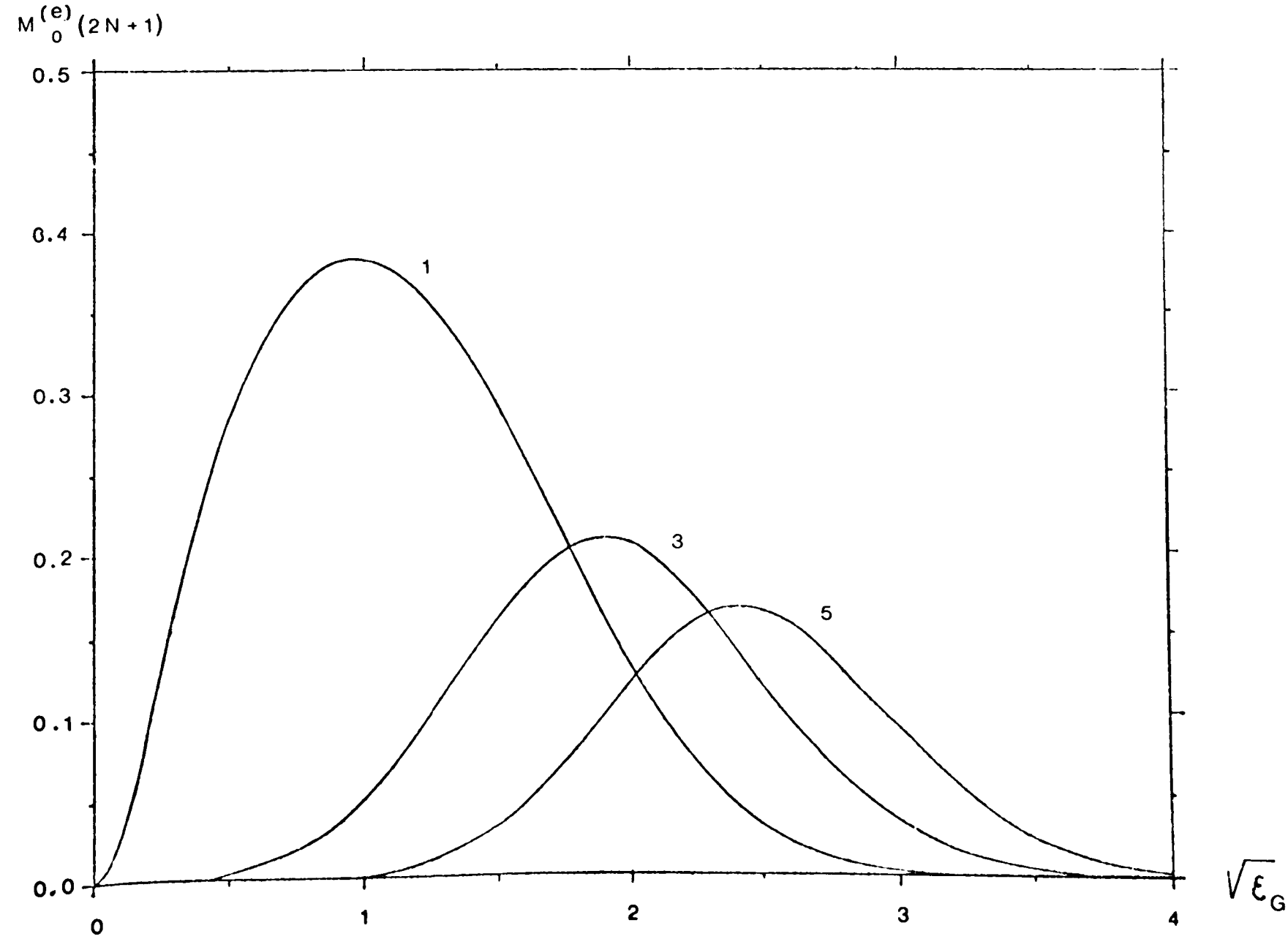


GRAPH 17

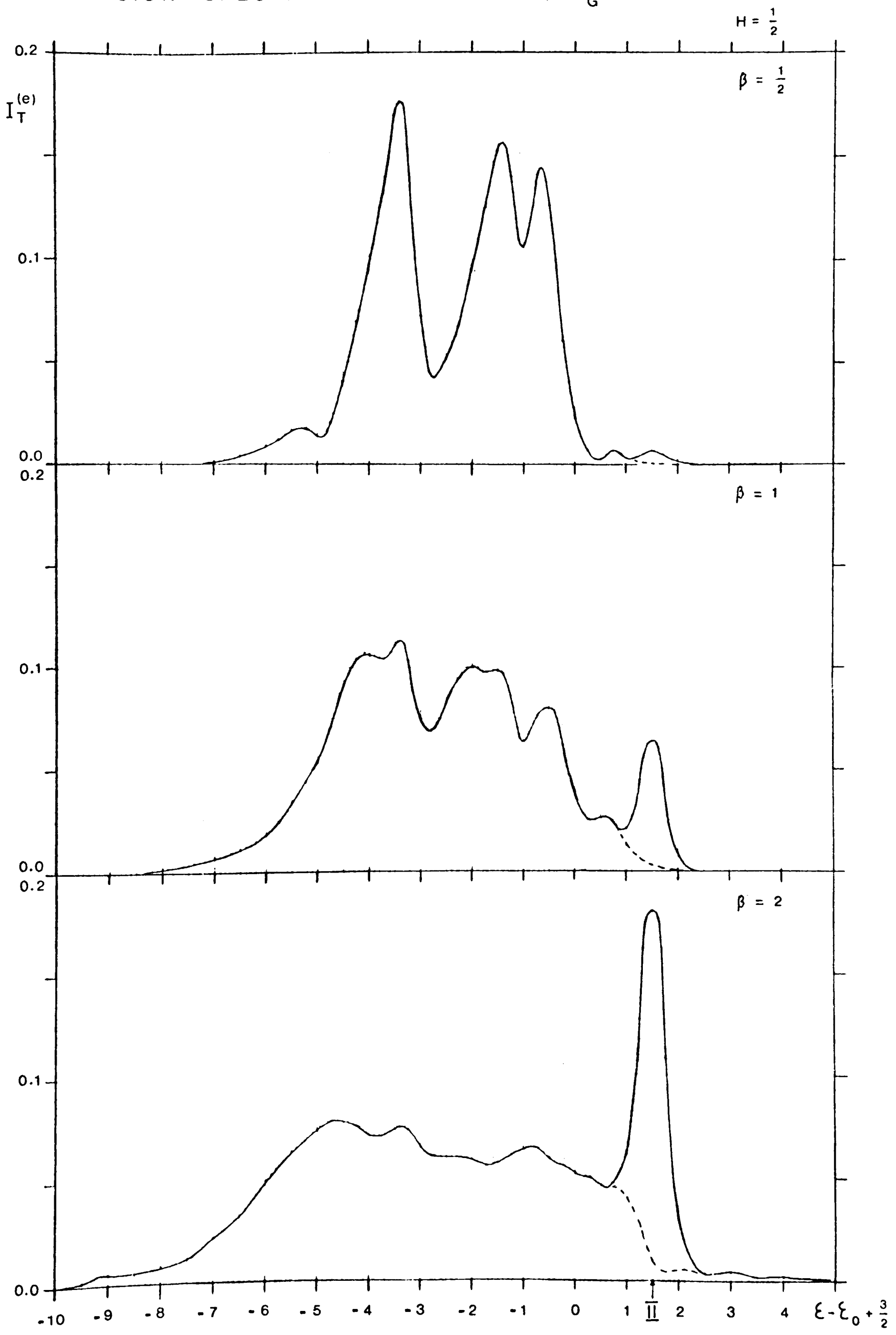
0-, 2-, 4 - PHONONS EMISSION LINES for $\delta = 0$



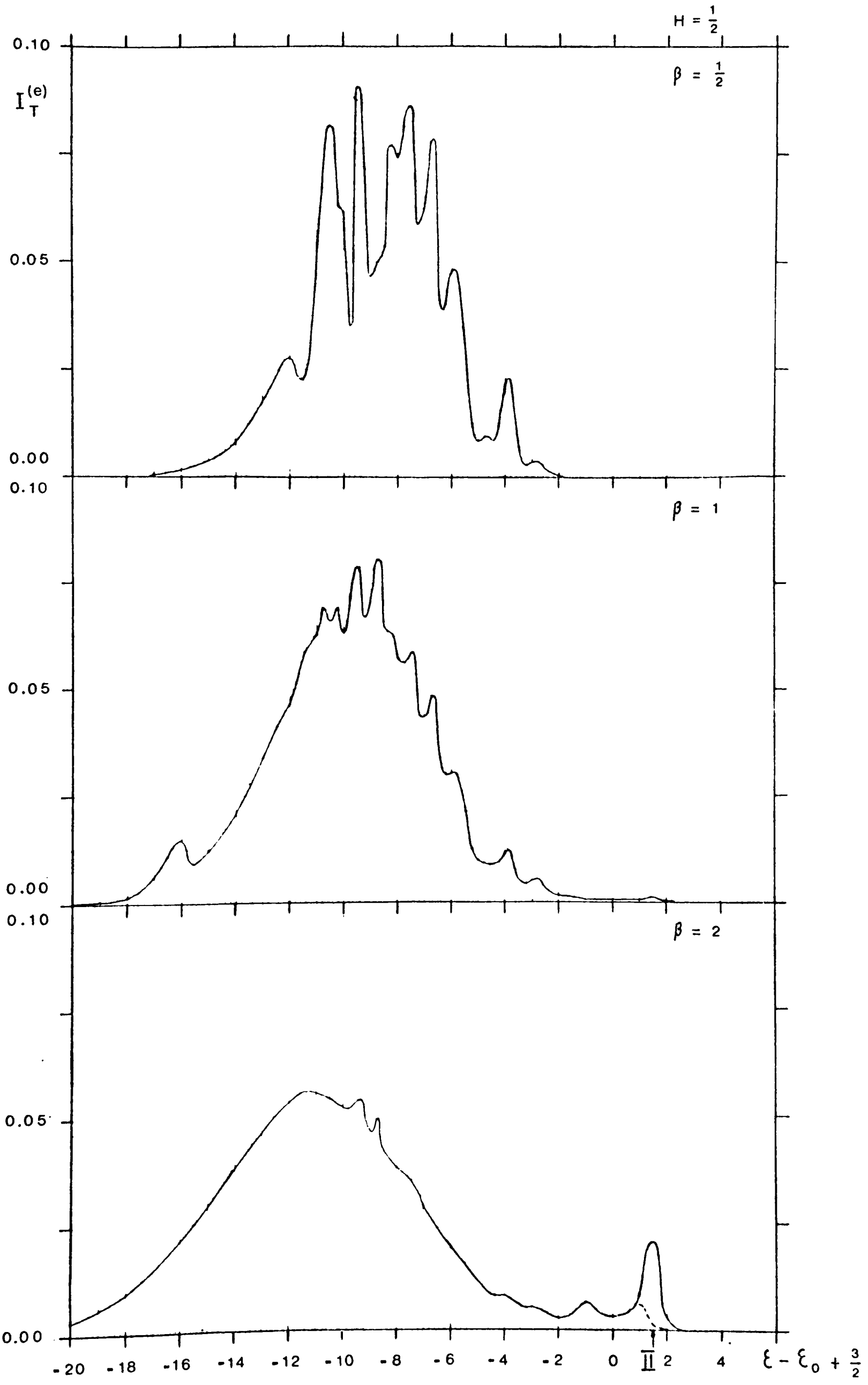
1-, 3-, 5 - PHONONS EMISSION LINES for $\delta = 0$



GRAPH 18

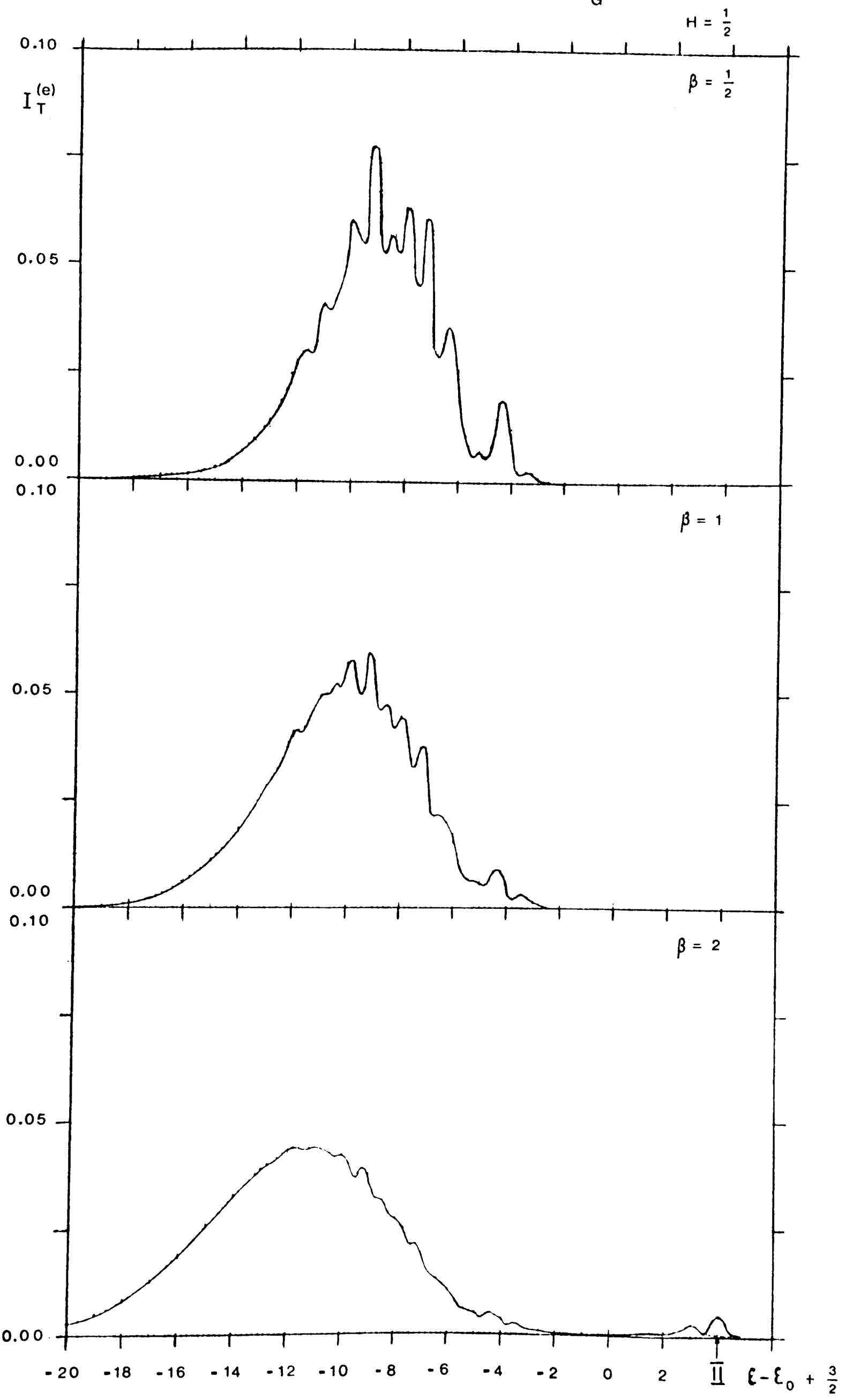

EMISSION SPECTRA at T >0 for δ=0, ε_G = 1
H = 1/2
β = 1/2
β = 1
β = 2
I_T^(e)
0.2
0.1
0.0
-10
-9
-8
-7
-6
-5
-4
-3
-2
-1
0
1
II
2
3
4
ε-ε_0 + 3/2

EMISSION SPECTRA at $T>0$ for $\delta=0$, $\varepsilon_G = 4$

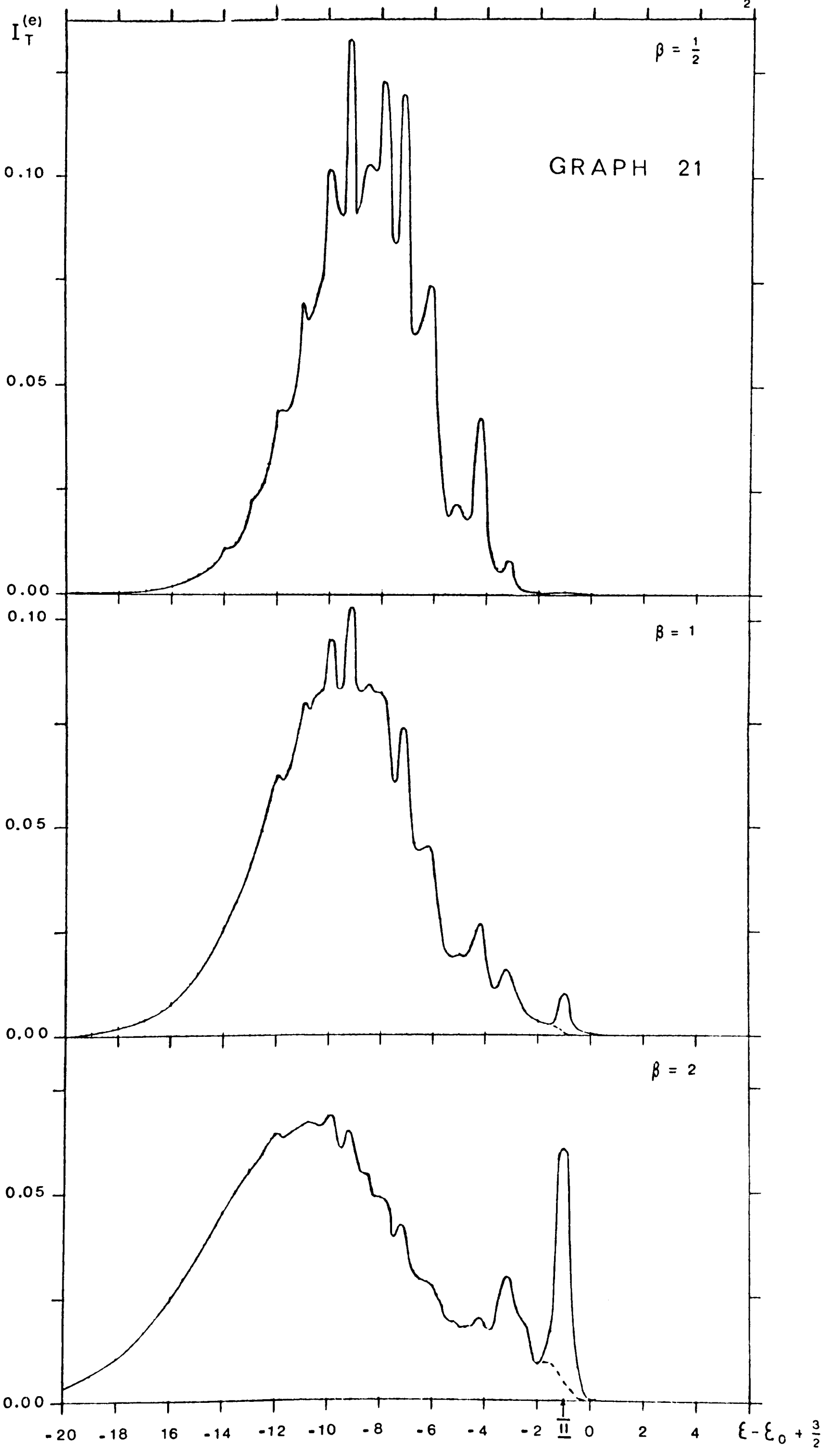


GRAPH 20

EMISSION SPECTRA at $T>0$ for $\delta = -2.5$, $\varepsilon_G = 4$



EMISSION SPECTRA at $T > 0$ for $d - 2.5$, $\xi_G = 4$



ABSORPTION LINES for $\delta = -2.5$ GRAPH 22

$M^{(a)}_{-2.5}(j)$

1
10^{-1}
10^{-2}
10^{-3}
10^{-4}

3 4 5 6 B = 0

C = 0

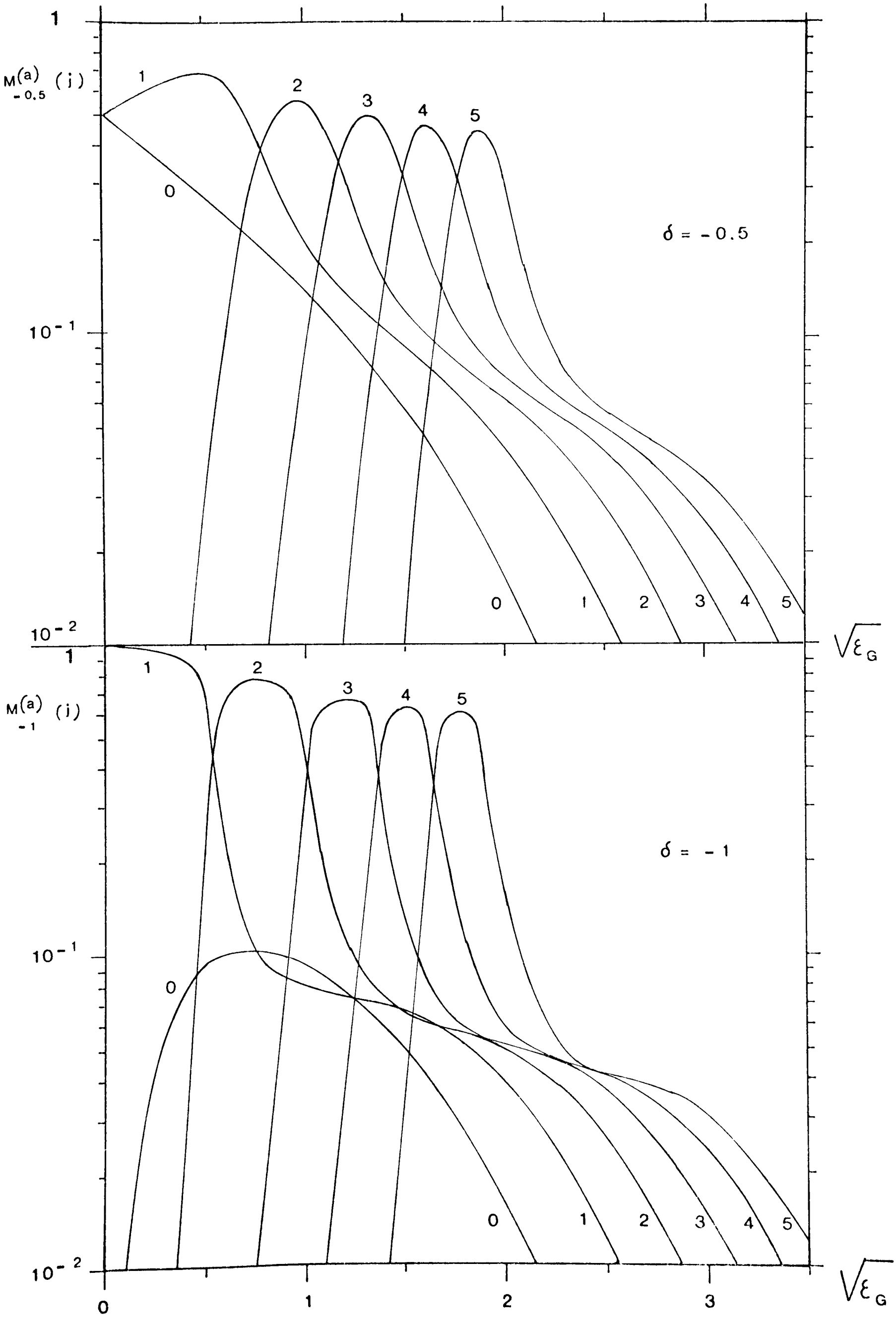
B = 1

A

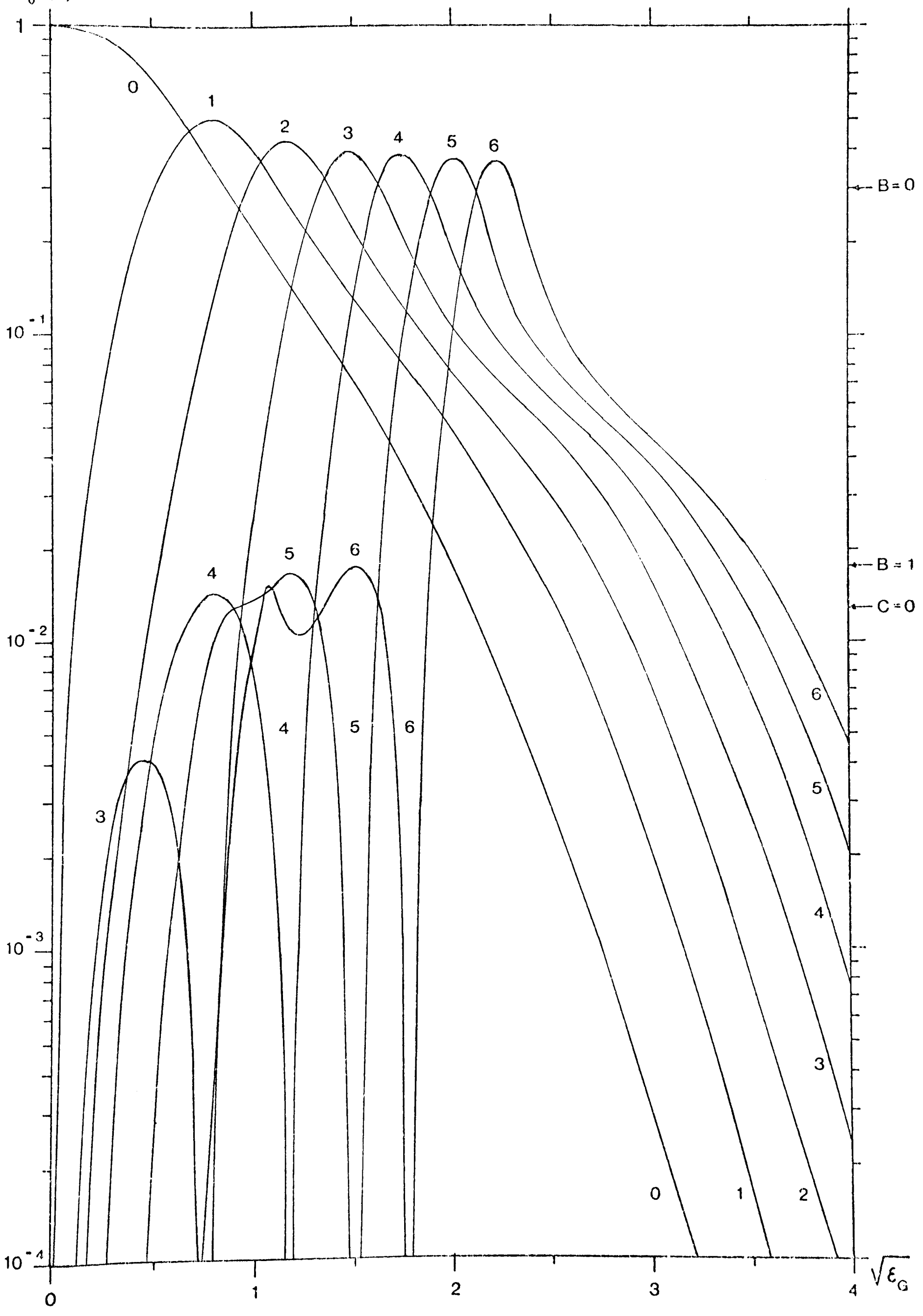
0 7 6 6 5 6 6 5 4 3 2 1 0

0 1 2 3 4 $\sqrt{\varepsilon_G}$

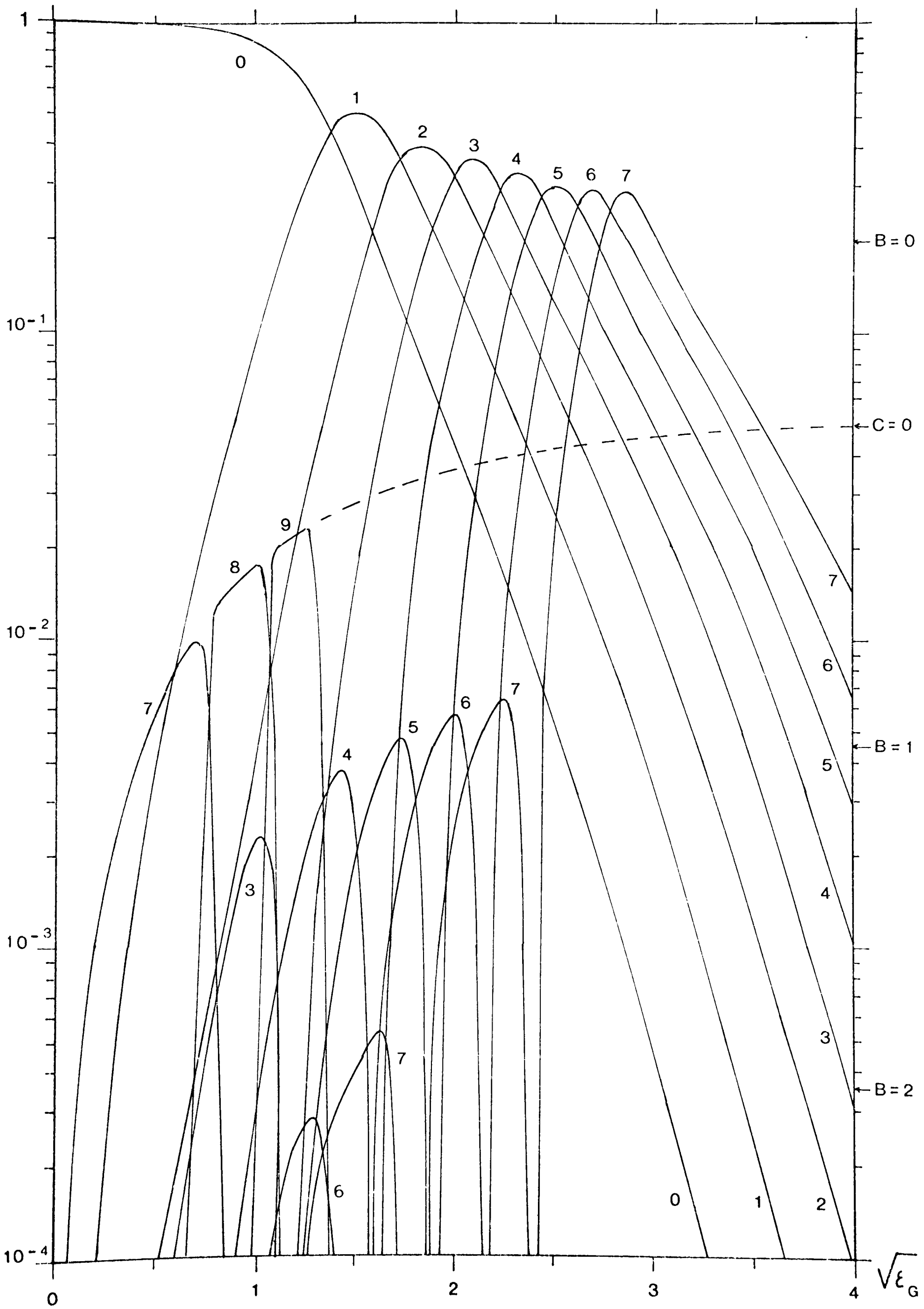
ABSORPTION LINES GRAPH 23

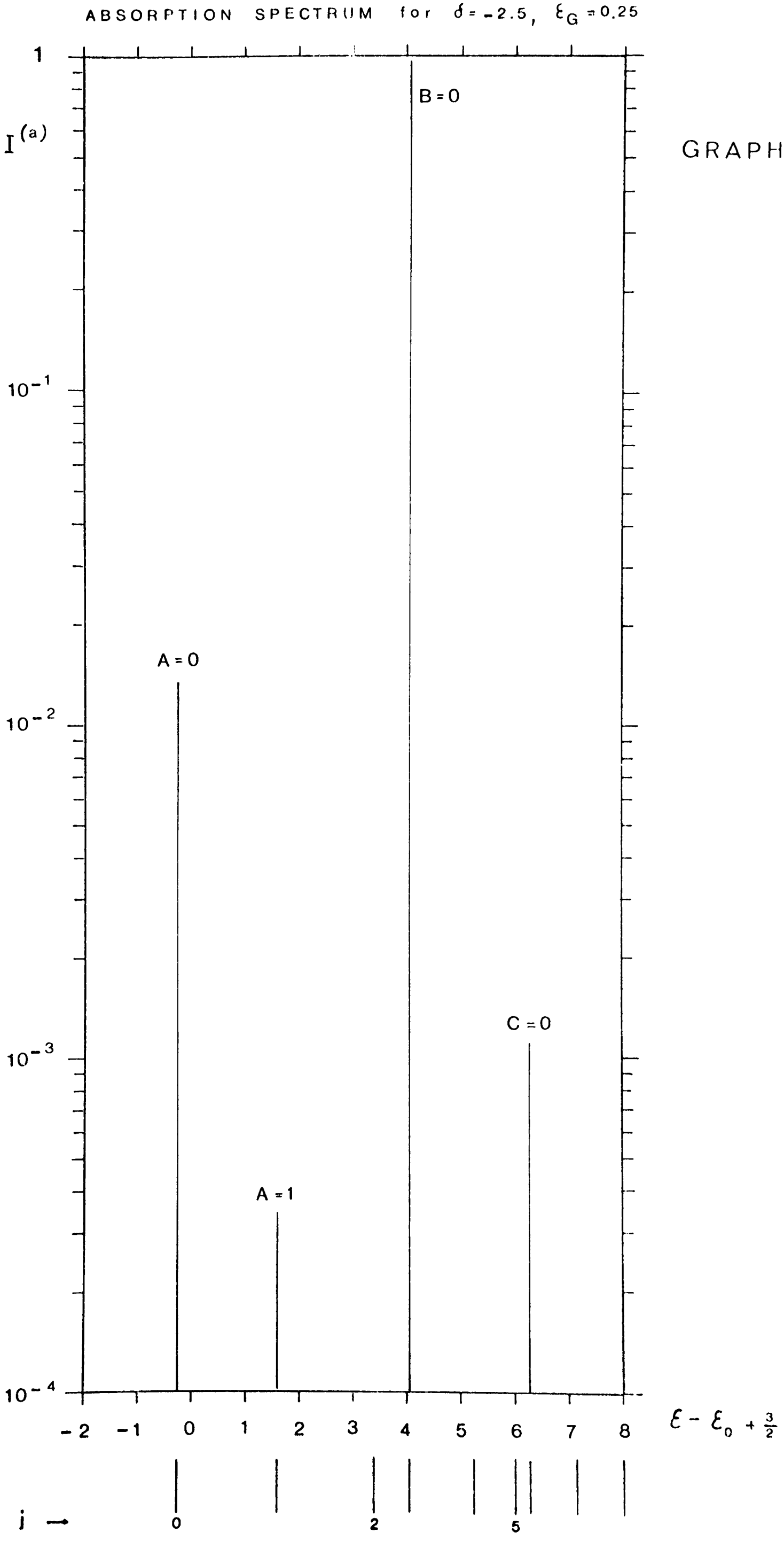


ABSORPTION LINES for $\delta = 0$ GRAPH 24



ABSORPTION LINES for $\delta = 2.5$ GRAPH 25




ABSORPTION SPECTRUM for δ = -2.5, ε_G = 0.25
1
I^(a)
10^-1
10^-2
10^-3
10^-4
A = 0
B = 0
C = 0
A = 1
-2 -1 0 1 2 3 4 5 6 7 8
ε - ε_0 + 3/2
j →
0
2
5

GRAPH 26

ABSORPTION SPECTRUM for $\delta = -2.5$, $\varepsilon_G = 1$

GRAPH 27

$I^{(a)}$

1

10^{-1}

10^{-2}

10^{-3}

10^{-4}

B = 0

A = 0

A = 1

A = 2

C = 0

B = 1

-3 -2 -1 0 1 2 3 4 5 6 7 8 9 $\varepsilon - \varepsilon_0 + \frac{3}{2}$

j → 0 5 10

ABSORPTION SPECTRUM for $\delta = -2.5$, $\varepsilon_G = 4$

GRAPH 28

$I^{(a)}$

1

10^{-1}

10^{-2}

10^{-3}

10^{-4}

A = 0

A = 1

A = 5

B = 0

B = 1

B = 2

B = 3

C = 0

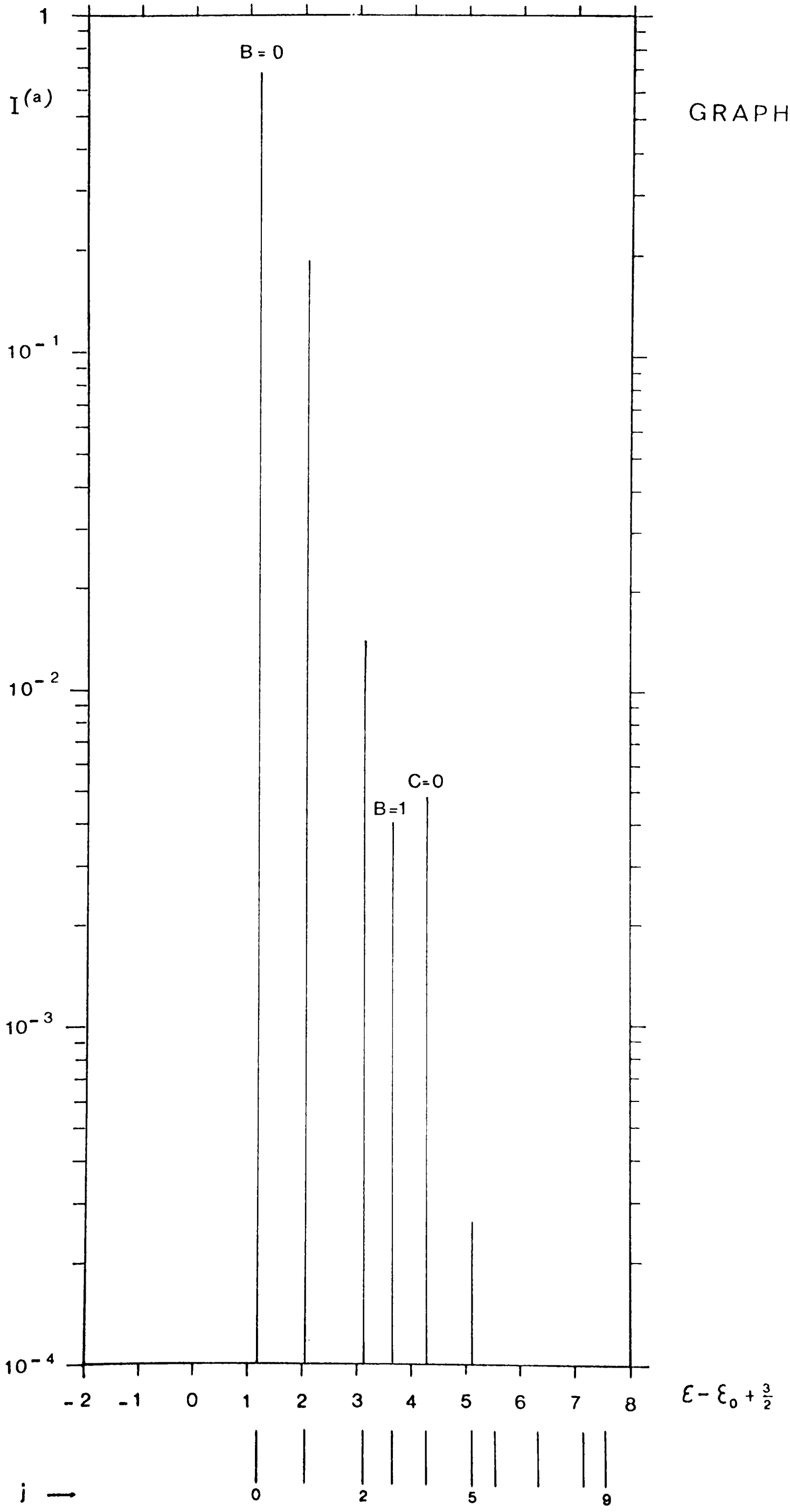
C = 1

-4 -3 -2 -1 0 1 2 3 4 5 6 7 8 9 10 11 $\varepsilon - \varepsilon_0 + \frac{3}{2}$

j → 0 5 10 15

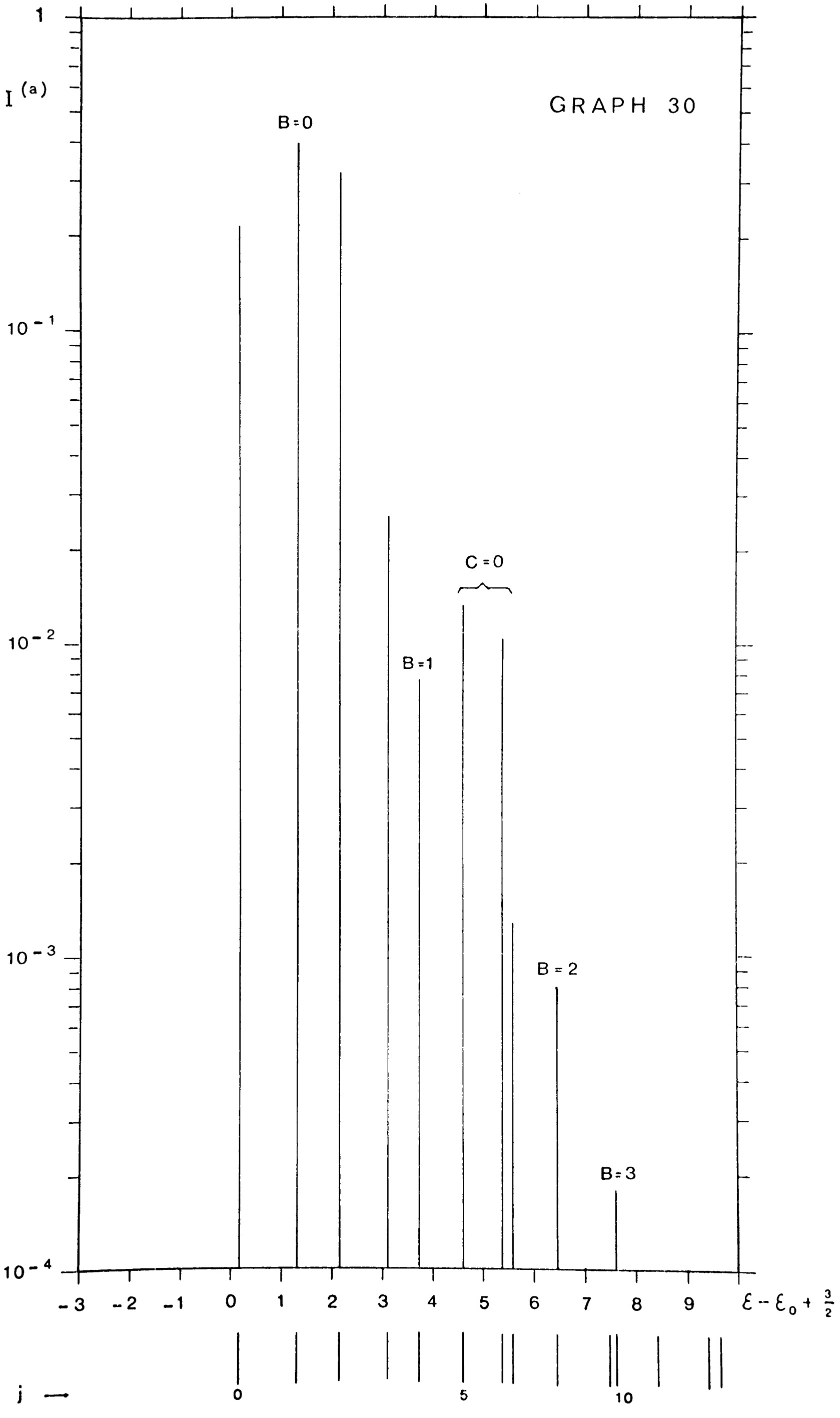
ABSORPTION SPECTRUM for $\delta = 0$, $\varepsilon_G = 0.25$

GRAPH 29



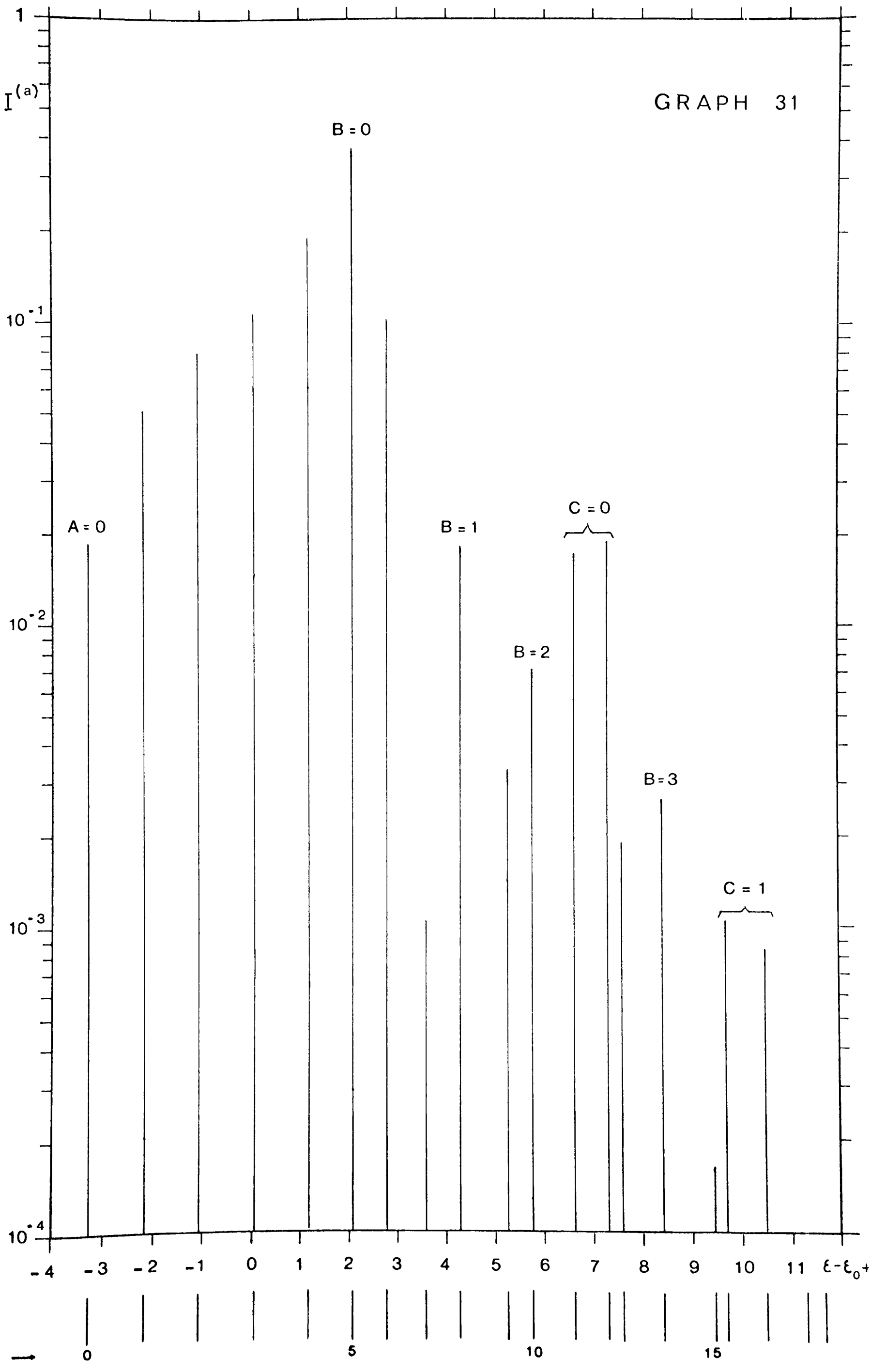
ABSORPTION SPECTRUM for $\delta = 0$, $\varepsilon_G = 1$

GRAPH 30



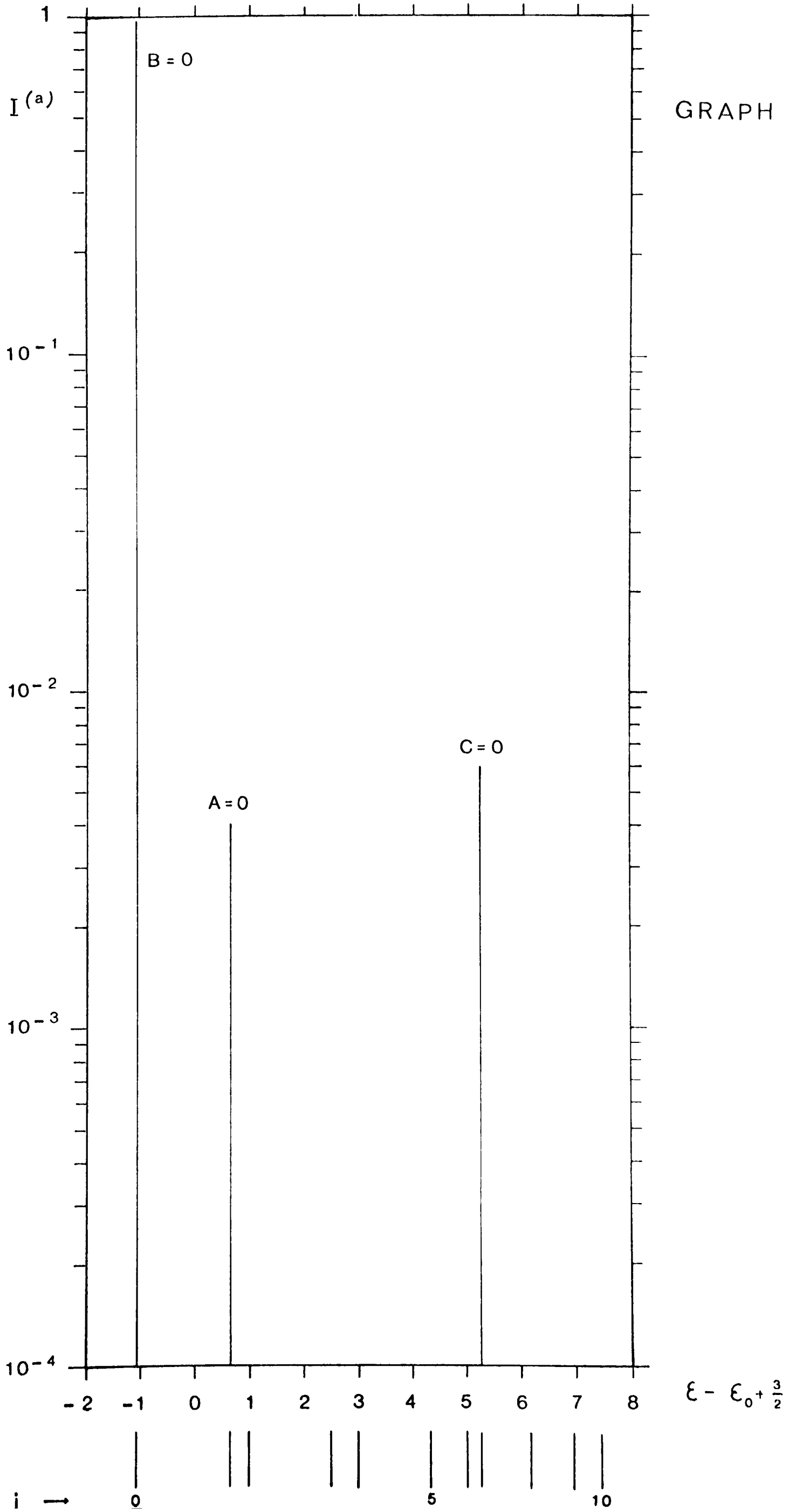
ABSORPTION SPECTRUM for $\delta = 0$, $\varepsilon_G = 4$

GRAPH 31



ABSORPTION SPECTRUM for $\delta = 2.5$, $\varepsilon_G = 0.25$

GRAPH 32



ABSORPTIUM SPECTRUM for $\delta = 2.5$, $\varepsilon_G = 1$

GRAPH 33

$I^{(a)}$

1

10^{-1}

10^{-2}

10^{-3}

10^{-4}

B = 0

B = 1

C = 0

C = 1

-3 -2 -1 0 1 2 3 4 5 6 7 8 9 $\varepsilon - \varepsilon_0 + \frac{3}{2}$

j →

0 5 10

ABSORPTIUM SPECTRUM for $\delta = 2.5$, $\varepsilon_G = 4$

GRAPH 34

$I^{(a)}$

1

10^{-1}

10^{-2}

10^{-3}

10^{-4}

A = 0

B = 0

B = 1

B = 2

B = 3

C = 0

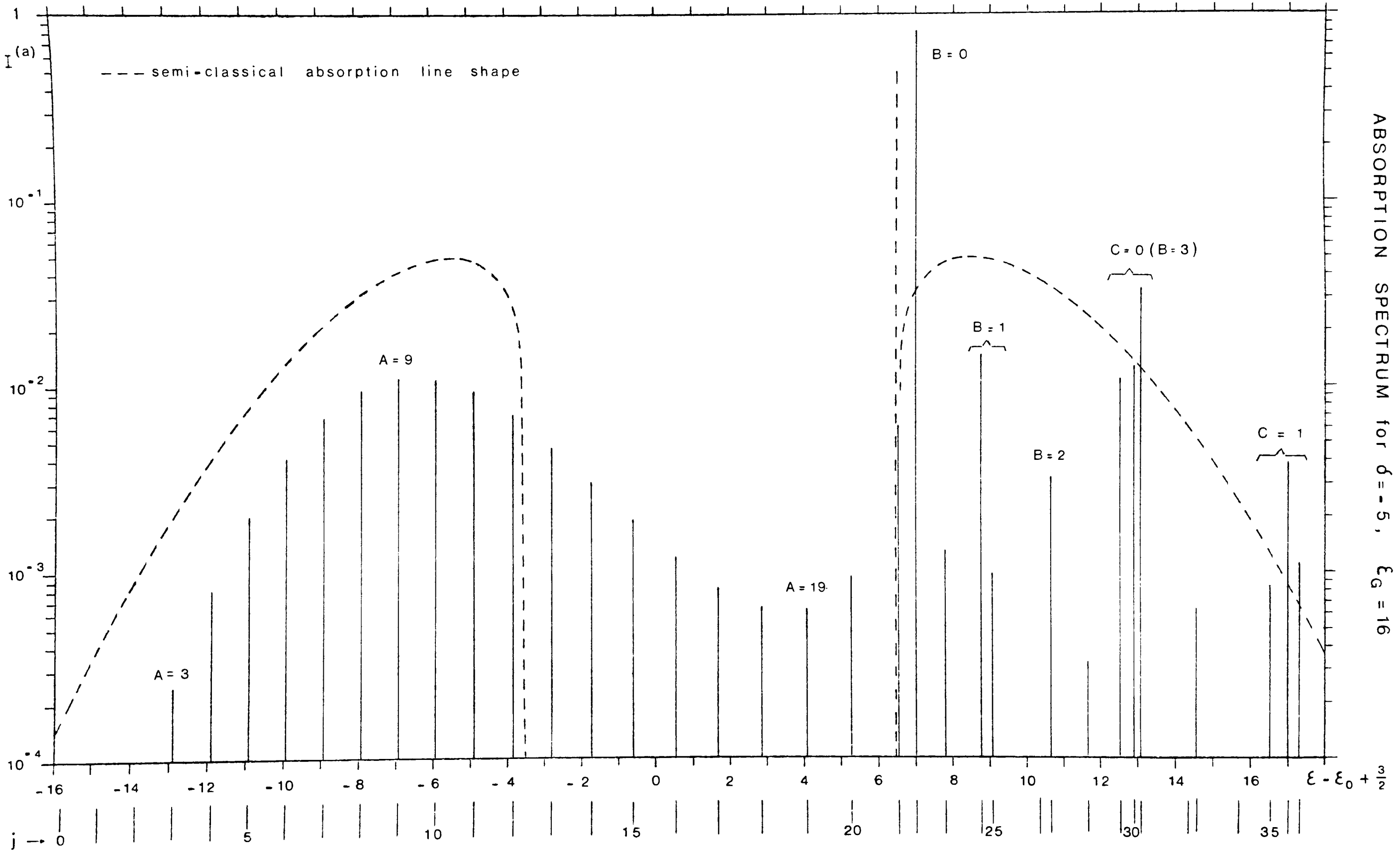
C = 1

$\varepsilon - \varepsilon_0 + \frac{3}{2}$

-4 -3 -2 -1 0 1 2 3 4 5 6 7 8 9 10 11

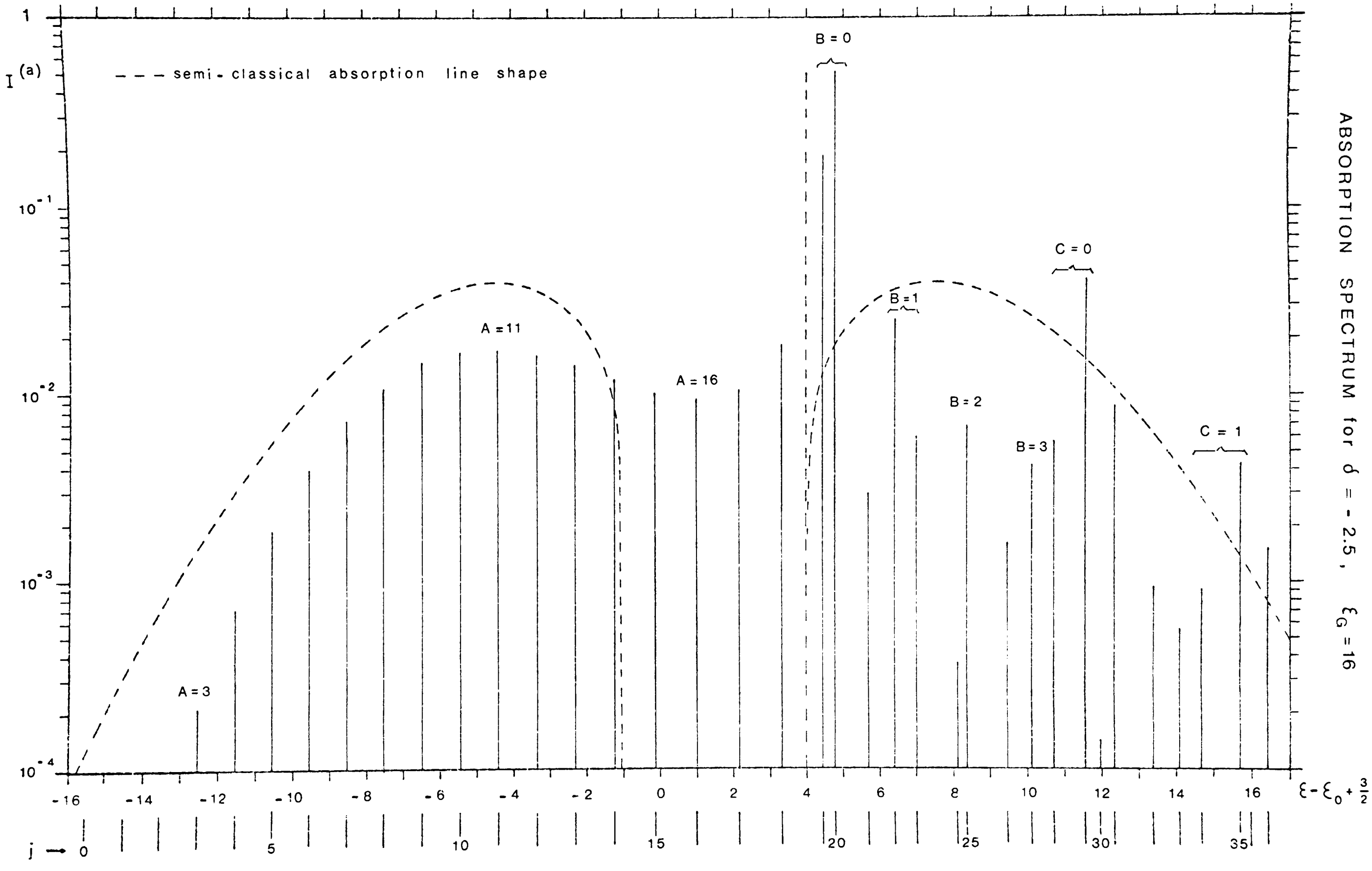
j → 0 5 10 15 20

GRAPH 35



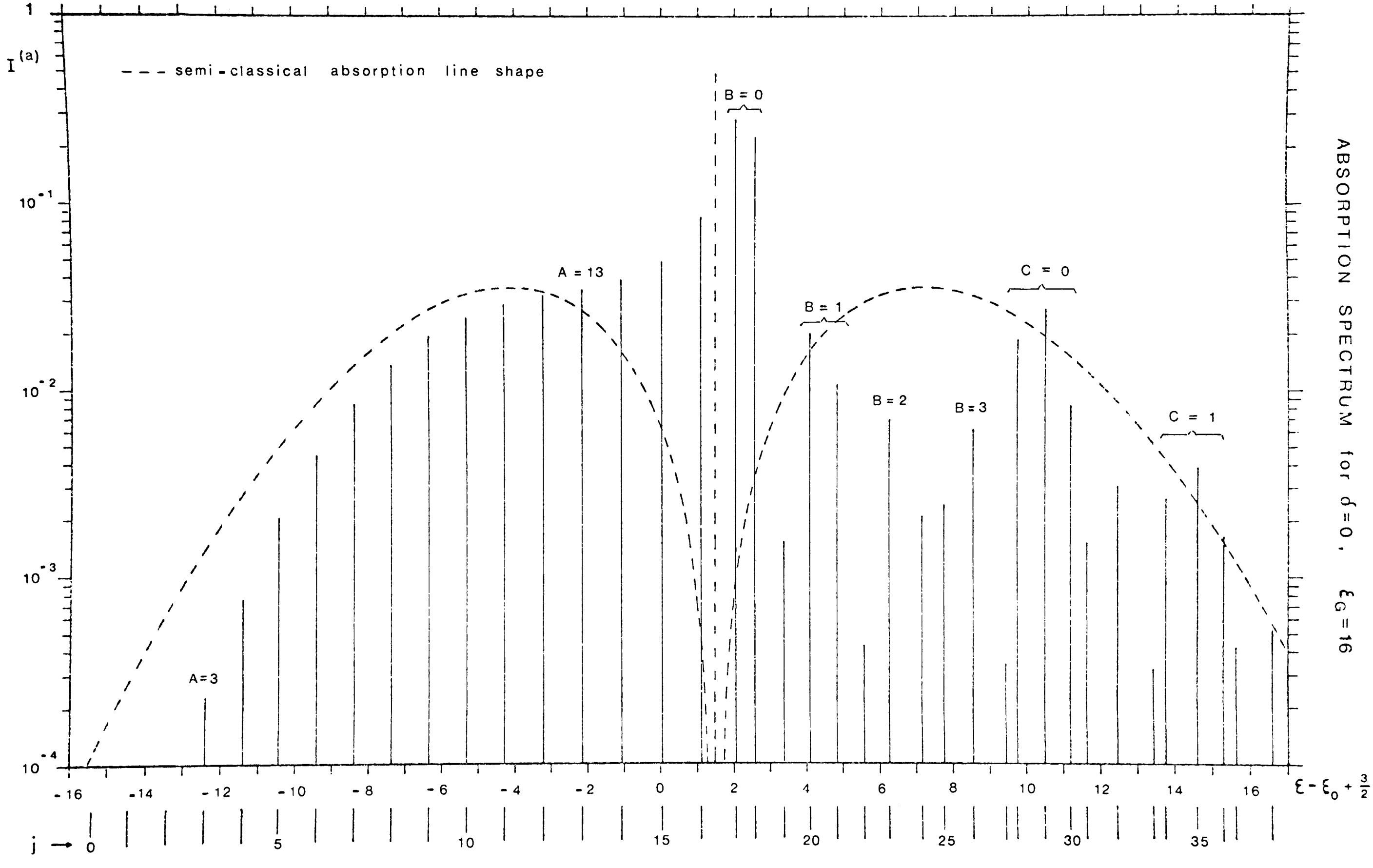
ABSORPTION SPECTRUM for $\sigma = -5$, $\varepsilon_G = 16$

GRAPH 36

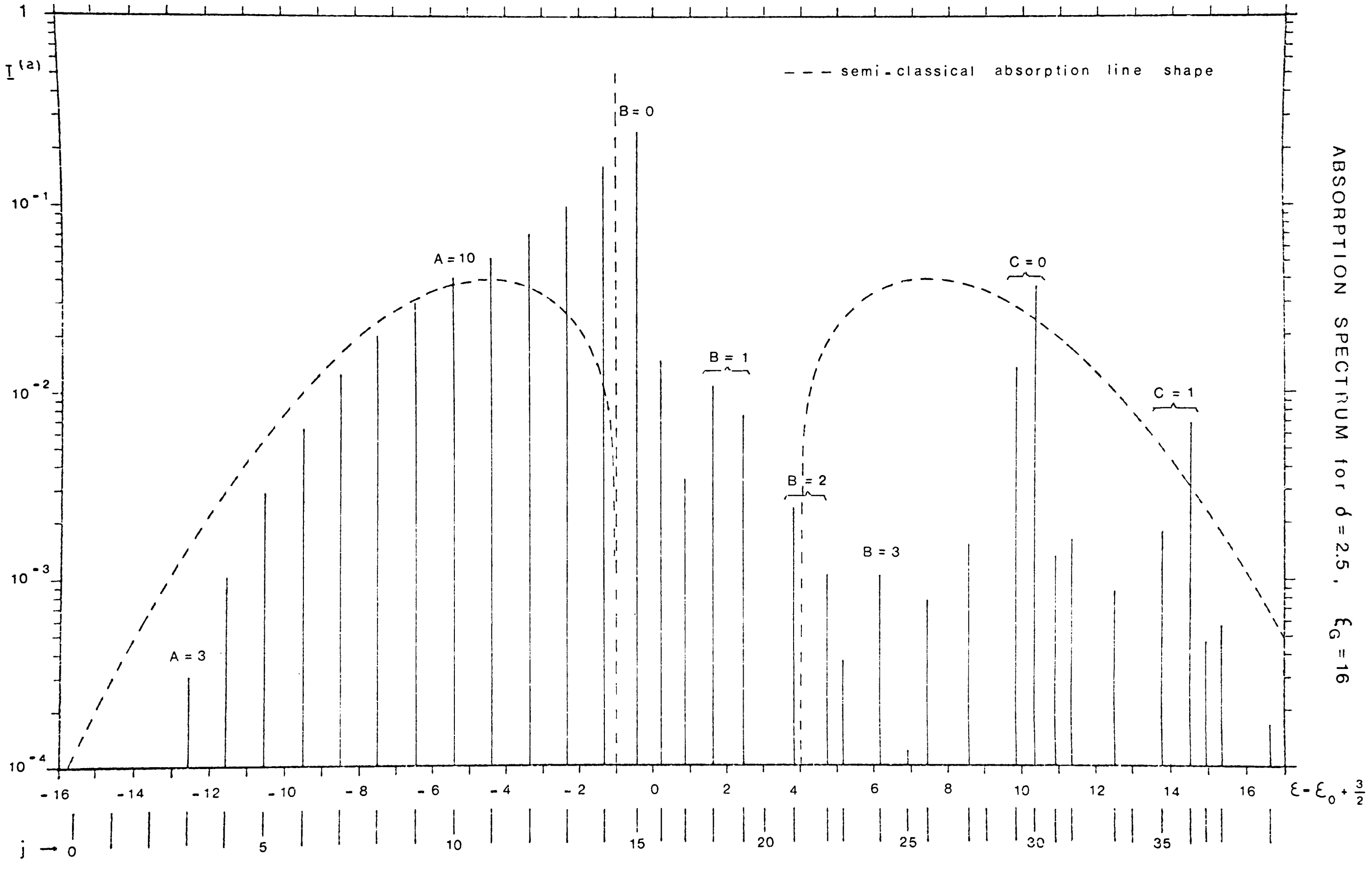


ABSORPTION SPECTRUM for $\delta = -2.5$, $\xi_G = 16$

GRAPH 37

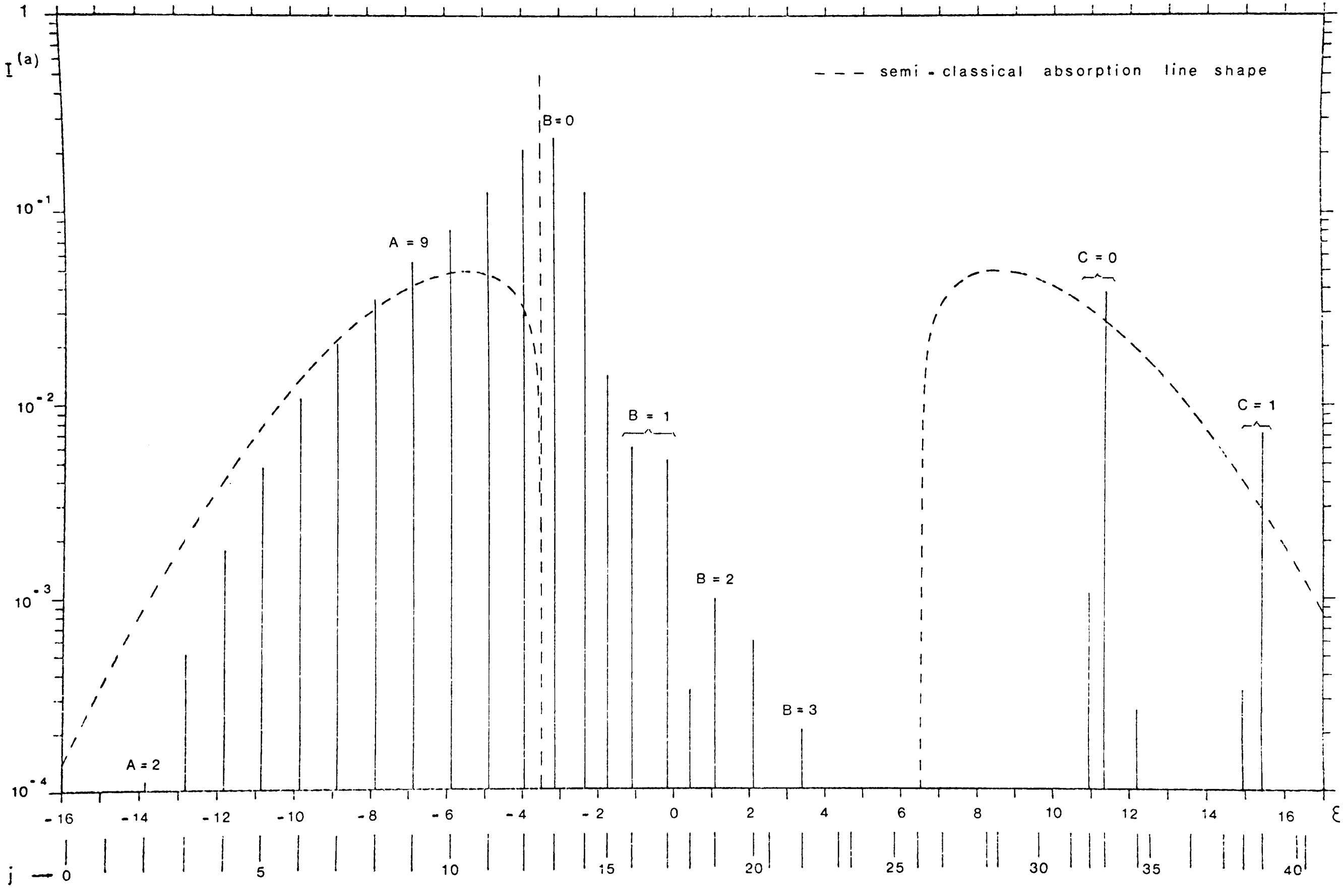

1
$I^{(a)}$
– – – semi-classical absorption line shape
10^{-1}
10^{-2}
10^{-3}
10^{-4}
B = 0
A = 13
B = 1
C = 0
B = 2
B = 3
C = 1
A = 3
-16 -14 -12 -10 -8 -6 -4 -2 0 2 4 6 8 10 12 14 16
$\varepsilon - \varepsilon_0 + \frac{3}{2}$
j → 0 5 10 15 20 25 30 35
ABSORPTION SPECTRUM for $\sigma = 0$, $\varepsilon_G = 16$

GRAPH 38



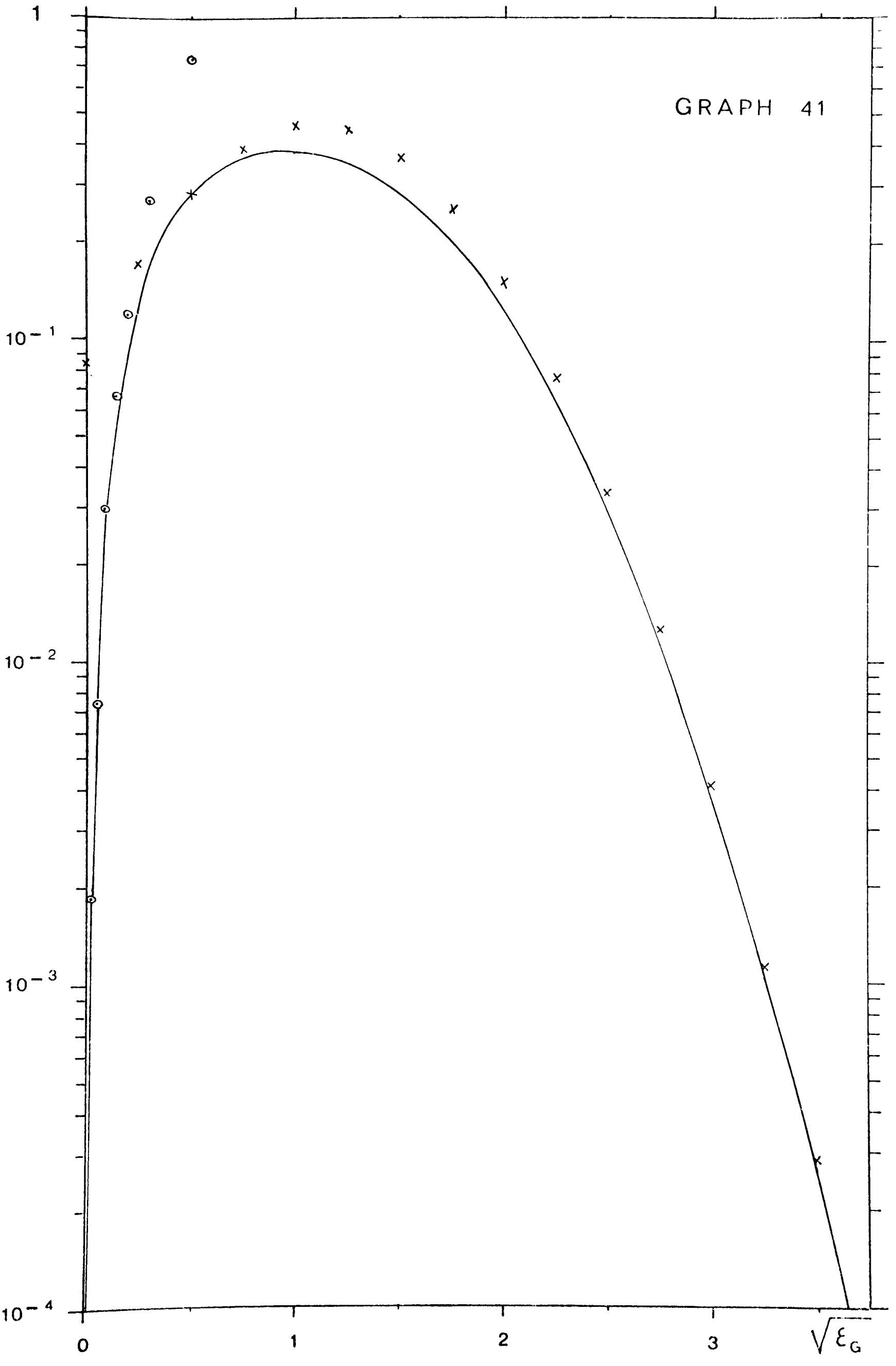
ABSORPTION SPECTRUM for $\delta = 2.5$, $\varepsilon_G = 16$

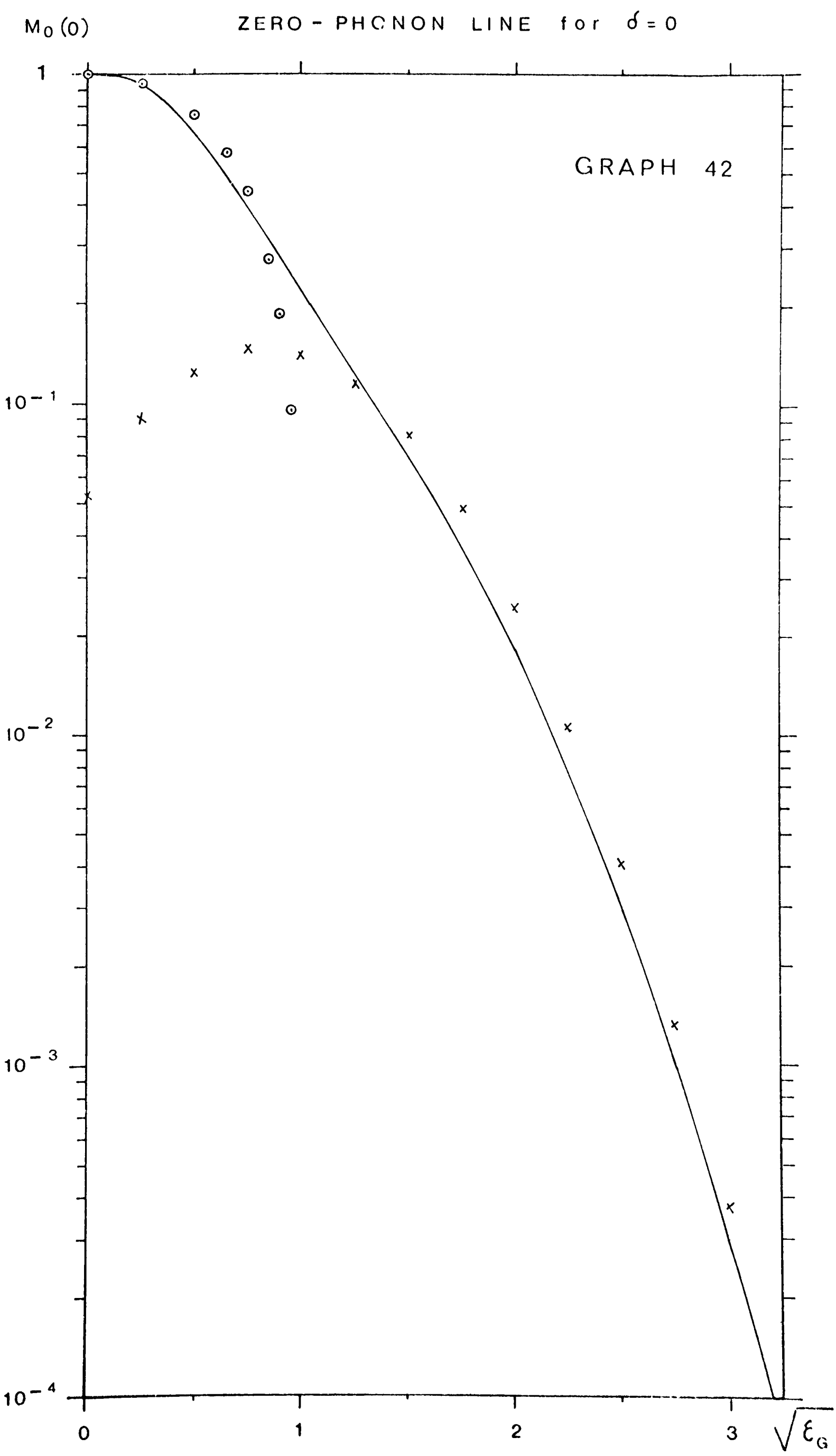
GRAPH 39


1
I (a)
10 - 1
10 - 2
10 - 3
10 - 4
– – – semi - classical absorption line shape
A = 9
A = 2
B = 0
B = 1
B = 2
B = 3
C = 0
C = 1
- 16
- 14
- 12
- 10
- 8
- 6
- 4
- 2
0
2
4
6
8
10
12
14
16
ε - ε0 + 3/2
j
0
5
10
15
20
25
30
35
40
ABSORPTION SPECTRUM for δ = 5 , εG = 16

$M_0^{(e)}(1)$ ONE - PHONON EMISSION LINE for $\delta = 0$

GRAPH 41

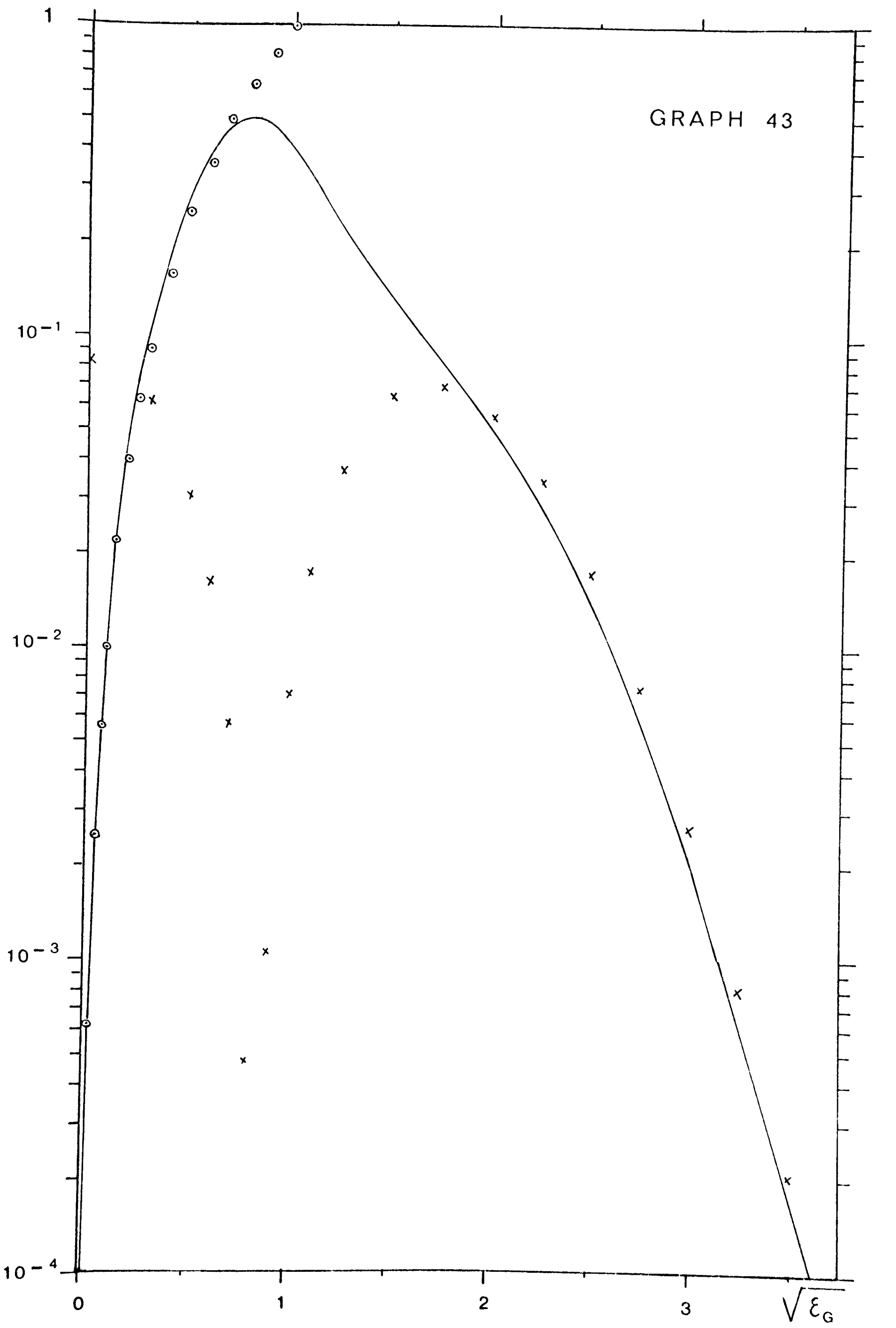



$M_0(0)$
ZERO - PHONON LINE for $\delta = 0$
GRAPH 42
1
10^{-1}
10^{-2}
10^{-3}
10^{-4}
0
1
2
3
$\sqrt{\epsilon_G}$
× × × strong
○ ○ ○ weak
} coupling approximation

$M_0^{(a)}(1)$

(j = 1) - ABSORPTION LINE for $\delta = 0$

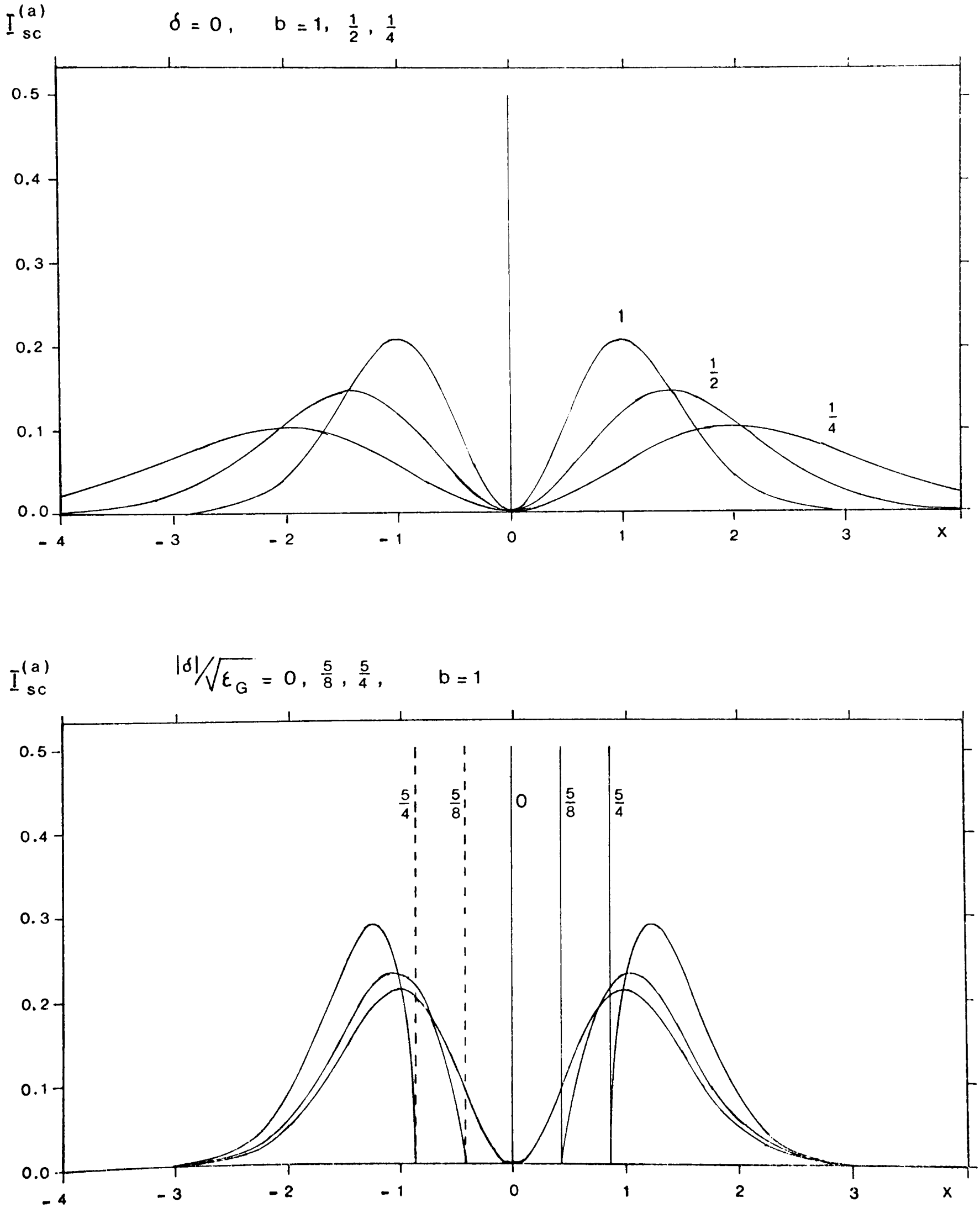
GRAPH 43



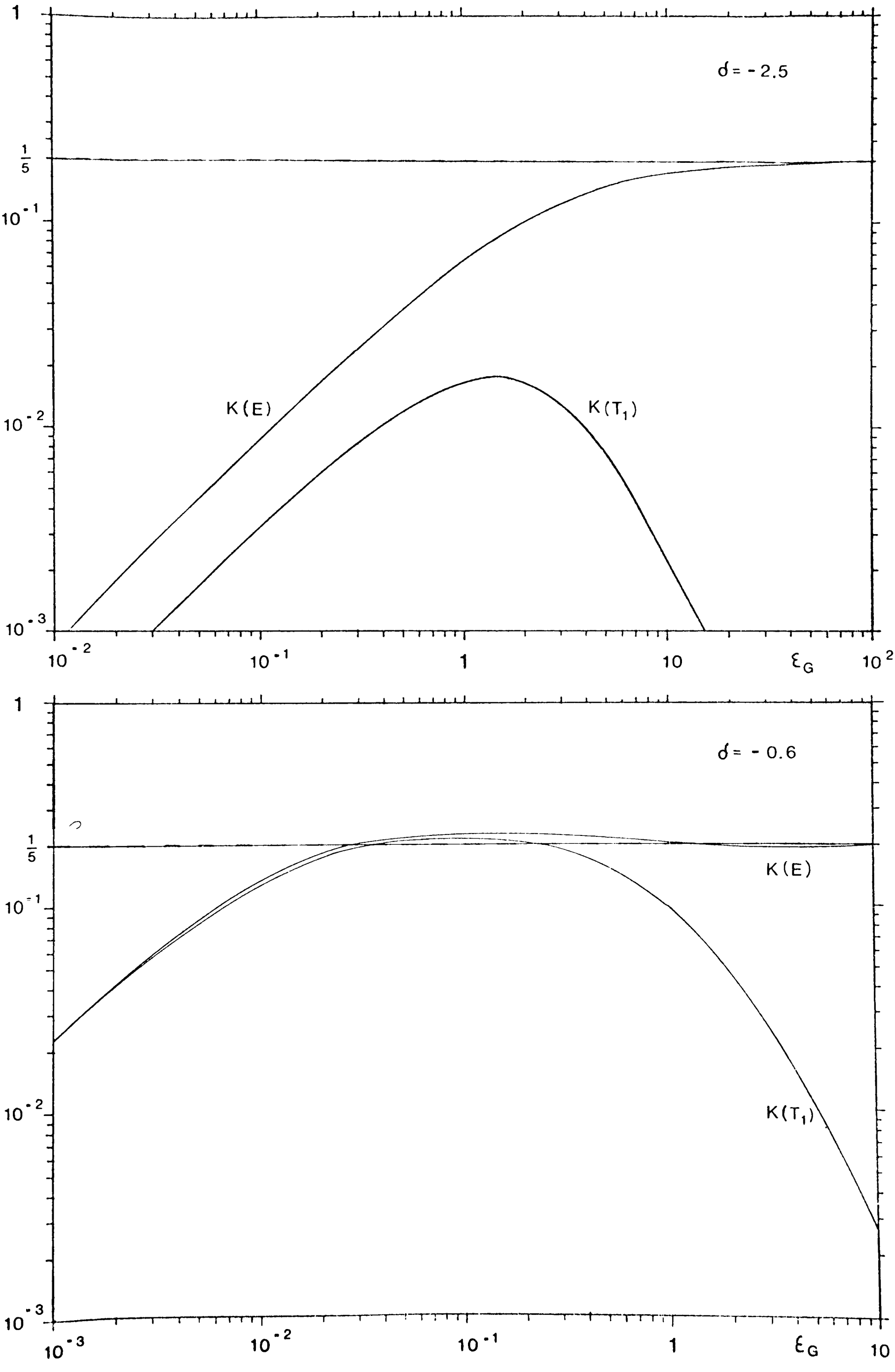
× × × strong
⊙ ⊙ ⊙ weak } coupling approximation

GRAPH 44

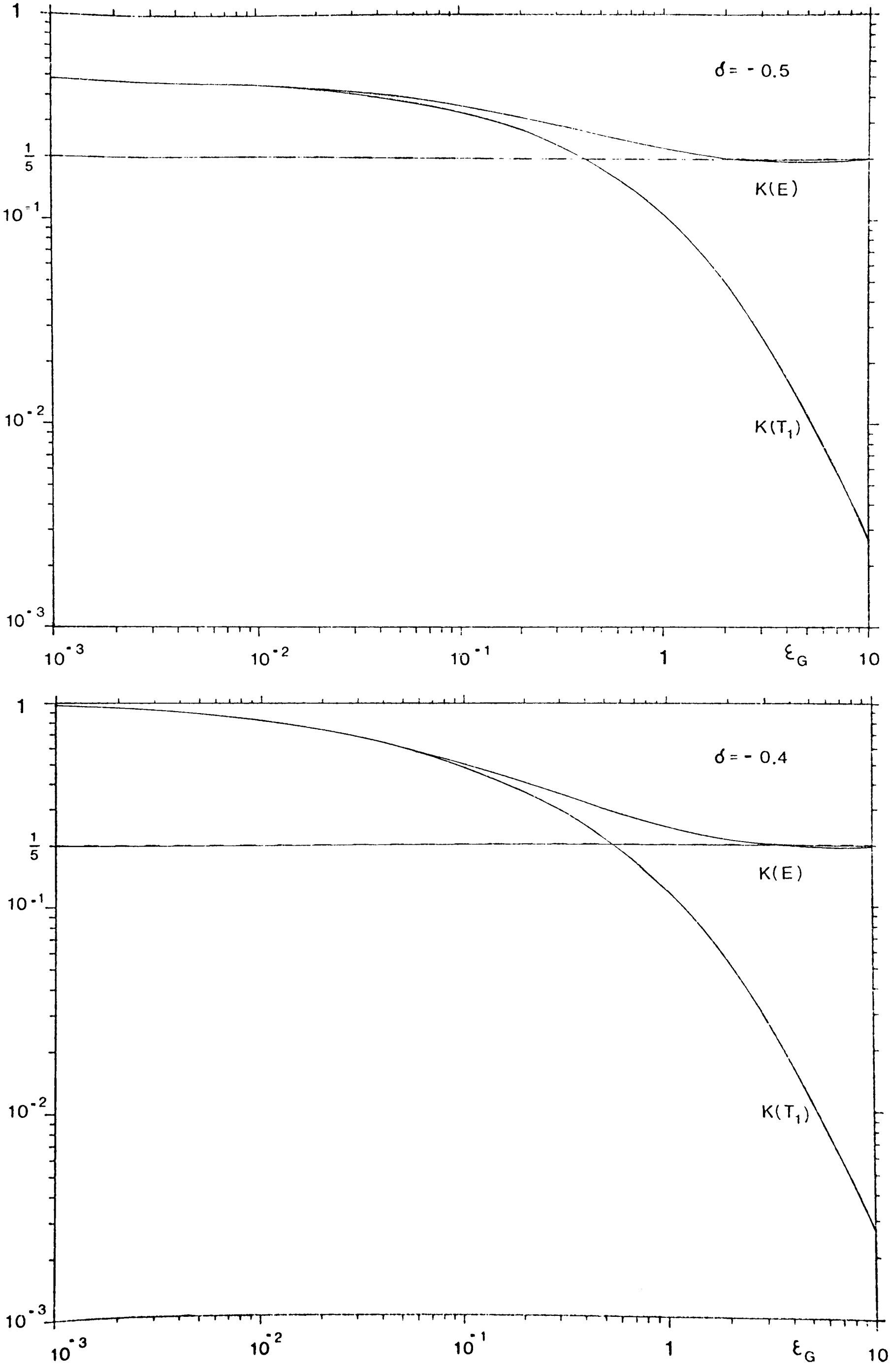
SEMI-CLASSICAL ABSORPTION BANDS



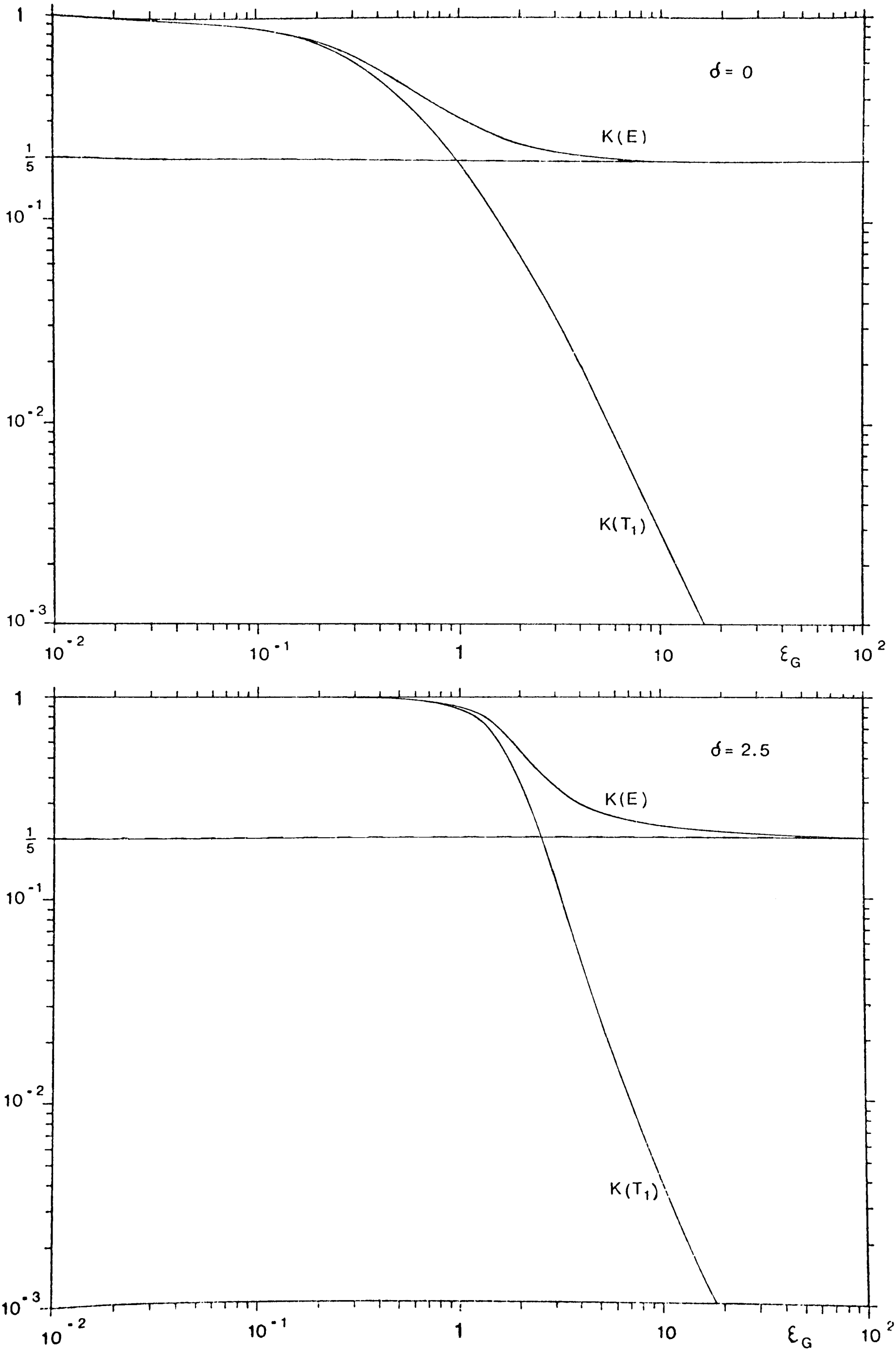
REDUCTION FACTORS GRAPH 45



REDUCTION FACTORS GRAPH 46



REDUCTION FACTORS GRAPH 47



APPENDIX: Jahn-Teller Systems in WKB Approximation

In the following we shall present some so far unpublished calculations made by O'Brien (1973) concerning the higher energy eigenstates of certain dynamically coupled JT systems. These calculations remove a difficulty in understanding the numerical results obtained from diagonalizing matrices (see § 11). The JT coupling can be regarded as producing a family of potential energy surfaces on which the system moves. If the kinetic energy is neglected, these surfaces intersect at the origin but remain smooth there. If the kinetic energy is properly taken into account, there appear centrifugal terms which are singular at the origin. Numerical calculations show that the higher energy levels correspond to the neglect of these centrifugal terms - it appears that the wave functions go right through these singularities without noticing them. The WKB method shows how that can happen and under what conditions. Moreover, it provides explicit expressions for the eigenfunctions and energy levels which - although these are only valid for higher energies - may be used in strongly coupled systems.

The WKB method is a way of obtaining approximate solutions of the one-dimensional Schrödinger equation for states well above the bottom of a potential well. It is usually described in standard textbooks (Messiah 1969, p. 231), and we shall only summarize it here briefly. The 1-d Schrödinger equation can be written

$$\frac{d^2\psi}{dx^2} + \frac{2m}{\hbar^2}\cdot\big(E - V(x)\big)\psi = 0 \qquad (A.1)$$

By treating $\hbar$ as a small parameter, we obtain approximate

solutions of the form

$$\psi = (E-V(x))^{-\frac{1}{2}} \cdot \exp\left\{ \pm \frac{i}{\hbar} \int \left[2m(E-V(x))\right]^{\frac{1}{2}} dx \right\} \qquad (A.2)$$

or

$$\psi = (V(x)-E)^{-\frac{1}{2}} \cdot \exp\left\{ \pm \frac{1}{\hbar} \int \left[2m(V(x)-E)\right]^{\frac{1}{2}} dx \right\} \qquad (A.3)$$

The solution (A.2) applies in the regions where $E \gg V(x)$ and represents a wave of wavelength $[2m(E-V(x))/\hbar^2]^{-\frac{1}{2}}$ with a modulation $(E-V(x))^{-\frac{1}{2}}$, and the approximation is good if $E-V(x)$ changes significantly only over several wavelengths. The solution (A.3) applies in regions where $V(x) \gg E$, and represents a ψ which either grows or decays exponentially. The complete solution is obtained by taking solutions of type (A.2 and A.3) and matching them over the boundaries where $E \cong V$, and the quantisation appears from the necessity of using only bounded solutions of type (A.3).

The WKB method can be extended to situations where several wave functions depend on the same independent variable through a system of coupled differential equations. We start off with a system of equations for a set of wave functions ψ_i, $i=1,\ldots,n$, all being functions of the same variable x,

$$\frac{d^2\psi_i}{dx^2} = \frac{1}{\hbar^2} A_{ij}(x)\, \psi_j \qquad (A.4)$$

where $A_{ij}(x)$ is a real symmetric square matrix, and summation over the repeated suffix is assumed. By analogy with the ordinary WKB approximation we look for a family of solutions of the form

$$\psi_r = \left\{ a_r^{(0)}(x) + \hbar\, a_r^{(1)}(x) + \ldots \right\} \cdot \left(\frac{dS}{dx}\right)^{-\frac{1}{2}} \cdot e^{\frac{iS}{\hbar}} \qquad (A.5)$$

Substituting these into the differential equations and picking out the largest terms (those in $\hbar^{-2}$) gives

$$A_{ij}(x)\ a_j^{(0)}(x) = -\left(\frac{dS}{dx}\right)^2 \cdot a_i^{o}(x) \qquad (A.6)$$

so that the solution is correct to this order as long as $-(dS/dx)^2$ is an eigenvalue of $A_{ij}(x)$, and $a_i^o(x)$ is the corresponding eigenvector. Clearly this solution is the one which would be obtained by first diagonalising $A_{ij}(x)$, and obtaining a set of energy surfaces on which the system is assumed to move without crossing from one surface to another. In order to work out the corrections to this assumption we apply the transformation which diagonalises $A_{ij}(x)$ to the original set of equations. Suppose that A is diagonalised by the orthogonal matrix M, so that $M_{i\ell}\ A_{ij}\ M_{jk} = \lambda_\ell\ \delta_{\ell k}$ and the eigenvectors are $\phi_i = M_{\ell i} \psi_\ell$ so that the system of coupled equations becomes

$$M_{\ell i}\ \frac{d^2 M_{\ell K}}{dx^2}\ \phi_K + 2M_{\ell i}\ \frac{d^2 M_{\ell K}}{dx} \cdot \frac{d\phi_K}{dx} + \frac{d^2\phi_i}{dx^2} = \frac{1}{\hbar^2}\ \lambda_k\ \phi_i\ \delta_{Ki} \qquad (A.7)$$

Then the solutions already obtained to order $\hbar^{-2}$ can be written

$$\phi_k = \delta_{ki} \left(\frac{dS_i}{dx}\right)^{-\frac{1}{2}} \cdot e^{-iS_i/\hbar}\ ,\ \left(\frac{dS_i}{dx}\right)^2 = -\lambda_i \qquad (A.8)$$

and substituting into the equations shows that the correction to order $\hbar^{-1}$ is given by

$$\phi_k = \hbar\ a_{ki} \left(\frac{dS_i}{dx}\right)^{\frac{1}{2}} \cdot e^{iS_i/\hbar}\ , \qquad (k \neq i) \qquad (A.9)$$

with $$a_{ki} = (\lambda_k - \lambda_i)^{-1} \cdot 2i\ M_{\ell k} \cdot \frac{dM_{\ell i}}{dx} \qquad (A.10)$$

This correction term remains small unless $\lambda_k \sim \lambda_i$ or

$(dM_{\ell i}/dx)$ becomes large. This means that the approximation may break down when the potential energy surfaces approach each other too closely. If two surfaces actually cross, that usually means that they are non-interacting, and hence that $(dM_{\ell i}/dx) = 0$, and the correction is not required. Since it is not usual for more than two energy surfaces to approach each other at the same point, it is convenient to consider a 2 x 2 problem. The orthogonal transformation M can then be taken to depend on a single parameter θ, and the coupled equations can be written

$$-\left(\frac{d\theta}{dx}\right)^2 \phi_1 + \frac{d^2\theta}{dx^2}\,\phi_2 + 2\,\frac{d\theta}{dx}\cdot\frac{d\phi_2}{dx} + \frac{d^2\phi_1}{dx^2} = -K_1^2\,\phi_1$$

$$-\left(\frac{d\theta}{dx}\right)^2 \phi_2 - \frac{d^2\theta}{dx^2}\,\phi_1 - 2\,\frac{d\theta}{dx}\cdot\frac{d\phi_1}{dx} + \frac{d^2\phi_2}{dx^2} = -K_2^2\,\phi_2 \qquad \text{(A.11)}$$

The first approximation corresponds to two independent oscillatory wave functions

$$\phi_1 = K_1^{-1/2}\cdot \exp\left(iK_1 x\right)\ ,\quad \phi_2 = K_2^{-1/2}\cdot \exp\left(iK_2 x\right) \qquad \text{(A.12)}$$

where K_1 and K_2 vary slowly with x. As the matching of the phase determines the allowed wave functions, it is important to consider the phase as x changes. The two extreme possibilities occur: (i) $|d\theta/dx| \ll |K_1 - K_2|$, (ii) $|d\theta/dx| \gg |K_1 - K_2|$. The first corresponds to a very slow change of state, and it can be shown that through this change the wave function can continue to be represented as $\exp\left\{(i/\hbar)\int(-\lambda(x))^{-\frac{1}{2}}dx\right\}$, and the system follows one energy surface adiabatically. In case (ii) the approximation may be made that $K_1 = K_2$. The coupled equations then reduce to a rotation of the principle axes of a 2-d oscillation,

and the phase change of the wave function is found simply by matching the states on either side of the rotation. There will be an intermediate zone between the slow and fast changes in θ, but high energy states tend towards case (ii) rather than (i).

We apply now the WKB method to the $(s+p) \otimes T_{1u}$ system. Ham (1973a) has shown that this PJT system has a set of coupled differential equations in a single variable. There are four such equations (7.14) and (7.15), but one of them, (7.15), is not coupled to the others. The solutions of (7.15) may be obtained by the ordinary WKB method. Near the origin they are spherical Bessel functions, and for large q they are parabolic cylinder functions. The matching condition gives

$$\varepsilon_{\delta}(II,NJ) = 2N + J + \tfrac{3}{2} - \delta \qquad (J \geq 1) \qquad (A.13)$$

with N=0,1,...,which agrees with (8.12).

Turning now to the three coupled equations (7.14), we find that f_1, f_2, f_3 are the inner wave functions which are uncoupled for small q and have the asymptotic forms

$$\begin{aligned} f_1 &= \frac{a_1}{q} \cdot \sin\left\{q\sqrt{2(\varepsilon - \delta)} - \tfrac{1}{2}J\pi\right\} \\ f_2 &= \frac{a_2}{q} \cdot \sin\left\{q\sqrt{2(\varepsilon + \delta)} - \tfrac{1}{2}(J-1)\pi\right\} \\ f_3 &= \frac{a_3}{q} \cdot \sin\left\{q\sqrt{2(\varepsilon + \delta)} - \tfrac{1}{2}(J+1)\pi\right\} \end{aligned} \qquad (A.14)$$

Ham (1973a) has also given the transformation to the outer wave function: (7.17) and (7.19). By putting $G_i = qF_i$ as in (11.10), the equations transform to the WKB form. When q is large enough, the equations uncouple and as before the

solutions bounded at infinity are the parabolic cylinder functions which are near q=0 of the form

$$G_1 = A_1 \cdot \cos\left\{q\sqrt{2\mathcal{E}} - 2\varkappa\sqrt{\mathcal{E}} + \frac{\pi}{4} - \tfrac{1}{2}\mathcal{E}\pi - \tfrac{1}{2}\varkappa^2\pi\right\}$$

$$G_2 = A_2 \cdot \cos\left\{q\sqrt{2\mathcal{E}} + 2\varkappa\sqrt{\mathcal{E}} + \frac{\pi}{4} - \tfrac{1}{2}\mathcal{E}\pi - \tfrac{1}{2}\varkappa^2\pi\right\} \qquad (A.15)$$

$$G_3 = A_3 \cdot \cos\left\{q\sqrt{2(\mathcal{E}+\delta)} + \frac{\pi}{4} - \tfrac{1}{2}E\pi\right\}$$

If we assume that E is large, so that $|d\theta/dq| \gg |K_1 - K_2|$ where the potential energy surfaces approach each other, then the inner and outer solutions just have to be matched at q=0. One such matching can be done if $A_1 = A_2 = \alpha_1 = 0$, which gives rise to

$$\mathcal{E}_\delta(I,BJ) = 2B + J + \tfrac{1}{2} - \delta \qquad (J \geq 1) \qquad (A.16)$$

with B = 0,1,... . The other type of matching corresponds to $A_3 = 0$, $A_1 = \pm A_2$, with an alternation of signs going along a sequence of energy levels for a given value of J. For each value of J the energy levels given by the matching conditions are

$$\mathcal{E}(I,A) = A + \tfrac{1}{2} - \mathcal{E}_G \qquad (A.17)$$

where A=0,1,... . The solutions (A.17) are only valid if $\mathcal{E} \gg 2\delta$, while (A.16) requires $(\mathcal{E} + \delta) \gg 1$. If δ were large, the mixture of G_1 and G_2 would be a slowly changing function of x, and in principle the matching could be done by evaluating the phase integral $\int (E-V(x))^{\frac{1}{2}}dx$ along each energy surface. This would involve elliptic integrals which would have to be evaluated numerically.